Studies into the rotational history of the minor planets

Thesis

STUDIES INTO THE ROTATIONAL HISTORY OF THE MINOR PLANETS

A Thesis submitted for the Degree of

Doctor of Philosophy

by

Andrew John Hollis

BSc(Eng) ACGI CEng MICE MIStructE

Physics Department
The Open University
1996

EX12

HIGHER DEGREES OFFICE

LIBRARY AUTHORISATION FORM

Please return this form to the Higher Degrees Office with the bound library copies of your thesis. All students should complete Part 1. Part 2 applies only to PhD students.

Student: ANDREW JOHN HOLLIS PI: M7021051

Degree: DOCTOR OF PHILOSOPHY

Thesis title: STUDIES INTO THE ROTATIONAL HISTORY OF THE MINOR PLANETS

Part 1 Open University Library Authorisation (to be completed by all students)

I confirm that I am willing for my thesis to be made available to readers by the Open University Library, and that it may be photocopied, subject to the discretion of the Librarian.

Signed: [signature] Date: 15 MAY 1996

Part 2 British Library Authorisation (to be completed by PhD students only)

If you want a copy of your PhD thesis to be held by the British Library, you must sign a British Doctoral Thesis Agreement Form. You should return it to the Higher Degrees Office with this form and your bound thesis. *You are also required to supply a third, unbound copy of your thesis.* The British Library will use this to make their microfilm copy; it will not be returned. Information on the presentation of the thesis is given in the Agreement Form.

If your thesis is part of a collaborative group project, you will need to obtain the signatures of others involved for the Agreement Form.

The University has agreed that the lodging of your thesis with the British Library should be voluntary. Please tick either (a) or (b) below to indicate your intentions.

(a) ☒ I am willing for the Open University to supply the British Library with a copy of my thesis. A signed Agreement Form and 3 copies of my thesis are attached (two bound as specified in Section 9.4 of the Research Degree Handbook and the third unbound).

(b) ☐ I do not wish the Open University to supply a copy of my thesis to the British Library.

Signed: [signature] Date: 15 MAY 1996

Abstract

Three aspects of the rotational history of the minor planets are considered - taxonomy, mathematical modelling and observation.

Following an introductory review of the basic characteristics and formation, the classification of asteroids is critically assessed and a new scheme based on the spectral characteristics is formulated using numerical taxonomy. It is noted that the asteroids within the basic S-type of other taxonomies can be distributed as two separate zones. the archetypal Juno-type S are found in the middle and outer parts of the main belt whilst a discrete Flora-type S class predominates in the inner portion of the main belt. The groups appear to be two easily distinguishable types probably representing compositional differences. The observed distribution of spin rates for different classes, and hence different surface compositions, is considered.

The collision evolution of the spin rates and spin axis orientations has been considered using a new model derived in this work. From this simple model the rotation geometry of precessing bodies can be derived and consideration of the nucleus of Comet P/Halley suggests that its spin axis is not aligned with any of the geometrical principal axes. Consideration of the geometry of rotation of 1220 Crocus suggests that it might be a binary asteroid. It is found that a random spin axis orientation for the asteroid belt would be expected to be consistent with the observed spin rate distribution.

Using the model and the equilibrium shapes of asteroids, calculations have been carried out to investigate the observability of free-precession of asteroids in terms of the maximum light curve amplitude due to free-precession. This shows that only large displacements of the angular velocity vector from the angular momentum vector would produce an amplitude sufficiently great to be detectable. Using a particle in a box model the expected number of examples of free-precession for different sizes of asteroid in the main visible at this time is estimated.

New observational data measured as part of this work is presented and analysed. Rotational light curves are examined to determine spin characteristics and whether complex rotations can be seen. As an example new data for 8 Flora has been obtained and, when combined with the digitised information from the international database, has allowed a new model for the shape and variegation to be proposed by combining the data measured as part of this project with the international data set. From this evidence it is clear that there is no evidence of free precession arising from collisions amongst asteroids in the recent past. In particular it is noted that a shortage of data constrains the accuracy of statistical data and many more quality measurements will be needed before a satisfactory picture of the evolution of minor planets can be presented.

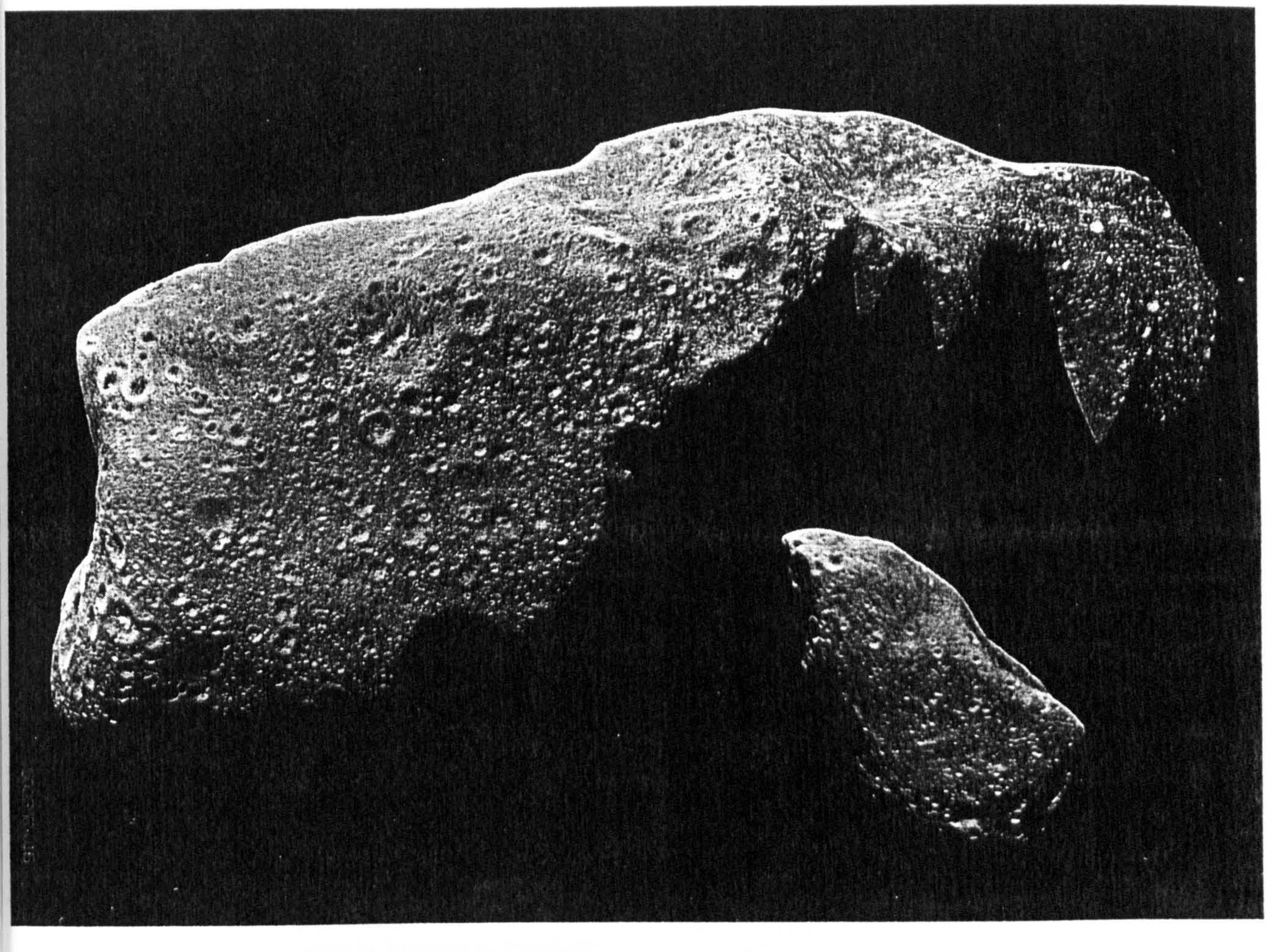

Frontispiece - Asteroid Images of 243 Ida and the smaller 951 Gaspra from the Gallileo Mission.
The images are combined on a single picture to the correct relative scale.

Contents

Figures

1. Review of the Basic Characteristics of Minor Planets

1.1 Historical Review

1.1.1 Discoveries

Prior to the introduction of the telescope the Solar System was thought to consist only of the seven bodies then known, namely the Sun, Moon, Mercury, Venus, Mars, Jupiter and Saturn. Since the time of Aristotle, the comets had been dismissed as "earthly exhalations" (see for example Whipple 1986). The first suggestion, at least in modern times, that there might be more bodies to be found in the Sun's family, appears to have been made by Kepler in his "Mysterium Cosmographicum" (Kepler 1595). Though he noted the large distance between Mars and Jupiter and that it could contain a planet he did not develop this idea further, perhaps because it would have introduced a difficulty into his theory of the construction of the Solar System. The discovery of four satellites of Jupiter by Galileo in 1610 was the first direct evidence of additional bodies in the Solar System.

An arithmetical relationship between the distances of the planets from the Sun was formulated by J.D. Tieze and inserted in the text of his German translation of Bonnet's "Contemplation de Nature" (Titius 1766). This relationship is a series predicting the semi-major axis of a planet's orbit in terms of that of the Earth. A gap in the sequence was found between Mars and Jupiter and the distances of any undiscovered planets exterior to Saturn were predicted. Johann Elert Bode (Bode 1772) popularised this formula and it became known as Bode's Law. The success of this Law was demonstrated in 1781 with the discovery of a planet, Uranus, by Herschel. It was initially announced as a comet (Herschel 1781), but was later confirmed as a planet - the first ever discovered as those already known were recognised from antiquity. This intensified the belief in a missing planet between Mars and Jupiter and so the scene was set for Piazzi to discover 1 Ceres on the night of 1801 January 1st (Piazzi 1802). It was found to orbit between Mars and Jupiter virtually in the place predicted by the Titius-Bode Law. There is a popular view that 1 Ceres was recovered by Olbers and von Zach on the first anniversary of its discovery (see for example Nieto 1972 or Ley 1963). In fact von Zach recovered it earlier - on 1801 December 7th (von Zach 1802 (i), (ii), (iii) and (iv) and Anon 1802). Three additional bodies (2 Pallas, 3 Juno and 4 Vesta) were discovered by March 1807.

The new planets were all faint and aroused speculation about their nature since they showed differences from both the major planets and the comets. Herschel (1802), using his "lucid disk micrometer", derived a value of 161.6 miles (259km) for the diameter of 1 Ceres and 147 miles (235km) for the diameter of 2 Pallas. In this method Herschel positioned a small disk of known diameter, illuminated by a lantern, at a known distance from the telescope. He then "threw the image of Mr Piazzi's star, seen in a 7-feet reflector, very near it, in order to have the projected picture of the star and the lucid disk side by side ...." He compared the apparent sizes of the two images and

deduced its size. He repeated the process with 2 Pallas and concluded that 1 Ceres and 2 Pallas were different from the known classes of Solar System body and, from their appearance, he coined the new name ASTEROID.

Sir Robert Ball (1901) admitted "of the physical conditions of the asteroids and of the character of their surfaces we are entirely ignorant". However the discovery of 433 Eros, by Witt in Berlin in 1898, attracted attention as it was the first asteroid to be discovered that did not stay between the orbits of Mars and Jupiter. Von Oppolzer (1901) noted that the apparent brightness of 433 Eros varied with a period of a few hours. This discovery prompted a special study of the asteroids at Harvard which revealed that 7 Iris was variable with an estimated period of six hours and thirteen minutes (the currently accepted period is just over seven hours) and that 15 Eunomia was also variable with a period of just over 6 hours (Thompson 1905). A key paper was published by Russell (1906) which discussed possible causes of such light variations (binary asteroids, elongated shape, or else albedo variations across the surface) on the assumption that they were caused by rotation of the asteroid. He considered the light curves from a mathematical viewpoint and concluded that all these causes could produce similarly shaped light curves which would be indistinguishable. He further concluded that there would be an infinite number of solutions of shape that would fit an observed light curve.

The problems addressed by Russell are still unsolved despite the great increase in data and improvements in techniques. They form the subject of this work.

1.1.2 Recent Studies

The asteroids have not been the subject of intense research until recent years. On the contrary, they were considered a nuisance by many astronomers as their trails frequently "spoilt" survey plates. Many of the discoveries were not followed up and the minor planets were lost. There has been a major effort recently to recover the missing bodies and only one, 719 Albert, remains lost.

Detailed observational studies began in 1949 when Kuiper and his team applied the then relatively new technique of photoelectric photometry to follow the brightness changes of asteroids. The increased precision of measurement enabled more asteroids to be studied without the bias errors inherent in visual observation. To complement this work, analytical methods have been developed to extract data about the physical conditions of the bodies namely rotation rates, surface structure and polar orientation. Roughly in parallel to these observations theoretical studies of the formation and evolution of the asteroids system began.

The first serious attempt to summarise the state of knowledge about the asteroids was the NASA publication "Physical Studies of the Minor Planets" (commonly known as "Asteroids 0"). Two state of the art books have since been published in the Arizona Space Science series, "Asteroids" edited by Gehrels and Matthews (1979) and "Asteroids II" edited by Binzel, Gehrels and Matthews (1989). These have provided the starting point for many studies of the minor planets.

The Galileo probe to Jupiter encountered 951 Gaspra in 1991 providing the first close up view of an asteroid and has since imaged 243 Ida. Several asteroid encounter missions have been proposed though most have been cut owing to economy measures. However ESA has taken a decision to concentrate on their own specific mission to multiple encounters of comets and asteroids starting in the late 1990s, this mission is known as ROSETTA (Schwehm and Hechler 1994). The success of the Infra-Red Astronomical Satellite (IRAS) has demonstrated the great potential for carrying out remote sensing of solar system objects from above the Earth's atmosphere. The Hubble Space Telescope (HST) may in due course provide data provided sufficient time can be made available. However the success of the repair mission is likely to mean that much of its future observing time will concentrate on deep space imaging.

1.2 Distribution and Orbital Dynamics

The minor planets appear starlike and are identified by their motion through the background star fields. A description of the search and identification procedure for discovering new asteroids is given by Taff (1984). Nearly 6000 have sufficiently well-determined orbits to be recovered at subsequent oppositions and have been allocated numbers, At any given instant they are distributed at all longitudes - as is illustrated by the longitude of the first 5405 on 1994 September 5.0 shown in Figure 1.1. Perhaps twice as many have preliminary orbits calculated (Marsden 1986 (i)) so that approximately 18000 are known.

All the known minor planets follow orbits that are prograde and of a relatively low inclination, see Figure 1.2. The vast majority have inclinations of less than 20°. The extreme value known is 2102 Tantalus with an inclination of 64°. The majority of the orbits have a low eccentricity and this is illustrated by Figure 1.3 where eccentricity is plotted versus semi-major axis. The orbits of asteroids appear to be governed solely by gravitational forces, unlike those of comets where the evolution of gaseous matter from the nucleus gives rise to a jet action which may accelerate or decelerate the comet depending on the direction of its axial rotation (Whipple 1981). This effect is not present in minor planets and a study by Ziolkowski (1983) concludes that other non-gravitational forces, such as radiation pressure, are not expected to be greater than the uncertainties in the calculated orbits.

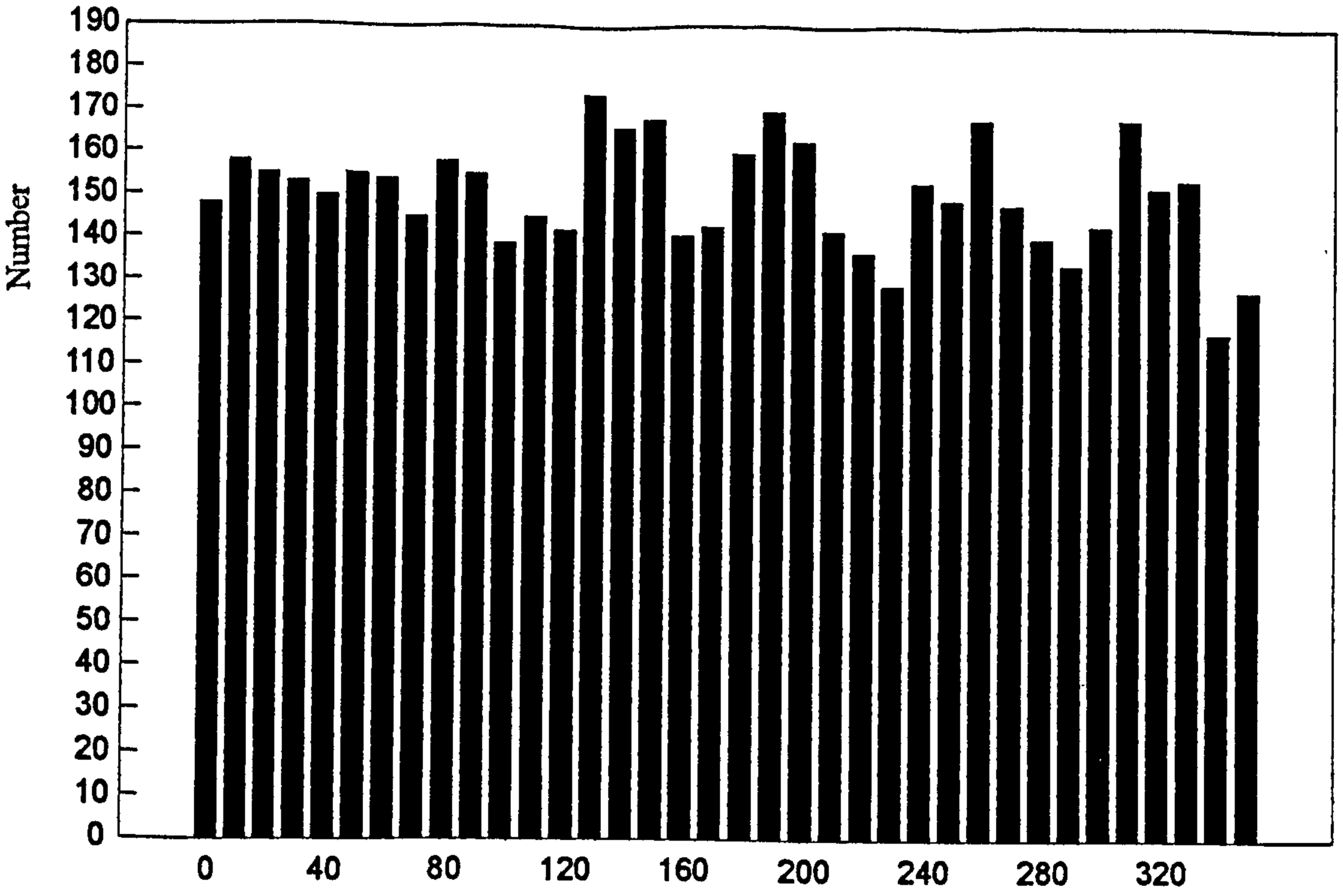

Figure 1.1 - Distribution in Heliocentric Longitude of the first 5405 Minor Planets on 1994 September 5.0
Bin size - 10 degrees, Source 1994 Ephemerides of the Minor Planets

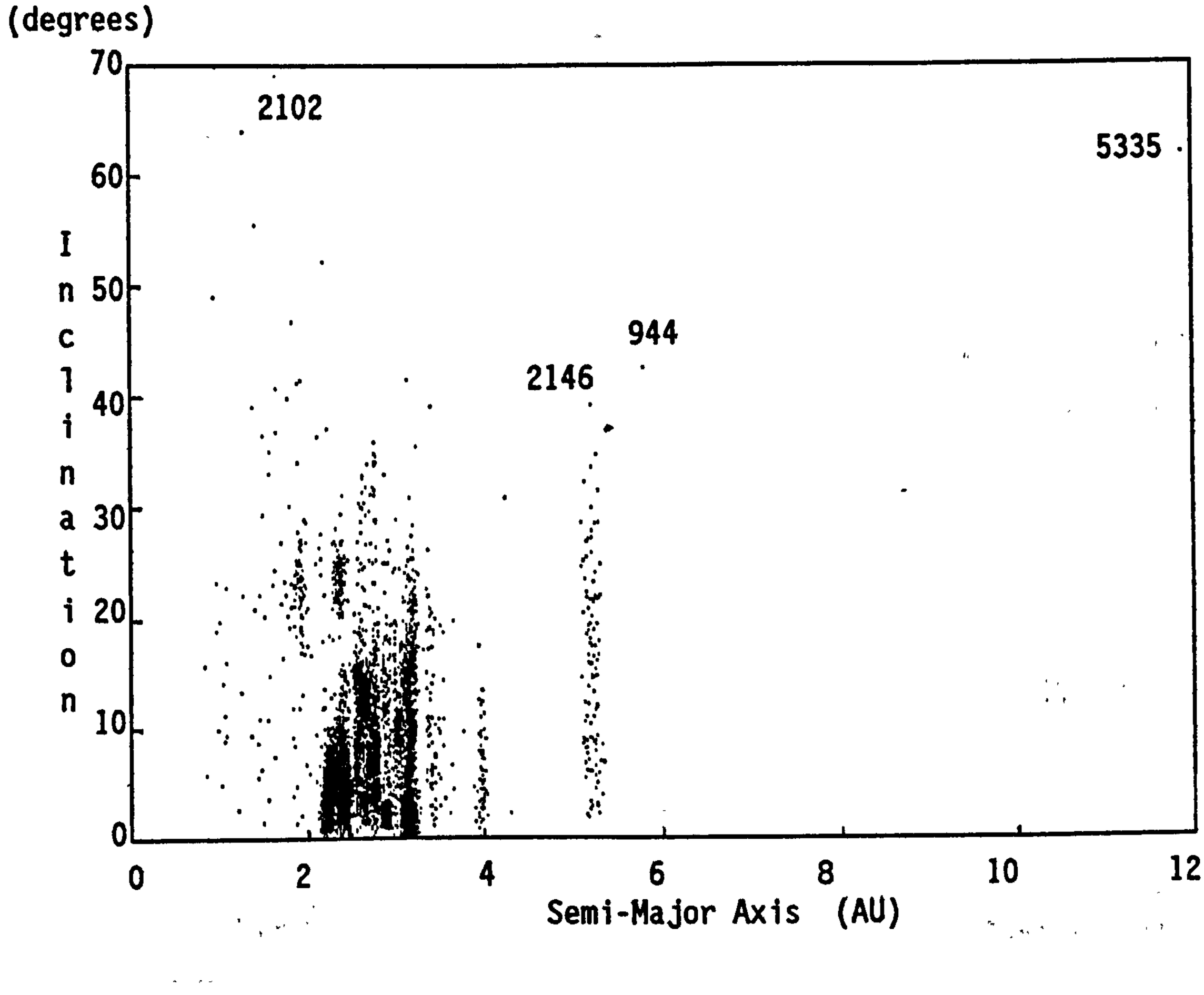

Figure 1.2 - Plot of the Orbital Inclination with respect to the Semi Major Axis for 5405 Asteroids.
Source 1994 Ephemerides of the Minor Planets

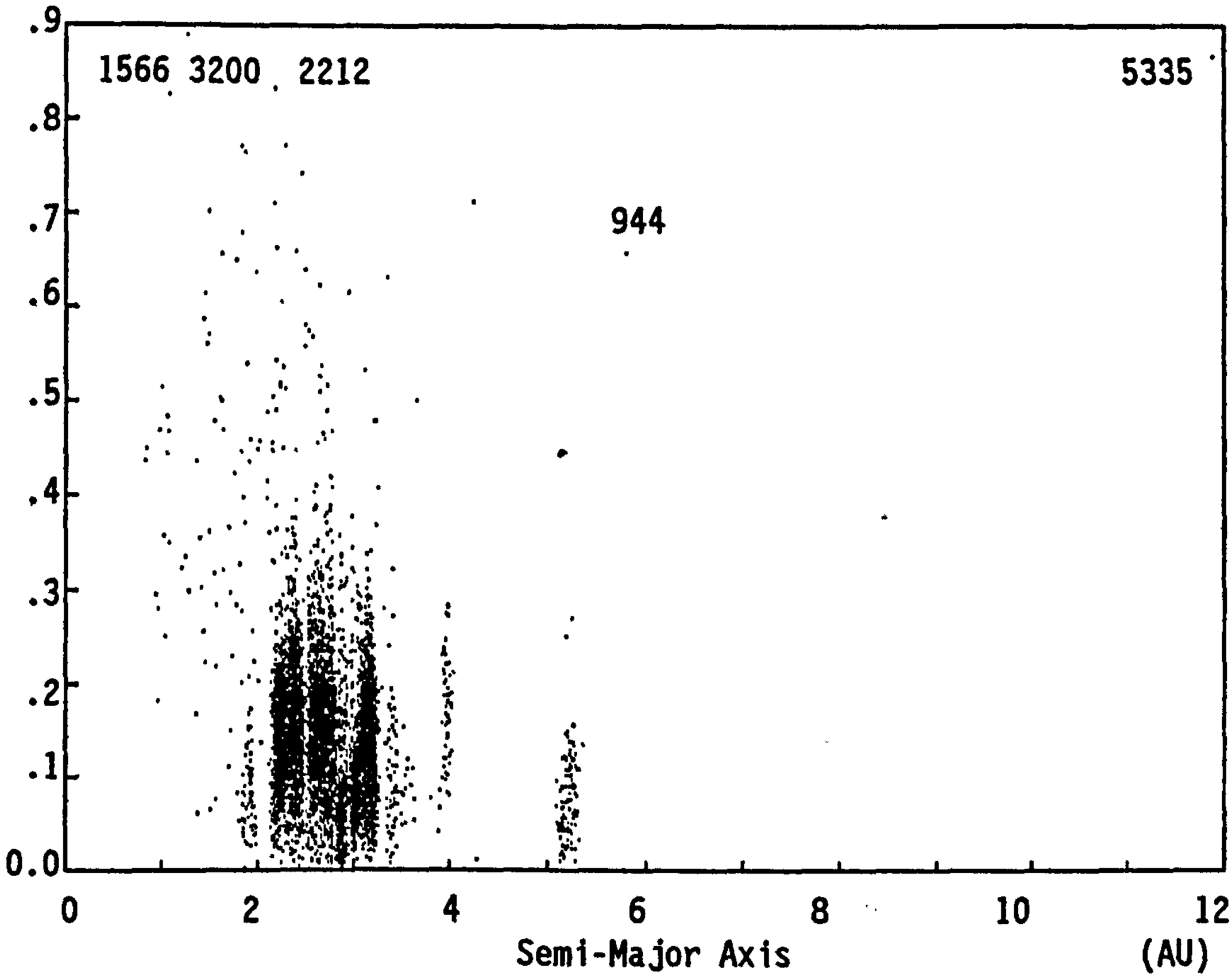

Figure 1.3 – Plot of the Orbital Eccentricity with respect to the Semi Major Axis for 5405 Asteroids. Source 1994 Ephemerides of the Minor Planets.

The orbits of both comets and minor planets are subject to gravitational perturbations - predominantly those due to Jupiter. The values of a, the semi-major axis, and i, the orbital inclination, change quasi-periodically in a timescale of less than 10^3 years (Bien and Schubart 1983).

Over 90% of the known asteroids follow orbits which lie wholly between the orbits of Mars and Jupiter. In 1866, when the number of asteroids known was only 85, Daniel Kirkwood was able to deduce the existence of orbital distances where the numbers of known asteroids appeared to be relatively high and others where there were gaps (Gradie et al. 1979). From a slightly larger sample he identified further structure within the asteroid belt in 1872. Jupiter is the main disturbing influence in the Solar System and the Kirkwood Gaps are always considered in terms of the ratio of their orbital period with that of Jupiter (known as resonance). The belt consists of a large number of subsidiary zones with apparent regions of depletion occurring at resonances of 3/1, 5/2, 7/3 and 2/1 though there are concentrations found at 3/2 (Hildas), 4/3 (Thule) and 1/1 (Trojans) (Greenberg and Scholl 1979). This effect is well illustrated by a cumulative plot of number versus heliocentric distance (see Figure 1.4). However the mechanism by which a resonance can cause a gap or an accumulation is still a matter of debate.

Outside the known planetary system is a disk of asteroids (Stern 1995). The Kuiper Belt (or Disk) was first proposed in the late 1940s. Calculations made in the early 1980s indicated that the reservoir of short period comets probably existed in a band just outside the planetary orbits. The first to be discovered was 1992QB1 and several more have since been identified (21 known in early 1995). All appear to be large (between 100km and 300km in diameter) and current estimates are that at least 10000 bodies exist in this belt. Currently four bodies are known which appear to have been perturbed from this belt toward the inner solar system. These bodies (now called 'Centaurs') occupy unstable orbits and the largest (2060 Chiron) was discovered by Kowal in 1977 and is currently near perihelion. Interest in these bodies has been heightened by the discovery that Chiron now has a coma making it cometary in appearance.

The presence of several bodies in similar orbits was first recognised by Hirayama (1918). He identified 9 groups of asteroids each group of which appeared to possess similar orbits. The possibility of a common parent body for each family was considered, inferring that catastrophic collisions occur within the asteroid belt (Gradie, Chapman and Williams 1979).

There are many similarities in the appearance of asteroids and of cometary nuclei. This has given rise to speculation that comets and asteroids may represent different stages in the evolution of the same type of body. A cometary nucleus that has lost its surface volatile components would appear telescopically the same as an asteroid at visible wavelengths. It could be possible for some of the observed minor planets to be extinct cometary nuclei though no examples were identified prior to

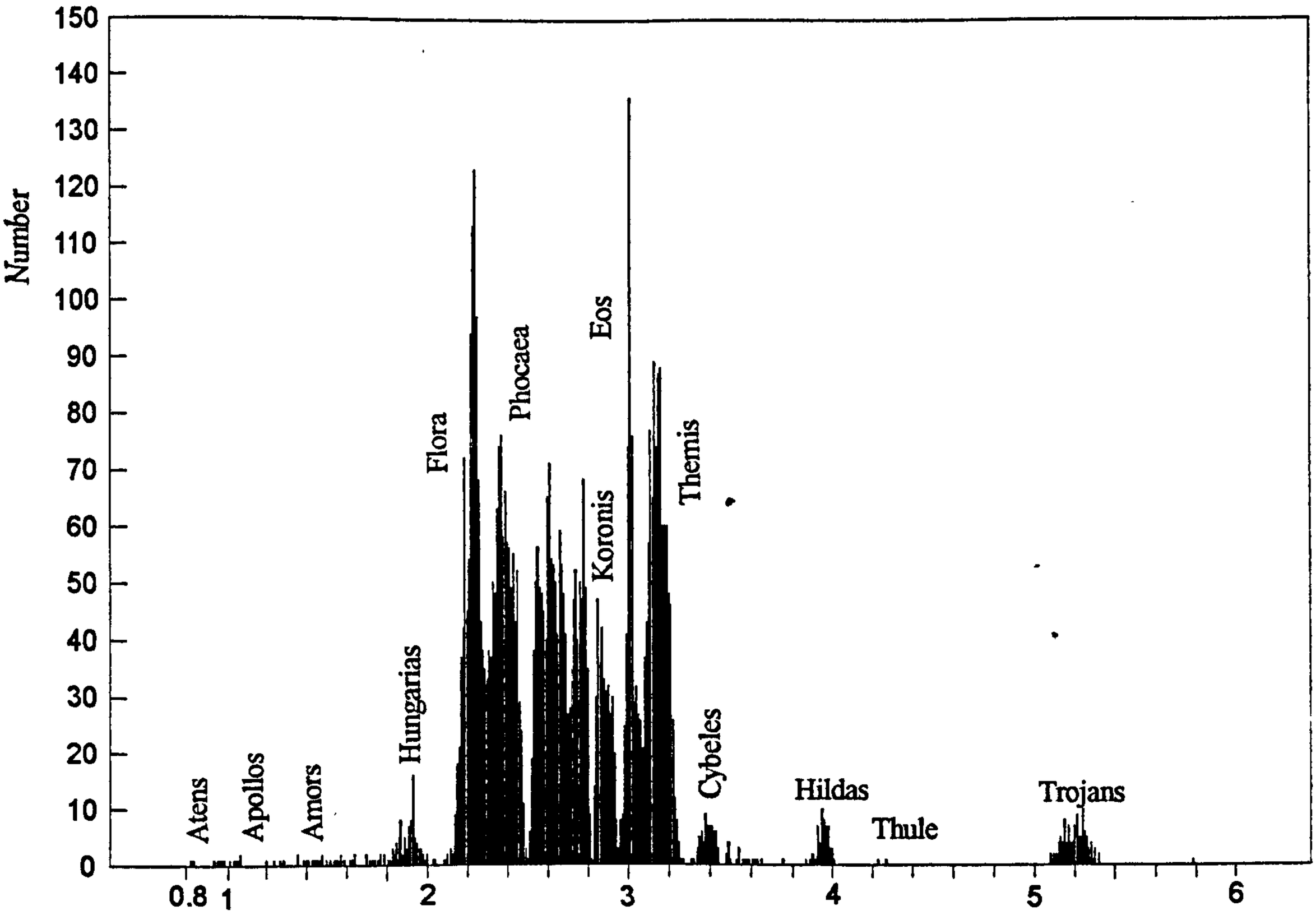

Figure 1.4 - The heliocentric distribution for 5401 asteroids from data in the 1994 Ephemerides of the Minor planets

1979 (Kresak 1979). But in that year, the identification of the asteroid 1979VA with the periodic comet 1949g (Wilson-Harrington) by Marsden suggests that many more examples have already been observed but not yet identified. Observation at infra-red wavelengths can show emission. Jupiter's satellite Io loses sulphur to the surrounding space and 1 Ceres has also been observed surrounded by a tenuous cloud (possibly of water vapour).

Minor planets which orbit in the Inner Solar System frequently come under the gravitational influence of the planets - predominantly Jupiter . The orbits are therefore not stable and calculations have indicated that the typical time of an object to remain in an Earth-Crossing orbit is of the order of 3 x 10^7 years (Shoemaker et al. 1979). There must be replacements perturbed into these orbits in the same timescale to account for the observed density.

1.3 Composition

The simplest view of asteroids, comets and meteoroids would be to consider them as planetesimals (Hartmann 1981), that is, debris left over from the formation of the larger bodies of the Solar System (e.g. Planets). This would happen if, by reason of their initial orbital location or subsequent orbital evolution, they failed to accrete to other planetesimals and form part of the larger bodies. More likely, some of the bodies represent the debris of catastrophic disruption of larger bodies brought about as a consequence of collisions. Planetesimals must have different compositions depending on their initial location in the Solar System. In the inner Solar System, where the Solar Nebula was hottest, only the metallic and silicate minerals could condense to form planetesimals - many of which accreted to form the Terrestrial Planets. At the distance of the outer regions of the asteroid belt the temperature of the Nebula was lower allowing carbon and water compounds to condense as well. At greater distances from the Sun it was colder still and so water ice is a common material - a major component in the composition of the satellites of Jupiter and Saturn. Further from the Sun the temperature is sufficiently low that methane ice can form. There is thus a steady transition in the composition of bodies which depends on their distance from the Sun and this has been observed, in the case of the planetary satellites, from telescopes on Earth and the space probes sent to the Outer Solar System.

The search for these isolated remnants assumed a special importance from the early 1970's when NASA began planning spacecraft missions beyond Mars and they wished to evaluate the potential danger of collision (Gehrels 1979) .

At this time it was realised that some of these objects may be planetesimals containing matter unmodified since condensation from the primitive Solar Nebula. Such bodies would offer a record of the early chemical composition of the Solar System and are of great scientific interest.

1.4 Physical Characteristics

The term minor planet or asteroid, names which are interchangeable, is applied to many Solar System bodies. They all possess similar characteristics, namely:-

1. They are smaller than the major planets. The estimated diameter of Pluto has been reduced recently and it (the smallest planet) is now considered to be 1423km (Sky and Telescope 1987). But Ceres is estimated to be only 913km diameter (Tedesco 1989), so there is no overlap between the sizes of the major and minor planets.

2. They are in orbit round the Sun. However there are similarities between many asteroids and some of the smaller planetary satellites. It is quite possible that a number of the latter are captured asteroids which may be in orbits of either a permanent or temporary nature (Carusi and Valsecchi 1979).

3. They are inert. The major characteristic of comets, the "hairy stars", is that in the inner Solar System they are surrounded by volatile elements that have boiled from the surface. The volatiles are water and organic ices which sublime when the cometary nucleus warms up on approaching the Sun.

The lower size limit for asteroids, to distinguish them from meteoroids, has not been defined. It is reasonable to consider any small object in solar orbit that can be remotely detected as an asteroid. Meteoroids are only detected during their passage through a planetary atmosphere (or when they impact a spacecraft). On this basis the minimum diameter of an asteroid could be set at 5 metres or less.

The asteroids are relatively small on the planetary scale and even the largest - Ceres - subtends an apparent angle of less than 1 arc second when seen from the Earth which means that the apparent disc cannot be directly resolved by a ground based telescope except where adaptive optics are used on a large telescope. It is only possible to directly measure the diameter of an asteroid and coarse surface features from a space platform such as the Hubble Space Telescope.

The largest asteroids appear to be almost spheroidal (since their rotational light curves are of very low amplitude <0.15 magnitudes); however many smaller asteroids show a high amplitude light curve at favourable aspects and thus may be elongated. Bell, Davis, Hartmann and Gaffey (1989) consider the possible evolution of shapes in terms of accretion and fragmentation and conclude that the previous assumption that spherical asteroids are accretion products and elongated ones are collision fragments is probably wrong.

From the Earth the most direct and accurate measure of the size and shape of an asteroid can be made on those rare occasions when an asteroid occults a star and the shadow passes across the Earth. A brighter star is preferred so that the change in brightness observed is relatively high. The shadow cast on the Earth is effectively the same size as the asteroid and by determining the start and finish times for an occultation it is possible to compute the length and direction of a chord across the asteroid. If many observers succeed in obtaining chords across the body it may be possible to construct the silhouette profile of the asteroid (see for example Maley 1984). Suitable opportunities in inhabited regions of the Earth are rare and usually seem to coincide with dense cloud cover! Despite these difficulties Millis and Elliot (1979) report the results of eight successful observing projects from 1958-1978, and since then several more occultations have been observed. More recently, astrometric data has become available on CD-ROM (such as the Guide Star Catalogue) and modern computer software is available so that many potential occultations can be predicted which will enable more successful observations to be secured..

1.5 Configuration

1.5.1 Variations in the Light Curve

The term configuration is used to describe the physical features of individual asteroids. These are usually derived from a study of variations in the received radiation, largely in the visible wavelengths. A study of time-dependent phenomena associated with the asteroids forms a large part of this work.

All asteroids exhibit a periodic variation in brightness presumably due to axial rotation, typically the amplitude is less than 0.2 magnitudes. This variation is mainly due to changes in the projected cross-sectional area as seen by an observer on the Earth (elongated shape), though the shadowing of large surface features, a variation of the surface albedo across the face of the asteroid or else mutual phenomena associated with two or more bodies in orbit around their common centre of gravity may also be present in the observed light curve (Chapman 1979). Contributions from all these causes may be present in the light curve of a given asteroid and it is extremely difficult to separate the effects due to each cause. Lupishko, Akimov and Belskaya (1983) propose a method based on a comparison of phase angle effects with those of the Moon for separating phase dependent phenomena and suggest that the effects caused by albedo variations could be greater than previously thought.

More than half of the known asteroids appear to have rotational light curves with amplitudes of less than 0.2 magnitudes at all heliocentric longitudes they are reasonably regular in shape. There are a few examples which seem to be almost spherical with amplitudes of less than 0.05 magnitudes (representing a 5% change in the projected plan area seen from earth) at all longitudes. There are some examples which are highly elongated and have amplitudes in excess of 1 magnitude. The

extreme example of this is 1620 Geographos which has a maximum amplitude at a favourable aspect of 2.03 magnitudes (Batrukov et al. 1993).

It may prove possible to invert a light curve to determine shape and topography of an asteroid (see Gehrels 1984) however to date no such complete result has been published.

1.5.2 Rotation Rates

The observed spin frequency of most asteroids lie in the range 0.5 revs/days and 6 revs/days though a few isolated examples have lower spin frequencies with the extreme at present known being 288 Glauke (Batrakov et al 1993) with a period of 1150 hours though this may represent an axial precession such as that discovered for 1220 Crocus (Binzel 1985). The fastest known rotator is 1566 Icarus (Batrakov et al 1993) which has an axial rotation period of about 2.273 hours.

The maximum rate that an asteroid can rotate is constrained by the strength of its gravitational field and the tensile strength of its weakest material. This aspect is considered later in this work. Fast rotating asteroids (such as 1566 Icarus) are probably composed of high strength materials. If the axial rotation rate is too high disruption will occur (Weidenschilling 1981). In the absence of direct information concerning the shape, asteroids are modelled as tri-axial ellipsoids (Farinella et al. 1981). From experiments using models, the theoretical shape of slowly rotating asteroids can be approximated to Maclaurin Spheroids and elongated bodies approximate to Jacobi Ellipsoids (Farinella, Paolicchi and Zappala 1981). Real asteroids (243 Ida and 951 Gaspra) show significant deviations from these idealised shapes and can be more accurately modelled once imaging data has been obtained, however in its absence the tri-axial ellipsoid appears to be a valid first approximation.

There have been several analyses of the population spin-frequency from which it is found that the mean spin-frequency is approximately 3 revolutions/day. The results must be treated with caution as there are selection effects since the information is only available from the biased population that we can observe from the Earth (Tedesco and Zappala 1980). This has been interpreted as the original spin frequency of bodies at the heliocentric distance of the asteroid belt. Harris (1979) proposes a method for modelling the evolution of rotation rates from the original value resulting from collisions in the asteroid belt. Binzel (1986) employs a slightly amended version in his dissertation and further modifications are considered later in this work. Figures 1.5 and 1.6 show the distribution of spin frequency and amplitude with diameter respectively and Figure 1.7 illustrates the observed amplitude plotted with respect to spin frequency.

Collisions may serve to increase or to decrease the rotation rate of an asteroid as the impacting body will rarely hit directly at the centre of mass. The main factors influencing the result of a collision

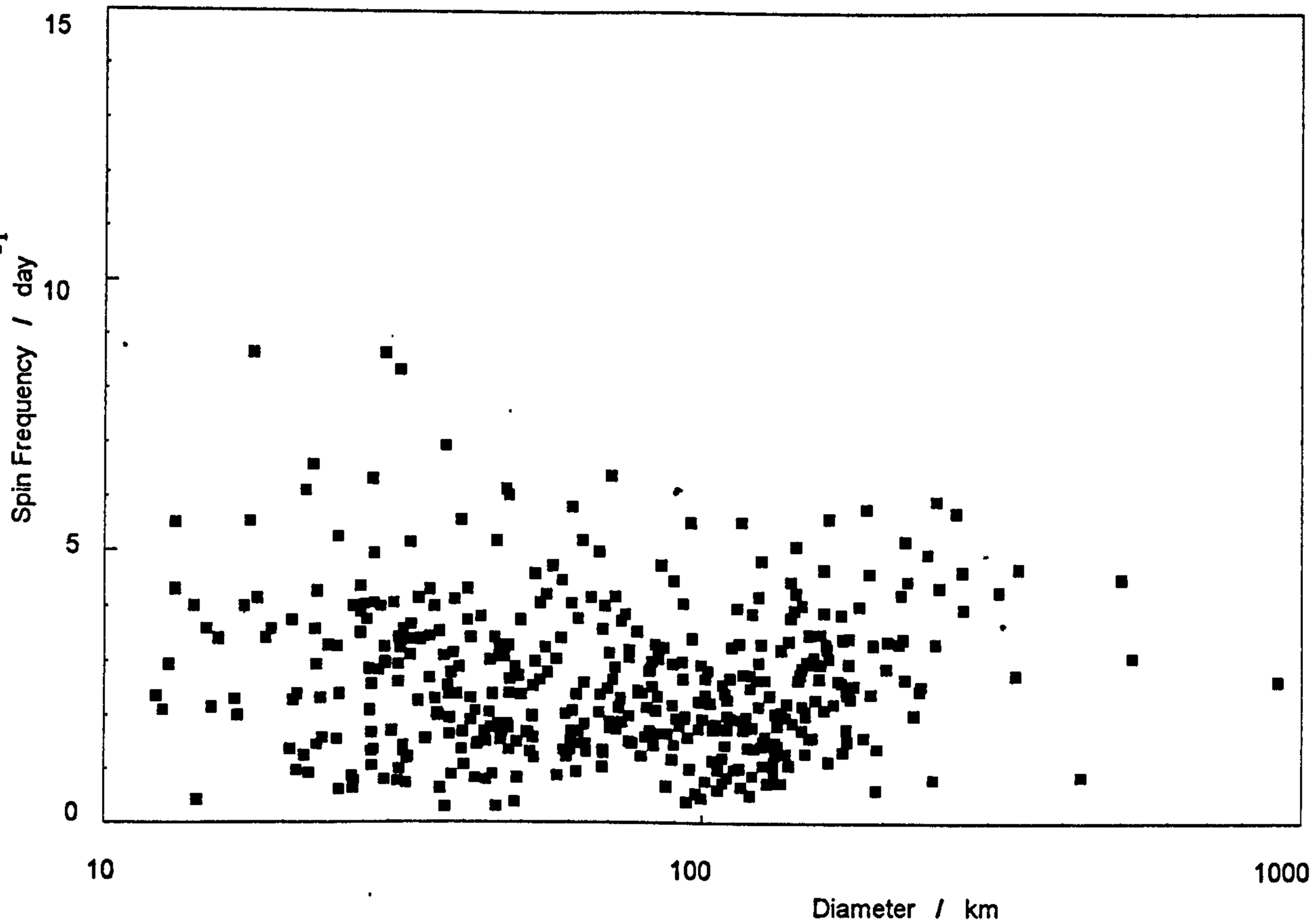

Figure 1.5 - A plot of spin frequency against diameter for the sample of asteroids given in the 1994 Ephemerides of the Minor Planets

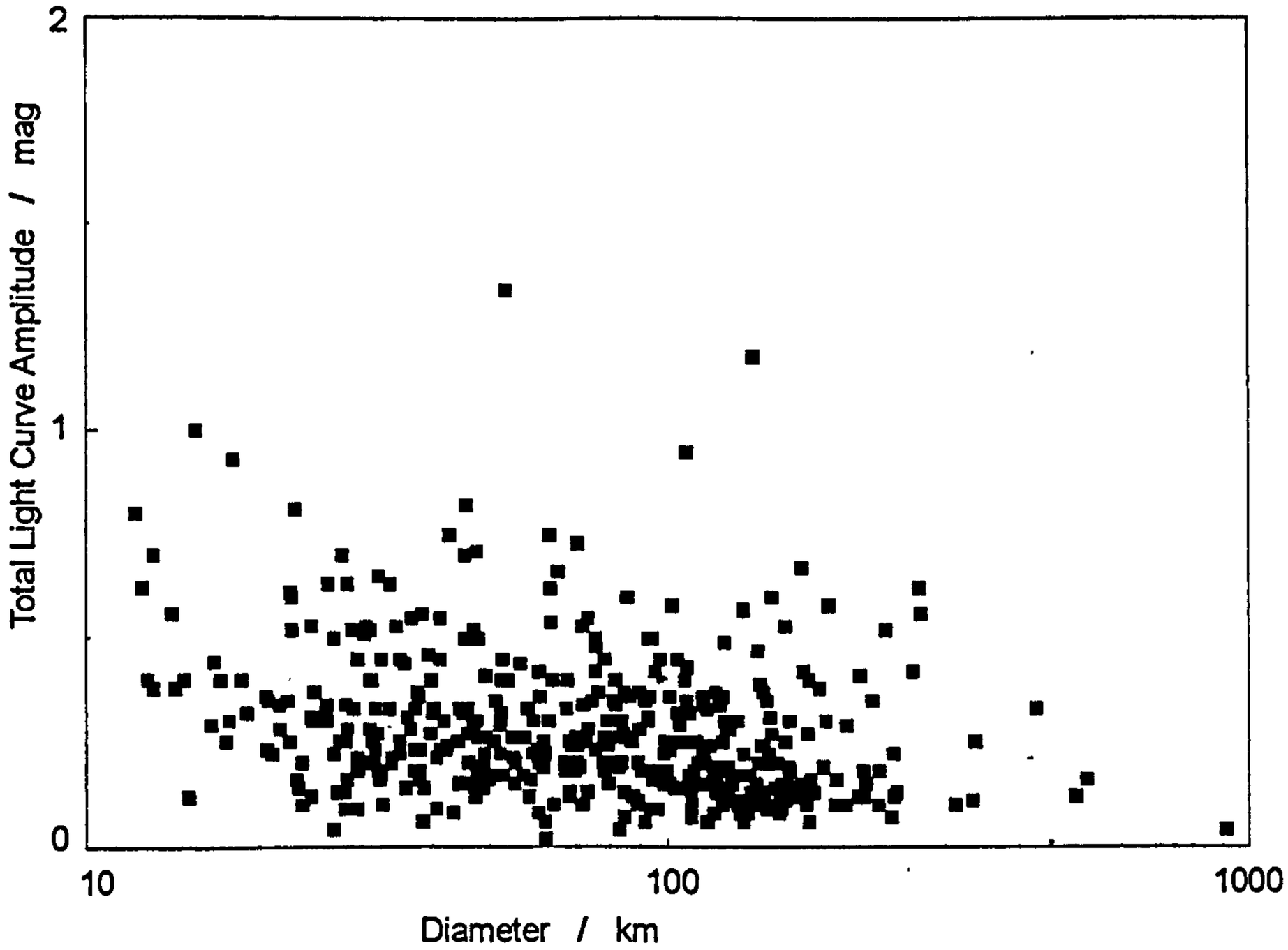

Figure 1.6 - A plot of total light curve amplitude against diameter for the sample of asteroids given in the 1994 Ephemerides of the Minor Planets

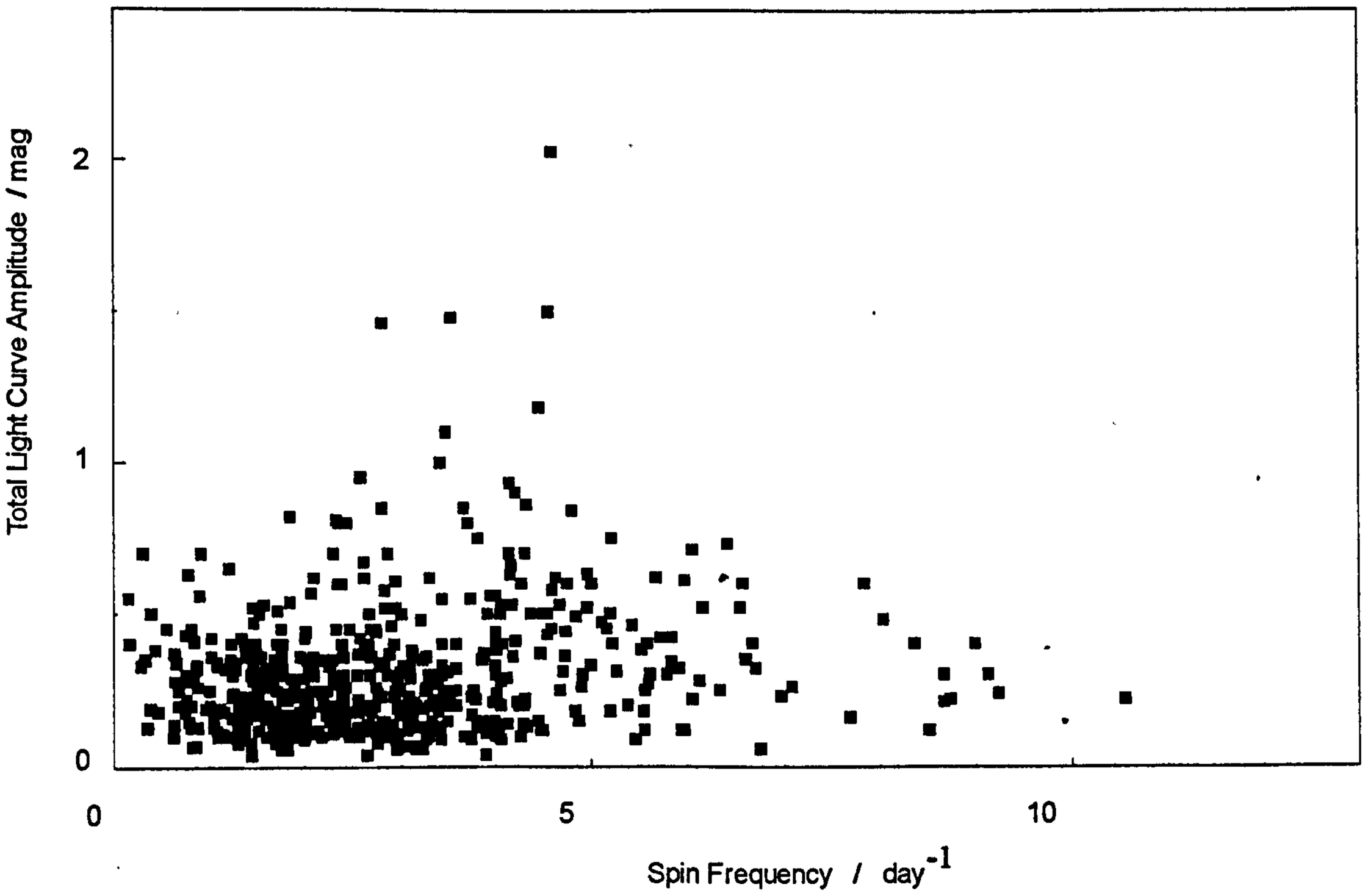

Figure 1.7 - A plot of spin frequency against total light curve amplitude for the sample of asteroids given in the 1994 Ephemerides of the Minor Planets

being the mass and velocity of the projectile and the impact parameter in both latitude and longitude. From the sample of rotation rates available at the time (1983), Dermott, Harris and Murray (1984) deduced that the large and small members of the belt rotated faster than asteroids of 50km to 150km diameter. It has been suggested that medium sized asteroids may be despun by the mechanism of angular momentum drain (Dobrovolskis and Burns 1984). In this case debris from an impact may be preferentially lost in the direction of rotation carrying angular momentum with it. Debris thrown in the opposite direction to the rotation may remain gravitationally bound to the asteroid. This component of angular momentum will be retained and tend to slow down the rotation. A smaller body will lose debris in both directions because of its small gravitational field whilst large asteroids will retain all the debris as their gravitational field is sufficient to prevent the escape of debris. Another idea, proposed by Halling (1984), interprets the spin frequency-diameter relationship as indicative of a modification of the internal structure of the asteroid during a process of accretion then differentiation followed by further accretion.

1.5.3 Polar Axis Orientation

The polar axes of the asteroids do not all point towards a similar direction in space (Harris and Burns 1979). If they did it would imply a common origin with little subsequent evolution. However if collisions have been an important evolutionary consideration, modification of the orientation of the polar axes would be expected. This is considered further later in this work.

If the spin-axis orientation is not perpendicular to the Earth's orbital plane then the light curve observed will not be the same at successive oppositions. A maximum amplitude will be found when the axis is perpendicular to the line of sight, a geometric case that, in the rest frame of the Earth, always occurs at a single pair of heliocentric longitudes 180° apart. No variation will be found if the polar axis lies along, or close to, the line of sight. In practice this latter case only occur for a few examples.

Two methods exist to estimate the orientation of the spin-axis. The photometric astrometry method (Taylor 1979) requires several complete light curves from a single opposition (Taylor recommends at least 6) so that a good estimate of the synodic rotation period can be made and in addition a similar number of light curves taken at various other oppositions and heliocentric longitudes. This method does not give any indication of the shape. The amplitude-aspect method (Zappala 1979) allows an estimation of the shape and also the polar orientation. The ratio of the axes a:b of the ellipsoid can be determined from the ratio of the maximum to minimum brightness when the aspect angle is 90°. The ratio of the long axis to the short axis is harder to determine and the amplitude aspect method allows many values for this, the smallest of which is usually assumed to be the correct value. The values derived from Galileo imagery at 951 Gaspra showed it to be 19km:7.5km:7km, corresponding to a:b

of 2.53 this compares with a value of 2.51 derived from the lightcurve (maximum amplitude 1.0 magnitudes). Insufficient data has been returned from the Galileo mission at the time of writing (March 1995) to comment on a similar comparison for 243 Ida.

In most cases the measured spin-axis orientation is fixed and precession is not seen. However, if collisions occur in the asteroid belt, it would be expected that an irregular light curve will result. This "irregular" light curve is produced by the combination of the axial rotation component and a precession induced by the impact (this is considered later). Internal energy dissipation will result eventually in the damping of the nutation angle. The body will resume simple rotation with no precession component. This has been considered by McAdoo and Burns (1974). Where a body is nearly spherical the precession will be damped out in a period of

$$T \sim 50\,\mu\,\tau / (\pi\, G\, \rho^2 .R^2) \qquad ....(1.1)$$

where

T is the time for the precession to damp out

R is the asteroid radius in kilometres

μ is the rigidity of the material

ρ is the material density

τ is the relaxation time of the material

The damping time for a given size and shape of body is dependant on its composition and internal structure. For a solid body composed of a homogenous rocky material of $\rho = 4$ gm/cc and $\mu = 10^{12}$ dynes/cm^2 and $\tau \sim 10^9$ secs equation 1.1 reduces to

$$T \sim 5\ 10^{10}\ R^{-2} \quad \text{years} \qquad ...(1.2)$$

(McAdoo and Burns 1974)

The value of μ is small for fluid or fractured bodies and τ is small for rigid bodies. Damping times can be several orders of magnitude lower in these cases than indicated from equation 1.2.

For an elongated rocky body they derive the following equation

$$T \sim 3 \,.\, 10^5 \,.\, P^3 \,.\, r^2 \,.\, (L/r)^2 \qquad ...(1.3)$$

(McAdoo and Burns 1974)

where

P is the axial rotation period in hours

r is the radius of the equivalent cylinder (with the same luminosity) in km

L is the half length of the equivalent cylinder in km

For P=10 hours and L/r=3 that this reduces to

$$T \sim 6 . 10^{9} . R^{-2}$$

where R is the radius of the circular body giving the same projected area viewed from the Earth. McAdoo and Burns are uncertain whether the difference in alignment time between results of similar shaped bodies using each of the two equations (Equation 1.2 and 1.3) is a real effect of the shape or due to the "roughness of the models".

Harris (1994) has reworked the model and identifies several asteroids with long rotation periods which may be undergoing complex rotation (combined axial and precession).

1.5.4 Minor Satellites

Imagery from Galileo has shown that 243 Ida has a satellite, now named Dactyl. This had been suggested as a means of explaining the observed light curves as early as 1906 (Russell 1906). Reports of satellite bodies to minor planets, christened minor satellites (van Flandern, Tedesco and Binzel 1979) were reported for several asteroids as secondary events had been detected preceding or following asteroid occultations. However definite proof was not available until the images of 243 Ida were downloaded in early 1994.

The major gravitational influence within the Solar System is the Sun. To a first approximation the motion of the planets and asteroids can be considered in terms of a three body problem since the gravitational influence of Jupiter is dominant among the planets. Whipple and White (1985) consider the stability of binary asteroids as the third body. They conclude that "the existence of binary asteroids is possible even for relatively small components (they consider diameters of 80km) and relatively large separation distances (12000km) between components". All the possible candidates for binary/satellite bodies have separation distances <1000km (Table 1 Hartmann 1979). The satellite of 243 Ida was found to be within this distance.

1.6 Evolution of the Asteroids

1.6.1 General Overview

When Ceres was discovered in 1801, it was at first assumed to be a major planet though it was much smaller than would be expected. The discovery of Pallas by Olbers in 1802 caused a further problem since if Ceres and Pallas were both major planets, the fact that they had similar orbits would not, in the view of that time, be allowable under Bode's Law. Olbers produced a solution by suggesting that the two bodies might be fragments from the disintegration of a single major planet and that other fragments might be found (see for example Nieto 1972). This idea seemed to be supported by the

discovery of Juno and Vesta in 1804 and 1807 respectively. Whilst many more asteroids have now been found it is still not possible to say whether they are fragments of one, or more, larger body. The question of the origin of the asteroids is part of the larger unsolved problem of the origin of the Solar System as a whole. Two main types of theory exist, encounter and nebula, and they are outlined below.

1. The encounter theory was proposed by Buffon in 1745 (see Cameron 1975) and seeks to explain the formation of the Solar System in terms of an encounter between the Sun and a passing star. This passing star caused the ejection some of the outer layers of the sun into a circumsolar disk which condensed to form the planets

2. The nebula theory was proposed by Descartes in 1644. The galaxy contains concentrations of gas and dust such as the Orion Nebula. In such regions the density of matter will be irregular and local condensations will occur. The net gravitational force will attract matter from the surrounding lower density areas. Eventually the cloud, or at least its central regions, will collapse to form a protostar or protostars which could give rise to stellar/planetary systems. The dust clouds surrounding many stars observed by IRAS and subsequently from the earth appear to support this theory.

1.6.2 The Formation of Planetesimals

The large cloud contracts under its own gravity. During this process, since the density is non-uniform, the cloud will fragment into many protostar regions (Meadows 1978). The protostar nebula that produced the Sun and planets was at least 3 Solar Masses (Cameron 1975). During the contraction of the Solar Nebula the gas and dust would become turbulent and the resulting shear forces would produce rotating eddies as in Weizsacker's theory (see Wood 1979). Contraction will increase the rotation rate since angular momentum will be conserved.

In the Solar System 99% of the mass is concentrated in the Sun whilst 98% of the angular momentum is carried by the planets (Singh 1970). This would suggest that there must have been a mechanism for transferring angular momentum to the regions remote from the Sun whilst condensation was occurring (Cameron 1975). In computations by Goldreich and Ward the first generation planetesimals of radius ~0.1km form by gravitational collapse and gas/dust drag on a timescale of the order of 1 year. These are gravitationally unstable and group in clusters of about 10000 members. In a timescale of a few thousand years the clusters contract to form second generation planetesimals with radii of about 5km. Further coalescence will proceed at a growth rate of about 15cm/year at 1AU (Goldreich and Ward 1973).

1.6.3 Planet Growth

The swarms of planetesimals, ~5km in diameter can only grow into planet size bodies by direct interaction. In practice this means that gravitational perturbations must modify the orbits of the clusters of planetesimals causing them to collide and coalesce (Cameron 1977). Hartmann (1978) has carried out investigations of the effect of collisions. A body released from rest and acting solely under gravitational forces, will impact a target at a velocity equal to the velocity of escape for the target. In practice there will be an initial relative velocity superimposed on this. In theory, for a rigid body a rebound velocity exceeding the velocity of escape from the target will mean they do not coalesce. Real bodies are elastic. Hartmann's experiments in the laboratory demonstrated that coalescence can occur at velocities up to twice the escape velocity.

Several computer simulations of the accretion of planetesimals have been carried out. Greenberg et al. (1978) report the results of simulations which illustrated that 1km planetesimals could grow to form 500km diameter bodies in only 10000 years. They interpret these as the seeds for future planet growth. Issacman and Sagan (1977), using the simplified method of Dole have calculated several alternative planetary systems including a Solar System analogue. Wetherill (1981) provides solutions, calculated by Cox, to the growth of the Terrestrial Planets. The effects of such impacts on rotation rates is considered in Chapter 5.

1.6.4 Formation of the Asteroids

Many asteroids are considered to be planetesimals which failed to form a planet. Some however are thought to be fragments of partially accreted bodies (Chapman 1981). The current total mass of the asteroid belt if it were incorporated in a single body is about an eighth that of the Moon (Bell et al 1989). This is significantly less than would be expected from the mass density of the rest of the Solar System suggesting that mass must have been ejected from the region (Hughes 1982) .

The asteroids may be the residue of the fragmentation of a large planet. Napier and Dodd (1973) consider the disruption of a 90 earth mass planet. They conclude that a chemical explosion, a close passage to Jupiter or what they describe as ".. a nuclear effect" could not account for the observed structure of the asteroid belt. It appears likely that the accretion of planetesimals in this region was incomplete, either because the gravitational influence of Jupiter disturbed the process or else because the density of planetesimals was insufficient to allow complete accretion.

Hughes (1994) has reviewed the likely evolution of the asteroid belt. From considerations of the mass density distribution he proposes that the currently observed belt is largely the product of fragmentation. This conclusion also provides an explanation for the apparent mass depletion in this

region. During the accretion phase the planetesimals had low eccentricity orbits and thus encounter velocities were low (Hoyle 1978). Any collision would tend to be non-disruptive and coalescence would occur. This allowed the growth of several large planets in the zone (estimated at 8 Mars sized bodies by Hughes) and the mass distribution index would be of the order of 1.65 (Hughes 1991). This would lead to about 640 asteroids larger than 1 Ceres, the largest current asteroid. Once the proto-Jupiter grew to a size when it could exert a perturbing influence on the asteroid belt the modification to asteroid orbits would increase encounter velocities. Fragmentation would become a significant influence and mass loss from the belt would occur due to perturbation. The currently observed mass distribution index is 2.0 indicative that fragmentation has been in progress for a long period of time (Hughes 1994).

In 1983 data from the Infra-Red Astronomical Satellite (IRAS) has revealed the presence of dust bands within the main asteroid belt (Sykes et al 1989). It is most likely that these bands are formed from the dust debris of collisions within the belt. Their existence suggests that collisions are a continuing process since the debris would be transported to the Inner Solar System by Pointing-Robertson drag. The continued existence of the bands implies a source of replenishment though their precise structure is likely to be variable.

The mechanisms responsible for the formation of the Solar System as a whole, and especially for the minor bodies within the system are still poorly constrained by the available evidence.

Further knowledge of conditions during the accretion process may be gained after samples of asteroid material have been obtained. In the meantime, the only approach is to try various models of the formation of the asteroids and to check them against parameters that can be measured from the Earth such as orbital elements, photometric rotation periods, spin-axis orientations, and spectrophotometric properties. Compositional differences can be noted by classifying asteroids of like surface properties and investigating differences in rotational properties which point to differences in the rotational history.

2. Scope of The Present Work

2.1 Classification

The classification of the asteroids is examined in Chapter 3 using numerical methods. The parameters used are derived from measurements of the surface characteristics and are thus related to the properties of the surface minerals. Initially the numerical taxonomy method is evaluated and a more appropriate way of applying it determined. Then the standard seven parameter classification scheme is considered and the effect of introducing small random errors into the input data is assessed to identify whether the classifications are valid and significant.

The effect of reducing the number of parameters on the classifications is investigated. Using these results, simplification of the classification schemes is discussed. A sample of 588 asteroids is classified using the published results of eight band photometry. The likelihood of differentiation and core formation in asteroids is considered to check whether classification of asteroids by surface characteristics could identify bodies with similar internal structure. The dependence on the structure on the fragmentation and spin rates is also discussed.

2.2 Projectile/Target Interaction

The overall evolutionary history is taken as build up from planetesimals and subsequent collisions between bodies. The evolution of the axial spin of asteroids is reviewed in Chapter 4. It is described in terms of classical mechanics. The processes of evolution of spin-rates, spin-axis orientation and modes of rotation are derived by considering the effects of collisions between planetesimals.

2.3 Evolution and Modes of Rotation

In Chapter 5 a collision model for the evolution of spin rates and spin axis orientations is formulated. This model describes the observed distribution of spin frequency and axial inclination with no mechanism (e.g. ejecta) required to carry away surplus angular momentum. It is shown that if the observed spin frequency distribution is modelled then a random orientation of spin axes is to be expected. Though observed orientation is not well known the indications are that they are randomly distributed. The rate of the occurrence of collisions is also discussed.

2.4 Observability of free precession

Using the collision model derived above and extending the work on equilibrium bodies carried out by Chandrasekar, graphs are presented which show that free precession could only be observed in a limited number of cases by light curve analysis as in the majority of cases the amplitude of the precession component is so small it would be lost in the noise.

2.5 Experimental Observation

In Chapter 7 a new design of photometer is described and its performance assessed. Sources of error are identified and quantified and recommendations for minimising their effects discussed.

2.6 Case Studies

In the first part of Chapter 8 a simple method of synthesising asteroid light curves, including precession and variegation, is derived. This is applied to the observed multi-mode rotation for Comet P/Halley and 1220 Crocus using results of observations by others. In the second part of this Chapter, observations of asteroids made using the equipment designed for this project are presented. These are analysed and compared with synthetic light curves (based on shape, variegation and precession parameters) to determine the possible configuration of the body and to derive synodic periods of rotation.

2.7 Future Work

The final Chapter identifies possible future extensions of this work.

3. Taxonomy of Asteroids

Abstract

The currently used schemes of classifying asteroids are considered and particular attention is given to the use of numerical taxonomy. After review it is applied to the seven parameter classification scheme and the effect of introducing errors into the data set considered illustrating that the major types remain distinct. The effect of reducing the number of parameters is assessed showing that simplification would still produce a valid classification. It is noted that the classical S-type splits significantly into two types which appear dependent on heliocentric distance.

A new scheme is prepared using the eight-colour survey which allows much finer classification to be derived. This confirms the conclusions about the subdivision of the S-type class.

The relevance of superficial features to internal structure and hence to spin rates is discussed.

Finally the relevance of classifying bodies solely on the basis of observed data from surface reflection is considered and some pitfalls are highlighted.

3.1 Review of classification schemes

3.1.1 Why Classify Asteroids ?

There are about 6000 numbered asteroids. These are asteroids with good orbits derived from observations over at least two oppositions. There are too many to allow detailed investigations to be made of every one. However if we can find similarities between individuals then by observing one we should be able to describe, at least in part, the remainder of the Group.

The brighter asteroids (those whose maximum opposition magnitude can reach 10th magnitude) have been well studied but most of the fainter examples (which are always fainter than about 16th magnitude) have not. The purpose of a classification scheme is to predict the surface properties of the fainter asteroids and to identify unusual objects for more intensive study. As the observed properties are those of the surface minerals the classification scheme characterises (at least in part) the composition of the asteroids and this gives clues regarding their evolutionary history. However there are limitations to the usability of any scheme. The main one is that with the increase in observation data there tends to be a proliferation in the number of subdivisions and the increasing complexity makes interpretation difficult. In practical terms every individual body will contain certain unique information which would justify separating it into its own class. This would defeat the objective of all classification schemes which is to group similar bodies whilst accepting that there will be differences between individual ones.

3.1.2 Early Classification Schemes

First attempts at classification involved plotting points on a colour-colour graph (U-B vs. B-V). Distinct clusters of points were found suggesting compositional differences (Bowell, and Lumme 1979) - see Figure 3.1. Two main types, called C and S, can be distinguished to allow quick classification of newly discovered objects (Zellner 1979 (i)). These names are derived from the similarity in observed characteristics between C-type asteroids and Carbonaceous Chondrite meteorite samples and between the S-type asteroids and the Stony-iron meteorites. The similarity in general characteristics between meteorites and asteroids is a strong indication that the former are fragments of asteroids produced probably by collisions within the main asteroid belt and subsequently perturbed by the gravitational field of Jupiter into orbits which intersect that of the Earth. There is a general review given by Greenberg and Nolan (1989).

Bowell and Lumme outline the advantages of including UBV colour indices in any classification scheme. They can be measured using only simple equipment which is available at virtually all observatories. Even faint objects may have their colour indices measured and hence be classified. Over half the asteroids have been classified solely using the colour indices. Unfortunately this data gives little insight into the nature of asteroid surfaces.

Introducing other factors allowed Bowell, Chapman, Morrison and Zellner (1978) to propose a new scheme. By considering seven basic parameters derived from three types of observation they recognised five classes of asteroid. Their scheme allows not only simple observational results (such as colour indices) but also considers others less easily obtained including spectral shape parameters, the strength of a spectral feature (the absorption line due to Fe^{++} near 950nm (Gaffey and McCord 1979)) and the geometric albedo - p_v (Chapman, Morrison, and Zellner, 1975). Bodies not falling into a standard class are designated U for Unclassifiable. The seven parameters are

a. Photometric Colour Indices

   1. The photometric colour index U-V

   2. The photometric colour index B-V

b. Narrow Band Spectrophotometry

   3. R/B - spectral reflectance at 700nm/ spectral reflectance at 400nm. This is the general slope of the spectrum from the B to R bands

   4. BEND a measure of the curvature of the reflection spectrum in the visible region. (Reflectance at 560nm - Reflectance at 400nm) -(Reflectance at 730nm - Reflectance at 560nm). The B and R points have been adjusted to be equidistant from the peak of the V band

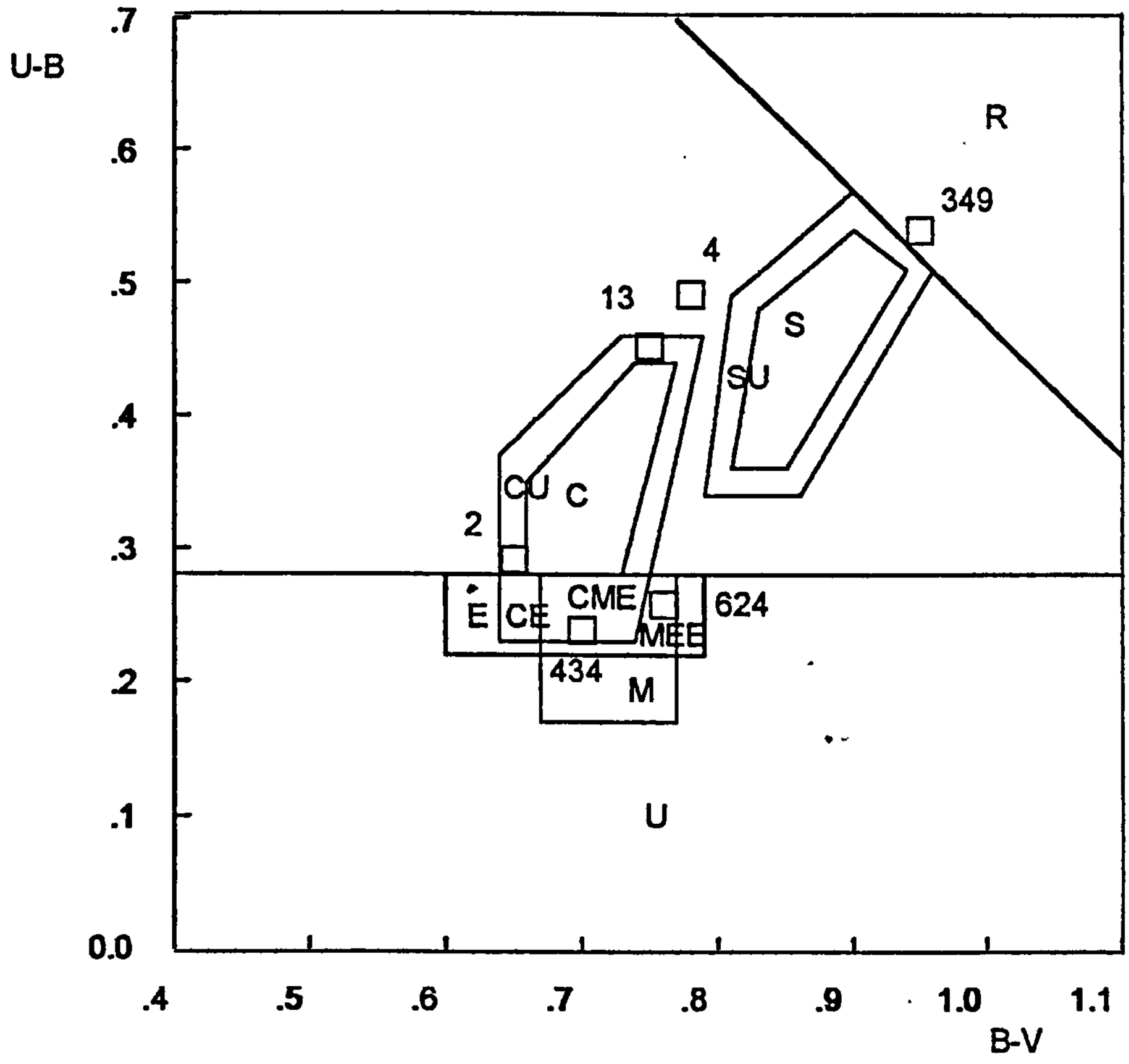

Figure 3.1 - U-B vs B-V plot showing the areas occupied by the different classes in the traditional classification scheme

5. DEPTH - the ratio of the reflectance at the bottom of the Fe^{++} absorption feature near 950nm with the highest reflectance on the short wavelength side of the band (a value of 1 would indicate no absorption feature is present). A strong absorption feature suggests the presence of silicates (pyroxene, olivine or feldspar)(Gaffey and McCord 1979).

c. Polarimetry and Radiometry

6. The geometric albedo in the photometric V band (p_V) which can be obtained from thermal radiometric or polarimetric data (Chapman, Morrison and Zellner 1975).

7. The minimum value of the polarisation curve (P_{min}). This is the value of the negative branch which occurs at approximately 10° phase angle. However this parameter is related to the albedo so it is not truly independent.

Additional parameters might allow further subdivision of the classes. The classes recognised in the general scheme are C, S, M, E, and R together with U. Multiple letter classifications exist, CMUE indicates 'not S or R' [indeed C really means 'not S, M, E or R'] but later reassignment to another as yet undefined class is possible (Zellner 1979 (i)).There are simple basic criteria for placement in a specific class and these are given in Table 3.1 and are shown graphically by Figure 3.1

Table 3. 1 Definition of Classes

(after Zellner 1979 (i))

	C	S	M	E	R
Albedo	<=0.065	0.065-0.23	0.065-0.23	>=0.23	>=0.16
P_{min}	1.20-2.15	0.58-0.96	0.86-1.35	<=0.40	<=0.70
R/B	1.00-1.40	1.34-2.07	1.06-1.34	0.9-1.35	>=0.70
BEND	0.00-0.20	0.00-0.20	<0.0-1.0	<=0.10	>=0.20
DEPTH	0.95-1.00	0.80-1.00	0.90-1.00	0.9-1.0	<=0.90
B-V	>=0.64a	b	0.67-0.77	0.6-0.79	c
U-B d	0.23-0.46a	>=0.34b	0.17-0.28	0.22-0.28	c

Type U means that an asteroid is Unclassifiable on the basis of the observational data.

The UBV parameters are the only classification parameters available for approximately half the asteroids that have been studied. To help classify these there are some additional notes which help define the regimes of each class when only UBV photometry is available.

Notes

a. The C-type asteroids occupy a box in the U-B/B-V diagram. The other edges of this region are given by

$$4.60(B-V) - 3.17 <= (U-B) <= (B-V) - 0.27$$

Type U is allowed 0.02 magnitudes inside the limits of the box if only UBV photometry is available which gives a small zone of type CU.

b. The S-type asteroids also occupy a box in this diagram. For this

$$B-V >= |(U-B)/7.0| + 0.74$$

$$1.70(B-V)-1.12 <= (U-B) <= (B-V) - 0.33$$

$$(U-V) <= 1.47$$

Type U is allowed 0.02 mag inside all the limits, except the last, when only UBV photometry is available giving a small zone of SU.

c. For class R the U-B and B-V indices are not considered individually but the overall index

$$U-V >= 1.47.$$

d. Type U is always allowed for U-B <= 0.28 when only UBV photometry is available. This is because it is not possible to decide whether an asteroid is C, M or E on this basis alone - or indeed whether it is none of these classes.

The designations C, S, M and E are derived from meteoritics since the spectrophotometric results from observing a C-type asteroid are similar to those obtained from Carbonaceous Chondrites and in the same way S (Stony-Iron), M (Metallic Nickel-Iron), and E (Enstatite) have meteorite analogues. Further classes have been added as considered necessary. Degewij and van Houten (1979) introduced class RD, for Reddish and Dark, (now abbreviated to D) which included some members of the Trojan family which showed characteristic spectral features.

Using natural groupings in the data there has been a general revision of classifications in the C- like group. Pallas, a unique low albedo object in a high inclination orbit has been given its own class, B-type. Three sub-groups have also been introduced. G-type is for atypical C- types which show similarities to Ceres. Types P (Pseudo-M) and F (Flat spectra, low albedo) were introduced by Gradie and Tedesco (1982).

All this has to be considered in terms of global photometry because surface features cannot be resolved. Even if they were, it is not possible to determine exact surface composition from the spectrum except that the presence of some classes of minerals (such as feldspars) may be detected (Gaffey and McCord 1979).

3.1.3 More recent Schemes - Numerical Taxonomy

Any classification scheme has the aim of placing asteroids in groups possessing similar properties. This can be done by assigning ranges, as typified by Figure 3.1, or by considering individual bodies mathematically as done in numerical taxonomy. This method expresses the similarity between two

objects in terms of a single number, called the similarity coefficient (Sokal and Sneath 1963). The method is impartial, but the outcome depends on the number and accuracy of the input parameters used.

The similarity coefficient (described below) is calculated between each of the sample members under investigation using the numerical values of the characteristics. The results are used to form a similarity matrix. Low values for the coefficient demonstrate a close similarity between two asteroids. The pair of asteroids (or group) with the lowest value of similarity coefficient are found and joined at this value of taxonomic distance. These bodies are then considered as a single object and the revised similarity coefficient from this to all other sample members is recalculated as the mean value of the coefficients for the group members. The next lowest value is found and the procedure repeated until all sample members are incorporated. When plotted, the dendrogram shows the linkages between asteroids and groups of asteroids. The method is often used for classification in microbiology but it has not been widely used in the field of asteroid research even though it has the great advantage of suggesting groupings independently of any preconceived ideas about the nature of asteroid surfaces.

McCheyne (1985) has examined a sample of 60 asteroids, representing approximately 1% of the observed asteroids. The results must be viewed with caution since the selection of this set may be biased by the fact that only the biggest and brightest have been studied in sufficient detail to allow the determination of the seven parameters used in this classification. Nevertheless the clean dendrogram suggests that this method allows a more precise classification than the apparently loose approach described earlier in this chapter.

Barucci et al (1987) have published a classification scheme based on G-mode analysis. They have used the eight colour survey data set of Zellner et al(1985) and in addition have used the albedo values derived from IRAS data. The method works in a similar manner to numerical taxonomy in that a single value is evaluated from the parameters considered. However the method of class assignment is different from that used in Numerical Taxonomy. The classifications derived using this method are, as would be expected, similar to both the results derived from numerical taxonomy and from the standard classification.

A three-parameter scheme using U-V and v-x colours together with visual albedo has been proposed by Tedesco et al. (1989). This has the benefit of simplicity in that the albedo and U-V colours are either known or can be easily derived. However their list only covers 357 asteroids so it is, at present, limited.

3.2 Scaling input parameters in Numerical Taxonomy

McCheyne (1985) examined the classification of 60 asteroids listed in the TRIAD file in terms of the seven classification parameters listed above.

The TRIAD file (Tucson Revised Index of Asteroid Data) contains a record of physical observations and other data. It was established in 1976 to ensure that all the reliable information about asteroids were available from one central source (Zellner 1979(ii)). A listing of the data held in this file, complete to 1979 June 20, is given in seven tables in the book 'Asteroids' edited by Gehrels and Matthews (1979) and subsequently updated in the Asteroids II Database contained in the book 'Asteroids II' (Binzel, Gehrels and Matthews 1989).

The similarity coefficient used by McCheyne (1985) is given by

$$S_{ij} = \sum_{k} (|x_{ik} - x_{jk}|^2 / n_{ij})^{0.5} \quad \ldots (3.1)$$

where S_{ij} is the coefficient of similarity between the i th and j th asteroid

x_{ik} is the k th parameter of the i th asteroid

n_{ij} is the number of parameters considered

To assess the validity of the method three dendrograms were prepared as part of the present work, the data analysis was done using a 48k Sinclair Spectrum microcomputer. The input data is taken from the TRIAD File. The U-B and B-V colours are given by Bowell, Gehrels and Zellner (1979). The narrowband photometric parameters R/B, BEND and DEPTH are tabulated by Morrison and Zellner (1979). McCheyne notes that parameters with a large range in comparison to the others could have a dominant effect if they are not scaled. He considered that the input data for the 60 asteroid sample did not require scaling. However the ranges are not the same and this is illustrated by Table 3.2

Table 3.2 Asteroid Classification -Maxima and Minima of Parameters

	Maximum	Minimum	Range
U-B	0.57	0.19	0.38
B-V	0.95	0.64	0.31
R/B	2.01	1.00	1.01
BEND	0.28	-0.05	0.33
DEPTH	1.00	0.71	0.29
Albedo	0.480	0.025	0.455
P_{min}	2.10	0.31	1.79

These parameters are those used in the seven parameter system and are defined in section 3.1.2. The mean value of these ranges is approximately 0.45.

The range of P_{min} is four times that of the mean and the range of R/B is also significantly higher than the mean. In the formula used by McCheyne a greater weight is given to these values than those with a smaller range unless some form of scaling is used to equalise the contributions from each parameter.

Figures 3.2 to 3.4 have been prepared as follows.

1.Using the same similarity coefficient as McCheyne, which is given in equation 3.1

2.Using a scaled version of equation 3.1

$$S_{ij}=\sum_{k}((|x_{ik}-x_{jk}|/(x_{kmax}-x_{kmin}))^2/n_{ij})^{0.5} \ldots (3.2)$$

In this case each of the input parameters will make an equal contribution to the similarity coefficient.

3.Using a linear scaled coefficient

$$S_{ij}=\sum_{k}(|x_{ik}-x_{jk}|/(x_{kmax}-x_{kmin}))/n_{ij} \quad \ldots. (3.3)$$

Equation 3.2 can be considered a least squares method. The linear option is considered to see whether it produces any major differences from the least squares version.

The resulting dendrograms are given in Figures 3.2 to 3.4. The current classifications of the asteroids are given adjacent to the asteroid number, the classification is taken from the Jet Propulsion Laboratory Asteroid Rotation Index (Harris and Young 1984).

Comparing the Figures it appears that scaling the similarity coefficients produces a more satisfactory dendrogram since the major divisions occur at a greater taxonomic distance in Figures 3.3 and 3.4 than with Figure 3.2. The three individual groups in the current scheme namely C-type, S-type and E-type separate in all cases. The current subgroupings in the C-type region only become apparent in the cases where the data is scaled (Figures 3.3 and 3.4) when the M-type asteroids group together.

Figures 3.3 and 3.4 produce essentially the same classification groups though - because of the "least squares" nature of equation 3.3 - separations generally occur at a greater taxonomic distance. Five main 'groups' can be seen. These correspond to the current types C, E, S, R and V. However it can be seen that the members of classification E (which always separate to form a discrete group) are less similar than the difference between the M and D types. The current C-types fall into two groupings. There is a Ceres-like group and a M/P/F Group. There appears to be no justification, from the dendrogram, for separating classes B, F and P on the basis of the seven parameters considered. The S-type grouping shows a close linkage and there is a possibility that 80 and 354 may form a subset of the S-type which is more significant than some of the sub-groups in the other sets.

3.3 An examination into the effect of introducing errors into the parameters used in Numerical Taxonomy

Because of the danger of bias, the effect of errors in the data has been studied further. To assess the size of errors needed to cause significant changes to the dendrograms three additional cases have been considered. The data taken from the TRIAD file have been subjected to a random error up to the value stated below. The error is introduced by the addition of the product of a*b*c where

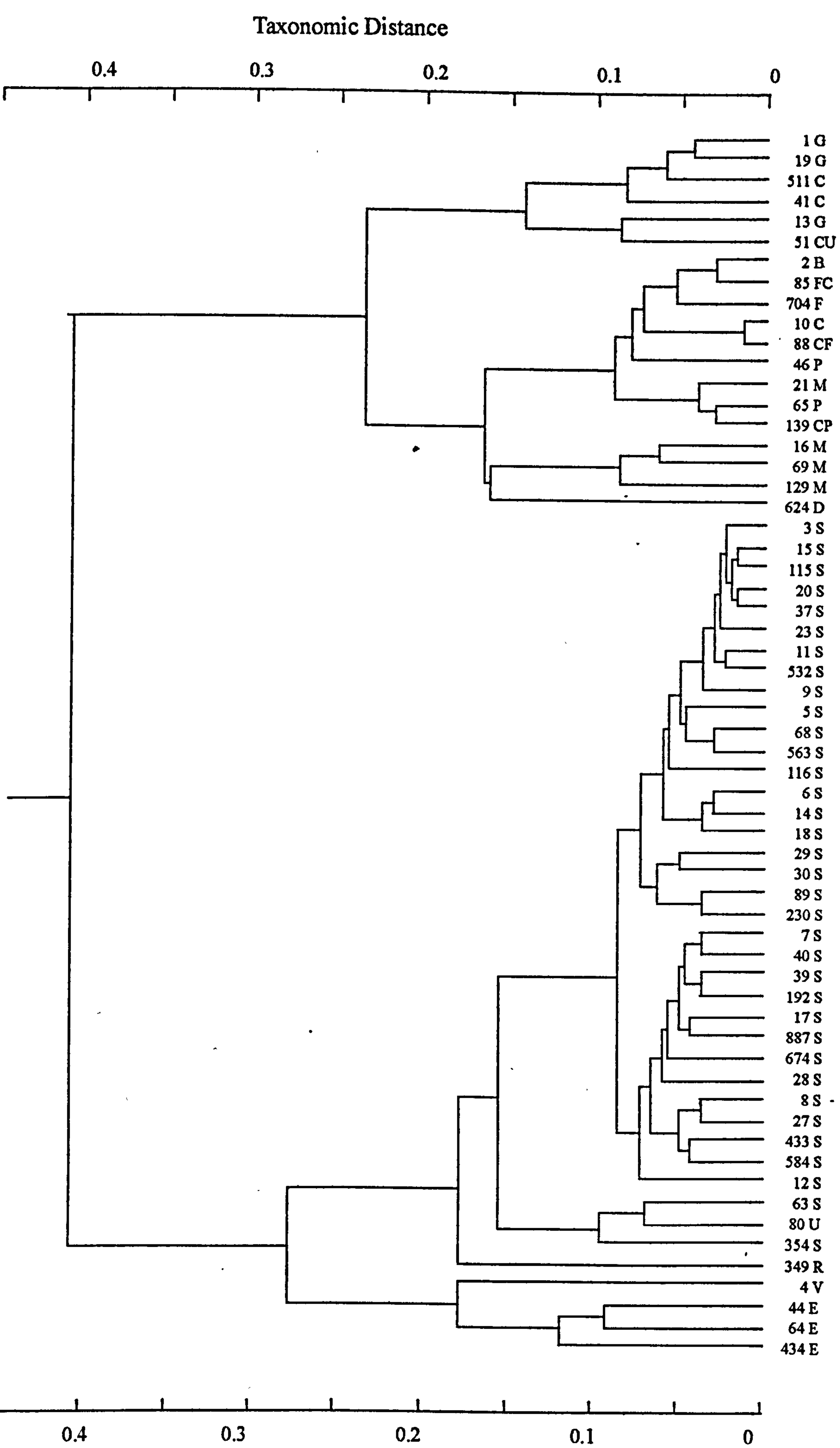

Figure 3.2 - Dendrogram for 60 asteroids using an unscaled, squared Similarity Coefficient
Taxonomic Distance 0 implies the bodies are indistinguishable
Taxonomic Distance 1 implies complete divergence

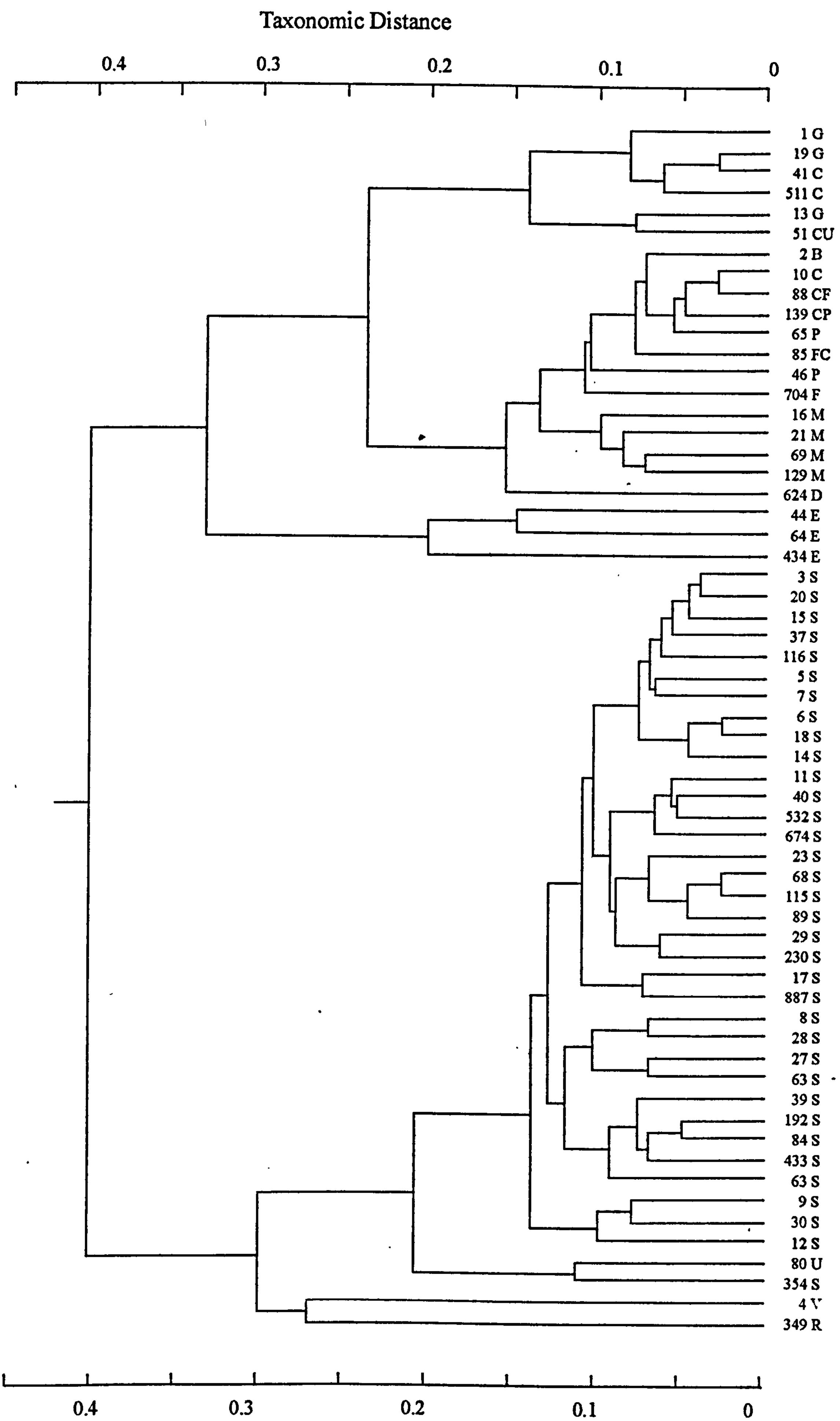

Figure 3.4 - Dendrogram for 60 asteroids using a scaled,linear Similarity Coefficient
Taxonomic Distance 0 implies the bodies are indistinguishable
Taxonomic Distance 1 implies complete divergence

a = a random number between -0.5 and +0.5.

b = the fractional error

c = the total range of the element under consideration (given in Table 3.2)

The resulting dendrograms have then been compared with Case 3 above to see the extent of changes produced by the introduction of the errors. The purpose of this is to determine an appropriate percentage error to be used for the investigation described in Section 3.5 and so single cases for each value of error have been calculated here.

(Cases 1, 2 and 3 are those considered previously)

4. Using equation 3.3 but with the input parameters subject to a random error of up to ± 1%.

5. Using equation 3.3 but with the input parameters subject to a random error of up to ± 5%.

Table 3.3 - Maximum Value of 5% Error on each Parameter
(ie 5% of the total range of each parameter)

U-B	0.02
B-V	0.015
R/B	0.05
BEND	0.017
DEPTH	0.015
Albedo	0.023
P_{min}	0.09

6. Using equation 3.3 but with the input parameters subject to a random error of up to ±10%.

When errors are introduced into the input data the effects are minimal at errors up to ±5%. When the input data has errors up to ±10% the structure of the C-type region breaks down completely. The major groups still remain separate. Increasing the error in the data tends to reduce the taxonomic distance of the linkages however the main groupings are of sufficient significance that the main structure of the dendrogram does not break down at the error levels considered. The maximum value of the error for each parameter in the 5% case is listed in Table 3.3. The main classification groups are therefore significant whilst the sub-classification in the C region must be viewed with caution unless additional parameters are used in the classification. Dendrograms of typical results are illustrated by Figures 3.5 to 3.7 for cases 4 to 6 respectively. The apparently disparate E group remain separate even with the maximum level of error introduced here.

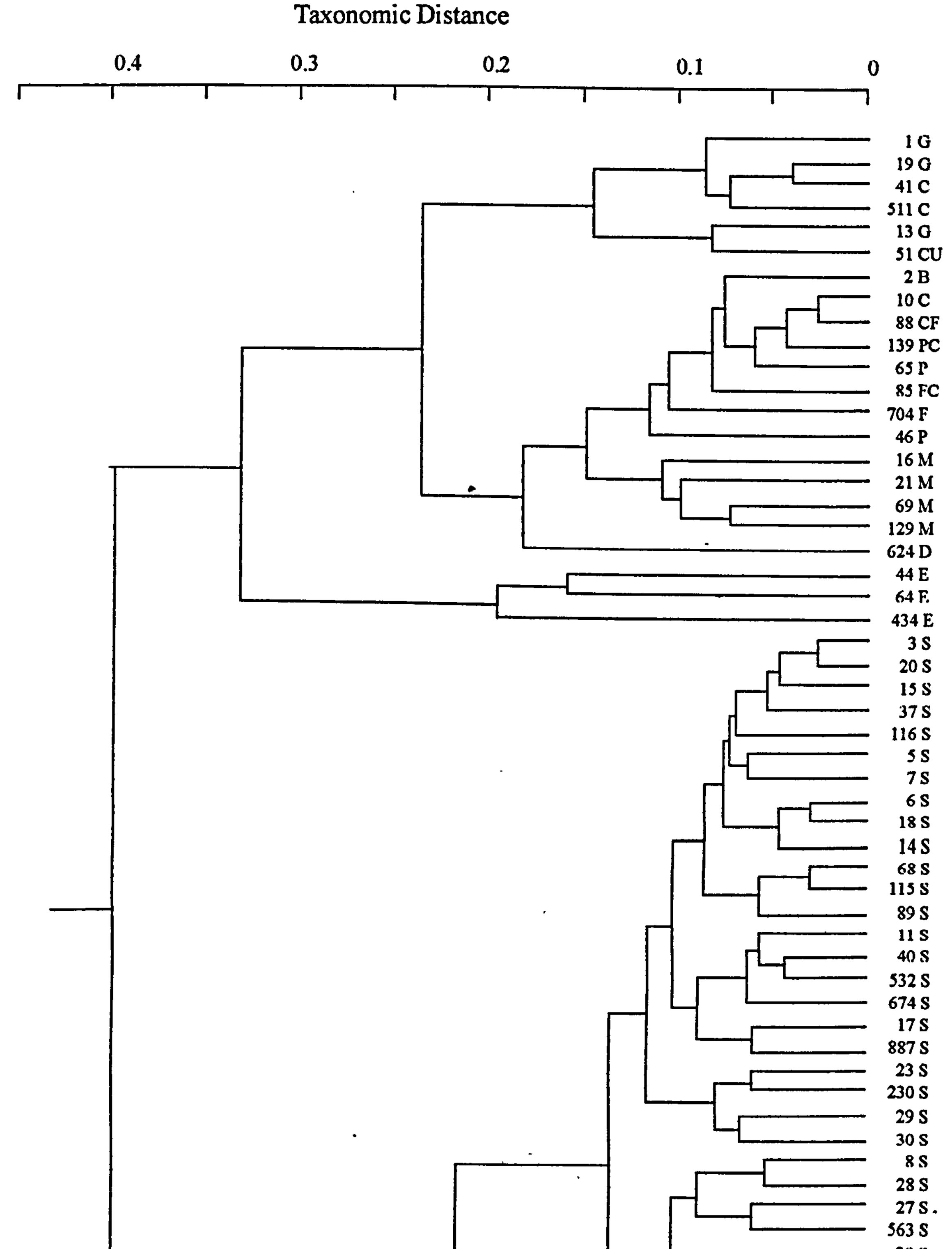

Figure 3.5 - Typical dendrogram for 60 asteroids using a scaled, linear Similarity Coefficient
Random error on the input data to a maximum of 1%
Taxonomic Distance 0 implies the bodies are indistinguishable
Taxonomic Distance 1 implies complete divergence

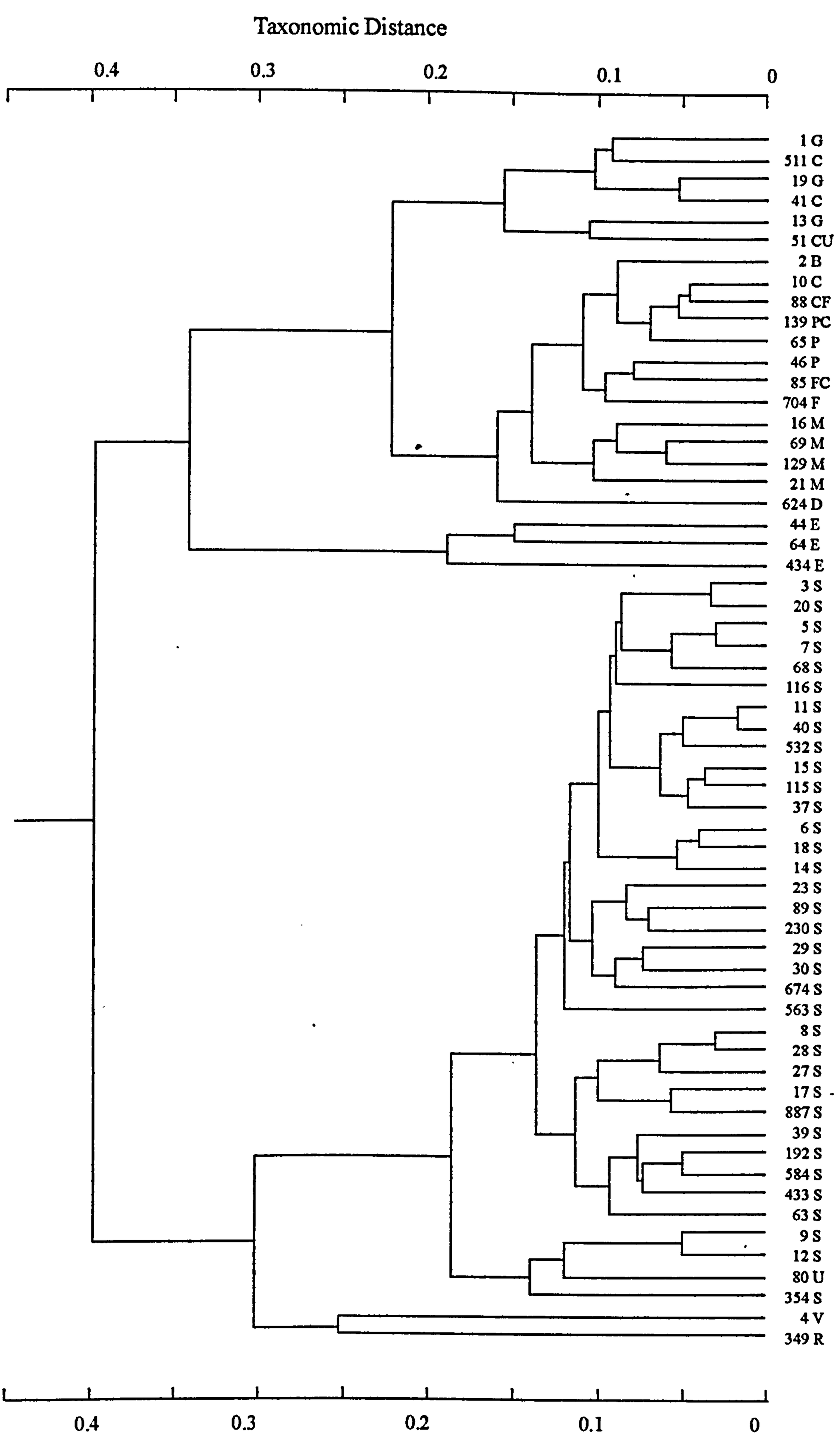

Figure 3.6 - Typical dendrogram for 60 asteroids using a scaled, linear Similarity Coefficient
Random error on the input data to a maximum of 5%
Taxonomic Distance 0 implies the bodies are indistinguishable
Taxonomic Distance 1 implies complete divergence

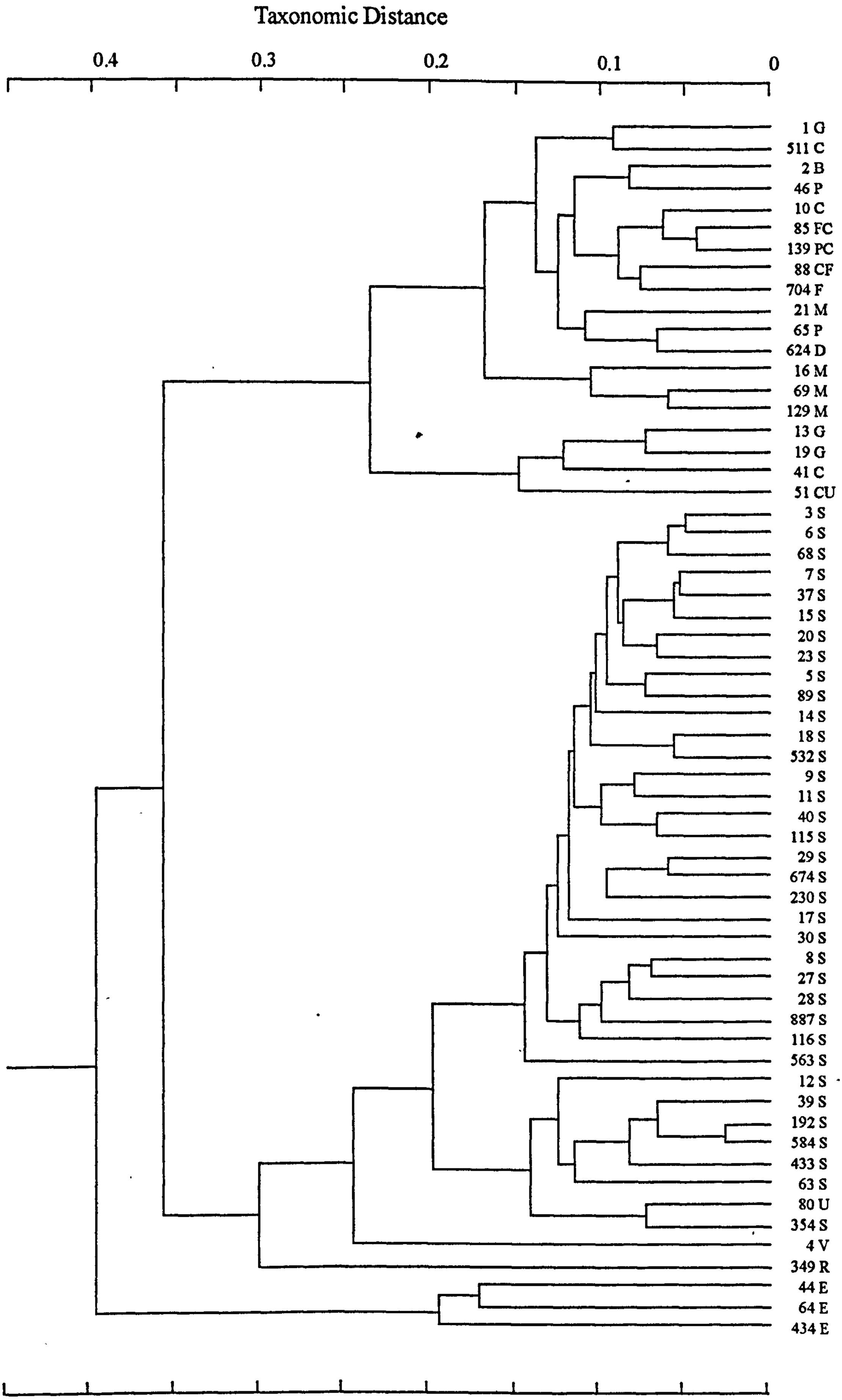

Figure 3.7 - Typical dendrogram for 60 asteroids using a scaled, linear Similarity Coefficient
Random error on the input data to a maximum of 10%
Taxonomic Distance 0 implies the bodies are indistinguishable
Taxonomic Distance 1 implies complete divergence

3.4 An investigation into the Significance of the Seven Parameters

To assess the significance of the seven parameters used in the standard classification scheme, and to determine whether it could be simplified, the effect of omitting various parameters has been studied by calculating the similarity between the asteroids using the numerical taxonomy method.

For each test, six sets of input data have been used; the standard set from the TRIAD file, and five sets having random errors of up to ±5%. This value, as determined in the previous section, should give only minor differences between dendrograms for the same input parameters. If the parameter in question does not add to the accuracy of the classification scheme then the resulting dendrogram should give a result similar to the standard scheme.

To facilitate intercomparison of the six individual dendrograms the calculated classes are presented in tabular form to show the main classes by omitting the calculated taxonomic distance for each test case. The H labels are introduced in this work to identify each grouping. They have no meaning beyond this.

Table 3.4 Main Classes derived by numerical taxonomy calculated following the investigation into reducing the number of data sets and consideration of likely errors

Class	Asteroid Number
H1 (Ceres-like)	1 13 19 41 51 511
H2 (Pallas-like)	2 10 46 65 85 88 139 704
H2a	16 21 69 129
H2b	624
H3 (E-type)	44 64 434
H4 (Juno-like)	3 5 6 7 11 14 15 18 20 23 37 40 68 89 115 532 674
H4a	17 27 29 30 116 230 563 887
H4b	8 9 12 28 39 63 192 433 584
H4b1	80 354
H5	4
H6	349

The numerical order within these groupings varies as different values of error are considered and is not significant. Groups H1 to H6 all represent defined separations which remain even if errors in the parameters at the ±10% level are introduced.

The large migration of objects within the H4 (Juno) group suggests that the minor structure is relatively insignificant. The sub-groups identified are H4b which is a Flora group, H4b1 which may represent a minor grouping within the Flora group, and H4a which contains members with factors in common with both the Juno and Flora subgroupings. It should be noted that, at the current time, there are no clear subdivisions recognised in the S-type (Juno) group in the standard scheme.

The C-type region, as currently classified, consists of several types which are separated by individual peculiarities. The dendrograms indicate the few significant groupings which exist.

The Ceres-like asteroids all group together, some examples have recently been classified as G and perhaps all should be given this designation.

The Pallas-like subset is slightly more complex and several distinct groupings are present. The most significant are the Metallic group 16, 69, 129 and probably 21, though the látter can be detached from the main grouping relatively easily.

624 Hektor forms a subset at a significant distance from the main Pallas-like members.

The E-type asteroids represent a significant grouping which always preserves a separate identity. However they are individually very dissimilar. They are grouped largely by virtue of their abnormally high albedo, low P_{min} and low U-B. They are more dissimilar than any of the structure inferred in the Juno-like group and it is likely that subsets will be formed if there are many more discovered.

Under this classification scheme much of the C-type region becomes simplified. Recent years have seen a proliferation of groups in this area of the dendrogram. These are not supported by the numerical analysis used here. Though each asteroid will be, in some ways, unique it would seem appropriate to rationalise this region as indicated in the H1 and H2 regions. There is no justification, under the seven parameter scheme, for subdividing group H2 which currently contains examples of type B, P, C, CF, PC, FC.

The effect of reducing the number of parameters used in classification from seven was considered next. Dendrograms were calculated, without consideration for errors, using firstly two parameters, U-B and B-V, and then two cases with three parameters, U-B, B-V and albedo, and also U-B, B-V and P_{min}.

The dendrogram produced using two parameters gives only a crude classification which is not close to the full scheme. The addition of albedo or P_{min} improves the matters greatly. The main groups

identified above have appeared, the minor structure is not as clear as with the seven parameters and the sub-groups have not separated. P_{min} and albedo are interdependent since one method of estimating the albedo is from the measurement of P_{min}. It should thus be possible to use one or the other in calculating the dendrogram. The two dendrograms, one omitting the albedo and one the P_{min}, are essentially the same as the basic seven parameter one.

If both P_{min} and albedo are omitted from the classification scheme, but the remaining five parameters are considered, there are only minor changes except that the H2a, H2b and H3 groups are seen as one group. It is thus essential to include albedo to allow the above groups to subdivide. Basically a three-parameter dendrogram can provide a useful classification bût a six-parameter one (excluding either albedo or P_{min}) would seem to give the most comprehensive subdivision.

3.5 A new Taxonomy of 588 Asteroids

Eight colour photometry of 588 asteroids has been published by Zellner, Tholen and Tedesco (1985). The wavebands observed lie between the Ultra-Violet (approximately 300 nm) and the Infra-Red (approx. 1100 nm). In all 589 objects were observed but one was subsequently rejected as a field star. The results of the eight-colour photometry are given as an absolute v magnitude and seven colour indices related to v. The colour indices were used to construct a classification for the 588 asteroids.

A new classification scheme has been calculated using this data set and numerical taxonomy (using equation 3.3) to identify similar bodies. The data set was sufficiently large that drawing a complete dendrogram would not have been realistic given the magnitudes of the errors quoted by Zellner et al. Since the classification has been calculated there are no initial preconceptions about the classification of any particular asteroid and each has been assigned to a class solely on the shape of its colour curve and its calculated similarity to the respective class "prototypes". The reflectance spectra of the asteroids for which each class is named is shown by Figure 3.8

The eight-colour light curves can be separated into two main groupings. Those which are non-linear in shape, listed in Table 3.5, and those which are substantially linear, listed in Tables 3.6 and 3.7. In addition there are a few bodies which do not fit easily into this scheme. These are entered in the Odd and Unique category. Each category includes many objects which have a close similarity coefficient (<0.1), there are also a few other bodies in each group which, because the full eight-colour photometry was not obtained, have been fitted by eye. To illustrate the distribution of the 588 members within the Solar System each group is listed by Zone. These are the same as those established by Zellner et al.. Figure 3.9 illustrates the distribution of the asteroid classes described here with heliocentric distance (a). A similar figure showing the distribution of the previous classification has been published by Zellner et al.(1985).

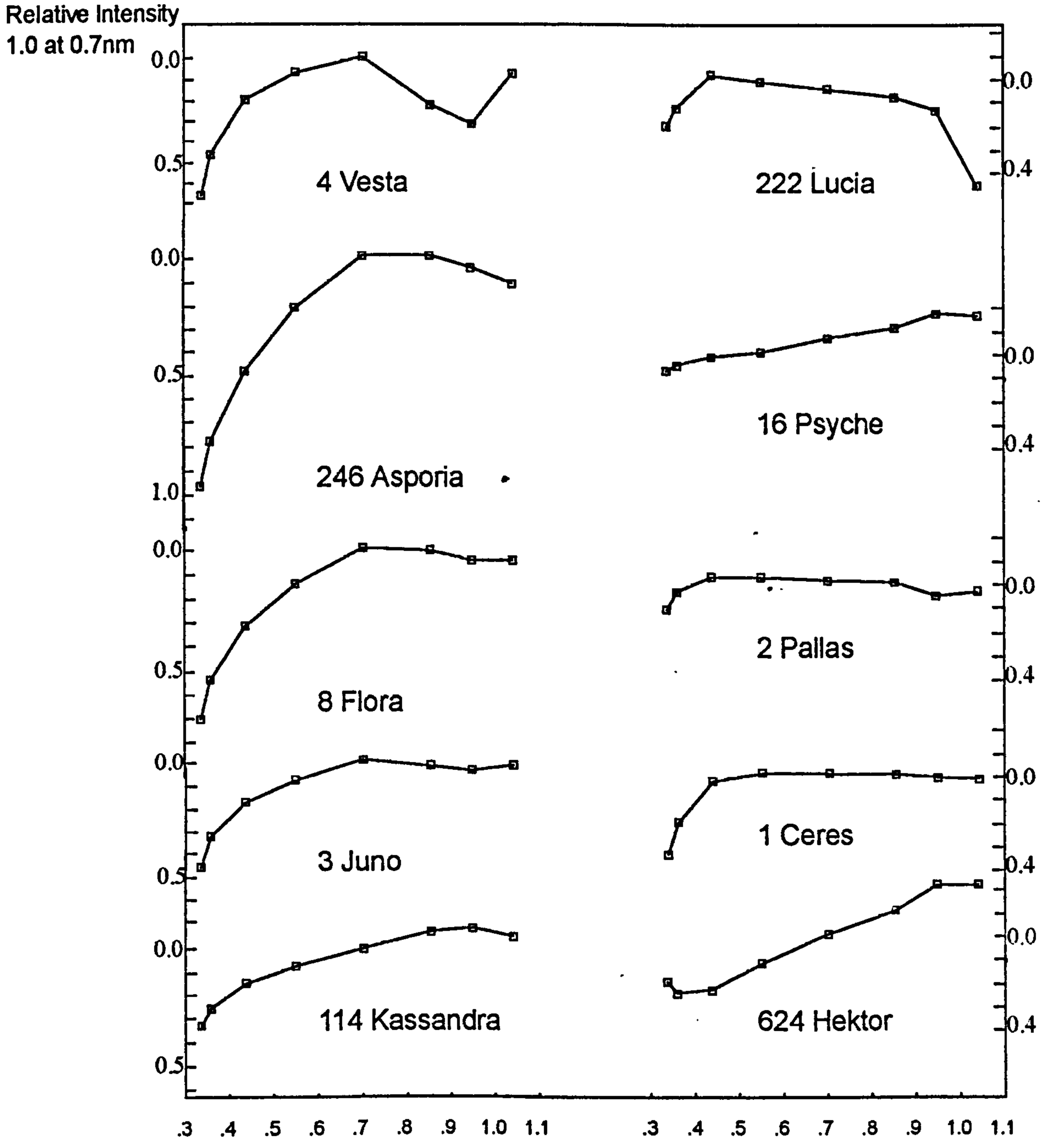

Figure 3.8 - Reflectance Spectra for the asteroid taxonomic classes introduced in this work

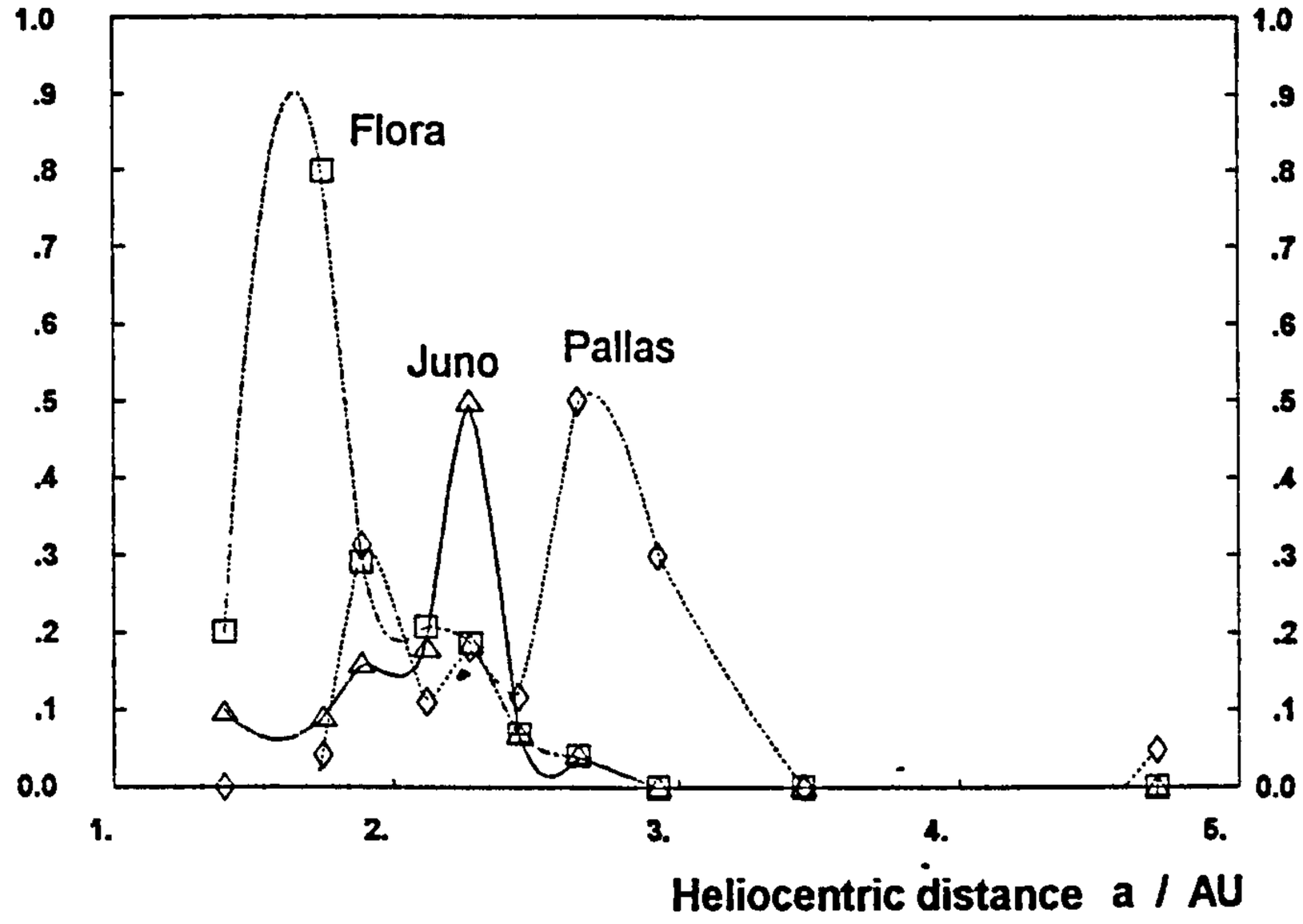

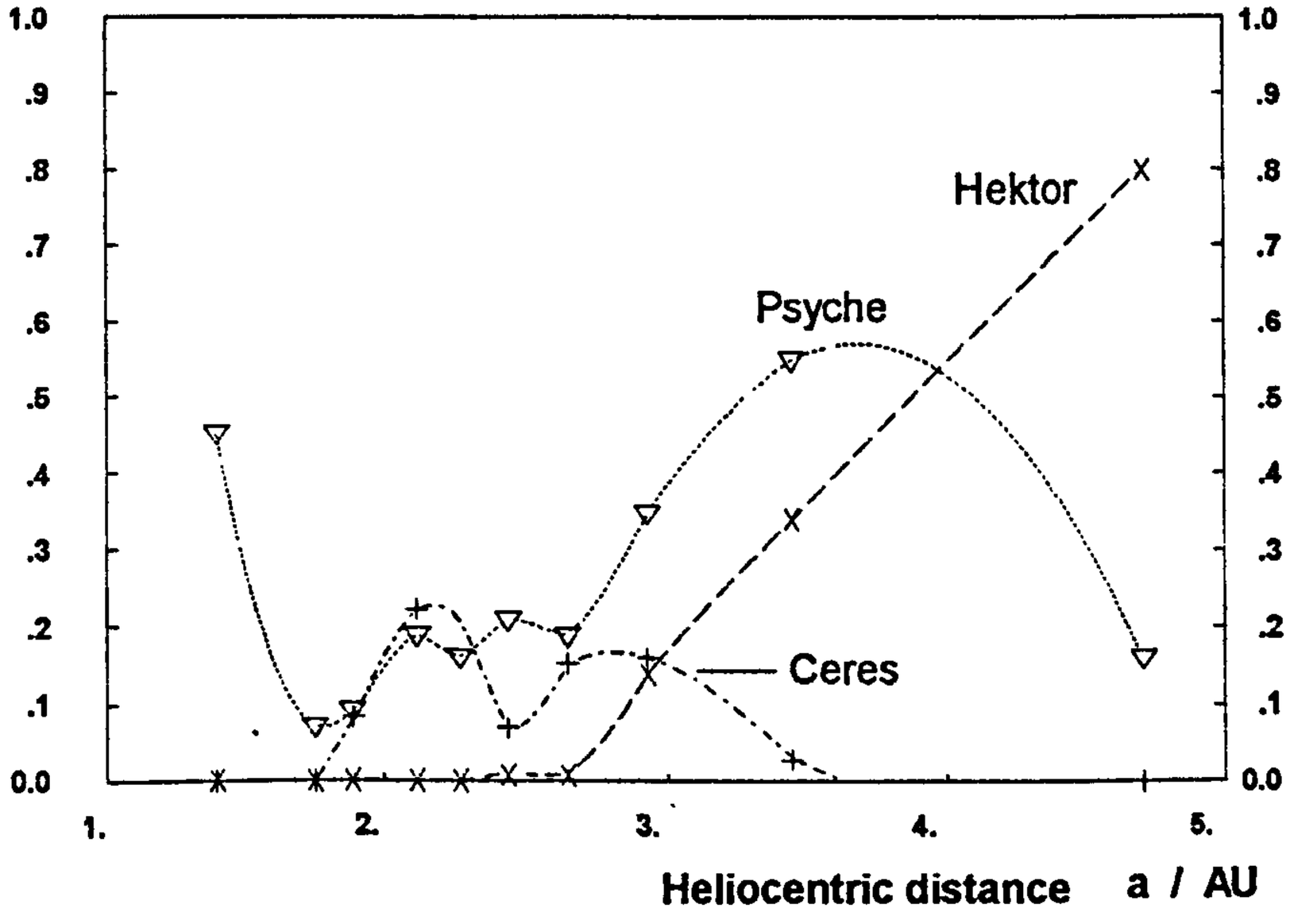

Figure 3.9 - Distribution of the Taxonomic Classes with respect to orbital semi-major axis

Table 3.2

Zone Group	AAA	Hungaria	Flora	MarsX	Phocaea	I	Nysa	IIa	IIb	Koronis	IIIa	Eos	IIIb	Themis	Cybele	Hilda	Trojan	Other
Vesta	1862					4												
Asporia							2501	246	446		289		863					
Flora	433	1019	8	512	25	9		14	28		33	639	108					692
	1627	1453	40	2744	323	11		15	39		349	651	196					
	1943	1509	80		1170	12		26	116			653	245					
	1981QA	2272	228			27		32	288				2090					
	1982DV		296			30		89	346									
	1982XB		352			42		101	354									
			364			63		103	374									
			376			67		119	387									
			443			79		170	563									
			496			113		459	579									
			540			118		472	631									
			548			169		480	675									
			851			189		582	980									
			864			198		616										
			901			219		660										
			937			234		714										
			951			287		925										
			1047			306		974										
			1078			470		1215										
			1088			477		1391										
			1133			571												
			1185			584												
			1249			1665												
			1307															
			1418															
			1422															
			1601															
			1619															
			1842															
			1990															
			2156															
			2411															
			2510															
Juno	887	2131	18	699	1310	6		3	68	158	61	221	57	515	483			
	1036	2577	43	1139	1584	7		5	71	167	179	339	181					
	1620				2050	17		23	82	208	471	529	509					
	1863				2830	20		29	148	243	478	562						
	1865					60		37	188	277		579						
	1982RA					115		124	236	462		661						
						186		204	264	761		775						
						192		258	394	811		798						
						230		389	416	962		1087						
						556		402	417	1245		1105						
						622		421	519	1336		1148						
								549	532	1350		1434						
								686		1442		1604						
								695				1711						
								897				2052						
								945				2111						
								1644				2345						
Kassandra	2100	2035				1236		114	739			740			570			
		2048						233	1251			1564						
		2491						476	1693									
								498										
								606										
								712										
								725										
								1284										
Lucia						282			213				222					
													1576					
													1581					
													2010					
Odd and Unique	1915	2735		1657			650		1724								958	
	1980WF	1981LA					969										1439	

Table 3.3

Zone Group	AAA	Hungaria	Flora	MarsX	Phocaea	I Nysa	IIa	IIb	Koronis	IIIa	Eos	IIIb	Themis	Cybele	Hilda	Trojan	Other
Psyche albedo >.10			336	475	83 1700	46 56 102 418 627 801 873 1275	216 275 322 365 521		406 497 551 613 705 773		276 368 506 663 746 1001 1171	223	65 73 87 107 420 522 536 643 790 909 1266 1390	153 499 748 1162 1212 1268 1345 1512 1754 1902 1911 2067 2760	617 659 1173	279
Psyche albedo <.25 >.10			132	1342	161 337	21 135	75 77 97 201 347 367 771 785	110 125 359 860		16 22 69 338 558 1124	92 184 250 382 755 931 1146 1461		1556			
Psyche albedo >.25	434					44	64	55									
Psyche albedo unknown	1025 1103 1355 1919 1920 2001 2083 2449						50	687		836 2407	768 849				190 1180 1529		
Pallas	1979VA		317	1508	105 654 1108	261 302 304 313 329 335 442 554 757 1080	142 750 877 1012 1076 1493 1650 1740 1768 2081 2139 2278 2279 2809 1981QF2	85 134 214 404 405 407 419 505 593 751	45 59 88 93 173 185 187 210 444 907 1021 1655	35 47 81 117 360 380 772 880	10 48 52 94 137 147 209 241 373 381 423 451 469 488 514 530 583 618 635 648 664 702 704 762 778 786 791 805 1061 1625 1794 2379	24 62 90 104 171 268 383 431 526 946 996 1445 1615 1691 1815 2405	225 229 466 713 733 1028 1154 1177 1579 1796 2196	1208	2 2060

Table 3.4

Zone Group	AAA	Hungaria	Flora	MarsX	Phocaea	I	Nysa	IIa	IIb	Koronis	IIIa	Eos	IIIb	Themis	Cybele	Hilda	Trojan	Other
Ceres					326	51	19	13	1		195	49		379	121	334		
					914	131		34	38		238	89			168			
					1963	345		58	41		386	95			414			
								66	54		776	106			566			
								70	128		804	120			1280			
								78	146			130			1467			
								98	156			159						
								99	200			211						
								109	206			350						
								111	266			508						
								144	410			511						
								145	559			602						
								194	821			640						
								232	1981VB									
								240										
								344										
								380										
								429										
								449										
								1277										
								1606										
Hector												308	2375		721	361	588	
															1167	1038	624	
															2208	1144	884	
															2266	1256	1143	
															2311	1269	1172	
																1578	1583	
																1746	1867	
																1748	2207	
																2246	2223	
																2312	2241	
																	2260	
																	2357	
																	2363	
																	2674	
																	1975QD	

Six non-linear Groups can be determined, four of these are a progressive flattening of a basic curve, the remaining two are more individual.

The Asporia Group is relatively rare. The five examples in this classification are distributed through the Main Belt. These bodies have a distinctive steeply curving spectrum. The Juno type (S) of the traditional classification scheme separates into two groups. One with a steeper curved spectrum showing similarities to Flora is found in the Near-Earth asteroids and the inner Main Belt.

The second, the traditional Juno type, has a flatter spectrum and is more numerous in the Outer Main Belt though it is also concentrated in the Near-Earth asteroids. The boundary between these two types is broad and some asteroids may be better placed in the other group, when additional observational data is available. It may be that the relative balance of the numbers in the AAA (Earth-Crossing Group) zone indicates that these were originally perturbed from the Main-Belt through collisions or gravitational interactions.

The Kassandra Group are asteroids with a shallow curved spectrum. They are quite distinctive and easily separated from both the Juno and the Linear spectrum classes. They are most frequent in the middle zone, Zone II, of the Main Belt, but the numbers identified are insufficient to determine whether this is a real family grouping or just an effect of observational selection

The final grouping comprise diverse bodies with similar spectra. Some are partially linear whilst 2010 for example is non-linear. The common feature they have is that the colour indices at the red end of the spectrum are greater than at the blue end giving an apparently backward slope to the spectrum.

Tables 3.5 and 3.6 give the classes of asteroid which have a substantially linear spectrum. The standard classification scheme gave Ceres and Pallas separate groupings and this was also found with this exercise. Indeed there is the possibility that a mid-Ceres/Pallas group also exists but the evidence was inconclusive. The distinctive features of these two Groups are that they both possess flat spectra but are UV-deficient. The depth of the UV deficiency determines whether a body is placed in the shallow Pallas group or the deeper Ceres group. Apart from a surplus of Pallas type in the Main Belt, both types are fairly well distributed in the asteroid belt. The Psyche-like group contains examples of both high and low albedo bodies. It is a Group that will subdivide into quite diverse types. For example consider the three bodies in the Nysa zone. 21 and 135 are low-albedo M types whilst 44 is a high-albedo E type. Insufficient precise albedo data is available for most of this group to allow significant conclusions to be drawn. Many are classified as CMEU (or more recently X) which allows any of the traditional classifications. On the basis of the eight-colour data however the C-type classification is not appropriate for these bodies. The spectrum is the opposite of that for 222 Lucia and shows a gentle increase in the colour index as the wavelength increases.

The final Group contains bodies similar to the Trojan asteroid 624 Hektor. They occur in the Outer Main Belt and beyond. The colour curve is redder and has a steeper gradient than the Psyche group.

The groupings produced in Section 3.4 represent a simplification of the classification by Bowell et al (1978) following a consideration of the effects of probable errors in the observed input parameters. This may be compared with the groupings derived in this new taxonomy. All the members of the H1 class are found within the "new" Ceres-like group. Most members of the H2 class are found within the "new" Pallas-like group though 46 and 65 have been placed in the low albedo Psyche-like group in the new classification.H3 (E-type).The final Group contains those bodies which are similar to the Trojan asteroid Hektor, number 624. H4 and its sub-groups all are S-types in the current classification. In the new classification the members form the Flora-like and Juno-like groups All members of the H4 group with the exception of 11 fall into the Juno group. H4a is equally split with 17,29,230,532 and 887 belonging to the Juno group. H4b and H4b1 fall into the Flora group with the exception of 192 which in the new classification remains with Juno. H5 contains Vesta which forms its own group whilst H6 contains 349 which is classified with Flora in the new system. 349 is an unusual case as it has a high albedo which influences its position in the "standard" scheme though its colour indices are normal for a Flora group member.

This scheme has several advantages over the seven-parameter classification. Each of the seven colour indices, referred to the v band, is independent of the others. This is not the case with the seven parameters of Bowell et al. where, for example, the P_{min} is related to the albedo. The colour index results show that the separation of the Flora-like from the Juno-like is real whereas this is not certain under the seven parameter scheme. The Hektor-like group can be shown to include a number of members in the main belt which are "classified" as U, unclassifiable, in the normal scheme. However a disadvantage is that the Psyche-like group cannot be subdivided without including the albedo data. Allowing for his latter proviso both methods of classification are valuable.

3.6 Rotation characteristics of the Classes

Figures 3.10 to 3.12 show the rotation characteristics of the five largest classes derived by the calculations made in the last section. The figures are plotted using data in the 1994 edition of the Ephemerides of the Minor Planets. The means and standard deviations for the complete sample and for the individual classes are given in Table 3.8. If the members of a class share a common evolutionary path then their rotational characteristics should mirror this. As some of the different classes will have a different evolutionary path it would seem likely that the rotational characteristics would show some variation between classes - this seems to be the case for the small data set currently available.

An inspection of the figures shows that all five classes have basically similar characteristics. However the Ceres and Pallas classes have amplitudes less than 1 magnitude and spin frequencies less than 5

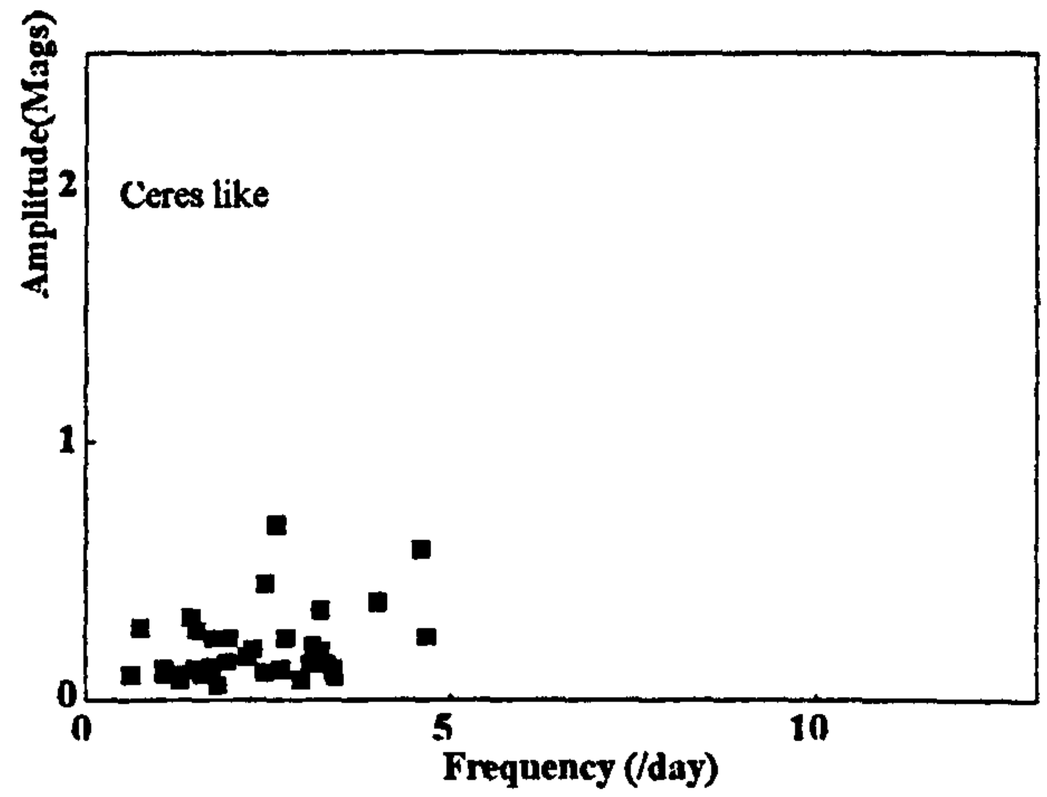

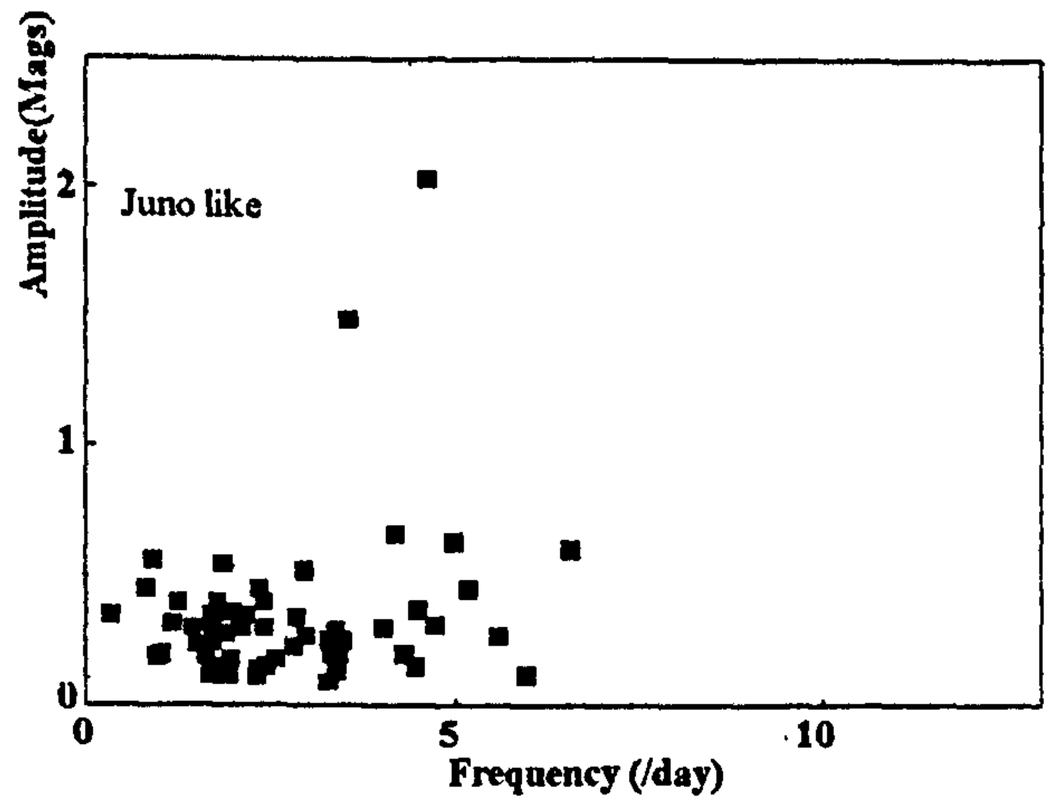

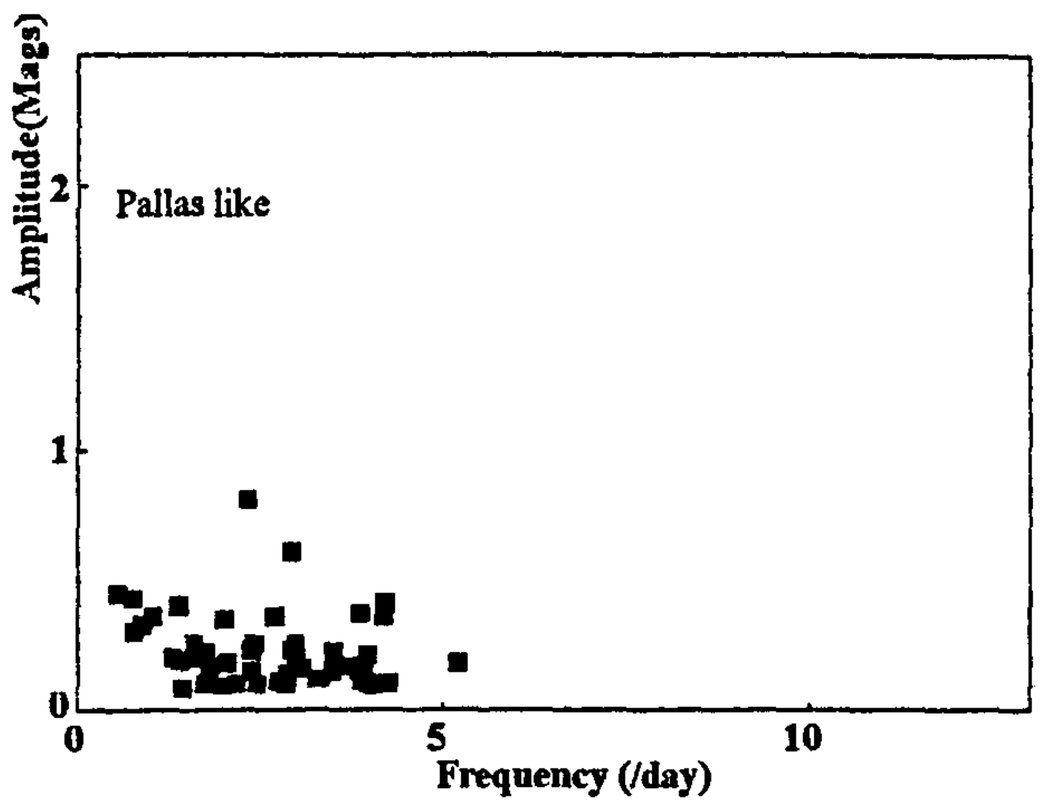

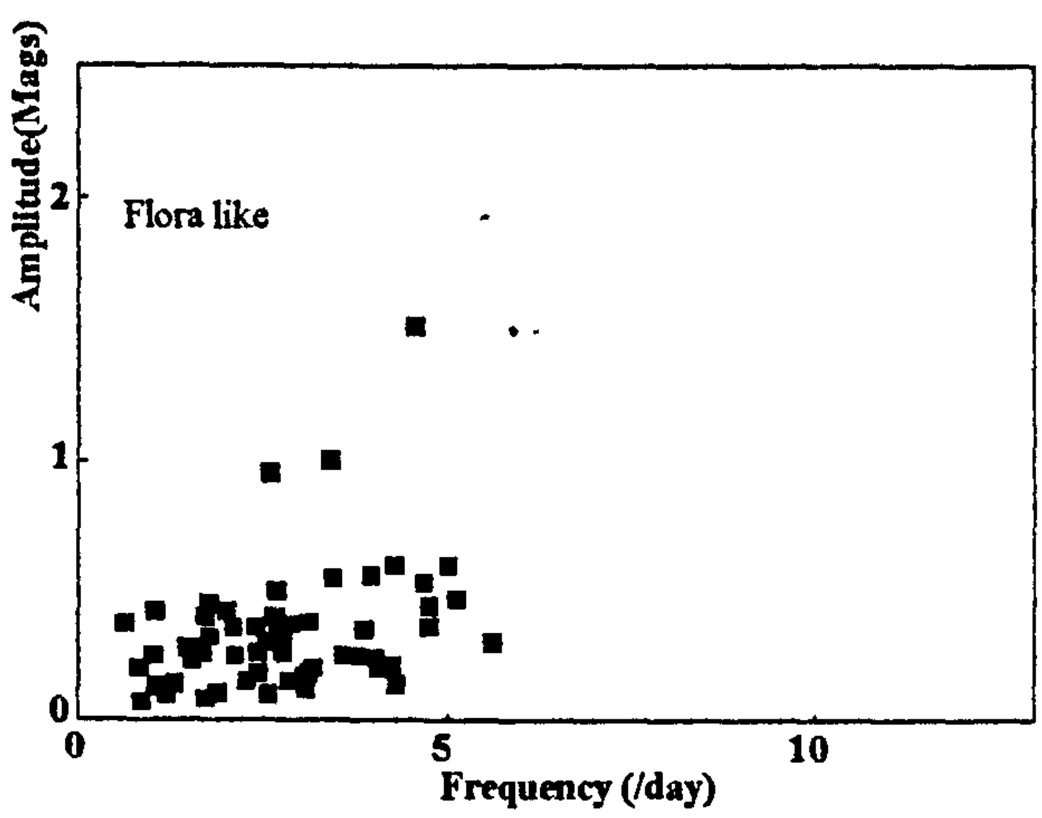

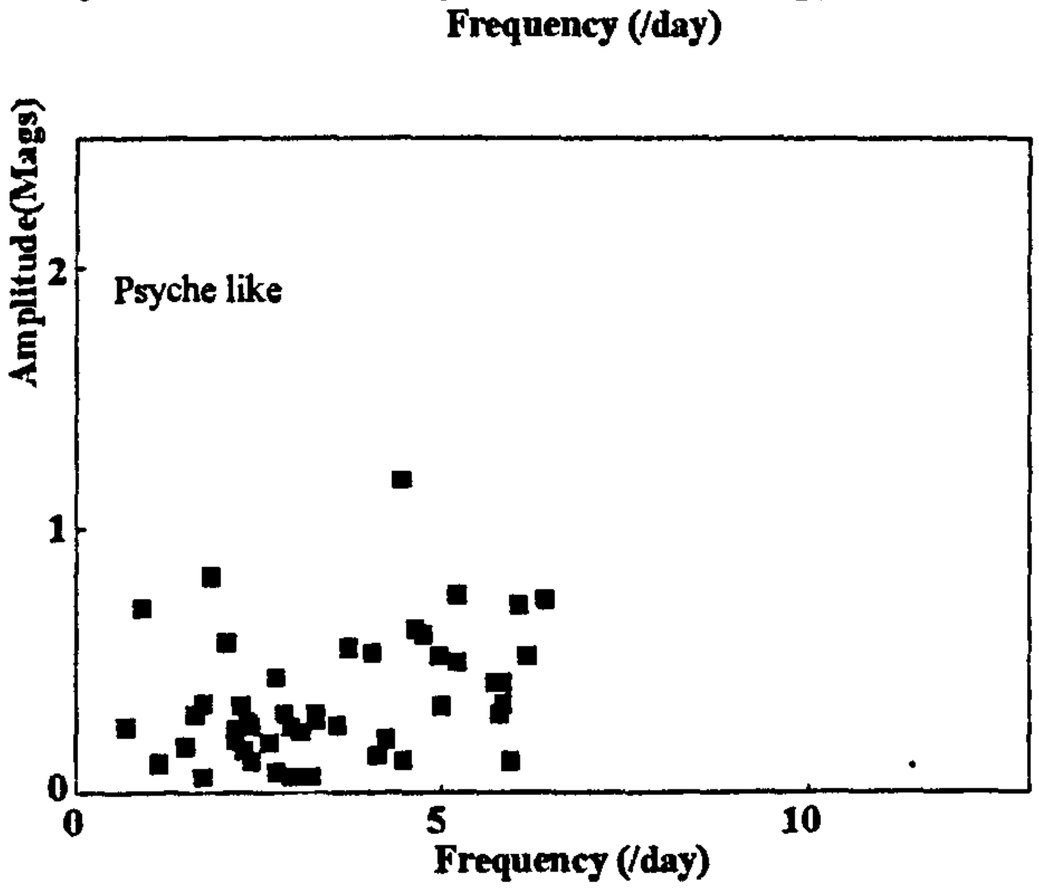

Figure 3.10 Graphs of Amplitude (Maximum - Minimum Magnitude) vs Spin Frequency for five classes in the new taxonomy

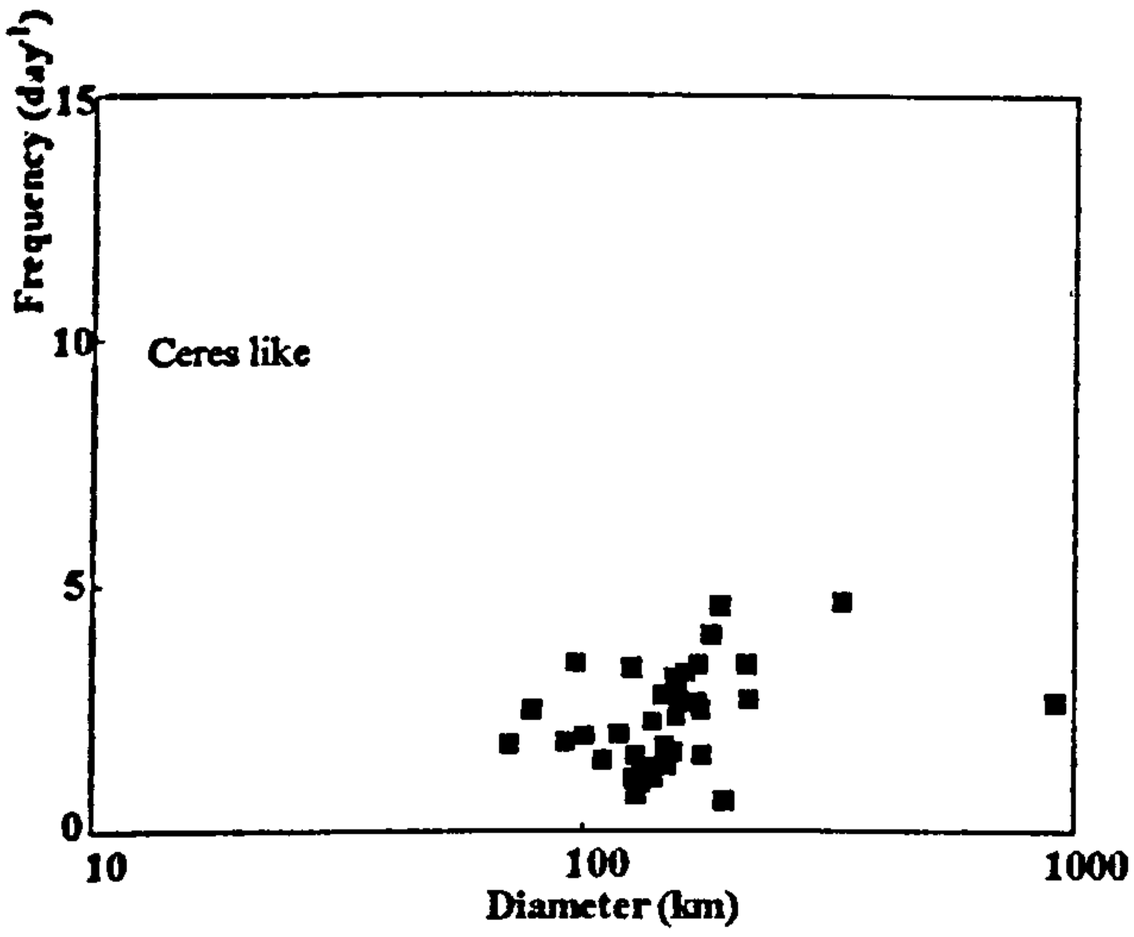

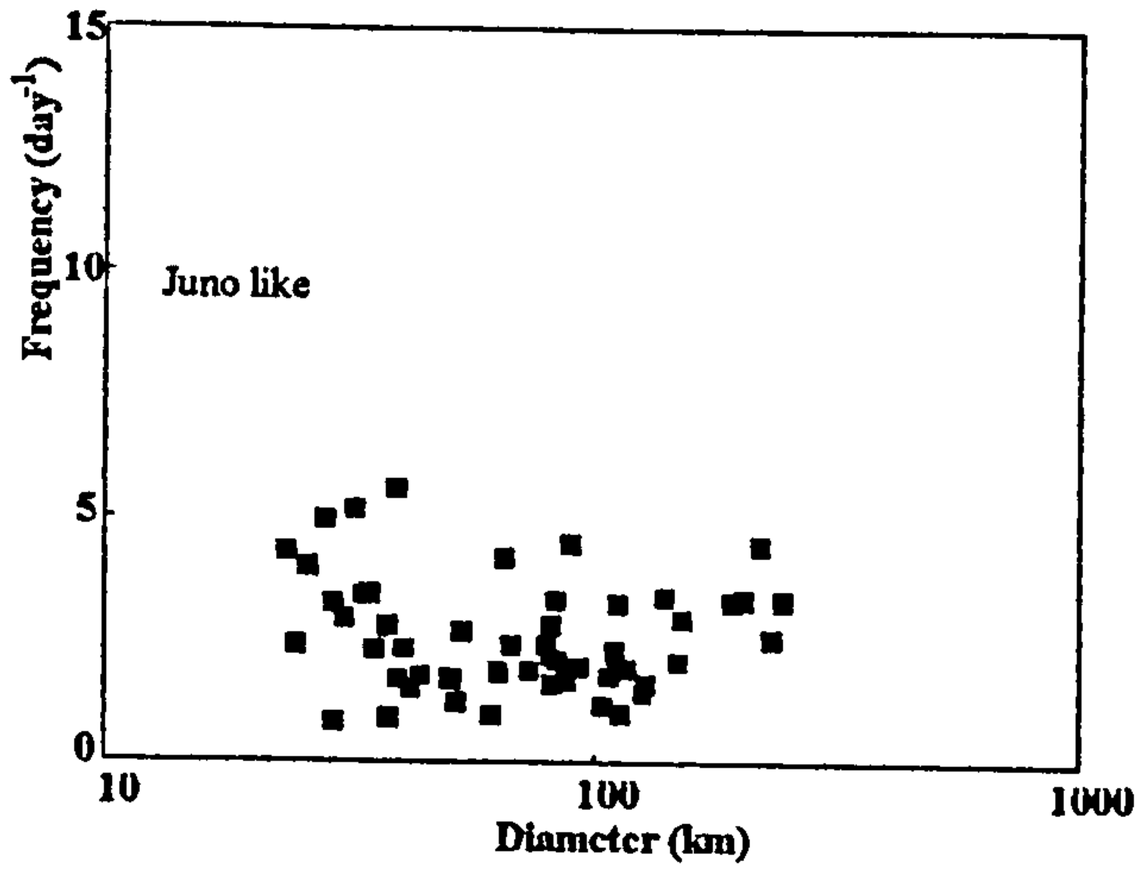

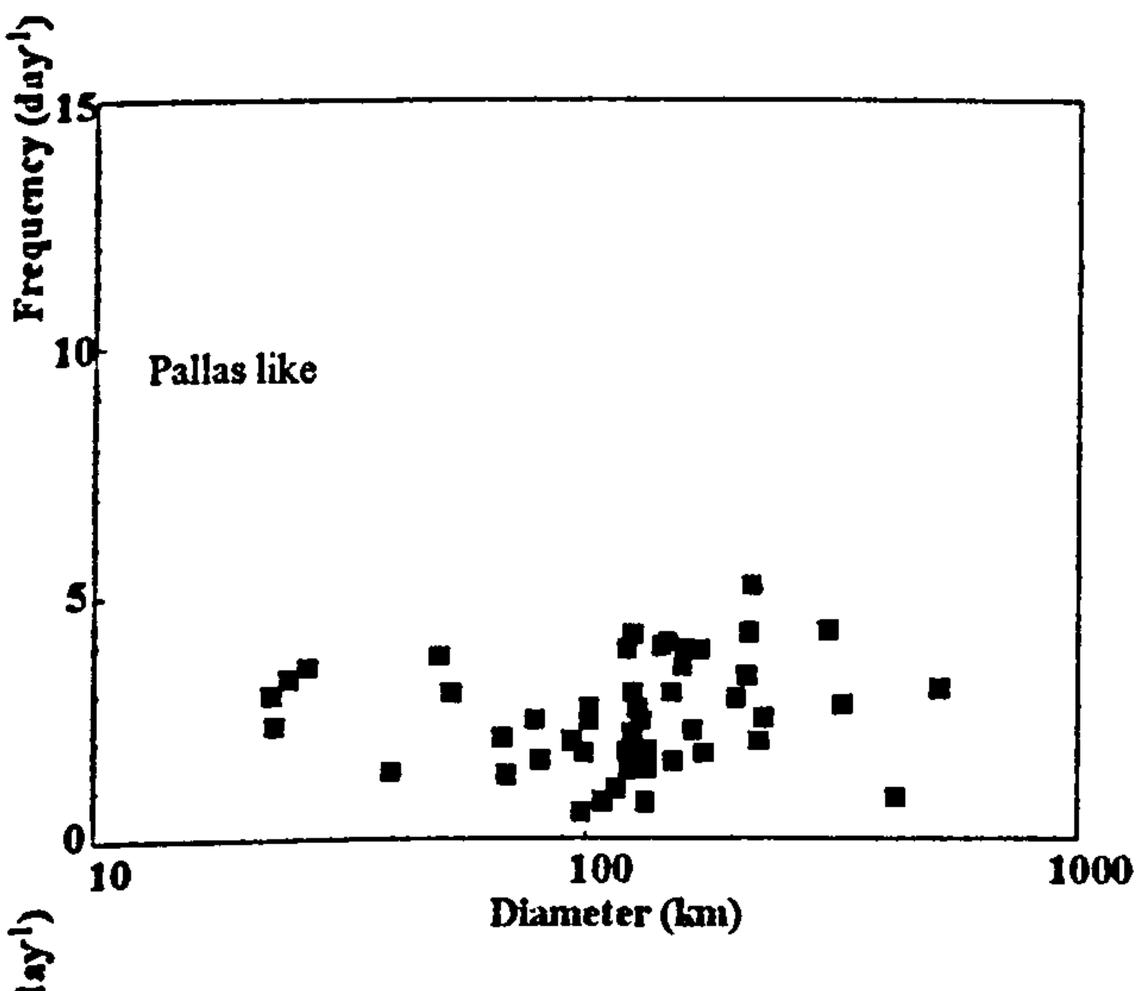

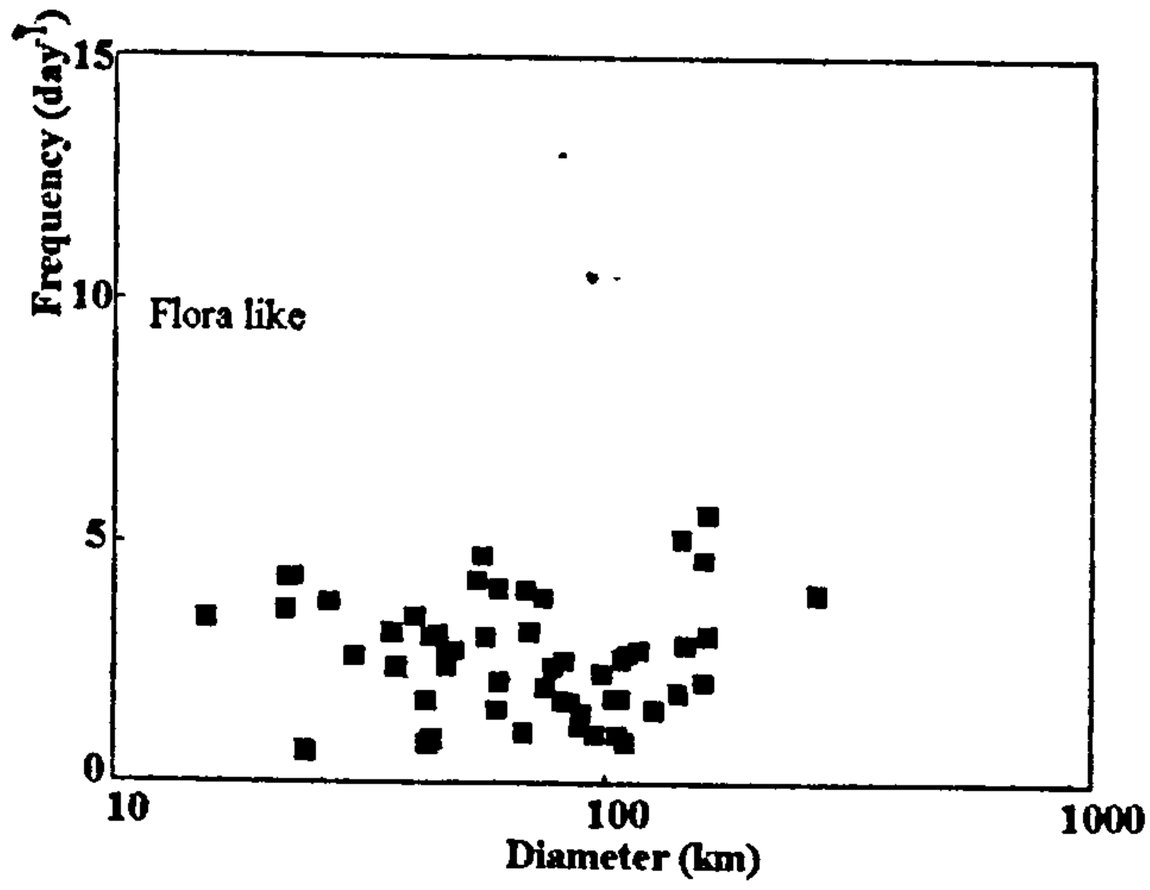

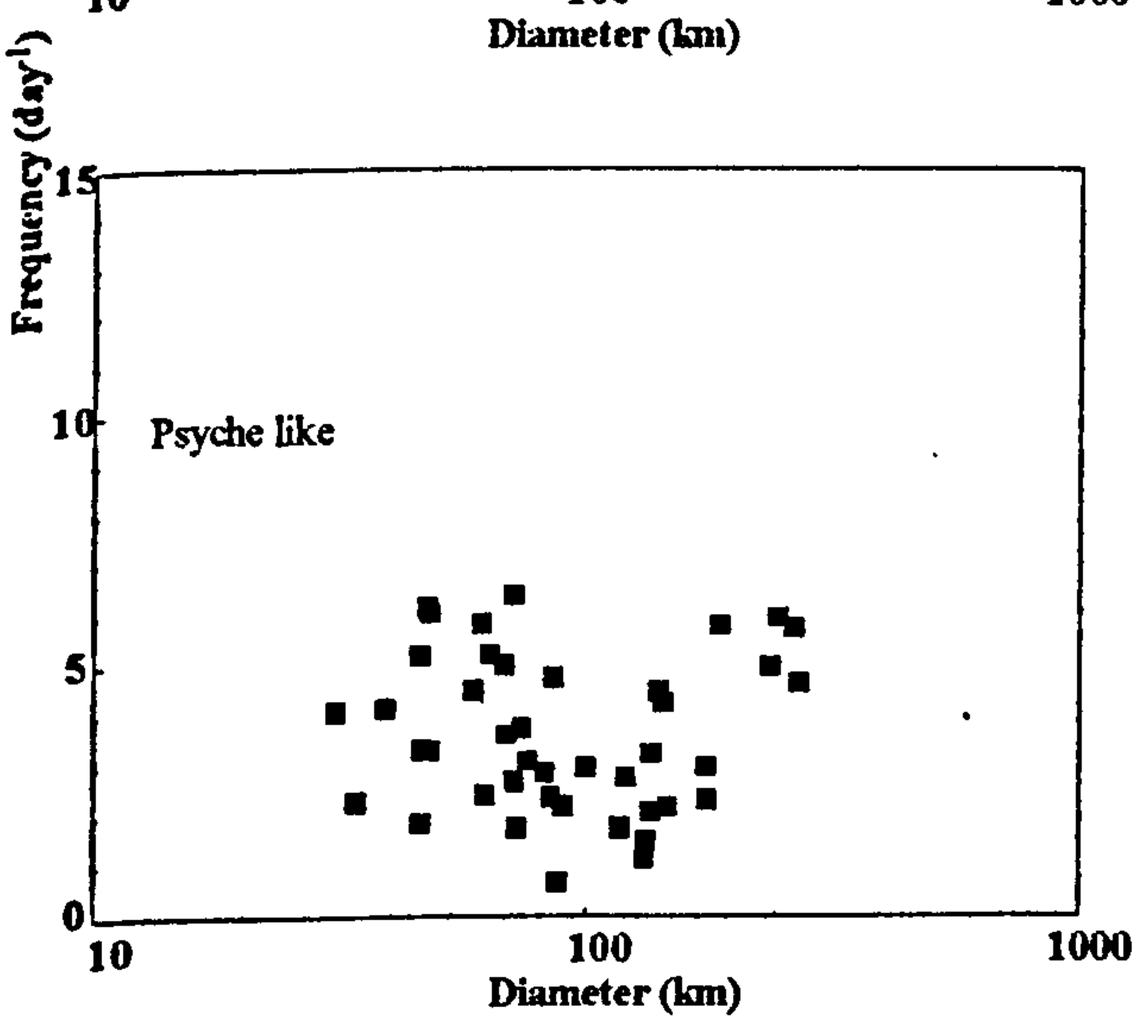

Figure 3.11 Graphs of Spin Frequency vs Diameter for five classes in the new taxonomy

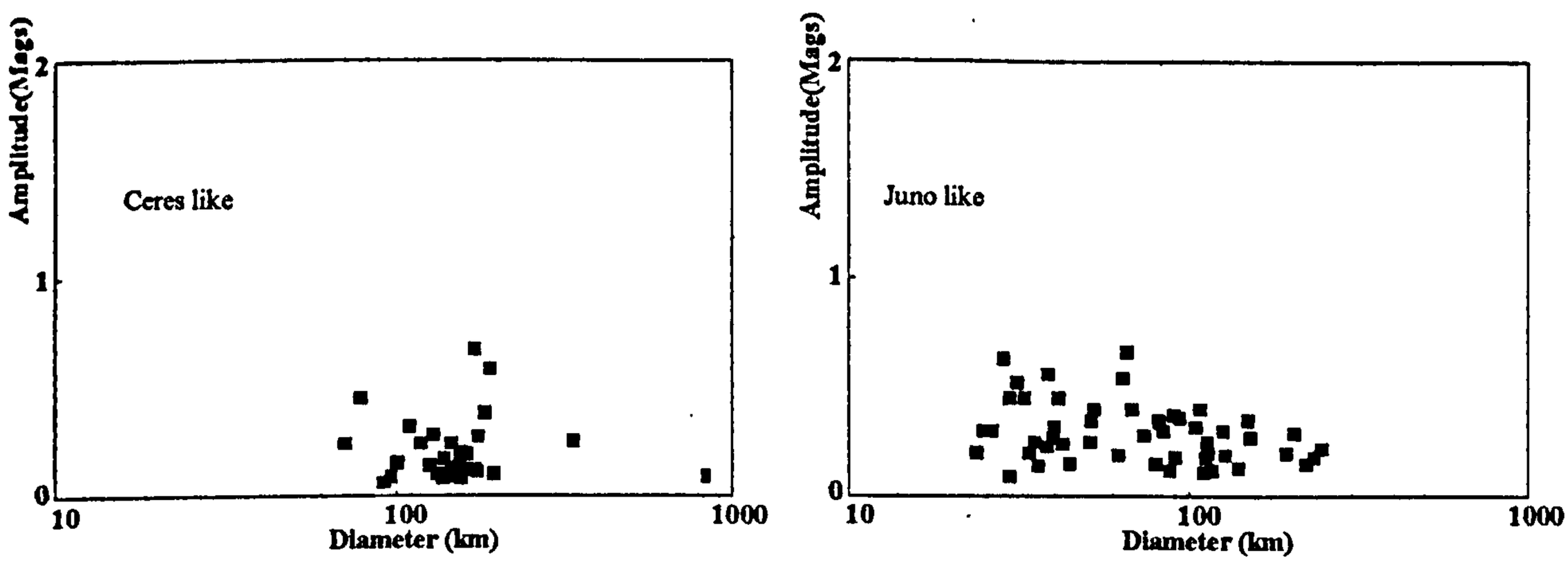

Figure 3.12 Graphs of Amplitude vs Diameter for five classes in the new taxonomy

per day whilst some examples of the Juno and Flora classes have amplitudes of up to 2 magnitudes and maximum spin frequencies in excess of 5 per day. The Psyche type have intermediate amplitudes (up to 1.5 magnitudes) with maximum spin frequencies in excess of 5 per day. Though the sample in each class is relatively small there is no reason to believe it is unrepresentative since the whole area of the amplitude-phase plot is equally accessible to measurement.

Table 3.8 Rotation Characteristics for the Sample and Classes from data in the Leningrad Ephemerides

	Mean Spin Frequency		Mean Amplitude	
Class	Day^{-1}	SD	Magnitudes	SD
Ceres	2.296	±1.026	.196	±.139
Pallas	2.562	±1.089	.215	±.145
Juno	2.562	±1.131	.282	±.122
Flora	2.612	±1.264	.303	±.157
Sample	2.652	±1.407	.310	±.220
Psyche	3.614	±1.536	.360	±.235

From light curve amplitudes Juno and Flora classes have very elongated members, the Psyche class has some medium elongated members whilst the Ceres and Pallas appear more spheroidal in shape. Juno and Flora classes may have evolved further than the others - possibly through impact processes.

3.7 Limitations of classification - A discussion of Surface Processes on Asteroids

Asteroids are classified on the basis of observations from Earth. As we are unable to probe a depth of more than at most a metre this refers to the structure of the surface . Just how reasonable is it to base classification on surface properties? We may well be grouping together dissimilar bodies on the basis of similar surface characteristics. The fundamental parameters of mass, volume, density, and internal structure remain unobserved and largely unobservable from the Earth.

To highlight the problem consider the three largest asteroids. The surface properties, determined from reflectance spectra of the largest, Ceres, are similar to those of carbonaceous chondrite meteorites. Samples of the latter have been examined in the laboratory and appear to be undifferentiated. This implies that they condensed early in the Solar System history and remained unmodified from that time. The next two largest bodies, Juno and Vesta, are both about half the diameter of Ceres but appear to be differentiated bodies. Taken at face value it would seem that in the middle of the main asteroid belt the conditions were not right for Ceres (a=2.8 A.U.) to differentiate, yet were right for the smaller Juno (a=2.7 A.U.) and Vesta (a=2.4 A.U.). Wood (1979) gives a graph showing the anticipated rise in temperature of the Earth during its early accretion. The rise in internal temperature increases with size due to lower radiation, the surface area (from which heat radiates away) depends on r^2 whereas the volume (and hence mass) depends on r^3 giving a lower radiation per

unit mass. It is a reasonable assumption that Ceres will have reached a higher temperature during accretion than Juno or Vesta. Bodies smaller than about 50km may be either partially accreted planetesimals or fragments produced by collisions. This appears not to be the case for the largest asteroids which are believed to be unmodified after the end of the accretion phase.

There are several possible explanations to account for apparent inconsistency of the surface of Ceres.

1. Internal rise in temperature, for example by radionuclide heating or electromagnetic induction, may have allowed internal melting and differentiation but heat loss to space or insufficient heat generation kept the surface temperature sufficiently low to prevent differentiation.

2. The primary accretion phase produced a body that differentiated as did Juno and Vesta. A secondary, post differentiation, accretion phase occurred which spread primitive undifferentiated material over the surface. But there is no known secondary accretion phase on the surfaces of the planets or satellites. The bombardment phase which gave rise to the craters observed on the surfaces of the Solar System bodies has effectively turned over the surface of those bodies but has not added a significant proportion of new material to the surface.

3. Ceres has attracted post accretion debris which has spread a thin layer of primitive material over the surface. It seems unlikely that this would have occurred on Ceres without some of the same effects being observed on the next two largest bodies.

4. Ceres accreted more slowly than Juno or Vesta and the consequential rise in temperature was much lower. This temperature was insufficient for differentiation. This seems unlikely since it requires conditions at the centre of the asteroid belt to be inhomogeneous.

5. Ceres may be an original undifferentiated body whilst Juno and Vesta may represent fragments of larger differentiated bodies which were disrupted after the proto-Jupiter accreted sufficiently for its gravitational influence to affect the main asteroid belt such that major collisions prevented further accretion and disrupted most of the major bodies. (see for example Hughes 1994)

6. Meteorite evidence may not be relevant to asteroids.

As none of the above seem convincing, what other processes could prevent the true character of an asteroid being deduced from the Earth? One possibility is that bombardment of the surface by meteoroids could result in localised melting and shock metamorphosis of the rock. If the rise in surface temperature were sufficient to melt a layer a few kilometres thick then differentiation may occur. A differentiated surface may overlie an undifferentiated interior. Micrometeoroid bombardment will modify the surface as, to a lesser extent, will bombardment by protons and alpha particles in the Solar Wind. Larger meteoroid impacts may mask the true nature of the asteroid by reworking the surface completely.

The extent of melting during the accretion process can be assessed by considering the temperature rise from an impact. If the kinetic energy of the projectile is totally converted into heat then the melted area of the target can be determined thus :-

Latent heat of fusion of rock - ~ 1.7 10^6 J kg mole^{-1} as kg mole for a typical rock ~ 170kg

Latent Heat of Fusion ~10^4 J kg^{-1}

Specific Heat of rock ~ 800 J Kg^{-1} °K^{-1}

Projectile velocity relative to target ≈5 km sec^{-1}

Kinetic Energy of Projectile 0.5 (5 . 10^3)^2 J kg^{-1}

Assumed initial temperature of accreting asteroid 300 °K

Melting Point of Rock ~1300 °K

Mass of asteroid melted by impact of a 1 kg projectile 0.5 (5 . 10^3)^2 / (800 . 10^3 + 10^3)
~ 16 kg

If the molten area is confined to a hemispherical bowl this result implies that the radius of molten matter will be 3.2 times the radius of the projectile. For small accreting bodies it is therefore unclear whether at any stage there will be complete melting and if this is the case then total differention to a heavy core, intermediate mantle and lightweight crust will not occur.

3.8 Conclusion

Numerical taxonomy applied to the eight-colour photometry data set recognises the same broad classifications derived by other schemes. Some minor reclassifications may be appropriate - either by way of subdivision or combination. This characteristic is recognised for each scheme by Tholen and Barucci (1989). An example of this is the subdivision of the S-class into two parts. An inner type (Flora like) and an outer type (Juno-like) which are found to be separate in my scheme.

To classify the greatest number of asteroids any scheme should rely on a few easily observed parameters. Further research is necessary to identify which are the most appropriate but it may well be that colour indices (such as U-V and V-R) and albedo may be the simplest. Colour indices may be directly determined at the telescope. However there is no doubt that the more parameters measured (such as the eight-colour survey) the easier it is to produce a correct classification.

There is some evidence for a weak correlation between class and spin properties

However precise the observations are, they must be used with caution because they may well group bodies that are only *superficially* alike. Similar-sized bodies with similar surfaces may well have undergone similar evolution but this may not be the case for bodies of differing sizes. Further research on the thermal and petrological history of small asteroids and planetesimals is needed to address this problem.

4. Projectile Target Interaction - a new model for the evolution of Spin Rates and Spin-Axis Orientation

Abstract

A new model for projectile/target interaction is derived from Newtonian mechanics by considering the target as a gyroscope. The model considers angular momentum transfer in terms of the modification to the value of the spin vector for the longitudinal component of the impact parameter and the orientation of the angular momentum vector for the latitudinal component. This method overcomes the need for angular momentum loss preferentially in the direction of rotation which was a basic necessity of the earlier models currently in use. In the short term a free precession is induced due to the misalignment of the angular momentum vector and the spin vector. Internal energy dissipation eventually damps this out and simple rotation with the two vectors aligned is the final equilibrium state.

4.1 Introduction

The evolution of the spin rates and axial orientations can be considered from two main viewpoints. Tidal interactions amongst the major planets have been used to account for the observed distribution of spin rates (Beletskii 1981), this method assumes that the planets formed by condensation. An alternative method assumes that after the formation of Goldreich-Ward planetesimals by condensation within the Solar Nebula subsequent planet growth is by collision and accretion. Harris (1979) has suggested a model for the collisional evolution of spin rates. Several modifications to this have been made and its latest form (Farinella et al 1992) provides an algorithm based on pure momentum transfer allowing for despinning by preferential mass loss in the direction of rotation. No model has been published prior to this work which considers the evolution of spin rates and spin axis orientations together.

To be successful a model must be capable of explaining the observed spin frequency distribution and the high angular momentum contained in elongated bodies with high spin frequencies (see Farinella et al 1981).

4.2 The rotation of a Rigid Body

The precise form of most asteroids remains unknown though modern observation techniques (such as adaptive optics and speckle interferometry) have allowed the reconstruction of images of the larger asteroids. At the time of writing the Galileo spacecraft has returned images of 951 Gaspra and 243 Ida which appear to confirm the earlier assumptions that asteroids are similar in conformation to the

Martian satellites. Various models exist which derive theoretical equilibrium shapes in terms of fluid or semi-fluid matter. It is plausible that during the accretion stage they became sufficiently hot to melt, either due to the conversion of the kinetic energy of impact to heat or else radionuclide heating due to the decay of short lived isotopes. As it cools, the asteroid will solidify. Though it will deform under stress it will behave, at least over short timescales, as a perfectly rigid body when considering the case of rotation with no external torque applied.

A third phase of evolution may well occur where subsequent collisions within the asteroid belt result in asteroids that are partially, or completely, fragmented (Davis et al 1989). These 'rubble-pile' asteroids will behave as a hybrid between fluid and solid bodies. The degree of interlock between fragments will decide whether a body behaves as a pseudo-solid or a pseudo-fluid body.

The rotation of a rigid body is a standard case in dynamics. The angular momentum, L, of which is the sum of the angular momenta of the particles forming that body.

$$\underset{\sim}{L_i} = (\underset{\sim}{r_i} \wedge m_i \underset{\sim}{v}) \qquad \ldots \quad 4.1$$

which in general terms is

$$\underset{\sim}{L_i} = \underset{\sim}{I_i} \cdot \underset{\sim}{\omega_i} \qquad \ldots \quad 4.2$$

where

$\underset{\sim}{L_i}$ = The angular momentum about the i axis

$\underset{\sim}{I_i}$ = The moment of inertia about the i axis

$\underset{\sim}{\omega_i}$ = The angular rotation rate about the i axis

If no external torque is applied to the body then angular momentum vector remains constant.

A regular asteroid has three mutually perpendicular inertia axes, denoted as X_p Y_p and Z_p . By convention the Z_p axis is the major principal axis and it is about this axis that the body's moment of inertia is a maximum. Pure rotation, that is when the angular velocity vector is aligned with the angular momentum vector, can only occur about one of the principal inertia axes. Rotation about two of these axes is an unstable equilibrium so that any disturbing influence, for example because of the imperfect rigidity of the body, will lead to misalignment of the two vectors. Energy dissipation, produced by flexure of the rocky crust for example, will ultimately lead to pure rotation about the major principal axis. The time for this alignment to occur has been discussed in Chapter 1.4.

In rotation which is torque free, the kinetic energy of rotation is given by

$$T = \sum_{i=1,3} 0.5 \cdot I_i \cdot \omega_i^2 \qquad \ldots \quad 4.3$$

which can be expressed in terms of the angular momentum (L) using equation 4.2 as

$$T = \Sigma\ 0.5 \,.\, L_i^2 / I_t \qquad \ldots\ 4.4$$

Lamy and Burns 1972

where

L_i is the sum of the angular momenta about the principal axes. i.e. the value of the angular momentum vector

I_t is the moment of inertia of the body about the direction of L_i

T reaches a minimum when I has a maximum value and occurs for rotation about the principal axis of inertia. The minimum energy state for rotation of a solid body with a given angular momentum, L, is for rotation about the principal axis. Since real bodies are not perfectly rigid there will be energy dissipated by internal flexure which will ultimately result in alignment of the angular momentum vector and the principal axis of inertia to give a pure rotation.

If the axis of rotation does not coincide with one of the principal axes then the body will perform a coning motion. The Z_p axis (defined earlier) will precess about the angular momentum vector and, at the same frequency, the axis of rotation will also precess about L (Figure 4.1). Conservation of angular momentum for this precessing state requires L, ω, and Z_p to lie in one plane (Curdt and Keller 1988).

4.3 External forces acting on a rotating body

A rotating planetary body should be considered as a gyroscope. Though this analogy is regularly applied to atomic particles and to inertial guidance systems it is not generally applied to planetesimal sized bodies. This application of this analogy is a standard case in text books (e.g. French 1971).

The presence of a source of external torque, for example a satellite, may introduce a gyroscopic precession - an example of which is the 25800 year Luni-Solar precession period for the Earth. In general terms a constant external source of torque is considered - e.g. the earth's gravitational field acting on a gyroscope or the Sun and Moon acting on the Earth. However current models do not consider that an instantaneous torque is applied during the impact of one body on another.

The mechanism of planet growth is the accretion of planetesimals. The basic mechanism is the collision of rotating non-rigid bodies. The change in translational motion and direction of the planetesimals satisfies the law of conservation of momentum. The magnitude of such change depends on the relative masses of the bodies, their relative velocity and the impact parameter. In addition there is a change in the angular motion of the bodies which depends on the same parameters plus the angular momentum already possessed in the system (the total angular momentum of the system will

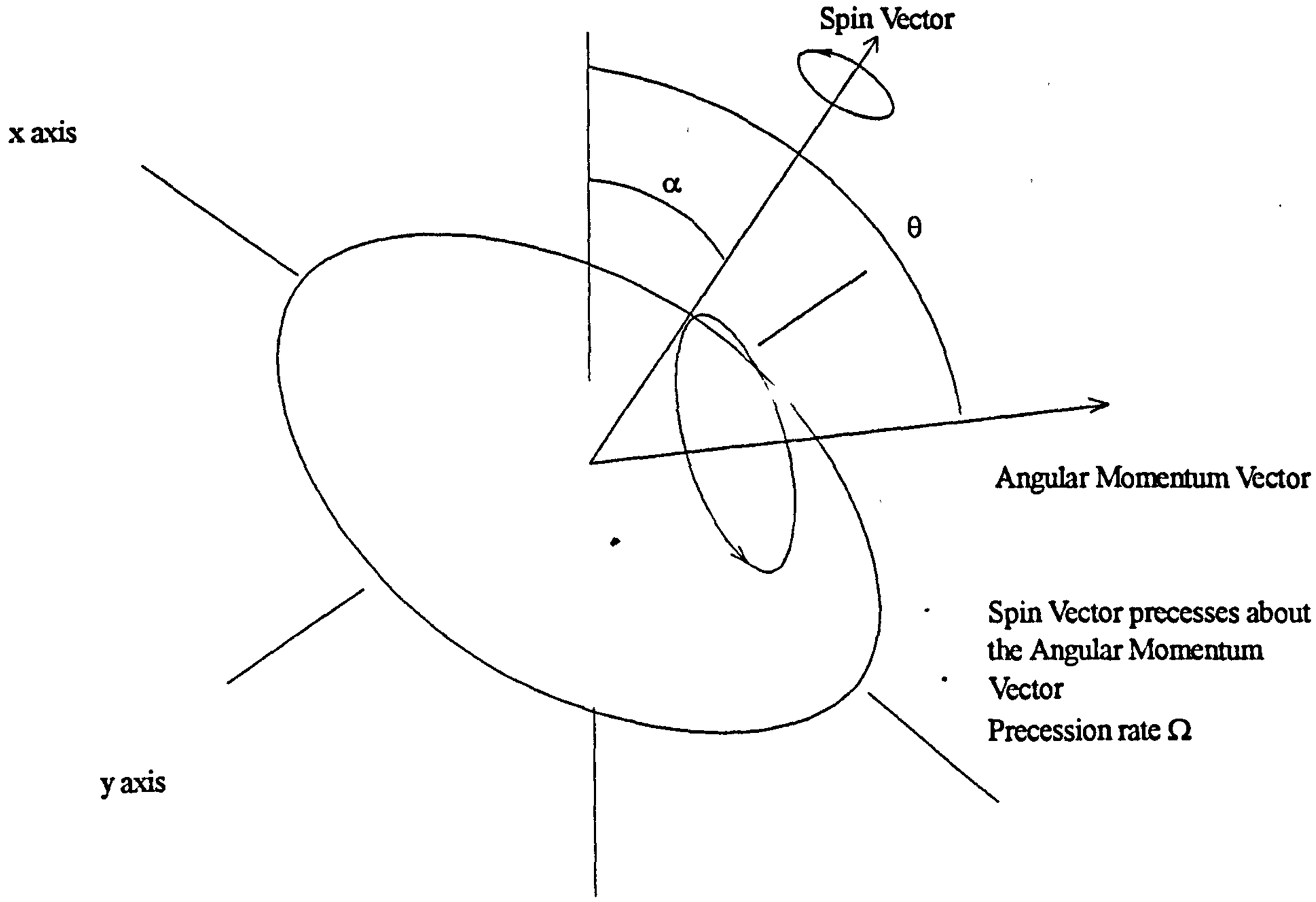

Figure 4.1 - Rotation Geometry for a freely precessing body

be conserved). The latter could lead to a change in the spin frequency or axial orientation of the bodies or both. If there is a misalignment of the angular momentum vector and the angular velocity vector introduced by the impact then a coning motion will be introduced which will be damped out due to internal friction in a timescale approximated by equations 1.2 or 1.3 (see Figure 4.2).

Using the method of McAdoo and Burns (1974) a spherical body of 1000 km diameter is estimated to have a damping time ~0.2 Myr, this increases to 20 Myr for a 100 km diameter body whilst a planetesimal of 10 km diameter has a damping time of 2000 Myr. These figures are only approximations and could be in error by a factor of 10. They do indicate that, if collisions have been a significant factor in the evolution of the Solar System then *the smaller asteroids may not have had sufficient time for the angular momentum vector to align with the principal axis. - We would thus expect to observe examples of the small bodies which still show precession.*

For a uniform density spherical body of mass M and radius a

$$I = 0.4 \,.\, M \,.\, a^2 \qquad \ldots\ldots \quad 4.5$$

In the rest frame of the target the projectile has linear momentum

$$\underset{\sim}{p} = m\ \underset{\sim}{v} \qquad \ldots \qquad .4.6$$

where

m = projectile mass

$\underset{\sim}{v}$ = velocity of projectile relative to target

From Newton's Third Law $- \underset{\sim}{F} = m\ \underset{\sim}{a}$ . . 4.7

so the impulse given to the target is equal to the change in linear momentum

$$\underset{\sim}{F} \,.\, \delta t = \delta \underset{\sim}{p} \qquad \ldots \quad 4.8$$

An impact between the projectile and target will produce several effects (see Figure 4.3).

1. The two bodies will either coalesce or else continue in motion separately. Linear momentum will be conserved.
2. There will be a change in the spin of the bodies after the impact from conversion of angular momentum associated with the parallel component of the impact parameter. (This is basically the longitude of the impact on the asteroid)
3. There will be a change in the orientation of the angular momentum vector. This results from the perpendicular component of the impact parameter (the latitude of the impact). Previous models have calculated the resultant vector assuming that it is derived by vector addition of the two perpendicular components (see Figure 4.4).

The change in orientation is given by

$$\delta\phi = \delta p / L_o \qquad \ldots\ldots \quad 4.9$$

The total angular momentum of the system will be conserved.

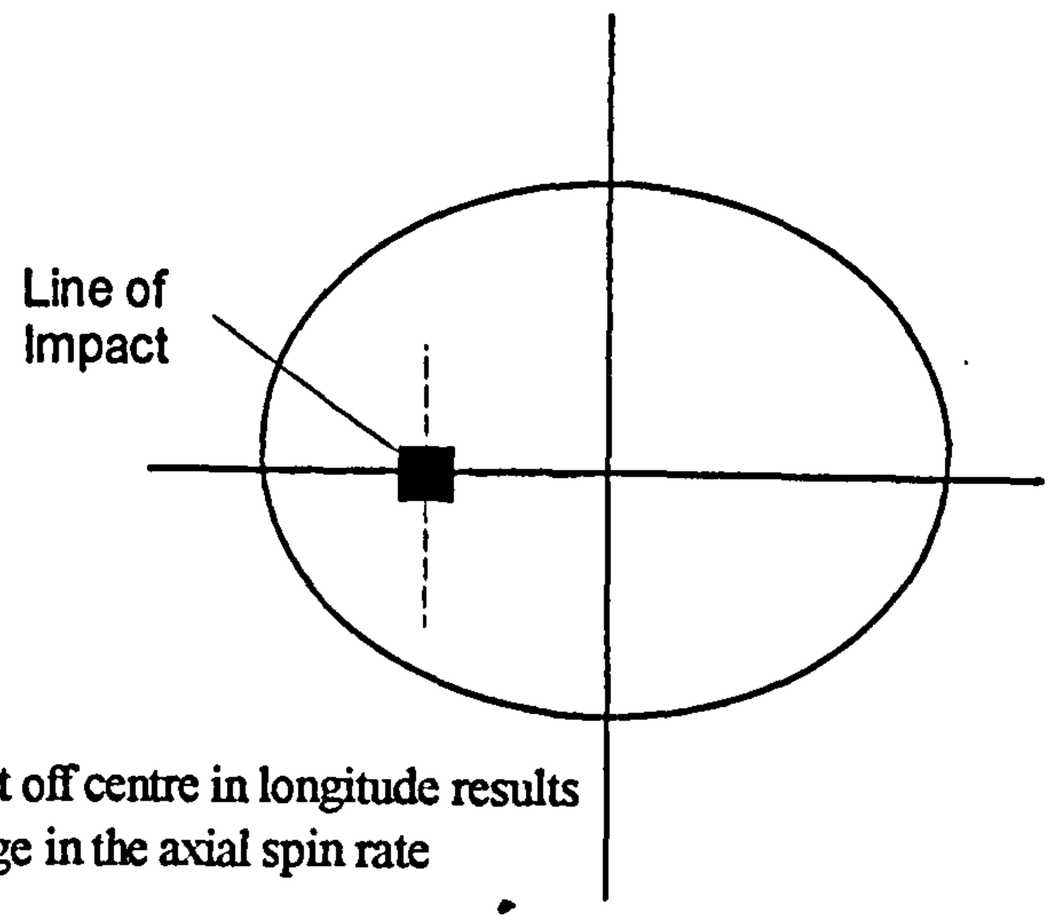

a) Impact off centre in longitude results in a change in the axial spin rate

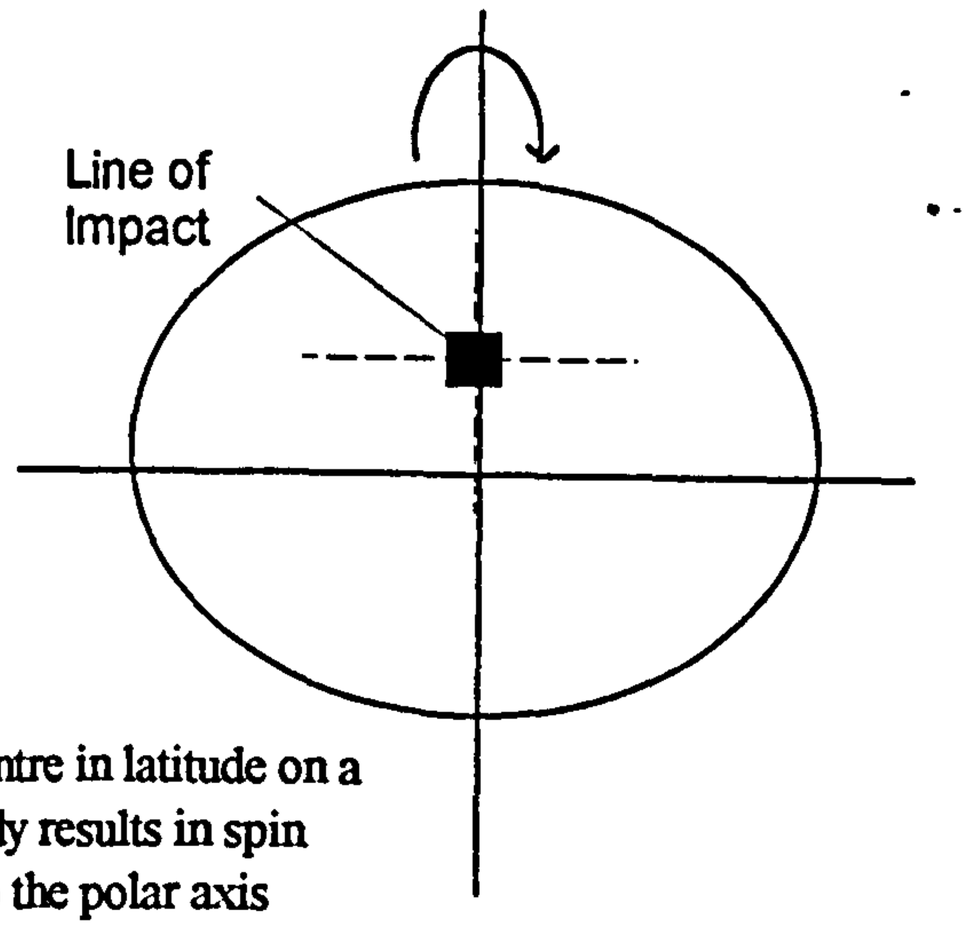

b) Impact off centre in latitude on a non-rotating body results in spin perpendicular to the polar axis

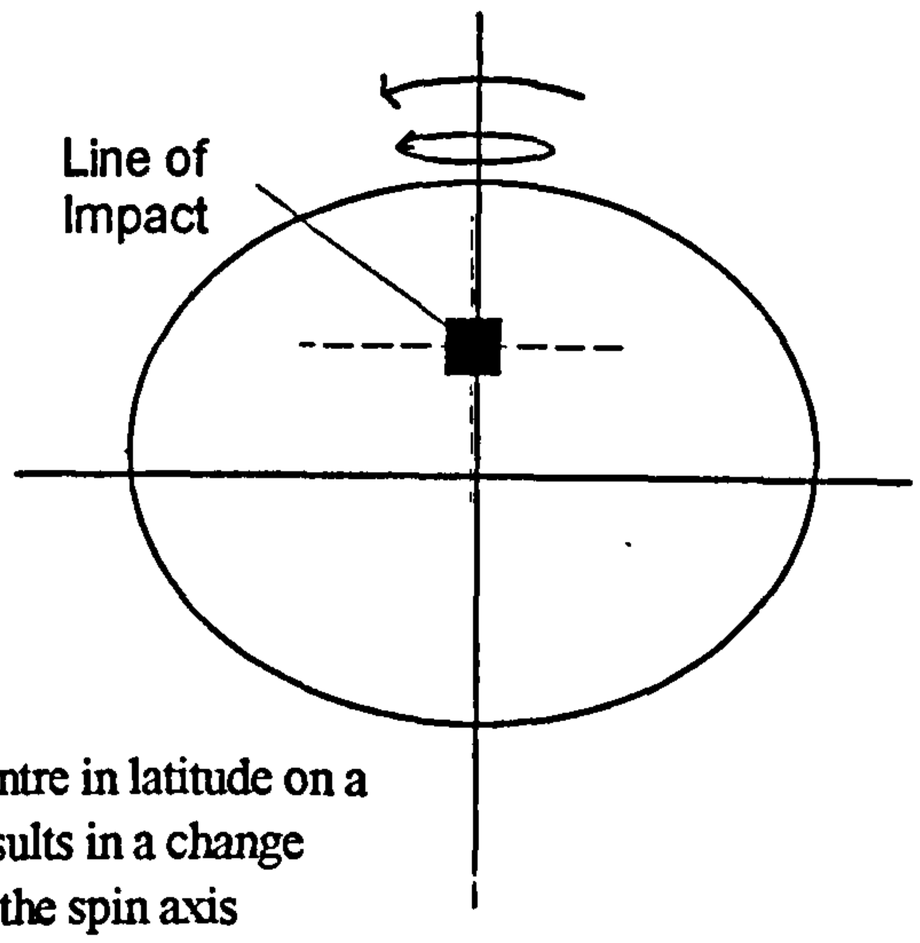

c) Impact off centre in latitude on a rotating body results in a change in orientation of the spin axis

Figure 4.2 - The effect of projectile collisions on target asteroids

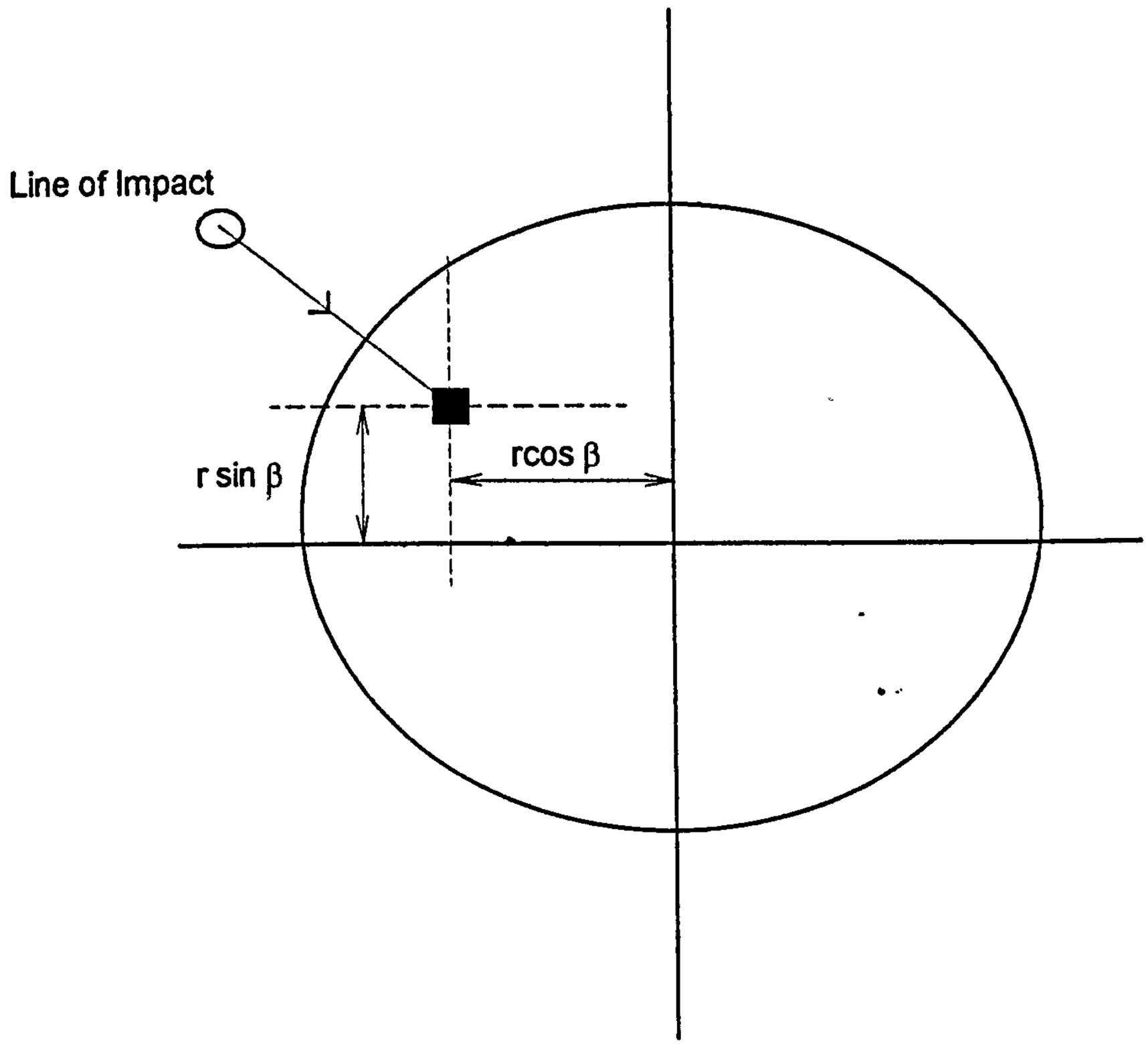

r cos β - longitude impact parameter

r sin β - latitude impact parameter

Figure 4.3 - Geometry of projectile/target interaction

For simple rotation the Angular Momentum Vector, **L**, and the spin vector, ω, align with the z axis

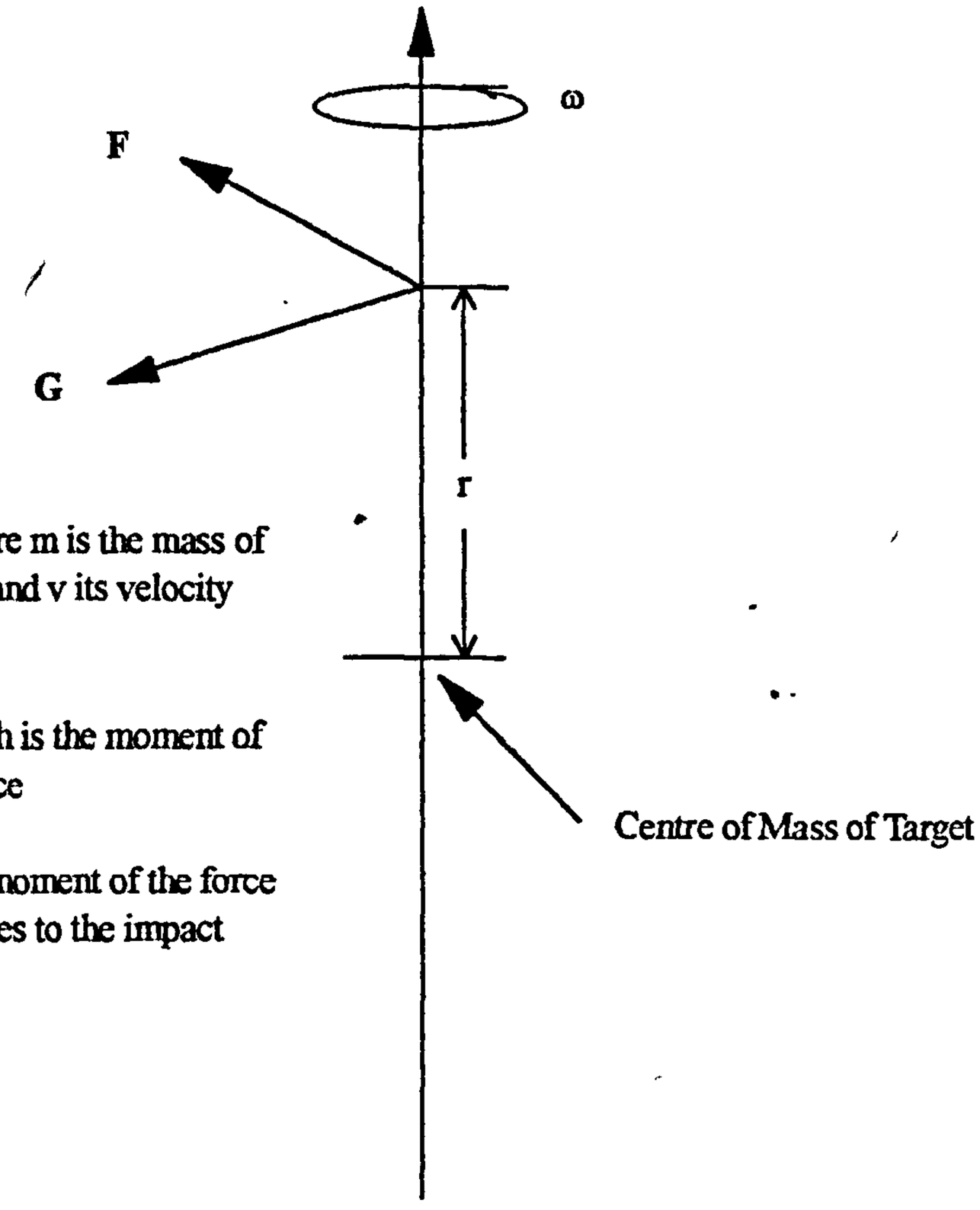

$\mathbf{F} = m\,\mathbf{v}$ where m is the mass of the projectile and v its velocity

$\mathbf{G} = \mathbf{r} \wedge \mathbf{v}$ which is the moment of the impact force

Note that the moment of the force is at right angles to the impact force.

Figure 4.4 - The vector geometry of projectile collision with a rotating asteroid

4.4 Free-Precession

For a non-rigid body - i.e. an asteroid - the change in the orientation of the angular momentum vector (L) will occur virtually instantaneously. Flexure within the body allows the direction of Z_p to remain constant. The direction of the angular velocity vector will also change. There will therefore be a coning motion such that Z_p and the angular velocity vector precess about L. By this means angular momentum is conserved. Energy dissipation within the body, caused by flexure, will result in a reduction of the coning angle and the orientation of Z_p and the angular velocity vector will realign with the orientation of L in the timescales indicated above. [Space platforms make use of special dampers to ensure that this re-alignment occurs in very short timescales - a description of the dampers used on the Giotto mission is given by Fertig, Marc and Schoenmaekers (1988).]

If the new body is altered by the accretion such that the axis of symmetry and the principal inertial axis do not align then a 'wobble' in the rotation is introduced. Impact melting and the spread of ejecta across the surface of the target will minimise this effect. Rubble pile or pseudo-fluid bodies will re-adjust their shapes in very short timescales, this may not occur with rigid bodies and it is possible that a modulation of the light curve due to this effect might be detectable. The amplitude of such a modulation will probably be less than 1% and as such it is unlikely to be detectable by earth based observatories. This is shown to be the case later in this work.

Simple models assume the shape of the minor bodies in the Solar System are triaxial ellipsoids. Though those bodies observed directly are not true ellipsoids they can be approximated to such shapes for theoretical studies. Most models assume that there is an axis of symmetry such that two of the moments of Inertia of the body are equal. Whilst this is only true for spheroidal bodies observation suggests that most of the minor bodies have two dimensions which differ by less than 10%. This is a sufficiently close approximation for the models in use at present. The assumption that the bodies perform as though they are rigid is valid only for consideration of the final aligned, e.g. damped case.

Light curves measured from Earth are consistent with the conclusion that the spin of asteroids can be considered in terms of pure axial rotation. If the spin vector is not aligned with the angular momentum vector, precession of the spin vector about the angular momentum vector occurs. In the absence of an external torque the precession is termed free precession. The frequencies for a spheroidal body can be described by

$$\Omega = (I_s/I - 1) . \omega . \cos \alpha \quad .. \ 4.10$$

(from Fowles 1981)

where Ω = rate of precession of the angular velocity vector about the axis of symmetry

$I_s = I_{zz}$ the moment of inertia about the symmetry axis

$I = I_{xx} = I_{yy}$ moment of inertia about the axes normal to the symmetry axis

ω = angular speed

α = the angle between the symmetry axis and the axis of rotation

The remaining expression to describe the orientation of the axes is

$$\tan\theta = I/I_s * \tan\alpha \qquad \ldots 4.11$$

where

θ is the angle between the angular momentum vector and the symmetry axis (Fowles 1981)

It can be seen that following an impact the spin vector does not remain aligned with the symmetry axis (see Figure 4,1). For asteroid shapes, the ratio I/I_s lies typically in the range of 0.3 to 3. This implies that for values of α close to 0° and 90° θ is approximately equal to α. For mid range values they can differ appreciably. This is considered further in Chapter 6.

5. The Collisional Evolution of Spin Frequency and Orientation of the Angular Momentum Vector during the accretion phase of asteroid evolution

Abstract

In this chapter the collision model derived earlier is applied to accretion by asteroids. When the observed spin frequency distribution of the asteroids is modelled it is shown that the spin axes of the asteroids should be aligned randomly. Though the number of known orientations of the axes of real asteroids is small, the calculated result appears to be in line with observation.

5.1 Review of Previous Models

The accretion of planetesimals to form larger bodies has been considered extensively (e.g. Wetherill 1989 and Ruzmaikina et al. 1989). During the early stages of accretion encounter velocities are low, since all orbits are similar, ~1 km/sec and accretion occurs with little shock modification to the target (Hartmann 1978). However the encounter velocity is pumped up, by gravitational interaction, to a value ~5 km/sec during the early stages as near misses modify the orbits of planetesimals. Later in the evolutionary process high velocity impacts between similar sized bodies occur and the subsequent fragmentation becomes a dominant factor and this is considered in 5.4.

The angular momentum of the projectile is added to the angular momentum of the target since angular momentum is conserved. The typical size of planetesimals is ~ (1 - 5) km (Goldreich and Ward 1973). At the later encounter velocities the orbital angular momentum (i.e. "translational") of the projectile is of the order of 10^3 that of the rotational angular momentum. It is thus a reasonable simplification to ignore the effect of rotation of the projectile.

Collisional models for the evolution of spin frequency have been developed to simulate the observed spin frequency distribution of the asteroids. The basic model (Harris 1979) uses projectiles selected at random to alter the angular momentum of the target. In these models the impact produces two results. The impact parameter - i.e. the impact longitude - serves to either speed up or reduce the spin frequency depending on the sense of the impact. The second result depends on the latitude of the impact. In the current implementations, which have been developed from that of Harris, the resultant momentum is treated as the vector sum of the two components and the net effect of this is always to increase the spin frequency (i.e. to speed up rotation). Increasing the spin frequency will ultimately lead to disruption of the target once the equatorial rotation stress reaches its Ultimate Tensile Stress. To prevent this end result, the model has been modified to allow angular momentum to be removed from the target by ejecta loss (Dobrovolskis and Burns 1984). Ejecta loss occurs when its velocity

exceeds the escape velocity of the target, the velocity of the ejecta is greater in the direction of rotation of the asteroid since velocities are added. A modified version of this model is used by Binzel (1986).

The orbital angular momentum of the projectile is considered as a linear momentum in current modelling of projectile/target interaction. Davis et al (1989) in their model consider that only a portion of the projectile's momentum modifies the angular momentum vector of the target. They use the experimental results of Fujiwara et al (1989) which showed that this proportion (the Transfer coefficient) is between 0.01 to 0.3.

5.2 A Revised Model

In Chapter 4 consideration was given to explaining projectile/target interaction in terms of gyroscopics. The use of this is developed further below when a simplified model of the accretion growth of asteroid is used to calculate the expected spin frequency and spin-axis orientation distribution. The objective of this exercise is to show the anticipated distribution of the spin orientation when the observed spin frequency distribution is modelled.

1. Assumptions

In this model the perpendicular component is considered as acting to modify the orientation of the angular momentum vector (Figure 5.1).

Several simplifications were accepted. Given the limited computing power available the aim was to illustrate effects rather than to provide quantitative solutions. Assumptions a, b, and c have been introduced to simplify and speed computation. Assumption d is made since only major catastrophic impacts will produce significant mass loss - smaller impacts will disturb material which will eventually return to the target under gravity. Assumption e has been introduced since in this model short term free-precessional effects are not a major item. The aim of this model is to illustrate that a random orientation of spin axes is to be expected if collision has been a factor in the evolution of the asteroid belt. For spherical homogeneous bodies precession is not detectable and so need not be considered (see Chapter 6).

a. All projectiles come from a single 180 degree sector

This assumption allows for a spread of impact angles but only from bodies in direct orbits. A projectile in a retrograde orbit is not allowed. This assumption is reasonable as the early rotating gas cloud will spin in a single direction - this is analogous to the rotation of the bath water round the plug hole. Assuming that the gas cloud has laminar flow prior to condensation then each particle will rotate about the centre of mass in the same sense. Retrograde orbits would be unstable as any body would be subject to perturbations from the major planets which would serve to modify the orbits such

Q_{change} is the change in orientation of the Target due to the latitudinal component of the Projectile impact

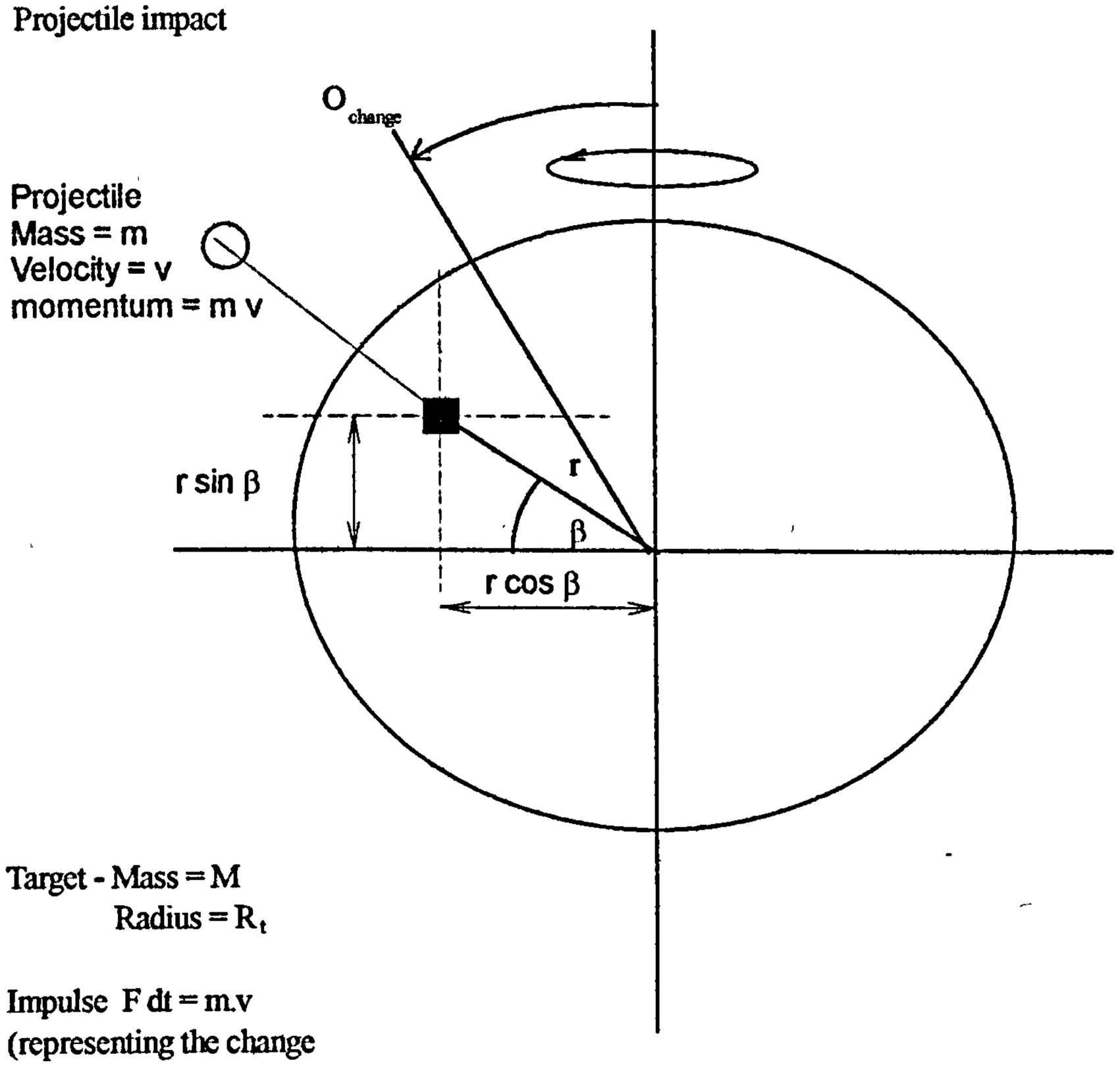

Target - Mass = M
Radius = R_t

Impulse F dt = m.v
(representing the change in linear momentum of the projectile)

r cos β is the latitudinal impact parameter which causes a change in the orientation of the spin axis

r sin β is the longitudinal impact parameter which causes a change in the axial spin rate

Figure 5.1 - Geometry of projectile/target interaction used in equations 5.1 and 5.3

that a collision with a body would occur or it would have its orbit modified to a more stable prograde orbit would result or else the body would be ejected from the Solar System.

b. All modifications to the orientation occur in the plane containing the Sun and Asteroid.

The nett effect of this is that model changes in orientation are only considered in a single plane at right angles to the assumed projectile approach direction. This will produce a greater reorientation than is likely to occur in practice. The target asteroid will usually either approach or be overtaken by a projectile in a similar orbit. In a real impact the range of angles at which the collision occurs could in individual cases deviate from this considerably, however the majority of impacts will occur at the assumed angle as most of the planetesimals will travel in similar orbits of low eccentricity at the early stages of accretion. However as shown by Hoyle (1978) during the later stages of evolution the range of eccentricities of orbits can be large which would render this assumption questionable as and the direction of approach can differ significantly from "head-on". It is shown later that as asteroids accrete, the spin axis modification due to an individual impact reduces.

c. Each trial run uses impacts by projectiles of a single mass

This simplification was accepted again as the objective of this study is to identify trends and not provide a definitive solution which models the true evolution. The mass of the projectile is defined in terms of a fraction of the initial mass of the target.

d. The projectile and target coalesce and there is no significant mass loss.

This is a simplification which should be valid for non-disruptive impacts. Since the observed asteroids are discrete bodies they either represent non-disrupted bodies or else fragments of previously larger bodies. To have mass loss, sufficient energy input is required to disperse fragments to infinity. Less input energy will mean that, with the passage of time, gravity will result in a recombination of the fragments. The target mass is reinitialised to include the mass of the projectile prior to the next impact. A simplified version of planet growth is modelled and as disruptive fragmentation is not considered this scenario is only applicable to the early stages of the evolution of the asteroids..

e. The effects of short term misalignments of the orientation of the angular momentum vector, the angular velocity vector and the direction of the minor axis of the spheroid are not considered.

This assumption implies that the body relaxes to the state where the orientations have aligned. This occurs instantaneously for a rigid body but can take long periods for semi-rigid and fluid bodies (as considered in Chapter 1).

2. Starting Parameters

Target Initial Conditions (assumed)

Radius	12.5 km
Density	3000 kg m^{-3}
Spin Frequency	3 day^{-1}
ω	0.000218 radians sec^{-1}
Angular Momentum Vector Alignment (taken as perpendicular to the invariable plane)	0 radians
I	$0.4 * M * R^2$
L	$I \omega$

Projectile Initial Conditions

Mean Velocity of Impact	5 km sec^{-1}
SD of Mean	0.5 km sec^{-1} (Normal Distribution assumed)

These values are derived from Ip (1977). Bottke et al (1994) re-examined this distribution. They find that though the mean value given above is reasonable it is raised by a relatively few high velocity collisions such that the *most likely* collision velocity is 4.4 Km/sec. The higher mean velocity and standard deviation have been retained as the results can then be related to those derived by Binzel and Harris. The mass proportion and the total number of projectiles used in each simulation are selected by the user.

3. Impact Effects

In this model the target is considered to possess both translational and rotational energy in a heliocentric coordinate system. The projectile is assumed to have only linear (the rotational energy of small bodies is significantly smaller than the translational energy at the relative velocities considered $<10^{-3}$).

The bodies are both in orbit around the Sun. They therefore have angular momentum both by virtue of their orbital motion and their axial rotation. In this model, since we are only concerned with the instant of collision and the resultant spin, the orbital angular momentum is considered in terms of

linear momentum. The translation portion is not considered further. The portion which results in a change of rotation momentum for the target is expressed as a transfer factor multiplied by the linear momentum and the impact parameter. The last two have dimensions MLT^{-1} and L and so have the same dimensions as angular momentum.

$$L_{imp} = \zeta \; m \; v \; s \qquad \ldots. \; (5.1)$$

where L_{imp} = Angular momentum transferred

ζ = Transfer Efficiency

v = Relative Velocity of impact

s = Impact Parameter ($R \cos(\theta)$)

$$\zeta = f \,.\, \cos^{h}(\theta) \qquad \ldots. \; (5.2)$$

where h = this index is a parameter determined experimentally

θ = Impact angle to the surface of the asteroid at the point of impact

f = Partition factor between orbital and rotational angular momentum. The value of this factor is determined by comparison between calculated values and the observed spin frequency distribution.

ζ has been determined experimentally by Fujiwara and Tsukamoto (1981) who determined that for impact angles of 60° ζ was 0.1 and hence h ~3. Schultz and Gault (1986) determined a value of 0.1 for ζ at impact angles of 75° implying that h ~1.7. A value of 1.7 has been used in this study and this value is confirmed by Yanagisawa et al (1991).

The factor f has been introduced in this study to make allowance for the transfer of orbital momentum from the projectile to rotational momentum of the resultant body. For fully rigid bodies with no internal friction this factor would be very small. The net result of a collision would be a pure transfer of orbital momentum. Nett rotational momentum arising from orbital momentum would tend to cancel as the projectile and target would each acquire rotational angular momentum of an equal value but in opposite senses, if coallescence occurs then these will cancel. For viscous fluid bodies the value of f would tend to 1 and virtually the whole value of the angular momentum of the projectile would be converted to rotational angular momentum in the system. The effect of changing the value of f is considered later in this study. A default value of 0.05 (implying a relatively rigid target) is found to produce a satisfactory model though this is an order of magnitude lower than the experimental value derived by Yanagisawa et al.

The parallel component of L_{imp} is added to L_o (the original angular momentum of the target) and the new spin frequency determined from this value and new mass (target plus projectile), radius etc.

The perpendicular component of L_{imp} is used to determine the change in the orientation of the target angular momentum vector

$$\theta_{change} = \tan^{-1}(\zeta \,.\, M_p \,.\, V_p \,.\, R_t \,.\, \sin(\beta)/L_{o)} \quad ...(5.3)$$

where θ_{change} = the change in target orientation of the angular momentum vector in radians

M_p = Projectile Mass

V_p = Projectile Velocity

$R_t.\sin(\beta)$ = Perpendicular impact parameter

L_o = Existing Angular Momentum of the target body

R_t = Target radius

5.3 Results and Discussion

The test for the model was that the results should, as far as possible, be similar to the observed spin frequency distribution. The sample of 505 real bodies given in the Asteroids II database gives the following result for the spin frequency (day^{-1}).

Max	Min	Mean	SD
10.5580	0.0209	2.778	1.678
(1566)	(288)		

Histograms of the data are given by Binzel et al (1989) which illustrate the sharp peaks in the distribution. These do not easily fit a simple distribution function and so the meaning of the SD is problematic. As the data set is relatively small when compared to the total population it is possible that the data is biassed by selection effects. The most probable value of the histogram set is 1.25 revolutions per day though the sample size is small and any value between 1.25 and 3.25 couls be realistic. More realistic is the value of the best fit Maxwellian distribution derived by Binzel which yields a probable value of approximately 2.2 revolutions per day.

Three exercises were carried out to investigate suitable values for the transfer efficiency and the projectile size to use. The results are summarised in Tables 5.1 to 5.3 and the accompanying graphs.

Table 5.1 (see Figure 5.2) The effect of single impacts to targets different starting mass ratios

Starting Conditions

Transfer Efficiency	.02	$[\cos(\theta)]^h$
Initial Target Spin Frequency	3	revs day^{-1}
Initial Orientation	0	radians
Number of Projectile Impacts	1	
Mass Proportion of Projectile	varies	
Number of Cases for each distribution	4000	

Spin Frequency

Log_{10} Mass Proportion	Mean	SD	Max	Min	Absolute Values Max	Min
-1	2.9609	3.831	15.301	-9.771	3.9479	2.803
-2	2.991702	.38834	4.249	1.796		
-3	2.998275	.038714	3.124	2.873		
-4	2.997756	.003806	3.010	2.984		
-5	2.997717	.000388	2.999	2.997		
-6	2.997716	.000037	2.9978	2.9976		
-7	2.997718	.000004	2.99773	2.99770		

Angular Momentum Vector Orientation

Log_{10} Mass Proportion	Mean	SD	Max	Min	Absolute Values Mean	SD
-1	0.0200	1.1296	1.4840	-1.4805	1.0560	0.4024
-2	-0.0029	0.3602	0.8081	-0.8097	0.2958	0.2057
-3	0.0000	0.0393	0.1014	-0.1066	0.0313	0.0237
-4	0.0000	0.0040	0.0112	-0.0104	0.0032	0.0024
-5	0.0000	0.0004	0.0011	-0.0011	0.0003	0.0002
-6	0.0000	0.0001	0.0001	-0.0001	0.0000	0.0000
-7	0.0000	0.0000	0.0000	0.0000	0.0000	0.0000

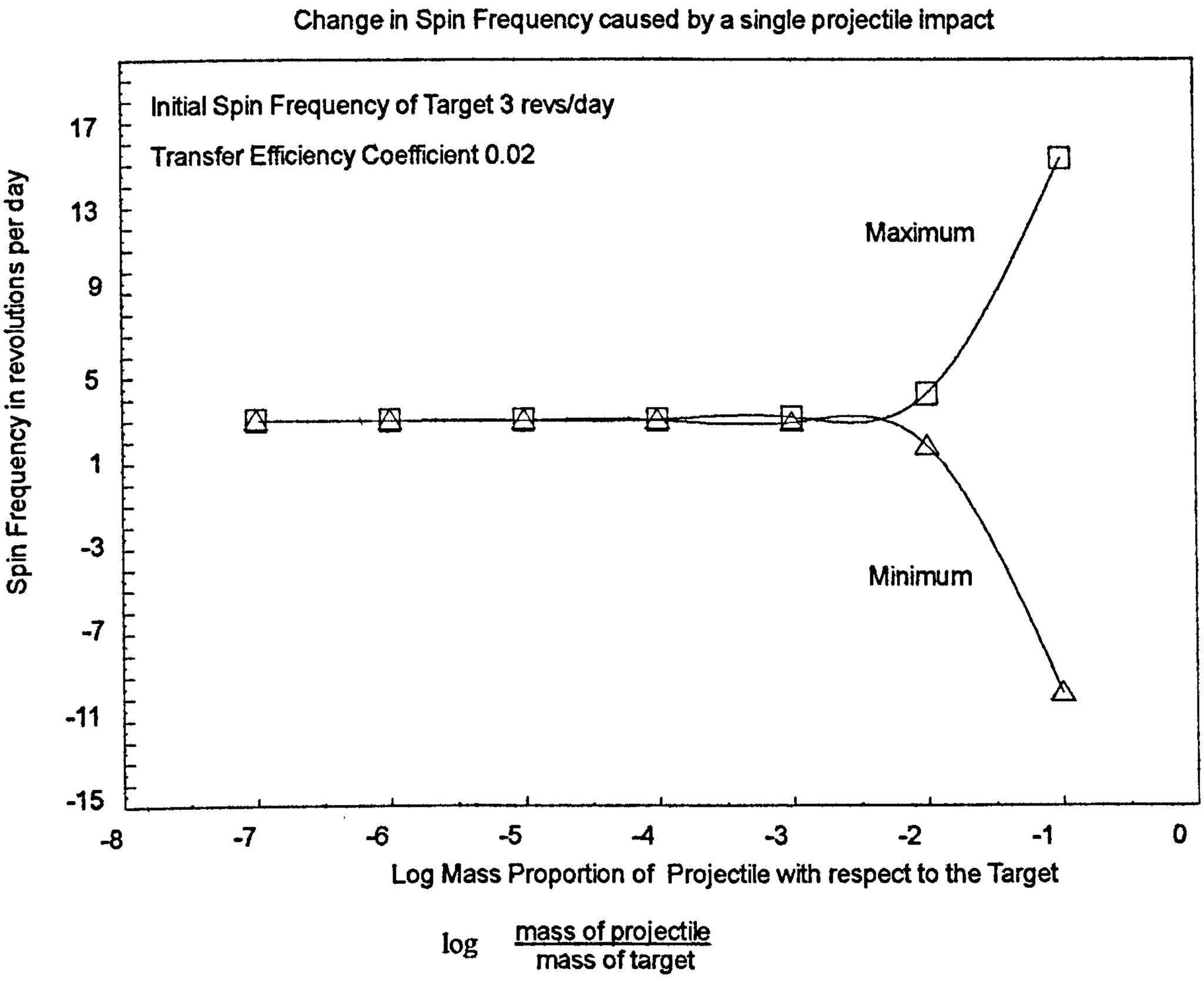

Figure 5.2 - Plot of the maximum and minimum spin frequencies generated by a single projectile impact on a target asteroid initially with a spin frequency of 3 revs/day. 4000 individual cases were calculated for each mass fraction of projectile. A momentum transfer efficiency of 0.02 $(\cos\theta)^h$ has been used (see text) The mean spin frequency after the impact is given in Table 5.1 ($\approx$2.99revs/day)

Table 5.2 (see Figure 5.3) The effect of single impacts to targets different starting mass ratios

Transfer Efficiency	0.05 $(\cos(\theta))^h$
Initial Spin Frequency	3 revs day^{-1}
Initial Orientation	0 radians
Number of Impacts	1
Mass Fraction of Projectile	Varies
Number of Cases for each distribution	4000

Spin Frequency

Log_{10} Mass Proportion	Mean	SD	Max,	Min	Absolute Values Mean	SD
-1	3.0350	2.6307	35.4671	-27.3920	7.8186	3.3900
-2	3.0121	0.9572	3.2139	-0.0717	3.0122	0.9571
-3	2.9960	0.0964	3.3081	2.6962		
-4	2.9976	0.0095	3.0279	2.9661		
-5	2.9977	0.0010	3.0007	2.9947		
-6	2.9977	0.0001	2.9980	2.9974		
-7	2.9977	0.0000	2.9978	2.9977		

Angular Momentum Vector Orientation

Log_{10} Mass Proportion	Mean	SD	Max	Min	Absolute Values Mean	SD
-1	-0.0219	1.3176	1.5361	-1.5318	1.2709	0.3485
-2	-0.0072	0.6731	1.1911	-1.2151	0.5804	0.3409
-3	-0.0018	0.0989	0.2488	-0.2742	0.0791	0.0593
-4	-0.0006	0.0101	0.0266	-0.0260	0.0081	0.0061
-5	0.0000	0.0010	0.0027	-0.0027	0.0008	0.0006
-6	0.0000	0.0001	0.0003	-0.0003	0.0001	0.0001
-7	0.0000	0.0000	0.0000	0.0000	0.0000	0.0000

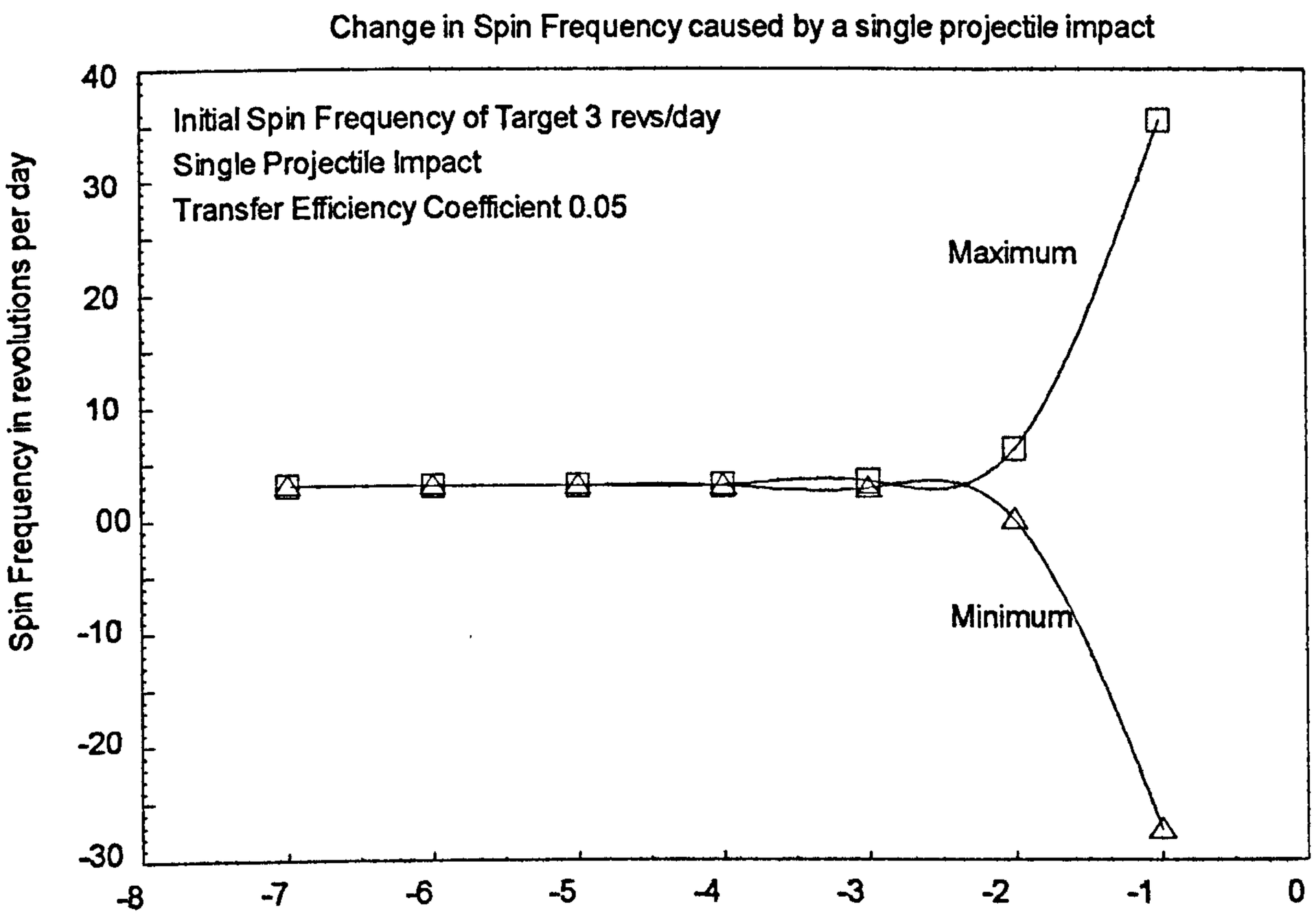

Figure 5.3 - Plot of the maximum and minimum spin frequencies generated by a single projectile impact on a target asteroid initially with a spin frequency of 3 revs/day. 4000 individual cases were calculated for each mass fraction of projectile. A momentum transfer efficiency of 0.05 (cos θ)^h has been used The mean spin frequency after the impact is given in Table 5.2 (~3.00revs/day)

Table 5.3 (see Figures 5.4 and 5.5) The effect of different values of the transfer factor

Transfer Efficiency		Factor * $(\cos(\theta))^h$	
Initial Spin Frequency		3 revs/day	
Initial Orientation		0 radians	
Mass Fraction of Projectile		0.01	
Number of Impacts	200	Number of Targets tested	200
Initial Target Mass	M	Final Target Mass	3 M
			[M (1 + 200 x 0.001]

Spin Frequency

Transfer Factor	Mean	SD	Max	Min	Absolute Values Mean	SD
0.0005	0.4810	0.0270	0.5660	0.4110		
0.001	0.4860	0.0530	0.6256	0.3507		
0.002	0.4940	0.1090	0.7620	0.1733		
0.005	0.4700	0.2680	1.1523	-0.2039	0.4709	0.9528
0.01	0.5160	0.5570	2.6603	-0.8314	0.6220	0.4431
0.02	0.5250	1.1970	3.2926	-2.5371	1.0900	0.7246
0.05	0.1380	2.4200	3.1630	-8.9810	1.8580	1.4836
0.1	0.9540	3.1120	19.1874	-21.9316	4.8790	3.7684
0.2	0.6883	10.9190	28.0840	-30.9170	8.4409	3.9277
0.5	-1.2020	28.3580	93.6007	-68.9731	22.2601	17.1732
1.0	0.4210	53.8350	170.3020	-162.3020	44.4153	33.2319

Angular Momentum Vector Orientation

Transfer Factor	Mean	SD	Max	Min	Absolute Values Mean	SD
0.0005	-0.0050	0.1660	0.3880	-0.4070	0.1340	0.0960
0.001	-0.0099	0.3560	0.8821	-1.1045	0.2830	0.2200
0.002	0.0310	0.7460	2.1940	-1.8380	0.5883	0.4649
0.005	-0.3820	2.8330	7.3200	-15.7700	1.9916	2.0777
0.01	0.1880	5.2700	20.0480	-20.5950	3.7207	3.7367
0.02	0.7970	7.6560	25.3276	-22.3795	5.5484	5.3025
0.05	0.7870	9.6350	37.1169	-35.2189	7.3965	3.3156
0.1	0.5780	9.6000	30.1812	-25.0467	7.3705	3.2912
0.2	-0.4992	8.5981	22.2340	-29.7570	3.8271	5.2663
0.5	-0.2600	9.7780	24.6346	-30.8537	7.7996	3.0106
1	-0.2050	9.4960	30.7986	-23.0811	7.5456	5.8197

From Tables 5.1 and 5.2, where only a single projectile impact is considered, it can be seen that a reasonable approximation to the observed spin frequency and standard deviation of the observation sample is given when the mass of the projectile is in the range 0.1 to 0.01 times the initial mass of the target. Table 5.3 supports a view that the efficiency of transfer of angular momentum from the projectile to the target is of the order of 0.05 * $(\cos(\theta))^h$ to give the required observed standard

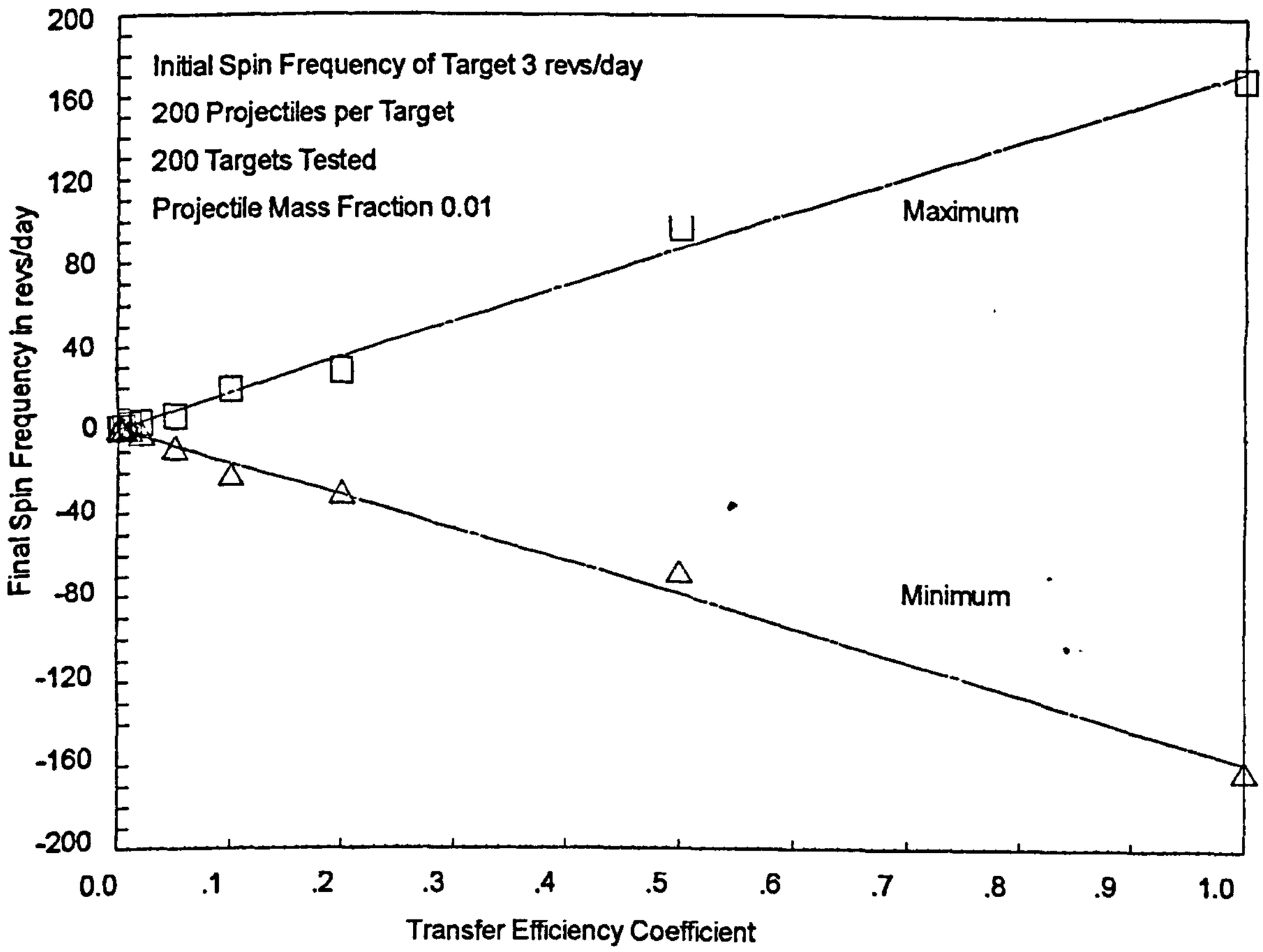

Figure 5.4 - Plot of the maximum and minimum spin frequencies generated by 200 projectile impacts on a target asteroid initially with a spin frequency of 3 revs/day. 200 individual cases were calculated for a mass fraction of projectile equal to 0.01. A momentum transfer efficiency of x (cos q)^h has been used and the value of x is plotted on the x-axis

deviation and this is therefore the value adopted for the remaining calculations in this Chapter. It should be remembered that the tabulated results of observations do not distinguish between prograde or retrograde rotation and that the absolute values from the calculations therefore have to be used in any comparison with the observed distribution. The maximum and minimum values derived are also similar to those known from observation which was a prerequisite of the exercise. Calculations by Weidenschilling (1981) suggest that the strength of materials which make up asteroids will not allow a higher spin frequency than about 12 revs/day without disruption. Exact modelling of the observed values is not to be expected from this exercise due to the generalised assumptions made earlier.

The effect on the orientation of the angular momentum vector is dramatic. Values of $2*\pi$ or greater are easily generated. Indeed it can be seen that the primary modification to an accreting asteroid is to the direction of the angular momentum vector. The damping time for realignment of the spin axis with the angular momentum vector has been considered in earlier chapters.

5.3.1 Accretion

As an additional check a series of calculations was performed to follow the growth of asteroids by accretion. The projectiles chosen were single sized and 0.01 times the initial mass of the target. The growth of the target from an initial mass of M to 2M, 5M and 10M is summarised in Table 5.4. It is seen that the spin frequency is substantially modified about the mean during the early stages of accretion but that as the target grows the effect of the projectile momentum diminishes as the addition of mass becomes the significant factor involved. The result is that as the target grows the mean spin frequency diminishes and so do the maximum and minimum values. Real asteroids will not mimic this result exactly as the mass of successive individual projectiles will vary in accordance with the distribution of bodies in the accretion zone. In the model considered here, the projectiles are single sizedwhich means initially they have a mass fraction of 0.01 which reduces in the final stage to a fraction of 0.001.

It has been suggested that the observed rotation rates of asteroids are indicative of initial conditions at the time of the formation of planetesimals. The calculation of the growth of targets suggests that the mean observed spin frequencies are probably lower than those of the original planetesimals due to the nett spin down as mass accumulates. [Pulsars on the other hand tend to spin up by accretion, this can be explained as material spirals in to the star from a single preferred direction aligned with its equator. Conservation of angular momentum will speed up rotation of the pulsar (in the same way as the spinning ice skater illustrates the rule).]

The orientation results obtained here suggest that any sample of asteroids should have angular momenta directed randomly in space. Few polar orientations have been determined and even fewer of

these are known reliably. However the indications given by Magnusson (1989) are that the polar axes known are aligned at random.

Table 5.4

Initial Spin Frequency	3 revs day^{-1}
Initial Orientation	0 radians
Mass Fraction of Projectile	0.01
Number of Targets tested	4000 (due to computer memory restrictions only 200 targets were calculated for 100M case)

Spin Frequency

Final Mass	No of Projectiles	Mean	SD	Max	Min	Absolute Values Mean	SD
2M	100	0.9420	3.5468	11.8772	-13.1016	2.9226	2.2193
5M	400	0.1616	1.9154	7.0886	-3.9287	1.5350	1.1570
10M	900	0.1050	1.0890	4.1689	-3.9185	0.8688	0.6648
100M	9900	-0.0148	0.1428	0.3643	-0.3825	0.1177	0.0822

Angular Momentum Vector Orientation

Final Mass	Projectile Number	Mean	SD	Maximum	Minimum	Absolute Values Mean	SD
2M	100	-0.0394	3.8706	30.9021	-25.9785	5.2292	4.4567
5M	400	0.0674	11.4566	54.1347	-50.6006	8.7391	7.4086
10M	900	-0.2898	15.1051	95.7305	-72.6782	11.5060	9.7908
100M	9900	0.9884	31.1450	113.0730	87.5764	22.6294	21.4219

A plot of the observed spin frequency vs diameter is given by Binzel et al (1989). This illustrates a trend to despinning of asteroids as the mass increases. However they also present running mean plots which illustrate that mean spin frequency increases with diameter for asteroids greater than ~150 km diameter. The sample of large asteroids is small and probably complete, however smaller asteroids show a selection effect - the sample is biased. Asteroids which appear bright have a more complete sample than those which are faint. The sample therefore is incomplete for smaller asteroids which are of low albedo or distant (or both). In addition observers have tended to avoid asteroids which have a low amplitude (where the measurement errors could be as great or greater than the amplitude) or long rotation periods (where light curve features may not be discernable during an observing run) because

of the difficulty in obtaining meaningful results. It is likely that the sample of real asteroids in each size category is too small for precise quantification.

The calculations indicate that spin frequencies as low as 0.01 revs per day occur and there is no mathematical reason why this value should not be even lower. Asteroids with low spin frequencies are known but the sample is probably incomplete for the reasons indicated above.

During the damping time, for alignment of the angular momentum vector and the angular velocity vector, precession occurs. A secondary light curve component will be present at the precession frequency. This is examined further later in this work.

An examination of the published values given in the Asteroids II Database indicates that the derived values of the orientation of the spin axes of individual asteroids seem to vary randomly with time. Though this could be a real effect due to precession it more likely represents uncertainties in the observations. Calculation using this model suggests that the angular momentum axes should be aligned at random. This probability is not ruled out by the published data.

Summarising the effect of accretion the following conclusions can be drawn.

a) Large projectiles (>0.1 target mass) modify the spin frequency and tend to cause spin-up (possibly retrograde).

b) Small projectiles (<0.005 target mass) add mass not angular momentum (L) and tend to reduce spin frequency.

c) Considering the target as a gyroscope eliminates the need to hypothesise additional mechanisms to carry away surplus angular momentum as the perpendicular component of the impact parameter modifies the direction of the angular momentum vector and is not "used" to increase the value of the spin vector.

d) Angular momentum vectors (and spin axis vectors of damped asteroids) are oriented at random. The current alignment is therefore unlikely to provide information about the preferred alignment during the early Solar System.

Using the model presented here no additional mechanisms are required to dispose of surplus or shortfalls of angular momentum. The angular momentum drain mechanism of Dobrovolskis and Burns is no longer essential to prevent spin-up as in previous models. The effect must occur but to a much less significant level than required by the Harris model (where it is crucial) and it only reduces the extremes of spin frequency observed to a small degree. A more thorough investigation of the effects of transfer efficiency and projectile mass will allow computation of a more precise match to the existing mass/spin frequency/angular momentum orientation.

5.4 Fragmentation as an Evolutionary Process

In the earlier part of this chapter consideration is given to accretion as a process for evolving observed asteroid spin rates and axial inclinations. The model given assumes that near 100% accretion occurs with no fragmentation effects. However as has been pointed out recently (eg Hughes 1994) collisions also serve to break down asteroid sized bodies.

Two effects can be considered in terms of fragmentation depending on the amount of energy involved in the impact. The simplest effect is the fragmentation of the target without mass loss. Disruption occurs when the input energy density exceeds the impact strength of the asteroid (Fujiwara et al. 1977).

$$E_k > S\,V_o$$

where E_k is the energy input
S is the impact strength
V_o is the target volume

This is the material strength of the asteroid and it is therefore independent of the spin characteristics. Fujiwara et al indicate that for asteroid materials (such as basalt) S is of the order of 10^6 to 10^7 Joules/ cu m. Energy is lost in vaporisation of projectile and target materials and in ejecta. O'Keefe and Ahrens (1977) suggest that 10% is lost to ejecta in vertical impacts with the proportion rising proportionally to the sixth power of the sine of the impact angle.

A greater energy budget is required to totally disrupt an asteroid. The energy must not only fragment the asteroid but also, to prevent reassemblage, send the fragments to infinity. The latter requires input of energy up to the total gravitational potential energy of the asteroid which is given by Cole (1984) as

$$E_g = -(\gamma_g * G * M_p^2) / R_p \qquad \ldots\ 5.5$$

where E_g = the gravitational energy
$\gamma_g = (1 - \alpha_p)$
α_p = the inertia factor (~ .8 for an oblate spheroid such as Saturn)
M_p = planetary mass
R_p = Mean planetary radius

This equation represents the energy required for a non-rotating asteroid. However as real asteroids rotate it provides an upper bound for the energy required to transport the fragments to infinity. As the rotational energy ($\frac{1}{2}I\omega^2$) is relatively small when compared to the gravitational energy it is acceptable to ignore its effect (at least to a first approximation). It is quite possible for partial disruption to occur

with some of the mass then reassembling. However a small amount of the mass could escape in fragments moving faster than the escape velocity removing much of the projectile energy. Indeed several successive impacts could produce similar effects to a single high energy one. Initially fragmentation, or partial fragmentation, may occur followed by mass loss with later impacts. In addition to removing energy from the target some of these impacts may well remove some angular momentum by the angular momentum drain mechanism of Dobrovolskis and Burns (1984). The effect of disruption on the rotation of the fragments is reviewed by Fujuiwara et al (1989). They note that there is a wide spread in rotation rate for the fragments (by a factor of ~10). The fastest rotating fragments appear to come from close to the point of impact. It is thus likely that the fastest observed rotators (such as 1566 Icarus) are collision fragments.

Asteroids that have not generated enough heat to melt either during accretion or by subsequent decay of radioactive nuclides may have shapes that do not represent equilibrium figures . If the central pressure is less than the material strength then the shape will remain as generated during accretion. The only asteroid massive enough to form an equilibrium figure due to self gravity is Ceres (Hughes 1991). Fragments of disrupted bodies will also tend to be irregular. It is not possible to determine origin from shape alone. Inferred composition suggests that large fragments exist as the metallic M-type and similar bodies appear to be composed of internal fragments from larger differentiated original bodies. These effects have not been considered further in this work.

5.5 Conclusion

The accretion model presented in this chapter confirms that the observed spin frequency distribution and random spin axis orientation could be a product of collisional evolution. A secondary result is the confirmation of likely precession angles in this event. Individual impacts can produce major alterations to the direction of the angular momentum vector - even complete reversal.

Asteroid disruption will tend to accentuate any observable effects (Binzel 1986).

6. The Observability of Free Precession in Asteroids

Abstract

In this chapter the model proposed in Chapter 4 is applied to the range of equilibrium shapes for asteroids (Maclaurin Spheroids and Jacobi Ellipsoids) for a range of angles between the Angular Momentum Vector and the Axial Spin Vector. From this the amplitudes of light variations due to axial rotation and free precession are derived together with the ratio between the spin and precession frequencies. It is found that the amplitude of free precessional elements of the light curve is only detectable for extreme cases.

6.1 Review

To date there have been no direct observations of free precession amongst the asteroids. If collisions have been a major factor in the evolution of asteroids then there should be many examples to be seen. On the other hand, if asteroids have remained largely unaffected by collisions after their initial accretion then they should exhibit simple rotation such that the spin vector is aligned with the angular momentum vector. This has been considered in chapters 1, 4 and 5.

That we have not detected free precession in asteroids does not imply that it is absent. Rather it indicates that either the observations have not been sufficiently precise (either due to the methodology employed or the absolute accuracy achieved) or that the effects are not observable for the majority of asteroids.

The object of this chapter is to consider the application of the spin model given in chapter 4 to the free precession case.

6.2 The Shape of an Asteroid

Any rotating self-gravitating body will tend to assume a shape for which the surface is normal to the resultant gravitational and rotational acceleration. This will only be successful if the body is sufficiently massive and deformable. During the accretion stages, the temperature of planetary bodies increases due to internal heat, decay of radioactive nuclides, and melting from projectile impacts.. This will reduce the internal tensile strength making the adoption of an equilibrium shape more likely.

The internal strength of a body is dependent on the composition and its evolution. If the body is fluid at some stage the strength is nil at this time. A body that has severe fracturing will also have an internal strength that is very small - it will not be zero as there will be interlock between the particles even if there is no bond strength. If the interior is not fractured then the internal strength will be of

the order of 10^9 N m^{-2} for basaltic rocks (Cole 1984). Above this pressure the lattice structure of the rock cannot be sustained, the material will show fluid behaviour and the body will take the shape of an equilibrium figure.

Using the value above Cole derives a radius of 100 km as the smallest size of planetary body that would be expected to assume an equilibrium shape. He admits that this limit is "to some extent arbitrary" so it would seem appropriate to consider this an upper bound. Smaller bodies he suggests will "have an irregular shape in general". Bell et al (1989) independently suggest that gravitational stresses exceed the crushing stresses of weak chondrite material at a diameter of about 150 km.

It should be remembered that the strength of materials decreases as temperature rises. During the accretion phase for a body there is a temperature rise (see for example Wood 1979). Even if this rise is not sufficient to melt the body it may be adequate to reduce the internal strength by several orders of magnitude. For this reason it is probable that equilibrium shapes will be found amongst asteroids significantly smaller than the above predictions (radius ~20-30km).

6.3 Equilibrium Shapes of Asteroids

The problem of the equilibrium shape of a planet was first considered by Newton in his Principia Mechanica. He predicted an oblateness of 1/230 for the Earth by assuming that it behaved as an homogeneous fluid rotating body. The value of 1/298.257 is currently adopted (BAA 1995) and the difference between this figure and that derived by Newton is attributed to the inhomogeneity of the Earth. A study of the motion of space vehicles in orbit around the earth has been used to derive a true shape. It departs from a simple spheroid and has a quite complex profile though the deviation is relatively minor (Cole 1978).

A generalised result of the above problem was derived by McLaurin in 1742. His model predicts the ellipticity of a rotating spheroid for a given angular momentum. The McLaurin spheroid (a=b>c) represents the approximate shape of the major planets and the larger or slower rotating asteroids where self-gravity is the dominant influence.

The possibility of ellipsoids with unequal major axes (a>b>c) was not considered until suggested by Lagrange in 1811 though in his derivation he concludes that the axes a and b must be equal. Jacobi in 1834 demonstrated that this conclusion was not correct and that as the angular momentum of the spheroid is increased it would eventually become unstable and elongate into an ellipsoid with axes a and b unequal. A series of triaxial ellipsoidal bodies could therefore satisfy equilibrium.

As the angular momentum is increased the ellipsoid body will become more elongated. Eventually the elongation becomes so large that the ellipsoid becomes unstable and fission will occur. Initially the products are of unequal mass but at high values of angular momentum the product is a pair of ellipsoidal bodies of equal mass (called Darwin ellipsoids). The greater part of the angular momentum of a binary system is contained in the orbital motion of the bodies about their common centre of gravity - much less in spin of the components.

The information in this section is taken from Chandrasekar (1969). His study is the classic treatise on the equilibrium shapes of self gravitating rotating bodies.

6.4 The Shapes of Asteroid Collision Debris

The data about the shapes of asteroids produced as collision debris has been derived from laboratory experiment. The current knowledge has recently been summarised by Fujiwara et al (1989). The results obtained indicate that there are no extreme shapes amongst fragments and the mean shape has proportions 2:1.414:1, though the scatter about the mean is large.

It is quite possible for figures that appear to be equilibrium shapes could be collision fragments. It is equally possible that a non-equilibrium shape may have begun as an equilibrium shape but that it has been sculpted to a different shape by the removal of surface matter by impacts.

The following conclusions have been given by Bell et al (1989)

1. Spherical Asteroids

a. Large slowly rotating asteroids in hydrostatic equilibrium

b. Spherical shape may arise in smaller weak asteroids due to "sandblasting" by small impactors.

2. Elongated Asteroids

a. Splintered collision fragments

b. Rapidly rotating 'rubble piles' which have adopted a near equilibrium shape.

c. Asymmetric sublimation of volatiles from initially spherical bodies.

d. Exaggeration of local topography during sublimation.

e. Exaggeration of axis ratios during sublimation on non-spherical bodies.

f. Preservation of primordial irregular shape produced by low velocity collisions, producing 'compound planetesimals'.

6.5 How Fast Can Asteroids Spin? (Does this affect the observed distribution)

It is has been stated that the fastest an asteroid can spin is the rate at which the force due to radial acceleration at the equator equals the surface gravity (Burns and Tedesco 1979). This would be realistic only if the asteroid possessed no internal strength and material could then be ejected into orbit. More reasonable would be to allow an internal strength such that 'bursting' occurred at a higher rotation, this is a classic case in mechanics (see eg French 1969).

The case of a body with no internal strength has been considered by Weidenschilling (1981) and

$$\omega_{max} = (4\pi G\rho/3)^{0.5} \qquad \text{.....(6.1)}$$

where G is the gravitational constant

ρ is the density of the asteroid

The maximum rotational rate for a given material strength ignoring gravitation is a standard case in Newtonian mechanics $\omega_{max} = (S/\rho)^{0.5}$ .....(6.2)

(French 1971)

where ω is the angular rotation speed of the asteroid

S is the ultimate tensile strength of the asteroid

ρ is the density of the asteroid

As the gravitational and rotational components act at right angles to each other combining the two gives

$$\omega_{max} = [(4\pi G\rho/3) + (S/\rho)]^{0.5} \quad .....(6.3)$$

The first term on the right side of the equation depends solely on the material density and the higher the density the higher the rotation rate. The second term depends on the ratio of S/ρ and in general the most significant factor will be the degree of fracturing within the asteroid. This in turn is likely to depend on the evolution of the asteroid as impacts will tend to produced a fractured "rubble pile".

An asteroid at rest in an equilibrium condition will adopt a spherical shape. As it begins to rotate the polar axis will flatten and the shape will deviate from a sphere with a=b>c. At the critical rotation rate it will start to elongate and a>b>c. The elongation will increase until fission occurs (see Section 6.3).

Weidenschilling (1981) has considered rotation in terms of these equilibrium figures. From this he derives a value of 0.53 times the rotation rate given by Burns and Tedesco as the maximum rate at which an asteroid can spin whilst retaining an equilibrium figure. During the McLaurin spheroid phase the eccentricity of the body (the flattening) increases as the spin rate increases reaching a maximum at the transition to the Jacobi ellipsoid phase. As the deformation increases, it increases the moment of inertia of the body so rapidly that the spin rate decreases for a given angular momentum budget.

For a fractured asteroid the vale of S is zero and the maximum rotation period is solely dependent on the material density. Weidenschilling has reduced Formula 6.2

$$P_s = 2 \,.\, \pi / \omega_s \sim 3.3\ (\rho)^{-0.5} \text{ hours...} \quad (6.4)$$

where P_s is the spin period in hours

ω_s is the angular velocity of rotation

ρ is the density in g cm^{-3}

A reasonable estimate for the density of an asteroid is 2500 kg m^{-3} which would correspond to a spin period of 2.1 hours using the above criterion. However, with the exception of a few small bodies, the typical shortest spin periods observed are ~4 hours. This would imply a material density of ~700kg m^{-3}

for 4 hours to represent the rotation rate at which 'bursting' of the asteroid occurs. However adopting Weidenschilling's criterion, the maximum spin rate for an equilibrium body of 0.53 ω_s we find that P_s is approximately 2.1 hours and the material density is 2500 kg m^{-3}. We would then expect that asteroids with spin periods shorter than ~4 hours must consist of very dense/heavy material such as metals if they are rotational equilibrium shapes or else represent collision debris.

6.6 How Fast Do Asteroids Spin?

The Asteroids II database gives observed rotation periods for 505 asteroids. Very few (only 5) are listed with rotation periods in excess of 100 hours - two of these (288 Glauke and 1220 Crocus) have periods in excess of 1000 hours. The great majority have spin periods between 6 hours and 15 hours. Very few are known with rotation periods less than the four hours given in the previous section. The shortest period is in the order of 1.5 hours (number 1566) this result implies either that if the asteroid has an equilibrium figure then the asteroid has a high density and internal strength or else it would have disrupted.

A graph of spin frequency (in revolutions per day) against number is given in Figure 6.1).

The vast majority of asteroids rotating with periods between ~4 hours and 15 hours could represent equilibrium shapes. However they could also represent collision debris or target bodies that have had fragments removed by collision. This is in good agreement with the 8-10 hour rotation period derived by Alfven (1964) for asteroids at the early stages of growth.

Slow rotation rates may be indicative of either collision despinning or alternatively they could indicate precession motion. This will be considered further in Section 6.8 however at this stage it is sufficient to note that the light curve of a spheroid under simple rotation is constant whilst the light curve of a precessing spheroid is not. The free precession period of a spheroid is longer than the axial rotation period and depends not only on its figure but also on the angle of misalignment between the axis c and the angular momentum vector. Slow rotating asteroids could be freely precessing asteroids.

Rapidly rotating asteroids are most probably collision fragments - a view supported since they are all very small, <10 km, in diameter.

6.7 Observing The Shape of Asteroids

Direct observation of the shape of an asteroid has, so far, only been obtained for 951 Gaspra and 243 Ida. The shape of several other asteroids has been reconstructed from speckle interferometry, radar echoes and through the use of adaptive optics. A limited view of shape has been determined from observation of stellar occultations by asteroids. However for the vast majority of asteroids the best estimate of dimensions has come from the light curve.

Direct observation is the most satisfactory method. Imagery from spacecraft allow the limb profiles to be viewed directly and, from a sequence of images as the asteroid rotates, the three shape parameters (a:b:c) can be determined. From a knowledge of the spacecraft's position these can be reduced to

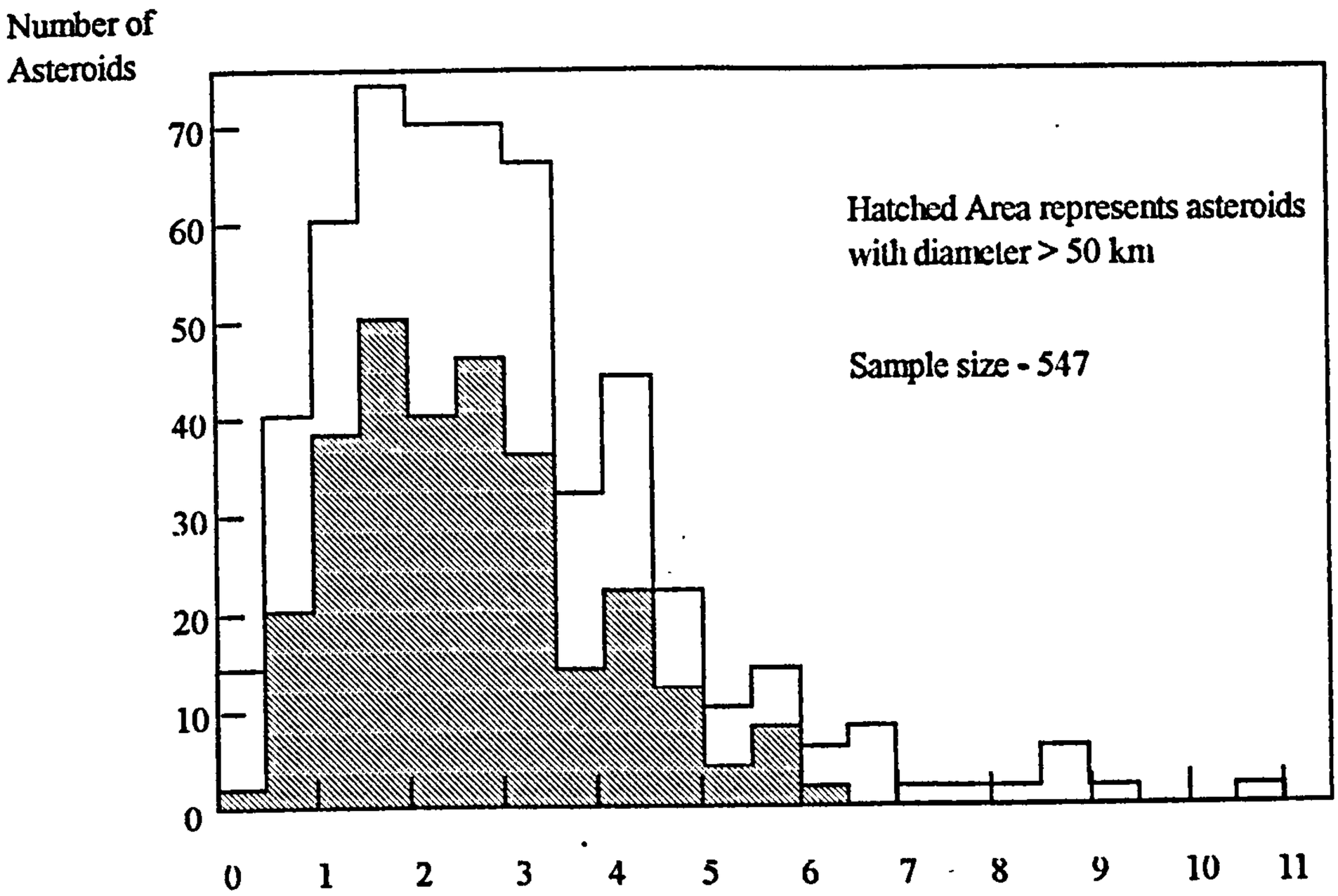

Figure 6.1 - Distribution of spin frequency
Source 1994 Ephemerides of the Minor Planets

dimensions in kilometres. However the use of spacecraft observation is likely to remain limited. Present proposals only allow observation of asteroids for missions with prime targets at the outer planets (Jupiter and Saturn). One other prospect remains and this is the use of the Hubble Space Telescope to directly image some asteroids. Observation of the surfaces of asteroids is not a high priority in the telescope schedule however images of a complete rotation of 4 Vesta have recently been published (Sky and Telescope 1995).

Speckle interferometry has only been carried out for larger asteroids. When obtained at several heliocentric longitudes it becomes possible to make reasonable estimates of a:b:c. Since only very few asteroids are suitable targets for speckle interferometry because of their relative faintness it is unlikely that many asteroids will be adequately studied for this purpose in the near future.

A stellar occultation by an asteroid is a comparatively rare event. Successful observation does allow the apparent cross-sectional shape of the asteroid at the instant of the occultation to be derived. This, of course, presupposes that an adequate number of chords have been obtained. It is also preferable that these be derived photoelectrically rather than visually to eliminate observer bias. The values of the two axes derived from this are accurate but only reflect the shape presented towards the earth at the instant of the occultation. Information from several occultations or, more likely, from one of the other methods outlined here is required to estimate the true shape of the asteroid.

A crude estimate of the shape of an asteroid can be made from the light curve provided that several light curves taken at different heliocentric longitudes are available. At some part of the orbit the aspect angle between the asteroid pole and the observers line of sight will reach 90°. At this time at maximum apparent brightness the apparent area is proportional to a.c and the minimum brightness is proportional to b.c where a, b and c are the lengths of the three main axes of the ellipsoid. From this the ratio of a:b can be derived. If the asteroid aspect angle is not 90° then the value of a:b derived will be less than the true value and represent a lower bound on the ratio. The error introduced in the ratio a:b is small for most asteroids provided that the aspect angle is within about 15° of a right angle. The problem comes in trying to derive an accurate figure for the ratio a:c or b:c.

The axis c is the minor axis of an asteroid. If the asteroid is in simple rotation it is also the direction of the angular momentum vector and the spin vector (ie the axis of rotation). It is only possible to get an accurate value for this dimension if the orientation of the spin vector is known so that the light curve can be modelled for all heliocentric longitudes. This is only well known for a handful of asteroids (Magnusson et al 1989). c can be derived from a study of the changes in the amplitude of the light curve with heliocentric longitude. The result is either a value for c or an overestimate of its value.

In cases where the observed amplitude of an asteroid lightcurve exceeds about 1 magnitude the possibility of binary asteroids still remains. A single body where a:b exceeds about 2.5 is not stable under equilibrium conditions and will divide. A collision fragment (ie a splinter) can exist this elongated but the work of Fujiwara et al (1989) suggest this would be rare and that large bodies would

not be stable. 216 Kleopatra and 624 Hektor may be too elongated to represent single bodies and could be binaries (Weidenschilling 1980). Radar images of the Earth approaching asteroid 4179 Toutatis suggest that it may comprise two bodies in contact.

6.8 Synthesis of Light Curve Amplitudes for Freely Precessing Asteroids

In order to determine whether free precession effects would be observable and also to investigate ways that free precession would be seen, a simple model has been set up. For the purposes of this investigation two equilibrium shapes of model asteroid have been considered - the Mclaurin spheroid, where a=b>c, and the Jacobi ellipsoid, with a>b>c. McLaurin spheroids have shapes between a:b:c of 1:1:1 and 1.72:1.72:1. Above this the equilibrium figure is the Jacobi ellipsoid and the shapes vary between limits of a:b:c of 1.72:1.72:1 and 3.07:1.23:1. The shapes of ellipsoid have been derived in accordance with the data given by Chandrasekar (1969).

The model has been used to determine the effect on the light curve of misalignment of the spin axis with respect to the principal axis (the z axis). Misalignments in the range of 0° to 90° have been investigated. The period of free precession has been derived from equation 4.10. The amplitude of the light curve due to primary rotation (axial spin) has been computed on the assumption it is a maximum (ie at an aspect angle of the rotation axis to the observer's line of sight of 90°). For the amplitude of light curve due to secondary rotation (free precession) the model assumes that one extreme of the precession rotation produces an aspect angle of 90° and that the aspect angle of the other extreme is as derived from equation 4.11. The two assumptions give the extreme maximum amplitudes for each rotation that can occur for each shape of body. In reality the favourable conditions will not occur very often. In practice the ratio between the two will remain similar.

Simple rotation - ie with no precession motion - occurs for the two following conditions. The terminology used is considered in Chapter 4 and illustrated by Figure 4.1.

The first and most common is when the spin axis is aligned with the z axis of the body - the minor axis. This is the axis about which the moment of inertia of the body is greatest and - for a given angular momentum - the spin vector has the lowest value (see equation 4.2). This is the stable equilibrium state since any misalignment between the spin axis and the z axis will tend to lead to a realignment of these axis due to elastic flexure of the body (see Chapter 4). For this case the angle α is 0°.

The second equilibrium is an unstable equilibrium when the spin axis is aligned with the x axis - the major axis of the body. In this case the angle α is 90°. Any misalignment from this equilibrium state will lead, through energy dissipation, to a progressive realignment of the spin vector with the z axis.

The results of the calculations (which were carried out on a Lotus 123 spreadsheet on an IBM compatible computer) are given in Table 6.1 for Mclaurin spheroids and Tables 6.2.1 and 6.2.2 for Jacobi ellipsoids. Plots of the results are given in Figures 6.2 to 6.5.

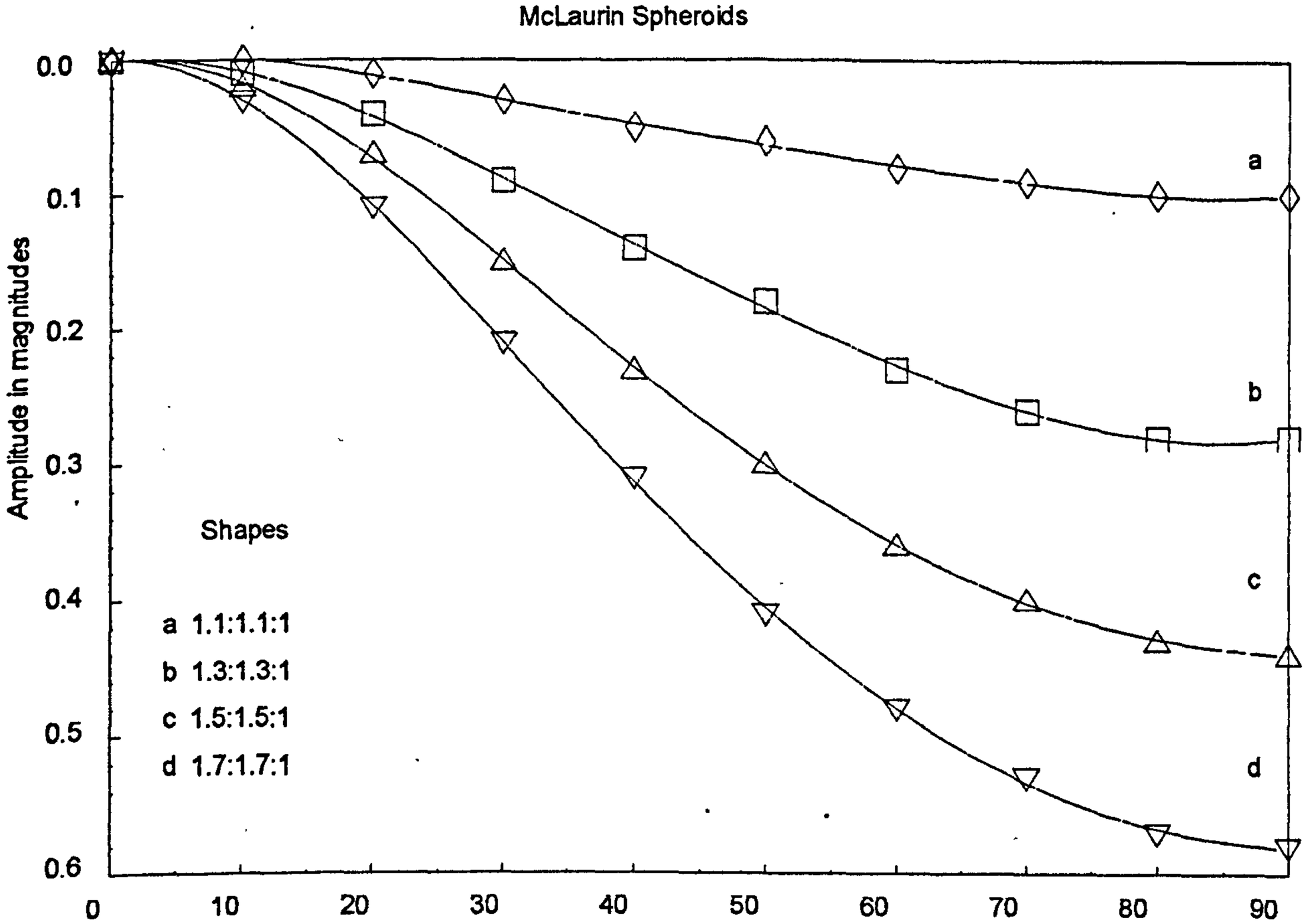

Figure 6.2 - Plot of the maximum amplitude of the secondary part of a light curve due to the free precession of McLaurin Spheroids

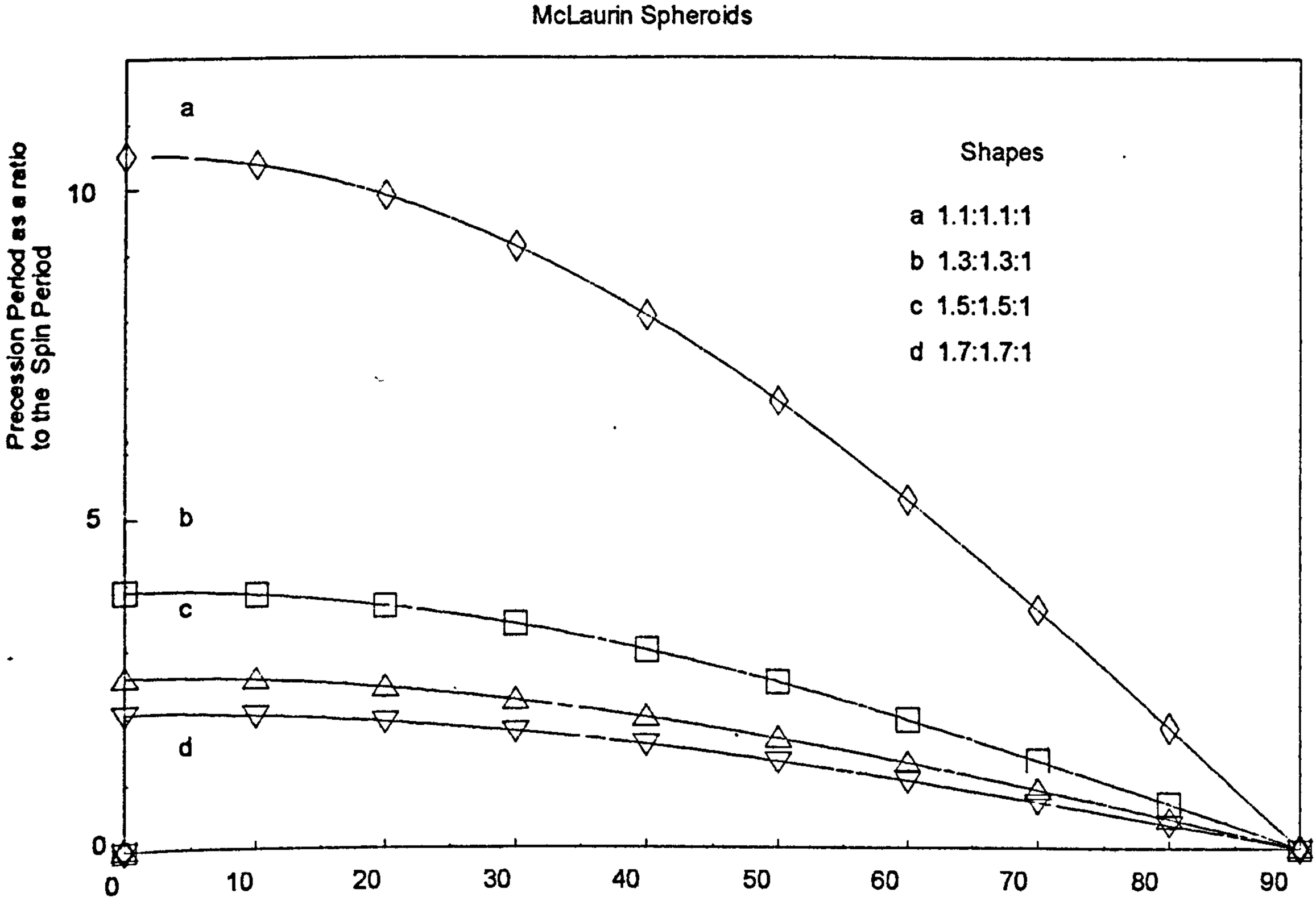

Figure 6.3 - Plot of the ratio between the precession period and the axial rotation period of a McLaurin Spheroid undergoing free precession

The rotation axis is taken as the z-axis of the body.

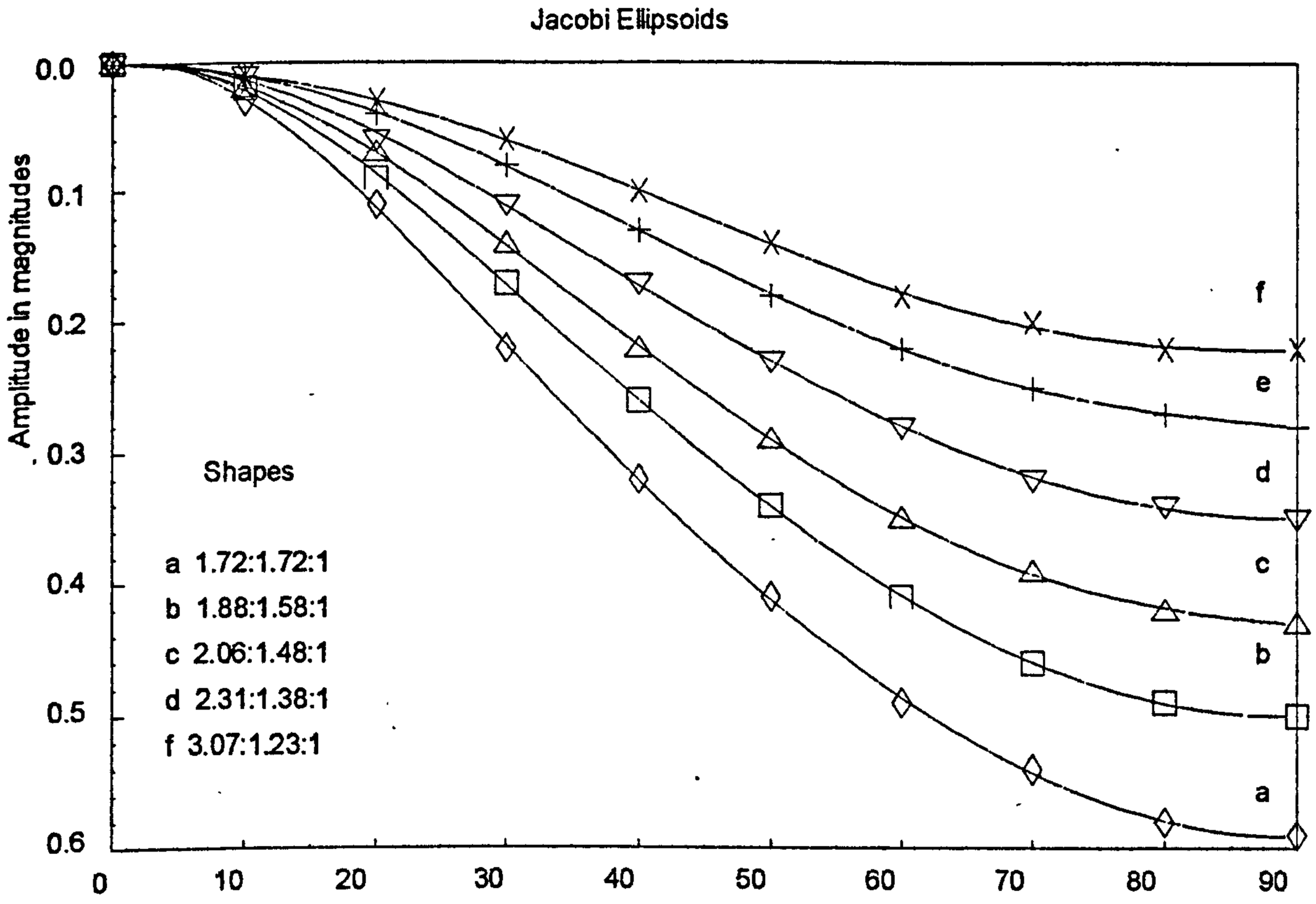

Figure 6.4 - Plot of the maximum amplitude of the secondary part of a light curve due to the free precession of Jacobi Ellipsoids

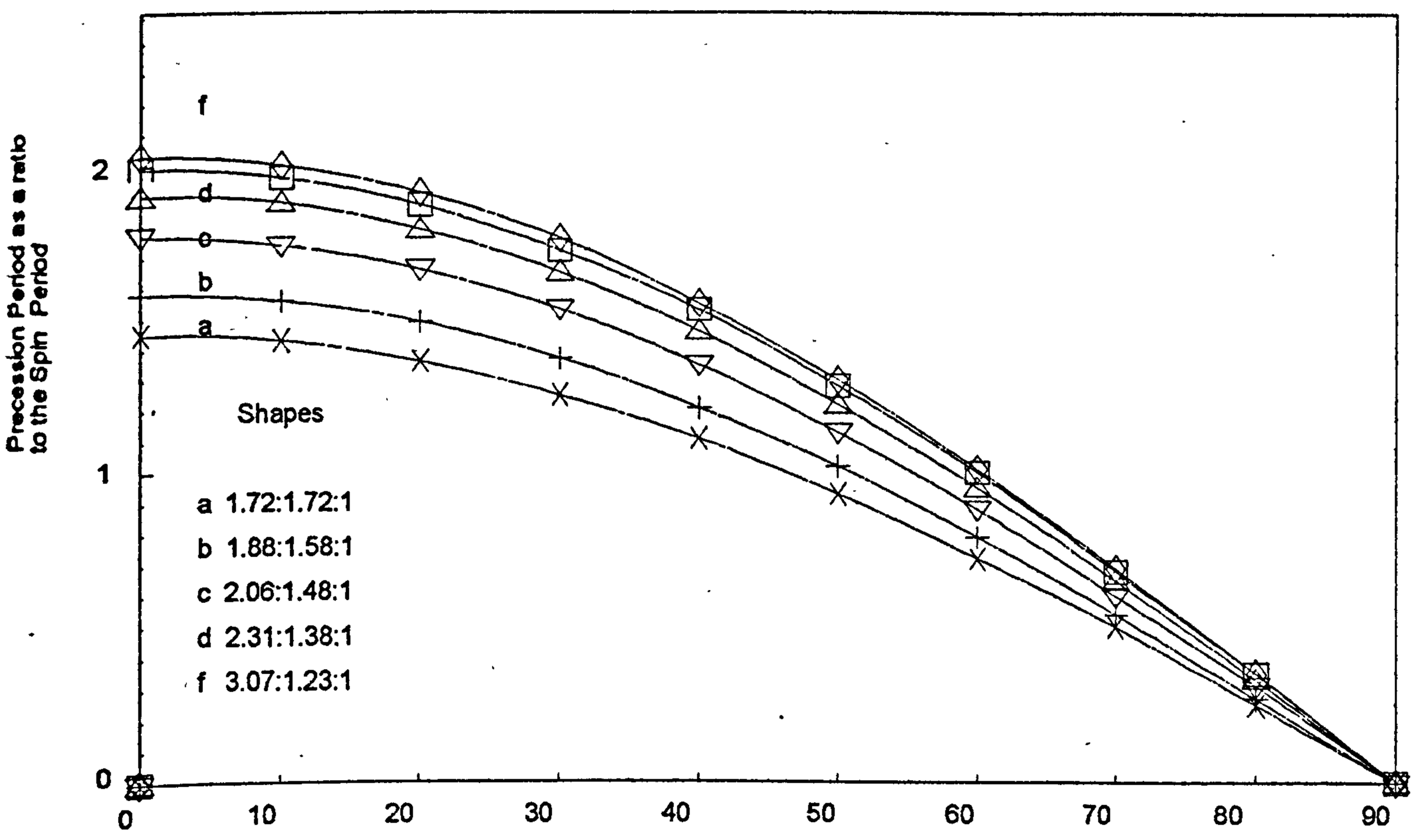

Figure 6.5 - Plot of the ratio between the precession period and the axial rotation period of a Jacobi Ellipsoid undergoing free precession

The tables contain results for precession of the two stable states where α is 0° and 90°. Neither of these columns have any real meaning but will allow interpolation angles close to the extrema. On the same basis the values are given for a sphere (a:b:c = 1:1:1) and again these have no real meaning as all axes are both major and minor.

6.9 Free Precession in Asteroids

In those cases where the predicted amplitude of the light curve is less than 0.02 magnitudes detection will prove impossible from the Earth as the anticipated errors in observation will mask it. In addition topographic or surface albedo variations are also likely to be at the same level. Detection from the Earth presupposes that sufficient observational data and continuity of data is available to allow identification.

The results given here illustrate that the effect of precession on the light curves of the two types of body are similar. However it is appropriate to consider the two shapes of body separately prior to making conclusions.

Table 6.1 - Precession Characteristics for McLaurin Spheroids

Lightcurve amplitudes in magnitudes

Angular displacement of the Spin Axis with respect to the z-axis	0	10	20	30	40	50	60	70	80	90
a:b:c	1.1:1.1:1									
Lightcurve amplitude Primary rotation	0	0.08	0.1	0.1	0.1	0.1	0.1	0.1	0.1	0.1
Lightcurve amplitude Secondary rotation	0	0	.0.01	0.03	0.05	0.06	0.08	0.09	0.1	0.1
Period of precession/Spin Period	10.52	10.36	9.89	9.11	8.06	3.76	5.26	3.6	1.83	0
a:b:c	1.2:1.2:1									
Lightcurve amplitude Primary rotation	0	-0.1	-0.16	-0.18	-0.19	-0.19	-0.2	-0.2	-0.2	-0.2
Lightcurve amplitude Secondary rotation	0	-0.01	-0.03	-0.06	-0.09	-0.12	-0.15	-0.18	-0.19	-0.2
Period of precession/Spin Period	5.55	5.46	5.21	4.8	4.25	3.56	2.77	1.9	0.96	0
a:b:c	1.3:1.3:1									
Lightcurve amplitude Primary rotation	0	-0.1	-0.2	-0.24	-0.26	-0.27	-0.28	-0.28	-0.28	-0.28
Lightcurve amplitude Secondary rotation	0	-0.01	-0.04	-0.09	-0.14	-0.18	-0.23	-0.26	-0.28	-0.28
Period of precession/Spin Period	3.9	3.84	3.66	3.38	2.99	2.51	1.95	1.33	0.68	0
a:b:c	1.4 1.4:1									
Lightcurve amplitude Primary rotation	0	-0.1	-0.22	-0.29	-0.33	-0.34	-0.36	-0.36	-0.36	-0.37
Lightcurve amplitude Secondary rotation	0	-0.02	-0.06	-0.12	-0.18	-0.24	-0.29	-0.33	-0.36	-0.37
Period of precession/Spin Period	3.08	3.04	2.9	2.67	2.36	1.98	1.54	1.05	0.54	0
a:b:c	1.5:1.5:1									
Lightcurve amplitude Primary rotation	0	-0.09	-0.23	-0.33	-0.38	-0.41	-0.42	-0.43	-0.44	-0.44
Lightcurve amplitude Secondary rotation	0	-0.02	-0.07	-0.15	-0.23	-0.3	-0.36	-0.4	-0.43	-0.44
Period of precession/Spin Period	2.6	2.56	2.44	2.25	1.99	1.67	1.3	0.89	0.45	0
a:b:c	1.6:1.6:1									
Lightcurve amplitude Primary rotation	0	-0.09	-0.24	-0.35	-0.42	-0.46	-0.49	-0.5	-0.51	-0.51
Lightcurve amplitude Secondary rotation	0	-0.02	-0.09	-0.18	-0.27	-0.35	-0.42	-0.47	-0.5	-0.51
Period of precession/Spin Period	2.28	2.25	2.14	1.98	1.75	1.47	1.14	0.78	0.4	0
a:b:c	1.7:1.7:1									
Lightcurve amplitude Primary rotation	0	-0.09	-0.24	-0.37	-0.46	-0.51	-0.54	-0.56	-0.57	-0.58
Lightcurve amplitude Secondary rotation	0	-0.03	-0.11	-0.21	-0.31	-0.41	-0.48	-0.53	-0.57	-0.58
Period of precession/Spin Period	2.06	2.03	1.93	1.78	1.58	1.32	1.03	0.7	0.36	0
a:b:c	1.72:1.72:1									
Lightcurve amplitude Primary rotation	0	-0.09	-0.24	-0.37	-0.46	-0.52	-0.55	-0.57	-0.58	-0.59
Lightcurve amplitude Secondary rotation	0	-0.03	-0.11	-0.22	-0.32	-0.41	-0.49	-0.54	-0.58	-0.59
Period of precession/Spin Period	2.03	2	1.91	1.76	1.55	1.30	1.01	0.69	0.35	0

Table 6.2.1 - Precession Characteristics for Jacobi Ellipsoids - Part 1

Lightcurve amplitudes in magnitudes

Angular displacement of the Spin Axis with respect to the z-axis	0	10	20	30	40	50	60	70	80	90
a:b:c 1.72:1.72:1										
Lightcurve amplitude Primary rotation	0.00	-0.09	-0.24	-0.37	-0.46	-0.52	-0.55	-0.57	-0.58	-0.59
Lightcurve amplitude Secondary rotation	0.00	-0.03	-0.11	-0.22	-0.32	-0.41	-0.49	-0.54	-0.58	-0.59
Period of precession/Spin Period	2.03	2.00	1.91	1.76	1.55	1.30	1.01	0.69	0.35	0.00
a:b:c 1.75:1.68:1										
Lightcurve amplitude Primary rotation	-0.04	-0.13	-0.28	-0.41	-0.49	-0.54	-0.58	-0.59	-0.61	-0.61
Lightcurve amplitude Secondary rotation	0.00	-0.03	-0.11	-0.20	-0.31	-0.40	-0.47	-0.52	-0.55	-0.56
Period of precession/Spin Period	2.03	2.00	1.90	1.76	1.55	1.30	1.01	0.69	0.35	0.00
a:b:c 1.79:1.65:1										
Lightcurve amplitude Primary rotation	-0.09	-0.17	-0.32	-0.44	-0.52	-0.57	-0.60	-0.62	-0.63	-0.63
Lightcurve amplitude Secondary rotation	0.00	-0.03	-0.10	-0.19	-0.29	-0.38	-0.45	-0.50	-0.53	-0.54
Period of precession/Spin Period	2.02	1.99	1.90	1.75	1.55	1.30	1.01	0.69	0.35	0.00
a:b:c 1.83:1.61:1										
Lightcurve amplitude Primary rotation	-0.14	-0.22	-0.36	-0.48	-0.55	-0.60	-0.63	-0.65	-0.66	-0.66
Lightcurve amplitude Secondary rotation	0.00	-0.03	-0.09	-0.18	-0.28	-0.36	-0.43	-0.48	-0.51	-0.52
Period of precession/Spin Period	2.01	1.98	1.89	1.74	1.54	1.29	1.00	0.69	0.35	0.00
a:b:c 1.88:1.58:1										
Lightcurve amplitude Primary rotation	-0.19	-0.27	-0.40	-0.51	-0.58	-0.63	-0.66	-0.67	-0.68	-0.69
Lightcurve amplitude Secondary rotation	0.00	-0.02	-0.09	-0.17	-0.26	-0.34	-0.41	-0.46	-0.49	-0.50
Period of precession/Spin Period	1.99	1.96	1.87	1.72	1.53	1.28	1.00	0.68	0.35	0.00
a:b:c 1.93:1.55:1										
Lightcurve amplitude Primary rotation	-0.24	-0.31	-0.45	-0.55	-0.62	-0.66	-0.69	-0.70	-0.71	-0.72
Lightcurve amplitude Secondary rotation	0.00	-0.02	-0.08	-0.16	-0.25	-0.32	-0.39	-0.44	-0.46	-0.47
Period of precession/Spin Period	1.97	1.94	1.85	1.70	1.51	1.27	0.98	0.67	0.34	0.00
a:b:c 1.99:1.51:1										
Lightcurve amplitude Primary rotation	-0.30	-0.37	-0.49	-0.59	-0.66	-0.70	-0.72	-0.74	-0.75	-0.75
Lightcurve amplitude Secondary rotation	0.00	-0.02	-0.08	-0.15	-0.23	-0.31	-0.37	-0.41	-0.44	-0.45
Period of precession/Spin Period	1.94	1.91	1.82	1.68	1.49	1.25	0.97	0.66	0.34	0.00
a:b:c 2.06:1.48:1										
Lightcurve amplitude Primary rotation	0.36	-0.42	-0.54	-0.63	-0.70	-0.73	-0.76	-0.77	-0.78	-0.78
Lightcurve amplitude Secondary rotation	0.00	-0.02	-0.07	-0.14	-0.22	-0.29	-0.35	-0.39	-0.42	-0.43
Period of precession/Spin Period	1.90	1.88	1.79	1.65	1.46	1.22	0.95	0.65	0.33	0.00

Table 6.2.2 - Precession Characteristics for Jacobi Ellipsoids - Part 2

Lightcurve amplitudes in magnitudes

Angular displacement of the Spin Axis with respect to the z-axis	0	10	20	30	40	50	60	70	80	90
a:b:c 2.13:1.45:1										
Lightcurve amplitude Primary rotation	-0.42	-0.48	-0.59	-0.68	-0.74	-0.78	-0.80	-0.81	-0.82	-0.82
Lightcurve amplitude Secondary rotation	0.00	-0.02	-0.07	-0.13	-0.20	-0.27	-0.33	-0.37	-0.39	-0.40
Period of precession/Spin Period	1.86	1.84	1.75	1.61	1.43	1.20	0.93	0.64	0.32	0.00
a:b:c 2.22:1.42:1										
Lightcurve amplitude Primary rotation	-0.49	-0.55	-0.65	-0.73	-0.79	-0.82	-0.84	-0.86	-0.86	-0.87
Lightcurve amplitude Secondary rotation	0.00	-0.02	-0.06	-0.12	-0.19	-0.25	-0.30	-0.34	-0.37	-0.38
Period of precession/Spin Period	1.81	1.78	1.70	1.57	1.39	1.16	0.91	0.62	0.31	0.00
a:b:c 2.31:1.38:1										
Lightcurve amplitude Primary rotation	-0.55	-0.61	-0.70	-0.78	-0.83	-0.87	-0.89	-0.90	-0.90	-0.91
Lightcurve amplitude Secondary rotation	0.00	-0.01	-0.06	-0.11	-0.17	-0.23	-0.28	-0.32	-0.34	-0.35
Period of precession/Spin Period	1.77	1.74	1.66	1.53	1.35	1.13	0.88	0.60	0.31	0.00
a:b:c 2.41:1.35:1										
Lightcurve amplitude Primary rotation	-0.63	-0.68	-0.77	-0.84	-0.89	-0.92	-0.94	-0.95	-0.95	-0.96
Lightcurve amplitude Secondary rotation	0.00	-0.01	-0.05	-0.10	-0.16	-0.21	-0.26	-0.30	-0.32	-0.33
Period of precession/Spin Period	1.71	1.68	1.61	1.48	1.31	1.10	0.85	0.58	0.30	0.00
a:b:c 2.54:1.32:1										
Lightcurve amplitude Primary rotation	-0.71	-0.75	-0.83	-0.90	-0.95	-0.98	-0.99	-1.00	-1.01	-1.01
Lightcurve amplitude Secondary rotation	0.00	-0.01	-0.05	-0.09	-0.15	-0.20	-0.24	-0.27	-0.29	-0.30
Period of precession/Spin Period	1.65	1.62	1.55	1.43	1.26	1.06	0.82	0.56	0.29	0.00
a:b:c 2.69:1.29:1										
Lightcurve amplitude Primary rotation	-0.80	-0.84	-0.91	-0.97	-1.01	-1.04	-1.06	-1.07	-1.07	-1.07
Lightcurve amplitude Secondary rotation	0.00	-0.01	-0.04	-0.08	-0.13	-0.18	-0.22	-0.25	-0.27	-0.28
Period of precession/Spin Period	1.58	1.56	1.49	1.37	1.21	1.02	0.79	0.54	0.27	0.00
a:b:c 2.86:1.26:1										
Lightcurve amplitude Primary rotation	-0.89	-0.93	-0.99	-1.05	-1.09	-1.11	-1.13	-1.13	-1.14	-1.14
Lightcurve amplitude Secondary rotation	0.00	-0.01	-0.04	-0.07	-0.12	-0.16	-0.20	-0.23	-0.24	-0.25
Period of precession/Spin Period	1.52	1.49	1.42	1.31	1.16	0.97	0.76	0.52	0.26	0.00
a:b:c 3.07:1.23:1										
Lightcurve amplitude Primary rotation	-1.00	-1.02	-1.08	-1.13	-1.17	-1.19	-1.20	-1.21	-1.22	-1.22
Lightcurve amplitude Secondary rotation	0.00	-0.01	-0.03	-0.06	-0.10	-0.14	-0.18	-0.20	-0.22	-0.22
Period of precession/Spin Period	1.45	1.43	1.36	1.25	1.11	0.93	0.72	0.50	0.25	0.00

The McLaurin spheroid in simple rotation shows no light variation since a=b. As the angle of misalignment increases the rotational light curve shows greater variations reaching a maximum when the angle attains 90° which corresponds to two mode rotation about both the long and the short axes. The greater the oblateness the greater the maximum amplitude as this depends on the ratio of a:c. The

amplitude of the light curve due to precessional rotation also increases as the angle of misalignment increases - its greatest difference from that due to simple rotation occurs at an angle of 45°. Precession periods - where the amplitude of lightcurve due to precession is greater than 0.05 magnitudes - are greater than about 5 times the spin period. Where the amplitude of the lightcurve due to precession is high (>0.2 magnitudes) the angle of misalignment is also relatively high (>40°). In these cases the period of precession varies between twice the spin period to an extreme much less than the spin period. It must be noted that the precession period is in general greater than the spin period where the angle of misalignment is less than about 60° however for extreme angles the precession period becomes significantly lower than that of axial spin.

With a Jacobi ellipsoid (since a>b) light variations due to rotation are relatively high and that due to precession relatively smaller. In general the same principles apply. As the angle of misalignment increases so does the amplitude of the rotational lightcurve and to a lesser extent the same is true for precession. The period of free precession varies between twice the spin period and perhaps a tenth.

If the modulated period is greater than about ten times the primary spin period and remains detectable then the body is probably undergoing forced precession due to an unseen companion and is beyond the scope of this work.

Precession periods that are an integral harmonic of the rotation period (2x, 3x etc) are unlikely to be recognised as such. If present the interpretation is likely to be made that the rotation period is that of the harmonic and that the light curve is complex with several (ie more than 2) maxima and minima. A similar argument applies if the precession period is a simple fraction of the rotation period.

Since it is unlikely that direct observation will be achieved in the near future it seems most probable that any discovery will be serendipitous - however there are several ways of increasing the chances of uncovering evidence of free precession.

6.10 Size Distribution of Freely Precessing Asteroids

The number of asteroids undergoing collision generated free precession in the asteroid belt depends on the rate at which asteroids are colliding and the rate at which the precession damps out. A simple particle in a box model has been used to estimate the likely size distribution which would be expected at the current time.

The size distribution of main belt asteroids has been calculated from the mass distribution index given by Hughes (1982) by setting the number of asteroids larger than 120km in diameter at 128. The damping time for each size of asteroids is calculated from the formula given in Chapter 1.

The impact probability per year is derived from

Asteroid cross sectional area x distance travelled in one yr x number density per yr

which can be expressed as

$$P = \pi r^2 V T n \qquad \text{.....(6.4)}$$

where r is the mean asteroid radius

n is the mean asteroid number density (assumed at 10^{-28} m^{-3})

V is the particle velocity

T is the number of seconds in a year $\sim 3 \cdot 10^7$

Table 6.3 Number of Freely Precessing asteroids larger than the specified diameter

Diameter D(km)	Number Smaller than D	Impact Probability/yr	Damping Time (yrs) calculated from Equation 1.2	Number existing now
500	2	10^{-10}	$8\ 10^5$	$8\ 10^{-5}$
200	30	$1.5\ 10^{-9}$	$5\ 10^6$	0.0075
100	238	$1.2\ 10^{-8}$	$2\ 10^7$	.24
50	1900	$9.5\ 10^{-8}$	$8\ 10^7$	7.6
20	30000	$1.5\ 10^{-6}$	$5\ 10^8$	750
10	240000	$1.2\ 10^{-5}$	$2\ 10^9$	24000

The results indicate that it is unlikely that large asteroids will be precessing. This is due to the small number and their short relaxation time. The number increases rapidly as the size reduces such that it appears likely that 10% of the population of 10 km diameter asteroids would be expected to be undergoing free precession at any time. Such small asteroids can only be observed with larger telescopes (typically >1 m aperture) or directly from space missions.

6.11 Possible ways of detecting Free Precession

Beat phenomena have not been recognised in asteroids (see for example Kopal 1970). However to detect beat phenomena it is preferable to have good coverage of the light curve of an asteroid over several continuous rotation periods - four or five. This has not yet been achieved and indeed is unlikely to be possible from Earth without a concerted global effort at a time of favourable weather conditions. Alternatively several complete light curves taken during the course of a week or two may be adequate to reveal any minor differences possibly attributable to precession. Similar techniques have been used to determine beat periods in short period Delta Scuti stars (see for example Walker 1986) where the periods are of the order of two or three hours.

The light curve of 44 Nysa is noted for changing shape during the course of an opposition. This is related to the changing viewing geometry - the sun-asteroid-earth angle (the phase angle) - and also the aspect angle - the polar axis inclination to the observer's line of sight. This effect may be sufficient to mask any variations in the light curve arising from precession of the spin axis. However it should be noted that if changes are seen in the shape of several lightcurves taken over the course of a couple of weeks when the phase angle is not changing rapidly, this could indicate a body in free precession.

Many asteroids are observed at several oppositions where the heliocentric longitudes and the phase angle are similar. If the form of the light curve at similar viewing conditions varies with time it would provide strong evidence of precession. 15 Eunomia has been observed under just such conditions and the amplitude and form of the light curve is always the same. For the vast majority of asteroids, such favourable circumstances do not occur.

The number of apparent extrema may vary during the course of an opposition. The viewing geometry for near polar aspect angles may yield only a single maximum and minimum for each rotation compared with a near equatorial aspect. If the aspect angle changes greatly during the precession cycle then the shape of the light curve could change quite dramatically over a period of a week or two.

6.12 Summary

In general any process which can give rise to asymmetry in a body could produce precessional motion. This could come from two different causes. First the displacement of the angular momentum vector from its initial orientation by the impact of projectiles as considered earlier in this work. A second cause, which has not been considered in this work, is the modification of the shape of the asteroid due to internal processes (such as sublimation) leading to a realignment of the principal axes of the asteroid such that the axis of maximum moment of inertia ceases to align with the angular momentum vector. The effects of each of these causes are the same and would not be distinguishable to the remote observer. Direct imaging of the surface could give clues as to which process is at work provided it produces visible effects (such as 'volcanic' eruptions).

In this Chapter the correlation between shape and spin of asteroids has been considered. Observations are unlikely to preclude free precession since for the majority of asteroids it will be unobservable (or at best extremely difficult) to detect from the surface of the Earth. Very few observations from spacecraft near asteroids are expected within the next few years. Typically encounters with main belt asteroids will only allow imaging for two or three weeks. However the NEAR (Near Earth Asteroid Rendezvous Mission) scheduled for launch in 1996 is intended to accompany 433 Eros as it will be in a similar orbit. Imaging for many months should be possible allowing the fully rotational characteristics to be determined. The Space Telescope could also be used for long term investigations if sufficient time were to be made available.

Precise shapes of very few asteroids are known accurately. Several examples appear to be close to equilibrium shape - eg 39 Laetitia, 45 Eugenia and 107 Camilla (Farinella et al 1981). The equilibrium shape may have been derived during formation or may result from internal fracturing during collision evolution resulting in a 'rubble pile' asteroid. However for the vast majority of asteroids the proportions are at best only a crude approximation. The majority of asteroids appear not to be equilibrium shapes (Magnusson et al 1989) which may indicate a significant internal strength. As the accuracy of shape determination improves the position may alter.

7. Design and Assessment of a Photoelectric Photometer

Abstract

A new low-cost design of dc photoelectric photometer based on a side window photomultiplier tube has been prepared. The photometer has been interfaced to a computer using a custom designed interface and used to obtain the measurements presented in Chapter 8. To overcome the previously identified shortcomings of dc photometers silica gel is used to desiccate the heads resulting in an 80 fold reductiorf in dark noise is typical. The numerical parameters of the photometer are given and it has been shown that in practice the performance is limited solely by sky conditions and photon statistics.

7.1 Introduction - Why Design a New Photometer?

Photometric study of the minor planets requires accurate instrumentation. Commercial designs of astronomical photometer are available, usually with suitably astronomical price tags of many thousands of pounds (see for example Ealing-Beck 1989). Expensive commercial equipment of this sort is generally beyond the means of most of the smaller amateur observatories. One prime objective of the present work was to use the current range of precision integrated circuits (IC's) to produce a design of photometer costing approximately ten times less than commercial designs yet capable of matching their performance. The result has been a successful design which may not contain all the features of a commercial instrument but is simple to operate and falls within the original cost/performance parameters desired. The intention has been to reduce noise and hence errors to a level that the photometer is essential limited in accuracy solely by atmospheric and photon noise.

The photometer design has been used on two telescopes systems during this project. The original system had two Newtonian reflectors mounted on German Equatorial Mountings. The main telescope was a 300mm aperture f/3.5 and the secondary telescope was a 130mm f/3.

The 300mm reflector has since been replaced by a 355mm f/10.6 Cassegrain and a 254mm f/16 Cassegrain operating as a twin telescope system on a single mounting (Figure 7.1). Using Cassegrain' telescopes makes the task of balancing and operation relatively easy. The arc described by the photometer head during the course of a night's observing is relatively small as it is carried axially at the rear of the telescope. With a Newtonian reflector the head is carried several metres above ground level and the weight is off the optical axis so that radial counterbalancing is required.

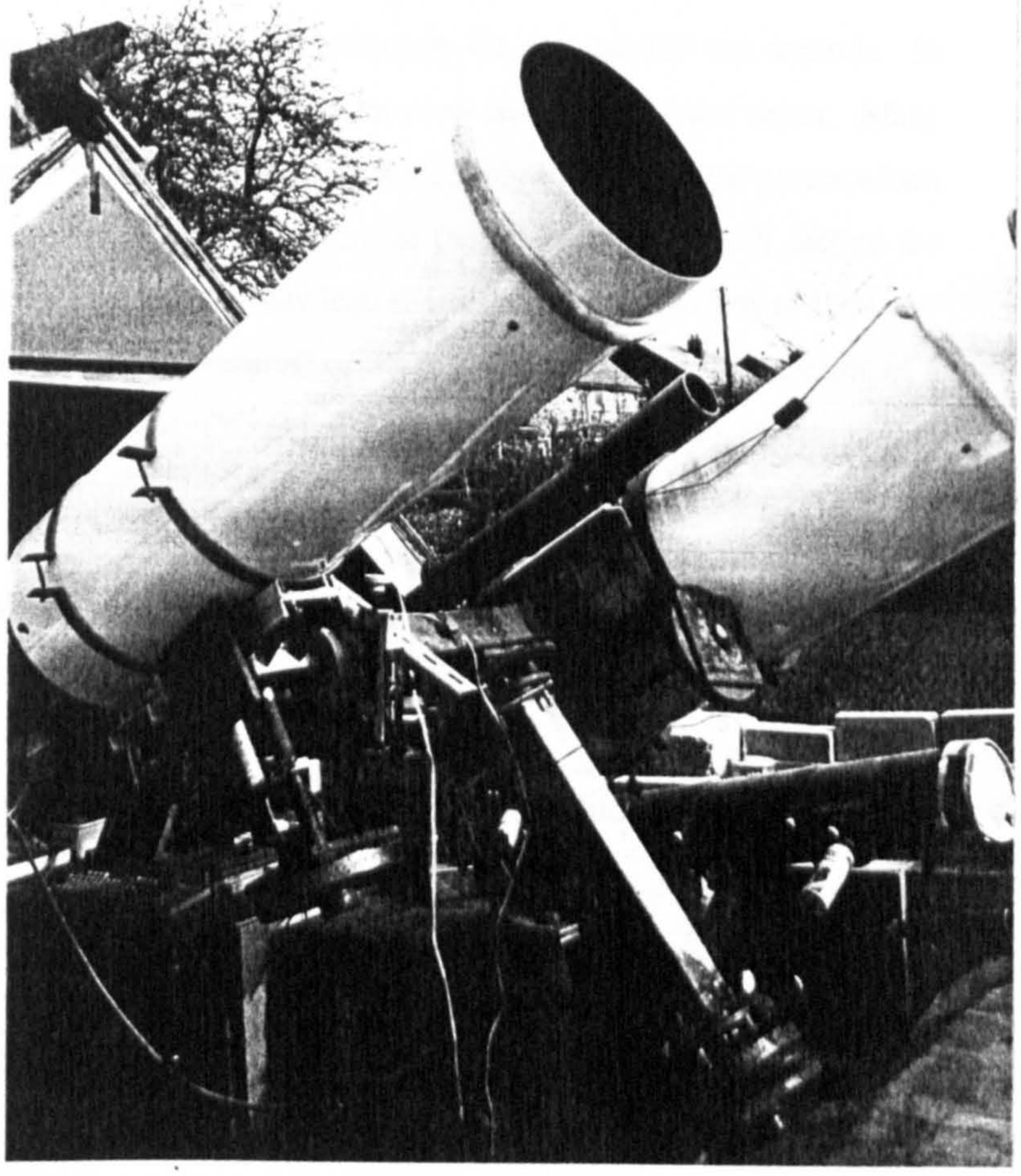

Figure 7.1 - Photograph of the observatory showing the telescopes and instrumentation

7.2 Photometer Head Design

One basic condition required was that the head should be no heavier than the body of a typical single-lens reflex camera. This was to allow it to be carried on most driven telescopes. The basic design is similar to that described by Stokes (1982). The photometer head is connected to the telescope using a standard 31.7mm push-fit flange. No additional bracing or telescope support has proved necessary.

Diaphragm apertures are provided corresponding to approximately 60, 90 and 120 arc seconds. In addition there is a wide aperture of 20 arc minutes to allow location and centering the object. Many observers select the diaphragm aperture without giving any consideration to the related errors which may be introduced. In general the maxim is that the errors in the telescope drive will dictate the minimum size of the aperture usable. This approach may lead to inaccuracies due to loss of light and if the aperture is reduced to, for example, 20 arc seconds or 30 arc seconds, an inevitable error of a few percent will be introduced in a measurement (Young, Talbert and Angione 1984). Inspection of a typical stellar profile with a 0.4 m aperture telescope under typical atmospheric seeing conditions (see Figure 7.2) shows that most of the energy of a star image is concentrated in a circle of radius 10 arcsecs but that a significant proportion of the image spreads at least 10 times further than this. The image may spread even further if the mirror coating is old or dusty.

The number of stellar diffraction rings passed through a given diaphragm aperture is approximated by

$$n = \frac{D\ r}{k\ \lambda} \qquad \ldots (7.1)$$

(KenKnight 1985)

where

n = the number of diffraction rings

D = telescope aperture in metres

r = radius of the diaphragm aperture in radians

k = a constant (This has been determined by KenKnight as typically 1.6)

λ= the wavelength of light in metres

Since an object is centred in the diaphragm aperture by eye, it is inevitable that it will not be placed exactly in the centre and a misalignment of from 10 to 20 rings will occur which corresponds to 5 to 10 arcsecs for a 300mm telescope. KenKnight reports that the change in transmission by an aperture for each ring of misalignment corresponds to

$$dP = 24 \,.\, K \,.\, (\pi)^{-2} \,.\, (n+1)^{-3} \qquad \ldots\ldots (7.2)$$

(eq 9 KenKnight 1985)

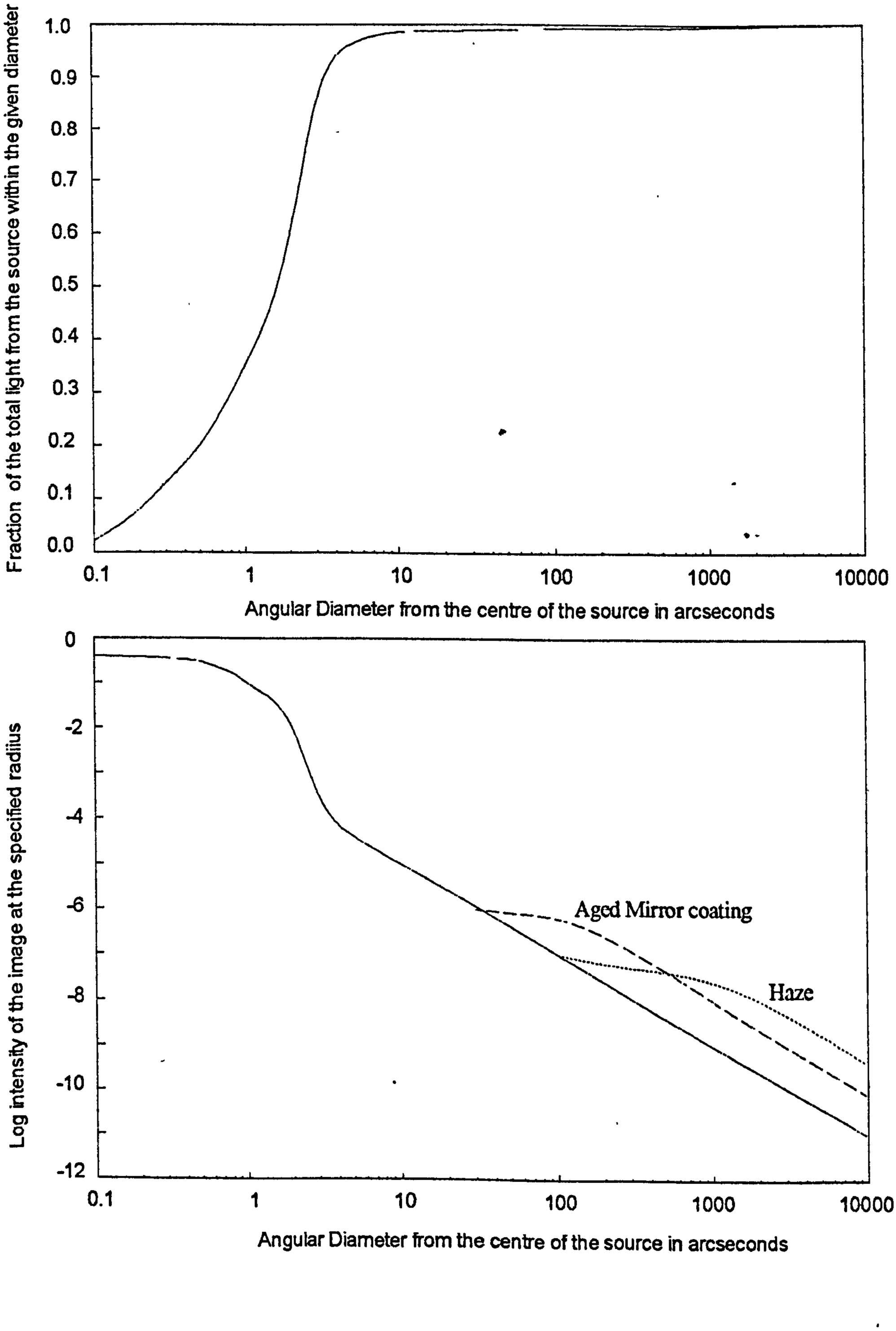

(After KenKnight)

Figure 7.2 - The profile of a stellar image. The upper graph shows the fraction of the total light contained within the specified radius. The lower graph shows the variation in the intensity of the image with respect to the radius.

where

K is a constant which depends on the accuracy of the surface figure of the mirror and the condition of its coating. KenKnight has determined a typical value for this of about 25

A diaphragm aperture as small as 42 arc seconds will therefore introduce a loss in a reading of at least 2% if the centring error is 20 rings (this corresponds to an error of 0.02 magnitudes). A common size of aperture is 60 arc seconds and the same misalignment will produce a loss of at least 0.7%. The effect of this error is reduced when differential photometry is used as the ratio of the measurements is taken. As long as the centring error is similar for measures of the object and the reference star the losses will cancel however in practice this is unlikely and so there will be a random error introduced into the readings due to miscentering. A practical solution is to use as wide an aperture as is practicable to ensure as much of the starlight as possible is transmitted even if some misalignment occurs.

The theoretical loss due to diffraction as the diaphragm aperture size varies is shown graphically in Figure 7.3.

The photometer head design includes a small mirror that can be flipped into the incoming light path to divert the beam through a relay lens to a 12mm focal length post-viewing eyepiece with illuminated cross-wires. This arrangement is used to centre the object in the diaphragm. The mirror is then flipped out of the light path to allow a reading to be taken.

A 19mm diameter 37.5mm focal length plano-convex lens is used as a Fabry lens positioned 40mm from the photocathode. By this means, a defocused image of the primary telescope mirror is cast onto the photocathode, which minimises both the effects of any variation of sensitivity across the face of the photocathode, and also the effects of any minor errors in the drive. In this design, the image spot is approximately 5mm in diameter at the photocathode (the minimum dimension of which is 8mm). Formulae for the design of Fabry lenses are given by Hall and Genet (1982) and Henden and Kaitchuck (1982).

Optical filters, approximately matching the Johnson UBV photometric system (Allen 1973), are carried on a sector plate positioned between the Fabry lens and the PMT. An exact match is not possible as the spectral response of the photocathode differs from that used originally to establish the system and the glass filters have a slightly different colour transmission from those originally used (and indeed between different production melts). The filters are 15mm squares of filter glass, 1mm or 2mm in thickness, supplied by Schott. The spectral response of the photomultiplier/filter combinations used calculated from the graphs by Schott (1985), are shown in Figure 7.4 together with the Johnson standard UBV passbands. Changes in the temperature of the filters can shift the passbands by up to 10

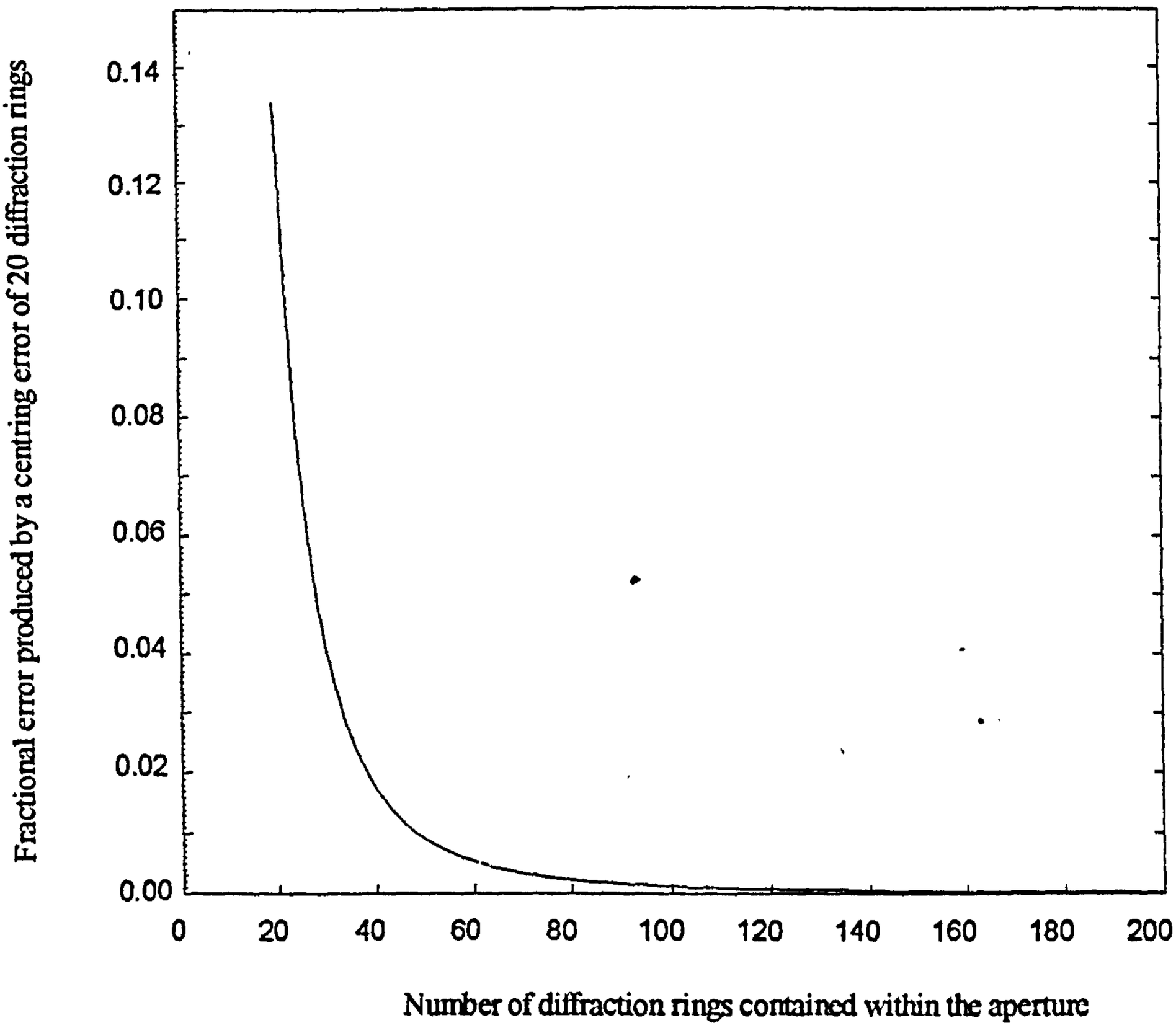

Figure 7.3 - The fractional loss in light transmitted through a diaphragm aperture due to misalignment of the source of 20 diffraction rings.
This can be related to diaphragm and telescope aperture sizes using Equation 7.1

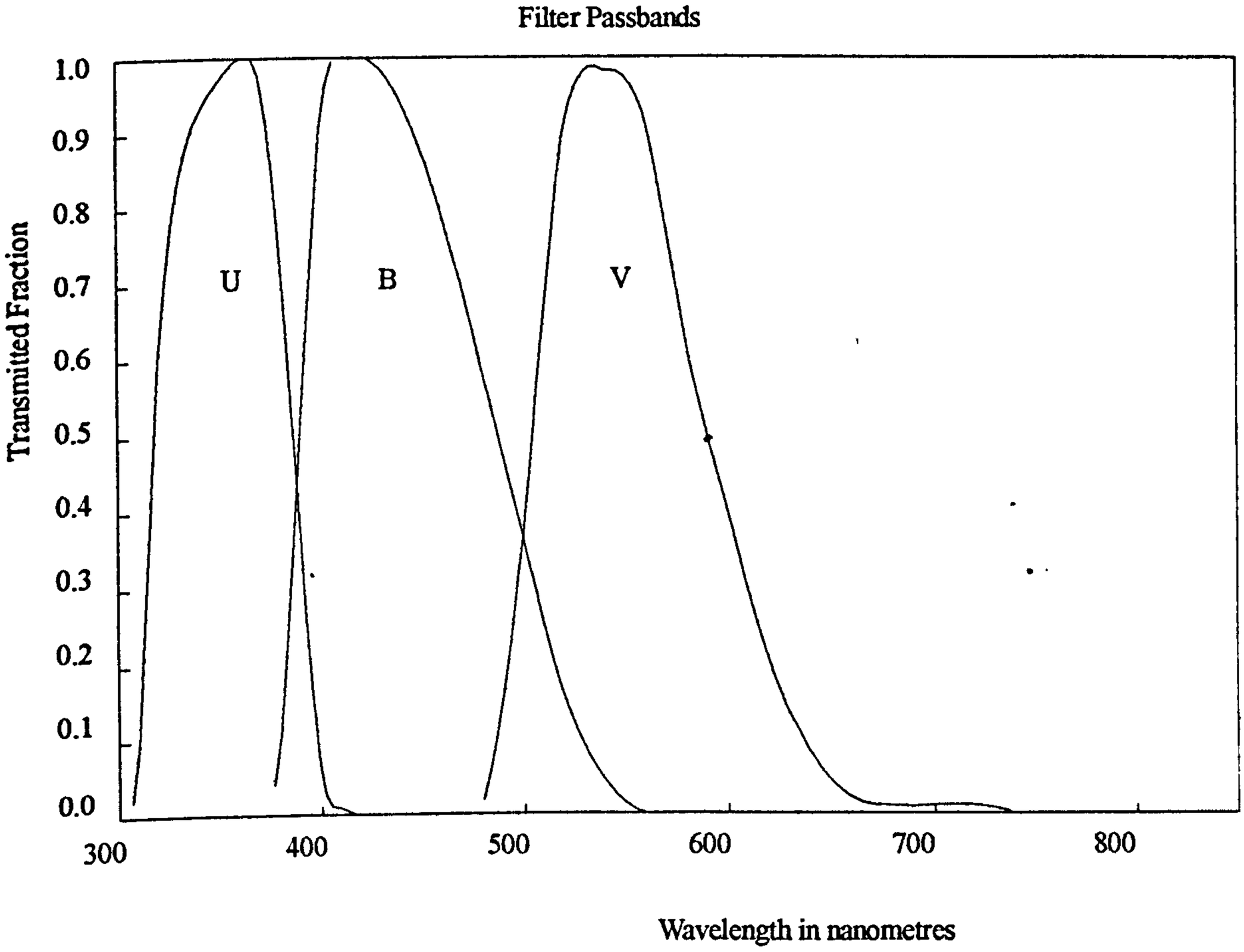

Figure 7.4 - Standard UBV passbands (according to Johnson - given in Allen 1973)

nanometers/°C (Young 1985). If observations are required to an accuracy of 0.001 magnitudes, then the temperature of the filters must be maintained within a few tenths of a degree during an observing run. The value of temperature for stabilisation is only significant if absolute photometry to millimagnitude accuracy is being carried out from high altitude observing sites.

The PMT, socket, dynode chain and head amplifier are also carried in the head, see Figure 7.5. No magnetic shielding for the PMT has been included. Side-window photomultiplier tubes have been used, which are less susceptible to errors from stray magnetic fields than end-window tubes. In practice no changes in photometer reading have been experienced which could be attributed to electromagnetic interference.

The complete photometer head weighs 0.7 kg. Adjustments can be made easily since one side of the head is detachable to allow access to the PMT and electronics. A schematic layout of the photometer is given in Figure 7.6.

7.3 Choice of Photomultiplier

The photomultiplier selected was a 1P21 side-window tube. This type of tube was used by Johnson and Morgan (1953) when the UBV photometric system was originally established, and later extended by Johnson and Harris (1954). This photometric system is wideband and is closely tied to the Morgan-Keenan (MK) stellar spectral classification.

Cooling the PMT is one method commonly employed to reduce the dark current. Cooling the tube to -20° C can reduce the dark current by a factor of at least 200. Changes in the temperature of the tube can give rise to changes in the sensitivity of the tube as illustrated in Figure 7.7 taken from Hamamatsu (1982). A typical value for this change is -0.5%/°C (Stubberfield 1985). Cooling with dry-ice can give rise to variations of temperature as the charge carried in the head sublimates (Miles 1986) resulting in variations in tube sensitivity. According to Rosen and Chromey (1985) gain variations may become an important source of error at the 1% level in pulse counting systems unless special precautions are taken. Electric cooling by the Peltier effect would hold the temperature and sensitivity constant (Walker 1986) but at the expense of increasing the weight of the head. The effect on the dark current of dehumidifying the head using silica gel desiccant that has been dried by heating in an oven has been measured during this project and is shown by Figure 7.8.

Experiments carried out in connection with this project have shown that the effects of dehumidifying and rehumidifying are reversible. A photomultiplier stored in a damp environment can be brought to a usable state in less than 24 hours. It is probable that the poor reputation of side-window

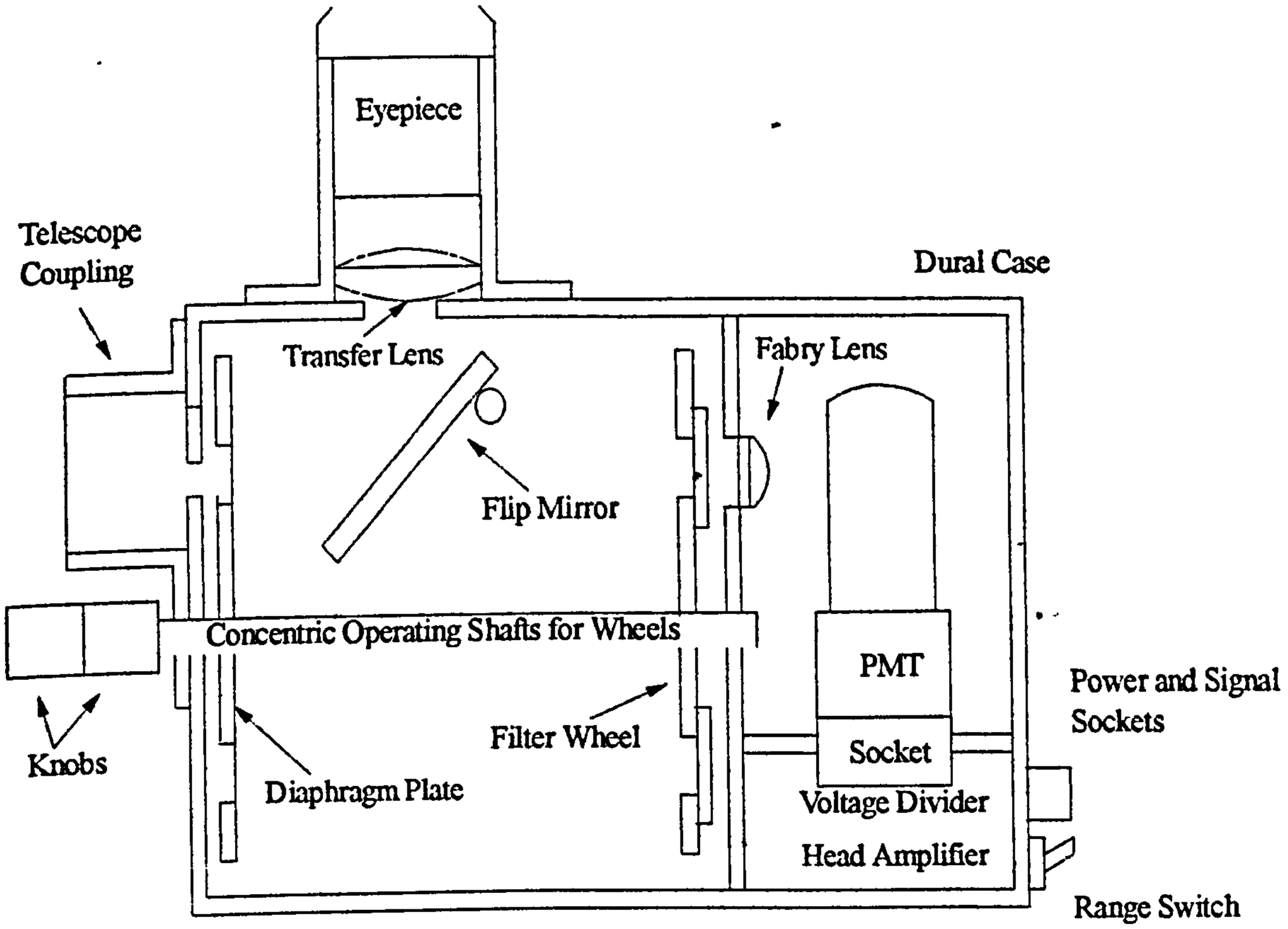

Figure 7.5 - General Arrangement of the Photometer Head
(Vertical Section)

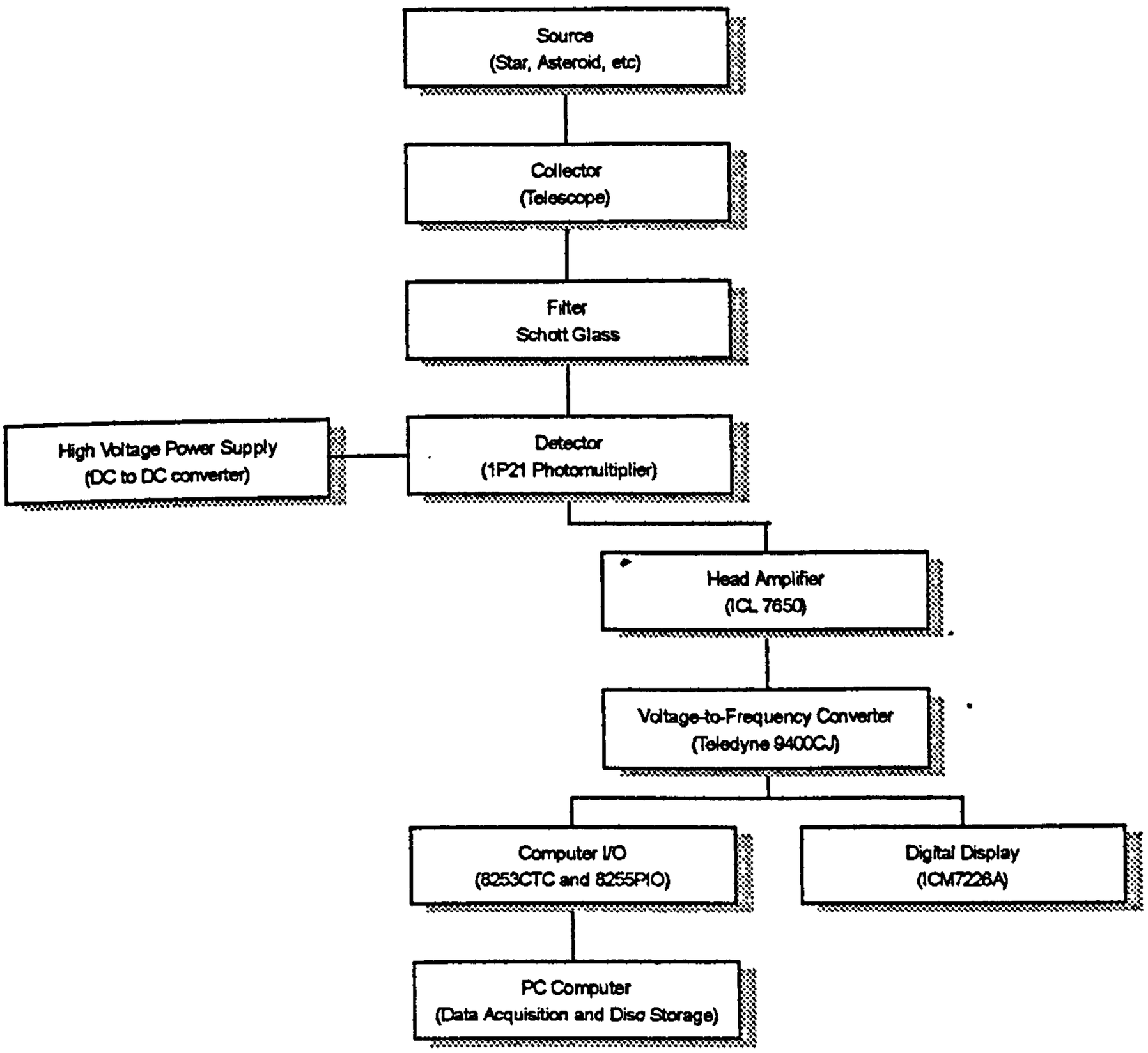

Figure 7.6 - Schematic Layout of the Photometer

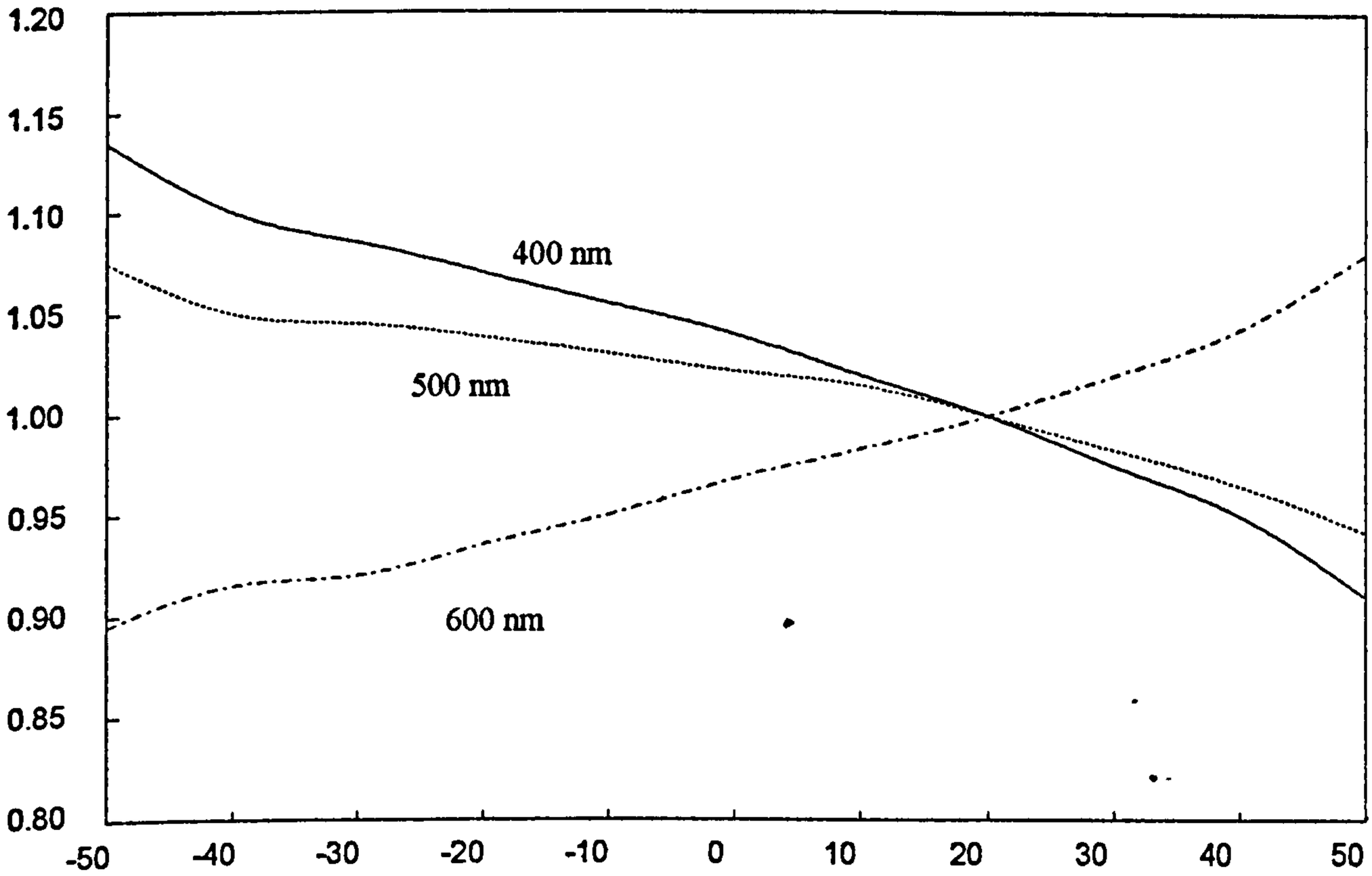

Figure 7.7 - The change in sensitivity of the 1P21 photomultiplier with changing temperature at three wavelengths source Hammamatsu UK

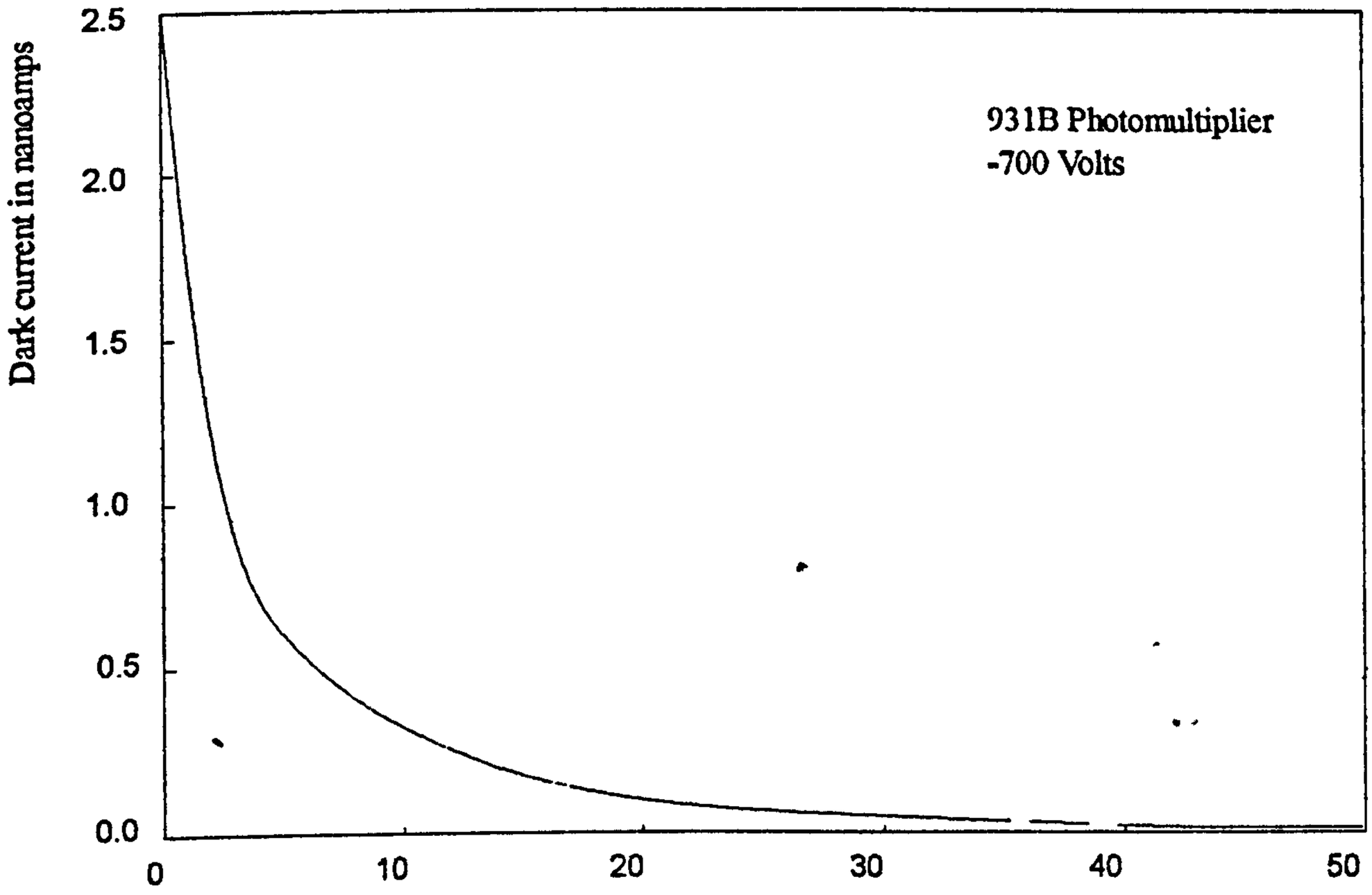

Experimental Data - Individual points not shown as data logged continuously

Figure 7.8 - The change in dark current with time as a photometer head is dehumidified from ambient conditions using silica gel as a dessicant

photomultipliers comes from their use undesiccated in humid environments, the results in Chapter 8 spcak for themselves.

In the 1P21 photomultiplier, photons pass through a borosilicate glass window and encounter the Sb-Cs type photocathode, where photoelectrons are generated. Nine semicircular dynodes amplify these photoelectrons. Several PMTs were used during the course of this project and all were manufactured by Hamamatsu. The certified dark current of each was less than 1 nanoamp at 1000 volts, 25°C and normal humidity. The typical rated sensitivity of the anode is 830 amps/lumen and the cathode is 50 amps/lumen under the same conditions. A corresponding amplification of 13.6 million is obtained at -1000 volts. At the typical operating voltage of -700 volts, the actual anode dark current recorded in the dehumidified head was 5 picoamps. At this voltage the current amplification is approximately 1 million (derived from the manufacturer's data). The typical anode response curve for the photomultiplier is illustrated by Figure 7.9.

The dynode resistor chain consists of eight 330 kilohm resistors from D1 to ground with the K-D1 resistor being 50% greater at 500 kilohm as recommended by the manufacturer.

Observation at the telescope indicates that the measured dark current corresponds to the signal received from a star of magnitude 14 using a 300mm aperture telescope. At a signal-to-noise ratio of 1 this would correspond to the lower limit for observation. The Shot noise on the dark current of 5 picoamps is 0.4 femtoamps for a 0.1 Hz bandwidth. The Equivalent Noise Input (ENI) is a measure of the amount of electromagnetic radiation, in Watts, required to produce a S/N ratio equal to 1 and is given by

$$ENI = \frac{(2 \,.\, q \,.\, I_{dB} \,.\, G \,.\, B)^{0.5}}{S} \qquad \ldots (7.3)$$

(Hamamatsu 1982)

where

q = the electron charge ($1.60 \,.\, 10^{-19}$ coulombs)

G = the current amplification

B = bandwidth (Hz)

S = anode radiant sensitivity (amps/watt)

I_{dB} = dark current in amps

The ENI of the 1P21 device employed under normal operating conditions is $2.2 \,.\, 10^{-18}$ Watts.

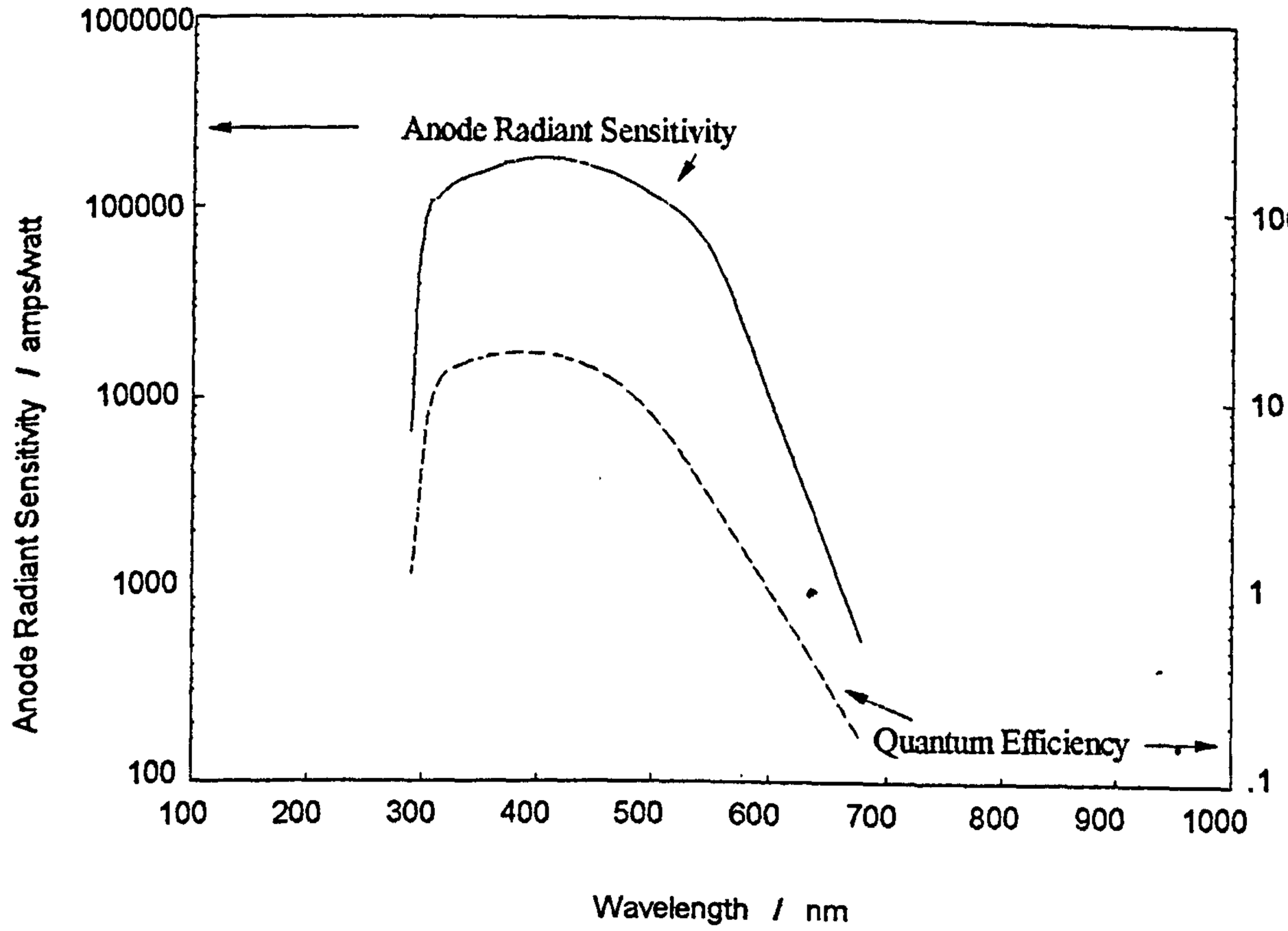

Figure 7.9 - The variation of Anode Radiant Sensitivity and Quantum Efficiency with respect to wavelength of light from the source for the Hammamatsu 1P21 Photomultiplier

7.4 High Voltage Power Supply

A photomultiplier requires a high dc voltage for operation. Each dynode requires a potential of about 100 volts and for the 1P21 it means a supply at -700 volts to -900 volts. The load is mainly that of the dynode chain and as this is a high resistance (3 Megohms) the power supply only needs to be capable of supplying a relatively low current (1 milliamp).

The gain of a photomultiplier can be expressed in the form

$$G = K \cdot V^{\alpha.n} \qquad \ldots (7.4)$$

(Hamamatsu 1982)

where

G is the gain of the tube

K is a constant

V is the applied voltage

n is the number of dynodes

α is a dynode coefficient (measured by Hamamatsu as typically 0.7 to 0.8)

For a nine-stage photomultiplier like the 1P21 type the tube gain is approximately proportional to the seventh power of the applied voltage (see Figure 7.10). For this reason it is advisable to regulate the output of the HV power supply so that both drift and instability are reduced to a minimum. Short term stability in the supply voltage over a time scale of 1 to 10 minutes should be ±0.1% or better, corresponding to a change of 0.7% in the photometer output. The resulting error in an observation would be 0.008 magnitudes. At an operating voltage of -700 volts this means that a steady drift of less than 1 volt over 30 minutes would be acceptable.

The basic design criterion was to produce a variable regulated HV power supply that can deliver -600 volts to -1000 volts at a maximum output current of 1.5 milliamps and with a short term drift of less than 1 volt/hour.

Commercial modules suitable for use with photometers are available but costly. The design prepared for this project can be constructed cheaply even including case and low-voltage power supply.

Three main methods are available for generating high voltages. The most simple of these is the use of a bank of batteries in series to achieve the voltage required. High voltage batteries tend to be expensive, are sensitive to ambient conditions and have a limited shelf life. A more practical alternative employs the mains electricity supply which is multiplied to the required voltage using a step-up transformer and then rectified. The output may be stabilised using high voltage Zener diodes. However the most satisfactory method is to use a dc-to-dc converter. The principles of this circuit are

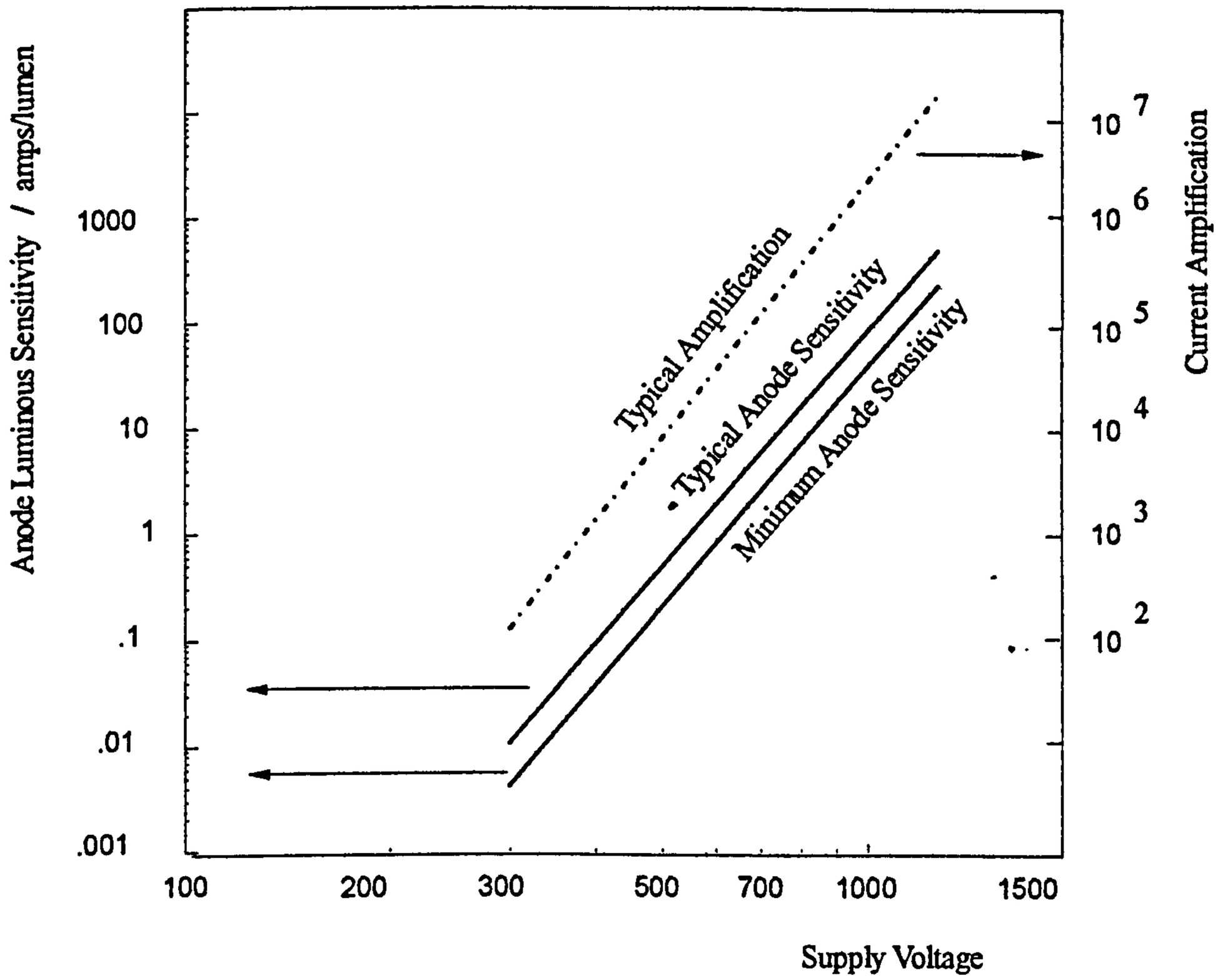

Figure 7.10 - The variation of the sensitivity and current amplification with supply voltage for the 1P21 Photomultiplier
Source Hammamatsu UK

discussed by Horowitz and Hill (1980). Here, a stabilised low-voltage dc drives an oscillator working in the range of 20 kHz to 55 kHz. The transformer is wound on a ferrite pot-core to produce an alternating high voltage source. This is then directly rectified or else rectified in conjunction with either voltage doubling or quadrupling. One practical design has been described by Hopkins (1981).

The new HV supply circuit presented here was designed with the assistance of T C Platt and is shown in Figure 7.11. It consists of a 50 kHz master oscillator driven by a 4069 CMOS IC (see Watson 1983) which pulses a VMOS driver transistor to provide the ac into the transformer. The transformer is wound on a standard RM6 pot-core. The output is fed to a voltage quadrupler/rectifier. The output is approximately 1800V. Voltage control is provided through a CA3140E op-amp used as a comparator. This IC has the great advantage that it can be fed from a single-polarity power supply. The non-inverting input of the op-amp is grounded to provide a fixed reference. The HV is fed to the inverting input through a 10 Megohm resistor, which is balanced by a reference voltage/variable resistance circuit. The output operates a current mirror which acts as a transistor switch which, when switched on, grounds the output of the master oscillator. Control is thus effected by altering the mark/space ratio of the pulses and adjustment of the output voltage is provided by the variable feedback resistance since

$$V_{out} = \frac{\text{Feedback Resistance . Reference Voltage}}{\text{Reference Resistance}} \quad \ldots\ldots \quad (7.5)$$

For values of reference voltage between 5V and 7V zener diodes are adequate. In this range they are adequately stable to changes in temperature and indeed 3.8V is a standard reference used in computers.

On test the finished device showed a stabilisation period of less than 30 minutes during which the drift was 6V (0.9%). After this initial warming-up period the output subsequently drifted by only 3 volts (0.5%) over 7 hours. During this test the temperature of the room varied by approximately 10°C from 19°C to 9°C. The maximum recorded short-term variation (0.01 sec) was 1.2 volts (0.2%). The measured variation in voltage is shown in Figure 7.12. As mentioned above, a steady drift has little effect on the accuracy of the final result provided that differential photometry is used. With this method, readings from the object under observation are bracketed by observations of the reference stars. The readings of the reference stars can be averaged to estimate their value at the time readings of the object were taken.

The Zener diode of the above instrument has since been replaced by a ZNREF025 2.5V precision reference voltage source. This is a stable reference at normal operating temperatures and has eliminated drift in the voltage supply.

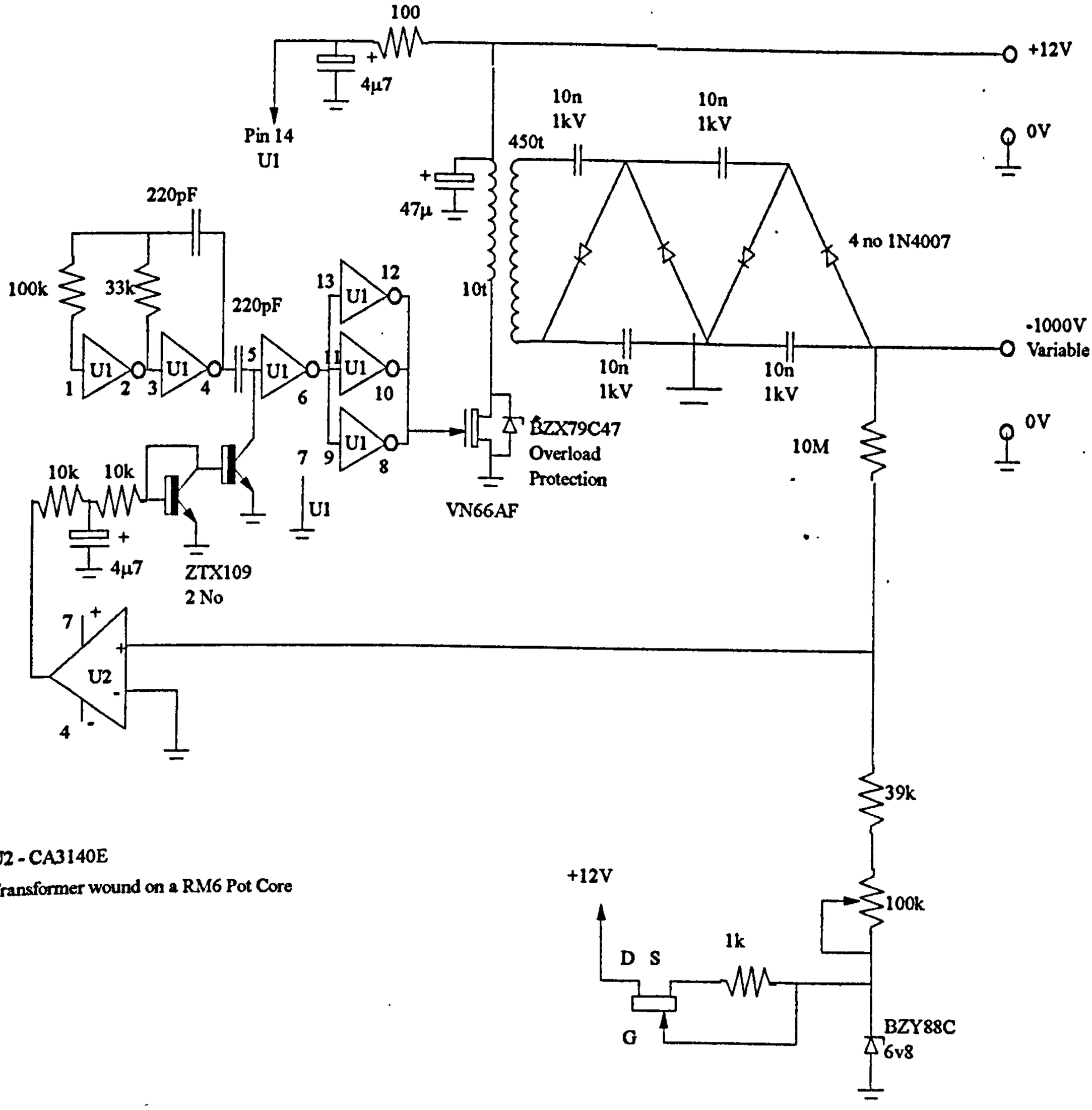

U2 - CA3140E

Transformer wound on a RM6 Pot Core

Figure 7.11 - Circuit diagram of the regulated high voltage power supply for the photomultiplier

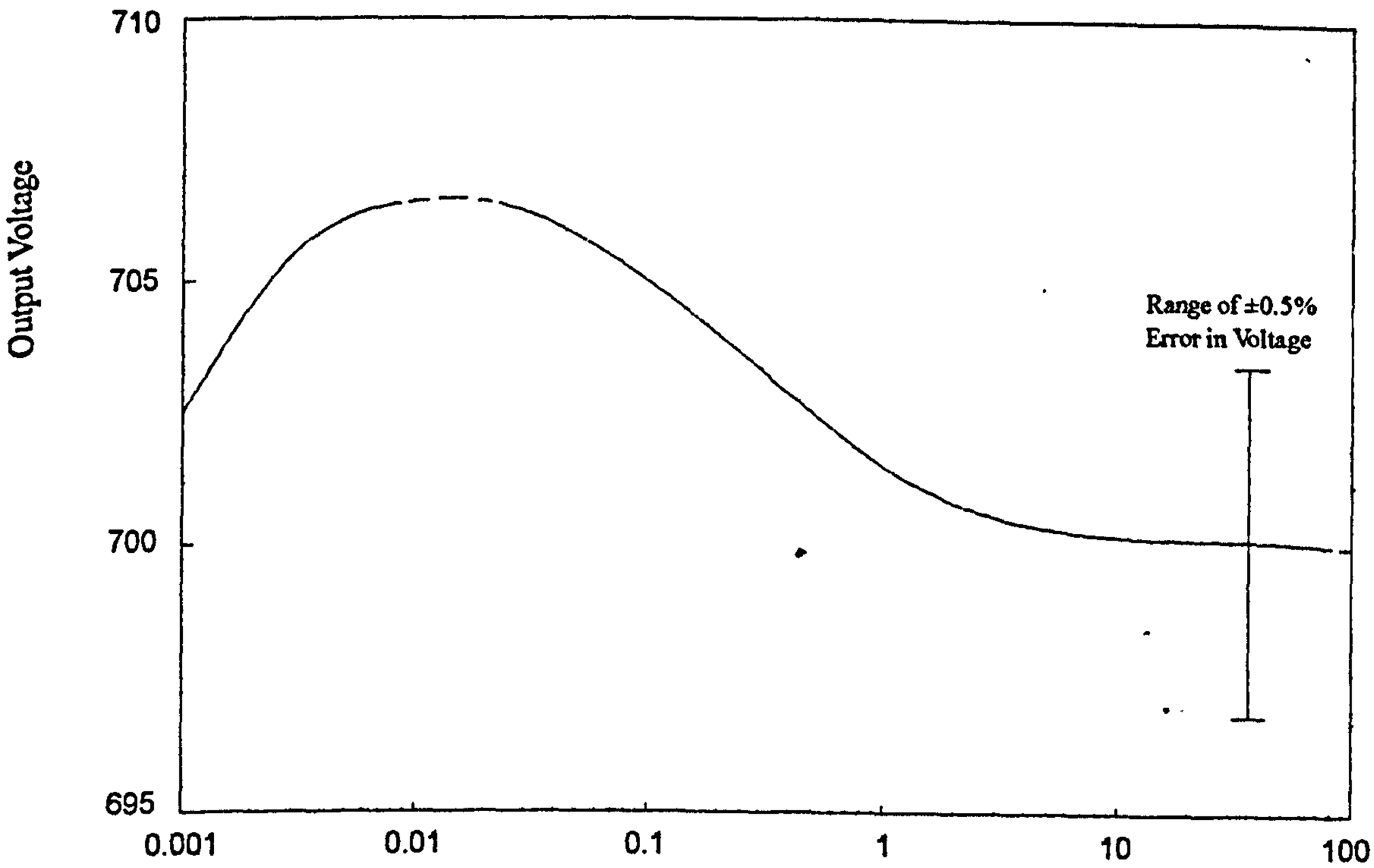

Figure 7.12 - The variation of output voltage with time as the High Voltage Power Supply warms up

7.5 Detector Electronics

In 1980, Intersil introduced the ICL7650 op-amp (Intersil 1980). This device has internal chopper stabilisation which reduces the input offset drift to 0.01 microvolts/°C (compared to the Analog Devices AD515, one of the best examples of earlier designs, with a typical drift of 15 to 25 microvolts/ °C). The typical input bias current at 25°C of the ICL7650 is 1.5 picoamps. With a $\pm$ 5 volt power supply it gives a maximum output of approximately 4.8 volts.

The circuit design makes use of this op-amp, operating as a current-to-voltage converter. The op-amp feedback resistor comprises a T-network of three small value resistors (see Dupuy 1983) to obtain a high equivalent resistance without using high value resistors. High value resistors pose handling problems as any external contamination (for example from fingers) can significantly affect the resistance by providing an external current leakage path. Low-value resistors should also be avoided owing to a significant contribution from Johnson noise, as discussed later in this section. The equivalent feedback resistance R of a T-network is given by

$$R_{eq} = R_{feedback} * (1 + R1 / R2) \qquad \text{..... (7.6)}$$

(see Figure 7.13)

The output voltage is related to the input current by Ohm's Law

$$V_{out} = - i_{in} \cdot R_{eq} \qquad \text{..... (7.7)}$$

The circuit designed for this project is shown in Figure 7.14. It will handle photocurrents between 1500 nanoamps and 0.025 nanoamps (full scale) in three gain ranges. It is built on double-sided, glass fibre, printed circuit board and the layout has been designed to minimise leakage currents and to screen areas where low currents occur.

The output is fed to a Teledyne 9400CJ V-to-F converter. The use of voltage-to-frequency conversion allows much greater accuracy than that attainable using a chart recorder. As there is a digital output there is a great dynamic range possible for each gain setting. A 9400CJ V-to-F is used for this design since it has a typical linearity of 0.01% when scaled for a maximum output of 10KHz (Teledyne 1980). The circuit design follows the recommendations of Teledyne but has been rescaled to give maximum output of 13 KHz for a 4.8 volt input. This output value was originally chosen because the computer compatible frequency/2 output, when counted for a 10 second gate period, yields 65536, corresponding to 2^{16} which was counted using 2 bytes of memory with a Z80 based computer. In this design

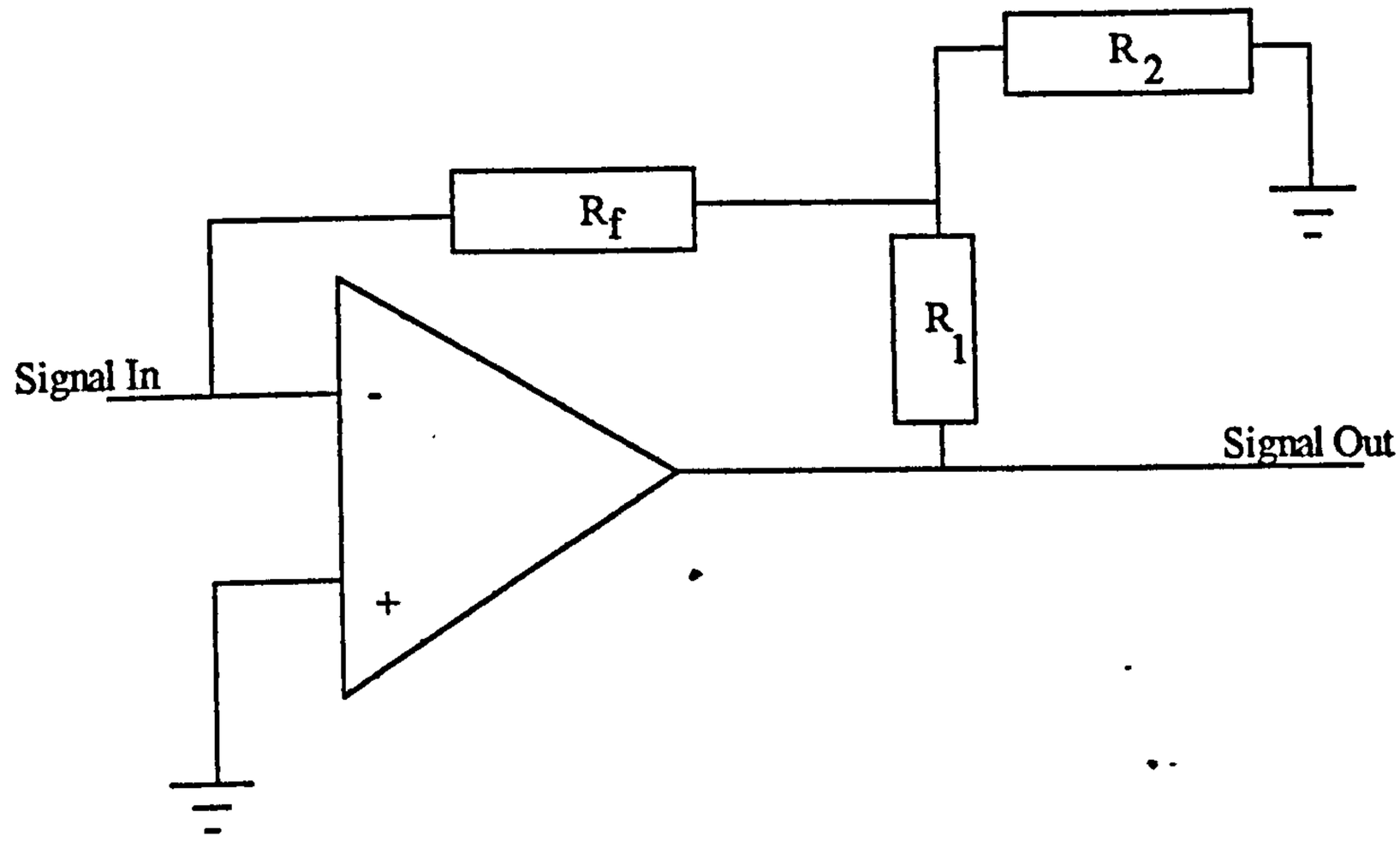

Figure 7.13 - Tee Circuit for Op-Amp Gain multiplication

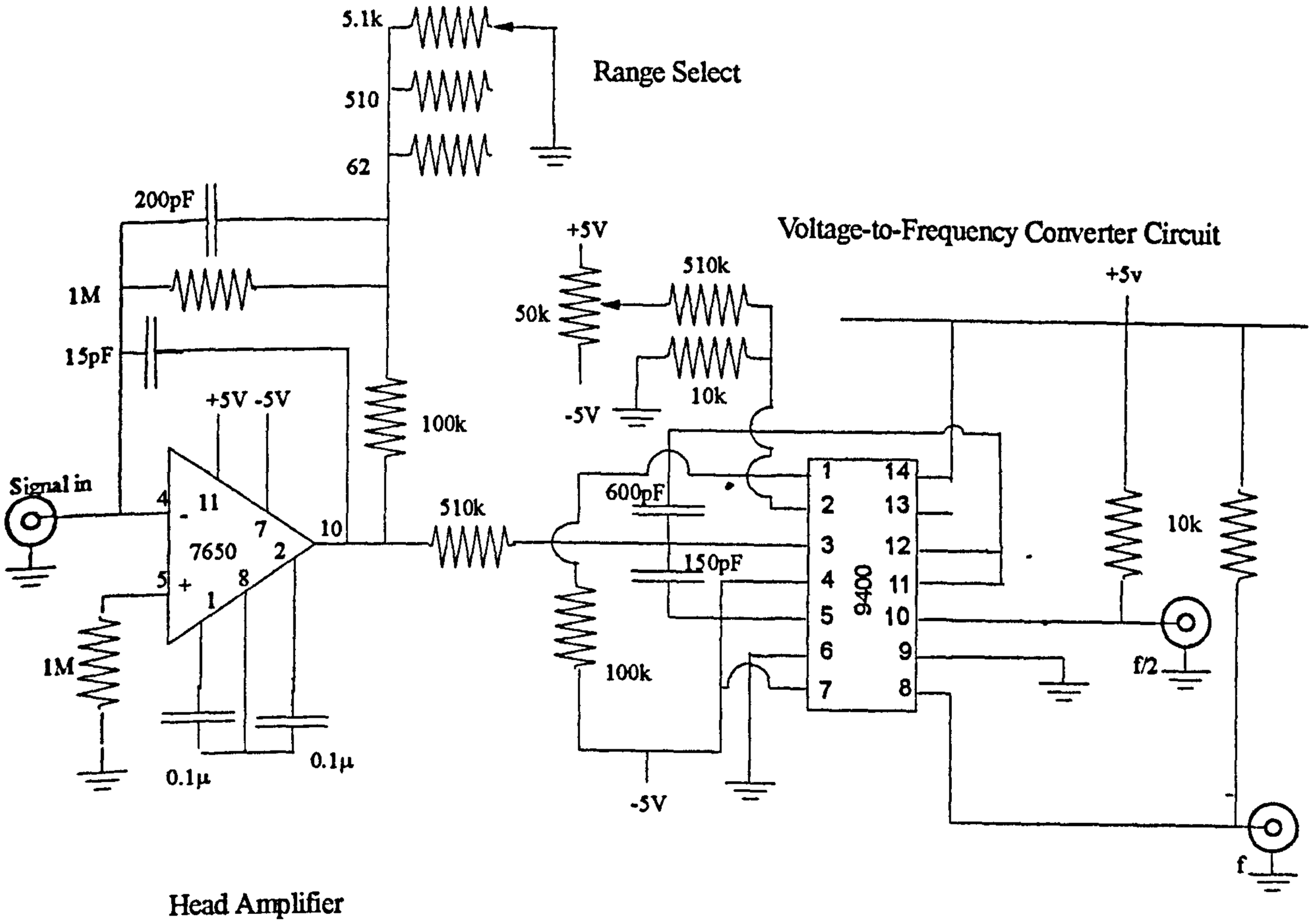

Head Amplifier

f - to frequency counter

f/2 - square wave output
to computer

Figure 7.14 - Circuit diagram for the Head Amplifier and the Voltage-to-Frequency Converter

$$f_{out} = V / (R_{in}\ V_{ref} . C_{ref}) \qquad \text{..... (7.8)}$$

The V-to-F used by DuPuy has no zero offset and an extra op-amp is used as a comparator. A third op-amp is used for second stage amplification to scale the input of the V-to-F. The 9400CJ V-to-F used here has a built-in offset null, and no second stage amplifier is necessary. This circuit is therefore much simpler than DuPuy's circuit. The offset is adjusted to give a count of about 20Hz on the highest gain setting of the amplifier. This ensures that a valid reading is obtained under all operating conditions since the V-to-F will not register voltages that are negative with respect to the nulling voltage.

The 9400 has two outputs. The frequency (f) output gives pulses of about 3 microseconds duration which will drive a frequency counter. The other output produces a square wave of frequency/2 (f/2) which is ideal for interfacing to a computer. For this circuit

$$f_{out} = 2.614 . 10^9 . i_{photocurrent}\ (1+10^5 / R_{gain}) \text{ ... (7.9)}$$

where $i_{photocurrent}$ is the photomultiplier output current in amps

R_{gain} is the value of the switched gain resistor

The high gain setting resistor is 62Ω and an output frequency of 1Hz represents a photocurrent of 0.23 microamps. For visual display and recording, the f output is fed to a frequency counter based on the ICM7226A IC in a circuit similar to that of the RS Components data sheet (RS 1982). This 10 MHz counter/display driver can be operated for gate times of 1 second or 10 seconds.

A full discussion of the sources of amplifier noise is given by Horowitz and Hill (1980). Two main sources should be considered in this application. These are Johnson noise and Shot noise.

Johnson noise is generated by the random movement of electrons in components. It is a white noise source which is dependent on the temperature only. The noise current is described by the following relationship

$$I_{noise}(rms) = (4 . k . T . B / R)^{0.5} \qquad \text{... (7.10)}$$

where k = Boltzmann's constant ($1.38 . 10^{-23} . V^2 Hz^{-1} ohm^{-1}$)

T = Absolute Temperature (°K)

B = Bandwidth in Hz

R = Resistance (ohms)

Shot noise is produced by the random elements of current flow. Like the Johnson noise it is a white noise source.

$$I_{noise}(rms) = (2 . q . I_{dc} . B)^{0.5} \qquad ..... (7.11)$$

where q = the electron charge ($1.60 . 10^{-19}$ coulombs)

B = Bandwidth in Hz

I_{dc} = dc current flow in amps

The bandwidth is equal to the reciprocal of the integration time when V-to-F conversion is used (Horowitz and Hill 1980). Assuming an observing temperature of 10°C and a T- resistor network of 1 Megohm, 100 kilohm and 62 ohm resistors, a 1 Hz bandwidth will produce a Johnson noise (rms) of 15.9 microamps. Increasing the integration time to 10 seconds will reduce this component to 5 microamps. This noise component is generated in the 62 ohm resistor. The other resistors contribute noise at least two orders of magnitude lower. Though termed noise, it is the random variation in this current which gives rise to errors in the observations (the noise on the noise current). Though not assessed specifically during this work the results obtained at the telescope suggest that the random variation is at least ten times lower than the Johnson noise.

For this design of amplifier, given a bandwidth of 1 Hz and a photocurrent of 1000 nanoamps, the Shot noise generated is only 0.6 microamps and so can be effectively ignored. For a dark current of 5 picoamps the Shot noise is only 0.0004 microamps, which is too low a value to affect the reading from the V-to-F.

When faint sources are measured the accuracy attainable is limited by the Johnson noise. Accuracy can only be improved by reducing the bandwidth, i.e. increasing the measurement time. If the integration time is increased from 10 seconds to 40 seconds the Johnson noise component is halved from 5 microamps to 2.5 microamps. The dark current of the system has been regularly measured during the course of each night's observation there is a variation as the external temperature changes and also as the system warms up. The variation during the course of several successive counts is found to be ±2 Hz corresponding to a noise on the dark current of approximately 0.5 microamps.

7.6 Computer Interfacing

Astronomical photometry and associated data acquisition is perfectly feasible manually, but data reduction is much simpler if a microcomputer can be used and many suitable programs have been published (such as Genet 1980 (i)). The options for carrying out some form of automation depend on the nature of the observing programme contemplated. One approach is to use the computer for

telescope control as well as for photometer control, thus dispensing with the observer altogether (Boyd, Genet and Hall 1984). Fully automating a telescope in this way is a difficult and time consuming process. However, successful designs have been completed and described in detail (Trueblood and Genet 1985). Automating only the photometer is easier but does require additional hardware including stepper motors and drivers for changing apertures and filter wheels (Fried and Mannery 1983, Zeilik and Elsdon 1982). The simplest form of computer interfacing is a direct link of the photometer V-to-F output to the computer which is used for recording the signal and reducing the data directly. One such system has been described by Genet (1980 (ii)).

The computer used in the present work is an Amstrad Portable PPC1640. Initially data was input manually using a compiled BASIC operating program. It has no I/O ports built in and so one was designed and built using an 8255 PIO interface chip and a crystal controlled oscillator running at 4MHz for integration timing. It is programmable to allow integration times between 0.02 and 20 seconds. It can be used for high speed occultation observation as well as conventional photometry.

The f/2 output of the V-to-F circuit is fed to the I/O device and the changes of state are read using an 8253 Counter/Timer IC.

The software has been custom written for this project using TurboBASIC and follows a sequence similar to that described by Fitzgerald and Shelton (1982). Data reduction follows outline schematics and formulae given in Henden and Kaitchuck (1982). However many improvements and enhancements have been added during use, allowing display of graphical reduced results during observation so that a check on progress can be made in real-time.

7.7 Reliability and Accuracy

The photometer system has seen extensive operation since commissioning in May 1983. It has proved reliable in operation though there is an occasional problem when extra pulses are recorded if certain electrical appliances are operated nearby - for example the switching of thermostats. Readings taken when this has happened are obviously too high and can be rejected by inspection. Fortunately this is a problem that arises infrequently.

The main sources of error inherent in the system have been discussed earlier the maximum value being the sum of the noise of the dark current of the photomultiplier and the noise on the Johnson noise in the main gain resistor (value 62Ω). Each of these have a basic current of 5 microamp and a random noise variation of the order of 0.1 of this. Other errors are introduced from the source and sky. The major source of error is photon noise. The detected photon flux can be approximated by

$$F \sim 1.06 \cdot 10^{6} \cdot A \cdot E \cdot 10^{-0.4(m-k)} \quad \text{..... (7.12)}$$

(Miles 1986)

where F = the photon flux in photons per second

A = Collecting area in cm^2

E = Collection efficiency ~0.017

m = Apparent visual magnitude of the source

k = Atmospheric extinction coefficient in the visual waveband in magnitudes per airmass (Typically 0.30 to 0.35 at the observing site)

E = is the product of the typical efficiency of the optical system (~0.35) and the sensitivity of the detector (~0.05) (Miles 1986). The value of E for the system is ~0.022 which is derive from the product of the efficiency of reflection at the two aluminised surfaces (65% assumed) and the transmission of the four glass/air surfaces (95% assumed).

For a source in the zenith taking k=0.3 Eq 7.12 reduces to

$$F = 23.8 \cdot 10^{3} \cdot A \cdot 10^{-0.4m} \quad \text{..... (7.13)}$$

(see Figure 7.15)(Miles 1986)

The current output of the photomultiplier is given by

$$\text{Photocurrent} = PMT_{gain} \cdot F \cdot q \quad \text{..... (7.14)}$$

PMT gain ~10^6

q is the electron charge ($1.60 \cdot 10^{-19}$ coulombs)

Hence a flux of 1 photoelectron/second produces a photocurrent of $0.16 \cdot 10^{-12}$ amps.

Using equation 7.9 if a 62 ohm scale resistor is used then a count rate of 1 Hz corresponds to a photocurrent of $0.23 \cdot 10^{-12}$ amps, i.e. a flux of 1.5 detected photoelectrons at the main mirror of the telescope gives a count rate of 1 Hz.

The photon noise error is the square root of the number of photons detected - which is the Poisson Statistics result and is applicable to any count. There is a variation in the number of photoelectrons produced by the photomultiplier per incident photon but this is averaged out during the integration.

Using a 300mm aperture telescope, a 10th magnitude source will produce ~1000 photoelectrons/second detected (corresponding to a photocurrent of ~ 1.6 nA). With a 10 second counting period ~10000 photoelectrons will be recorded and the photon noise will be ~100 which is 1% of the signal (corresponding to an accuracy of 0.01 magnitudes - see Figure 7.15). For a 12th

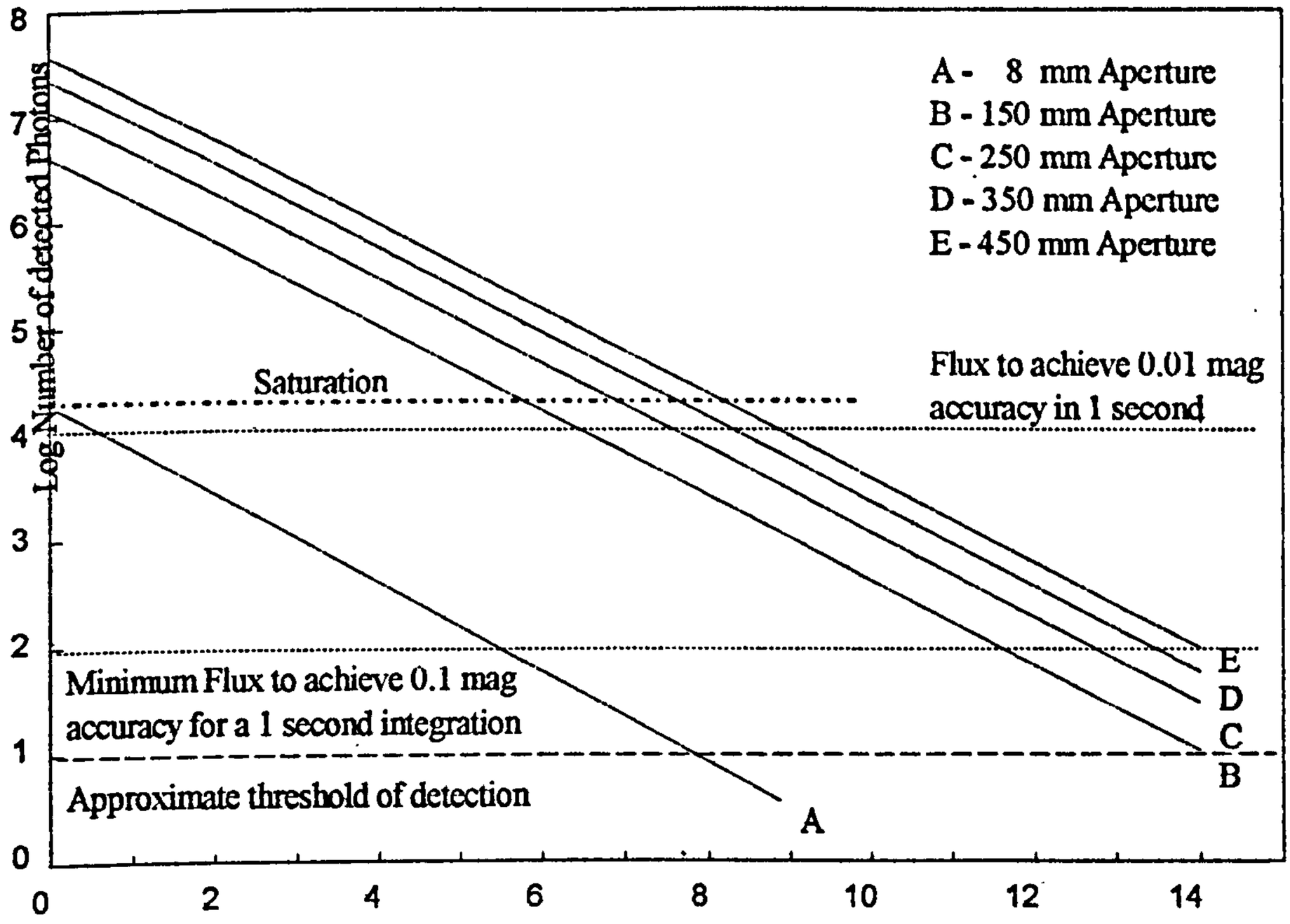

Saturation - The maximum measurement possible on the most sensitive setting of this photometer design without overloading the head amplifier

This graph is based on a fractional airmass of 1 (source in the zenith)
PMT gain 10^6

Figure 7.15 - A graph showing the Photon Flux from sources of magnitudes for a range of telescope apertures.
The 8mm aperture (representing the fully dark adapted human eye) is also given for comparative purposes.

magnitude source (~110 photoelectrons/second) a 10 second integration period gives a count of 1100 photoelectrons and a noise error of 3%. It is necessary to increase the counting time to 90 seconds to detect a sufficient number of photoelectrons to reduce the photon noise error to less than the 1% level.

The typical sky brightness (using an 84 arc second diaphragm) on moonless nights and with little light pollution produces 20 photoelectrons per second which is equivalent to a star of V magnitude ~13. The typical photon noise error is 0.07 magnitudes but this is only significant if faint sources are to be measured (fainter than mag 12) when a smaller diaphragm aperture could be used. The use of small apertures (<~40 arcsecs) can cause problems in centring the object in the aperture (see earlier) and also if the telescope drive has much backlash which could easily give rise to greater errors than the noise in the sky count with a larger aperture.

~10000 photoelectrons must be detected before the error due to photon noise is reduced to 0.01 magnitudes. The integration time must be sufficiently long to allow this.

Other sources of error are introduced by the atmosphere. The movement of air cells in the atmosphere gives rise to unsteadiness in the stellar image (scintillation or 'seeing'). The cells are typically ~125mm in diameter (Hall and Genet 1982) and their effect is random. Larger apertures reduce the effects by covering several cells. In practice scintillation is the greatest source of inaccuracy in the measurement of bright sources whilst the measurement of faint sources (count rates <1 KHz) is essentially limited by photon noise.

Variations in the sky transparency also limit accuracy and are often the major limiting factor. The use of two telescopes taking simultaneous measures of the asteroid and comparison star largely eliminates errors from this cause. Systematic errors of a lower order can also be introduced if the value of the atmospheric extinction coefficient is incorrectly estimated or measured. An error of 0.1 magnitudes per airmass will give an error of 0.001 magnitudes in the final reduction if the difference in airmass between the object and the comparison is 0.01. There is a second-order extinction coefficient which depends on the colour index of the source. An error of 0.01 magnitudes per airmass in this coefficient will give rise to an error of 0.003 magnitudes if the difference in the B-V index for the object and the comparison is 0.3 magnitudes.

It is difficult to build a photometer that is an exact match to the Johnson UBV system because of variations in the filter glass and detector sensitivity. So it is necessary to determine the instrumental scale factors (the transformation coefficients) to convert results to the standard system. Errors in the zero points cancel if differential photometry is used and the scale factors are applied to the colour indices. As with the second-order coefficients an error of 0.01 in the scale factor will give rise to an error of 0.003 magnitudes if the B-V indices of the source and comparison differ by 0.3 magnitudes.

It is possible to reduce error by choosing a comparison of the same or similar colour index to the object. A full discussion of the sources of error is given by Hall and Genet (1982).

7.8 Recent Developments in Photometry

The design of photometer described in this chapter has been in use for several years. There has been a general improvement in the equipment. The most notable of these is that the head amplifiers are now constructed on screened fibre glass printed circuit boards. The purpose of this has been to reduce noise currents arising from both leakage currents and magnetic fields. This has reduced the noise on the dark current by a significant factor.

Developments in solid state technology have not produced a more cost effective or better design for the electronics. Experiments with the nominally lower noise ICL7652 shower no advantage over the ICL7650, it is probable that the benefits in noise reduction from the PMT by desiccating with silica gel are similarly experienced by the head amplifier circuit.

Recently CCD cameras have become readily available. The adoption of such cameras for use by the television companies has seen a great improvement in quality and a major reduction in price. Observers have been experimenting with their use for photometry and several asteroid light curves have been published in the ALPO Minor Planet Bulletin. In the past several factors have held back progress in this field.

1 CCDs have been very expensive and the sensitivity of individual pixels has been highly variable. In addition to these factors the chips have been small. Developments in the near future are likely to lead to inexpensive large chips (eg 1024 pixels square).

2 Early CCDs only had a low resolution (dynamic range). Currently 8-bit, 12-bit and 16-bit resolution is readily available. There is a trade off between sensitivity and computer memory usage and probably the best compromise is 12-bit sensitivity (1 part in 4096) which is the level achieved by the photometer described in this chapter.

3 Images use up a great deal of computer memory. A 512 pixel square CCD with 12-bit accuracy produces an image which requires 384 kB (this is a small image). With a typical observing run, 20 images per hour would be required for perhaps 6 hours and these would require 45 MB of storage. Allowing for calibration images, dark images, etc perhaps 50 MB would be required for processing. Recent falls in the price of computer memory have halved the priced of hard disks during 1994, however this storage space may prove hard to find if many night's data storage is

required. The advent of cheap tape or optical disk storage may improve matters in the near future.

4 The use of filters to match the standard UBVRI response curves is necessary. To ensure an even focus each passband must use filters of the same thickness so several neutral filters are necessary for this. The required thickness is 4mm. At present suitable filter holders are not readily available and are very expensive.

CCDs however have many advantages in the simplicity of target acquisition and also in that differential photometry is possible directly from each image as comparison, asteroid and sky measures can be made from a single image. Indeed, as many of the field stars will prove suitable for use in photometry, a useful by-product will be the identification of new variable stars during the course of this operation. One other major advantage is that the images are available for archiving, allowing remeasurement at a future time if required - photomultipliers do not store images so that not independent checking of measurements is possible. CCD photometry will shortly establish a place as the most important technique available for all but the brightest asteroids where pixel saturation is likely to prove a problem. There are many advantages to the use of CCDs including

1. Differential photometry can be carried out directly from each image when suitable comparison stars are nearby.
2. Images can be stored and are available for reprocessing if more information is found (such as the variability of a comparison star).
3. There is the certainty of target acquisition. Even if the asteroid is initially misidentified its motion will be detectable after several images and appropriate reprocessing is possible. (non-target asteroids can also be identified).
4. Astrometry can also be carried out from each image by using the Hubble Guide Star Catalogue.

8. Case Studies

Abstract

A model for synthetic light curve generation and light curve analysis based on a rotating 'spotty' (ie variegated) ellipsoid is derived. It is used, in conjunction with the geometric model derived in Chapter 4, to analyse results from space observation of Comet P/Halley and Binzel's observation of 1220 Crocus confirming the state of free precession of the former and forced precession of the latter. Other asteroid light curves measured using the photometer design described in Chapter 7 are given and analysed using the model. Some general guidelines for obtaining light curves are formulated. The overall conclusion is that there is no evidence of recent collisions affecting the asteroids studied. The measured light curves when considered with others indicate that the database rotation periods given for 8 Flora and 115 Thyra are incorrect.

8.1 Introduction

This chapter gives the results of investigations into the rotation of some smaller bodies in the Solar System in relation to their rotation modes. Two separate studies have been undertaken. The first pair cover Comet P/Halley and asteroid 1220 Crocus. Each of these bodies has been described in the literature as multi-periodic. The geometry of this is investigated in the light of the model presented earlier in this work to derive the geometric configuration.

For the remainder of the chapter the results of photometric observation of several asteroids is presented. These observations were made using the equipment described earlier at three observatories - Marton Green, Ormada and Manley. Ormada Observatory was relocated to Marton Green in 1989 and is operated by the writer and Manley Observatory is operated by Dr R Miles using Celestron 350mm and 280mm Schmidt-Cassegrains (the writer acting as co-observer). One light curve of 7 Iris was measured by the late J Ells using a semi-automatic telescope in 1989 at the writer's request. The observations have been compared to light curves generated using a simple model of a rotating ellipsoid with a single circular dark or light spot so as to derive the spin period and shape.

8.2 Light curve Inversion and Synthesis

Russell (1906) can be considered as the first person to tackle the inversion of asteroid light curves from a numerical standpoint. He concluded that it is not possible to determine, from an examination of the light curve alone, the basic cause of variation. It is not possible to discriminate between shape, albedo (or topography), or duplicity from an examination of variations in the reflected light. The modern observer has a much wider range of techniques available than Russell and observations

(including those from space) are possible at all wavelengths in narrow band and polarised light. Modern computational techniques allow rapid investigation of problems that would have seemed intractable in earlier years. However though complete inversion has yet to be successfully carried out some of the basic features of the asteroid can be inferred.

The light curve can be decomposed into its Fourier coefficients and a synthetic light curve calculated (Harris and Lupishko 1989). One problem found in this approach is that gaps in the data (from incomplete light curves) may generate light curves which correspond to a highly improbable shape or variegation. This is illustrated by the third order Fourier fit to the observations presented later in this work (Figure 8.1). In such cases the synthetic curve may show spurious periodicities longer than the true rotation period which do not correspond to any plausible rotation for a real body. Fourier analysis is therefore a poor way of deducing shapes and so has not been used in this work.

Laboratory experiments have been used to model lightcurves. The main experiment is the SAM (System of Asteroid Model) which makes use of laboratory photometric observation of models to construct rotational lightcurves for a range of aspect and phase angles (Barucci et al 1982). Their model does not allow measurement at very small phase angles simply because of the physical obstruction of the light source by the photometer.

Mathematical models all follow the basic premise that asteroids are triaxial ellipsoids (Magnusson et al 1989). In practical terms there is no disagreement between this simple approximation and those bodies which have been observed so far. Once an asteroid has been imaged then its light curve may be modelled by using its actual shape.

8.3 A Simple Photometric Model allowing Precession and Albedo Variations

The apparent magnitude of an asteroid is proportional to the instantaneous illuminated area perpendicular to the observer's line of sight (Pospieszalska-Surdej and Surdej 1985). The projected area for a fully illuminated ellipsoid is given by

$$S = \pi * abc\,[(\sin A)^2\{(\sin \psi / a)^2+(\cos \psi / b)^2\}+ (\cos A / c)^2]^{0.5} \qquad \ldots\ 8.1$$

where S = Area of ellipsoid

$a > b > c$ are the axes of the ellipsoid

A = the aspect angle of the pole to the line of sight

ψ= the rotational phase (maximum at $\psi = 0$ and minimum at $\psi = \pi/2$)

The Central Meridian faces the Earth at ψ=0 and corresponds to the maximum projected cross sectional area. For non-zero values of phase angle, consideration of the reflection process is required.

Using the Hapke-Irvine reflection law, Surdej and Louis (quoted in Barsuhn 1983) determined that the instantaneous cross section approximation is still valid.

The variation in brightness with increasing phase angle has been extensively modelled. Models have to explain all observed effects, which are :-

The change in illuminated fraction (the phase)

A large increase in apparent brightness at very low phase angles due to multiple internal reflections in the surface grains (The opposition brightening or surge).

The large decrease in apparent brightness at high phase angles due to multiple shadowing of surface grains. This effect can only be observed in spacecraft imagery and in asteroids which pass near to the Earth.

Lumme and Bowell studied this effect and produced a two-parameter model (Lumme and Bowell 1981 (i) and (ii)). The two parameter magnitude system was adopted by the IAU in 1985 and described by Marsden (1985). A fuller description of the implementation is given by Bowell et al (1989).

Many asteroids exhibit a change in the overall amplitude of the light curves as the phase angle changes. In most cases this can be explained as a change in the aspect angle. It is also possible that shadows produced by topographic features or due to irregular shape may also contribute to this. This effect will only be observable for large scale features.

Precession can be considered as rotation of the axis decomposed into two planes, a movement at right angles to the line of sight of the observer and one parallel to the line of sight. Movement at right angles to the line of sight does not give rise to any variation in the intensity of received light - it only alters the position angle of the pole. Movement along the observer's line of sight alters the angle that the polar axis makes with this line (the aspect angle). The effect of precession on the light curve may thus be modelled by varying the value of A in a periodic manner. This has been done by Sher (1971), Barsuhn (1983) and others.

For the simple requirements of this model it is sufficient to consider variations at zero phase angle. Albedo effects can be introduced in a simple way by considering rotation of a circular spot at a defined latitude and longitude which may have an albedo of 0 (dark 'spot') or 1 (bright 'spot'). Though this is unlikely for a real body *the effect on shapes of theoretical light curves gives effects similar to those observed in real light curves.* It does not give a true estimate for the size of a real spot as the albedo of real features will typically lie in the range 0.02-0.40. Local areas with a higher albedo than the surroundings may modify the observed light curve. However it must be appreciated that albedo differences of only a few percent will tend to be lost in the noise component of the observations. More

complex light curves may be modelled using more than one albedo feature but in this work it has only been attempted for 4 Vesta. Other shapes of feature may give a better fit though this has not been attempted in this work. The synthetic light curves are plotted together with the measured brightness of the target asteroids and considered in Sections 8.6 to 8.16.

A composite light curve can be assembled using measurements made on a single, or several nights. A correction has to be applied to each night's measurements so that they are standardised. Usually one night is taken as the base reference and a composite light curve can be assembled using measurements made on a single, or several nights. Magnitude corrections are then applied to the other night's data to allow for the changing heliocentric and geocentric distance and the change in phase angle from this reference night. Composite light curves are assembled using a range of trial periods, shapes and albedo features which are compared with a light curve synthesised using Equation 8.1. The period, shape and albedo features are derived by minimising the squares of the deviations of measured from calculated values for each point.

8.4 The rotation of the nucleus of Comet P/Halley

During its recent return to the inner solar system, P/Halley was studied by five spacecraft in 1983. Studies of comets and asteroids are closely related, as in many ways they appear to have a common origin and may represent differing stages in the evolution of bodies (see for example Weissman et al 1989).

Results from the Soviet Vega Mission (2 probes) suggested that the nucleus is an irregular ellipsoid of approximate dimensions 14km:7.5km:7.5km and a rotation period of 2.2 days (Sagdeev et al 1986). Observations of C and CN molecular emissions in the inner coma suggested a rotation period of 7.4 days (Millis and Schleicher 1986). Observations of the shapes of gas jets on the nucleus were consistent with a rotation period of about 2.08 days (Vaisberg et al 1986).

Julian (1987) describes the observed rotations of the nucleus in terms of two modes of free precession which he terms a long axis mode and a short axis mode, depending about which geometric axis the precession occurs. The feasibility of each of these modes is considered below.

The dimension of the nucleus of P/Halley was derived from images taken during the close flyby by the Giotto probe. The size is approximately a triaxial ellipsoid of 16km:8km:7.5km. However the shape is very irregular and Julian models it in terms of a dynamically equivalent ellipsoid of 16:8:7. For the purpose of this work an axis of symmetry about the x axis will be assumed leading to an equivalent shape which has been assumed as 16:7.5:7.5.

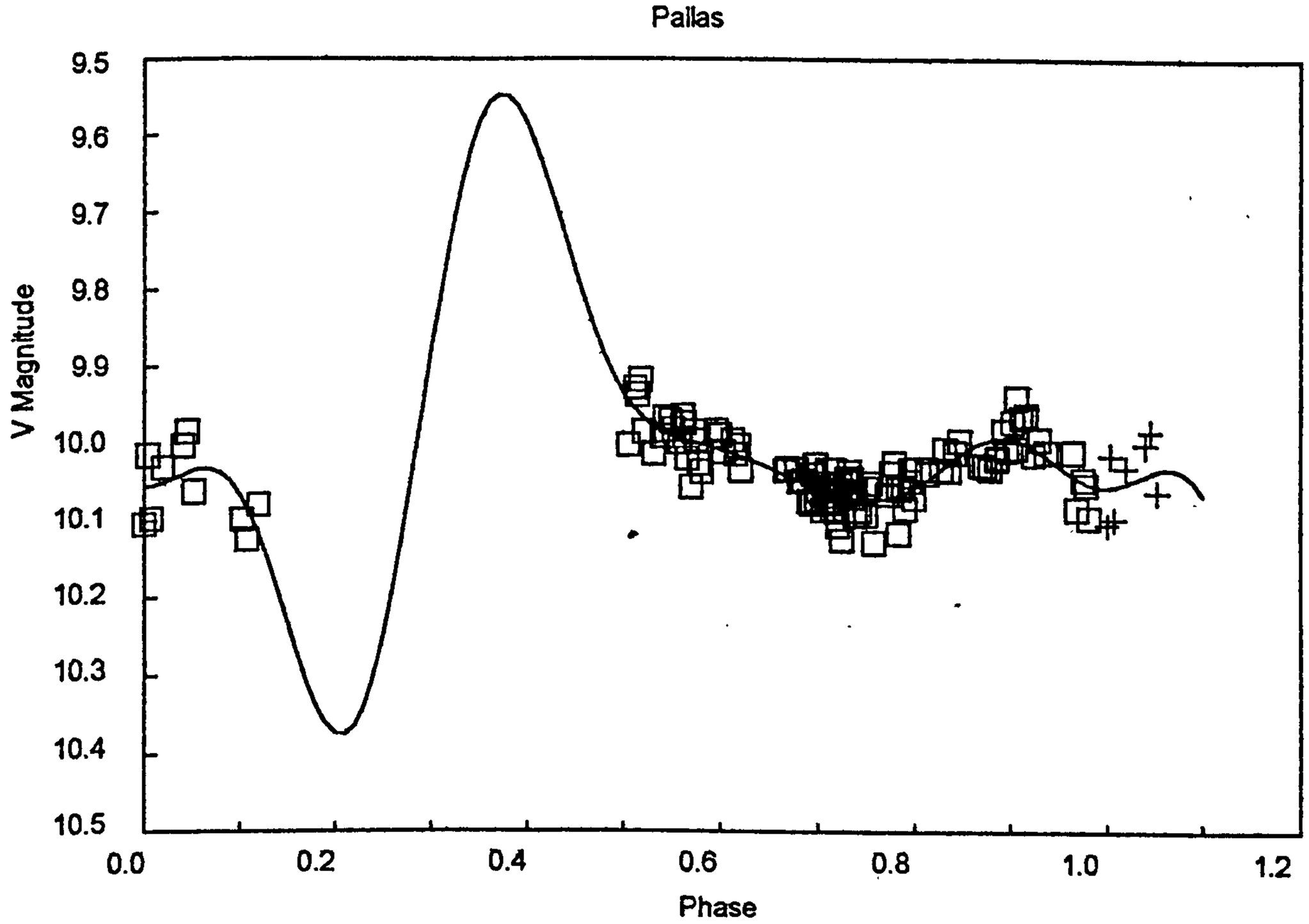

Figure 8.1 - The measured light curve of 2 Pallas and the third order Fourier fit showing how gaps in the data are not plausibly modelled using this approach

The Moment of Inertia for an ellipsoid with axes a and b is given by $I = \frac{2M(a^2 + b^2)}{5}$

Hence $$I_s = \frac{0.4 * M (7.5^2 + 7.5^2)}{4}$$

$$= 112.5 * \text{constant}$$

$$I = \frac{0.4 * M (16^2 + 7.5^2)}{4}$$

$$= 312.5 * \text{constant}$$

$$I_s / I = 0.36$$

from Chapter 4 $\Omega/\omega = (I_s/I - 1) * \cos\alpha$

The two angular frequencies are 1/2.2 rotations per day and 1/7.4 rotations per day.

Ω/ω = 2.2/7.4 or 7.4/2.2 corresponding to $\cos\alpha$ = -0.46 or -5.25

since $\cos\alpha$ cannot be less than -1 it follows that α = -62.3°

$\tan\theta = I/I_s * \tan\alpha$ hence θ = -79.3°

$\theta - \alpha$ = 17° implying a 'wobble' amplitude of 34° which is close to the value of 26° derived by Sekanina (1987).

The calculations illustrate that the angle between the symmetry axis of the nucleus of Comet Halley and the spin vector is -62.3° (117.7°) with a rotation period of 2.2 days and that the angle between the symmetry axis and the angular momentum vector is -79.3° (100.7°) with a precession period of 7.4 days. This conclusion is in line with that for the short axis mode given by Julian and is illustrated in Figure 8.2. Julian also derives an acceptable result for the long axis mode where the shorter period is the precession superimposed on a lower value angular spin vector. However this result is forbidden under the solution presented here as it requires a $\cos\alpha < -1$ (the angle between the symmetry axis and the spin vector).

Belton (1990) and Samarasinha and A'Hearn (1991) consider the dynamical constraints on the nuclear rotation. They conclude that axial rotation is most likely about the long axis. *They do not consider the possibility that the spin axis may not be aligned with one of the principal geometric axes, whereas this is the conclusion presented in this work.* The importance of the rotation of the nucleus of Comet P/Halley in relation to this work is that it shows how a body in free precession may be identified from its light curve and has allowed the testing of the free-precession model on the rotation of a real body.

8.5 The rotation of 1220 Crocus - evidence for a binary system?

1220 Crocus was observed by Binzel (1985). His initial observations indicated a relatively large amplitude (0.87 magnitudes) with a slow rotation (Period 30.7 days). Further investigation suggested

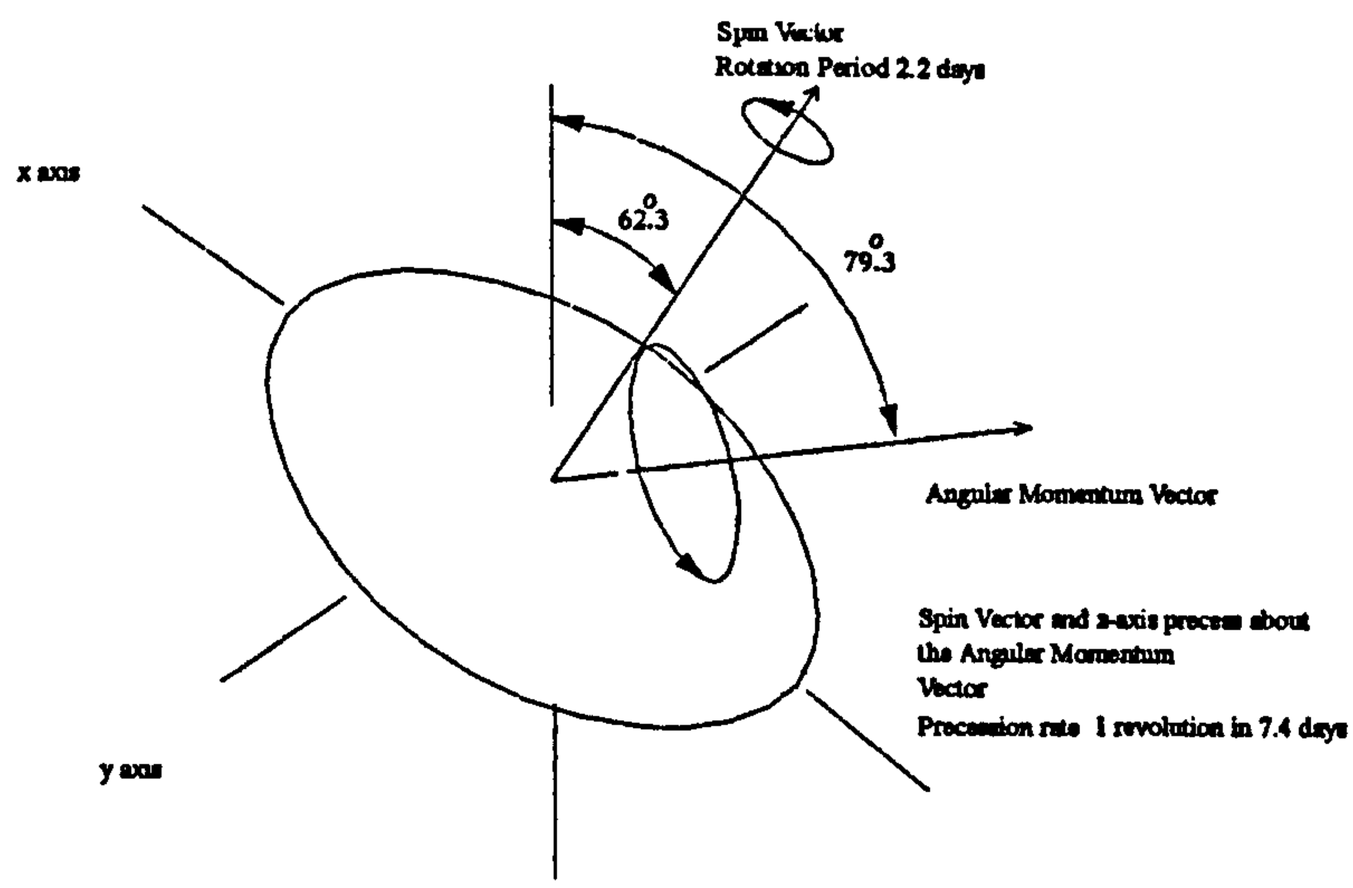

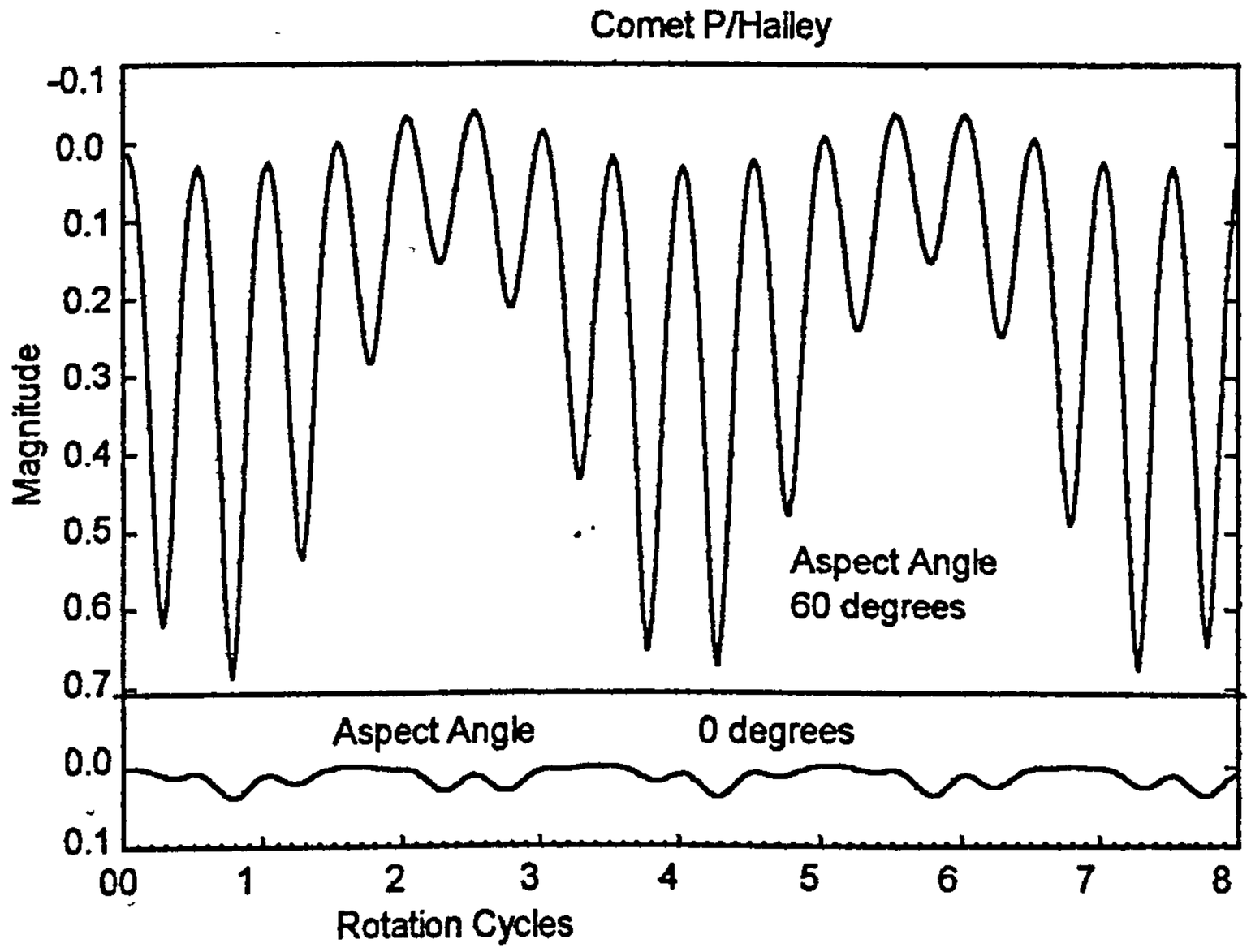

Synthetic Light Curves

Figure 8.2 - Rotation geometry for the nucleus of Comet P/Halley and the synthetic light curve derived in this wortk

that there could be a second period visible in the data with a short period (7.9 hours) and a small amplitude (0.15 magnitudes).

As part of his investigation he presents synthetic light curves for a freely precessing model and one undergoing forced precession due to an unseen torque. His light curves differ. The free precession model shows a constant mean brightness with the short period variation modulated over the longer period one, (ie similar to AM radio waveforms). In his forced precession model the mean brightness varies as that of the longer period and the short period lightcurve is superimposed on this.

Free precession has been considered in Chapter 4 and is the state that would be induced by the impact of a projectile. The angular velocity vector remains aligned with the principal axis of the asteroid, but has an angular displacement from the angular momentum vector induced by the impact. The angular velocity vector will precess about the angular momentum vector. However flexure of the body will result in energy being dissipated producing a reduction of the angular displacement. The end state would be reached when the angular momentum vector, the angular velocity vector and the principal axis are all aligned and simple single axis rotation occurs.

Binzel derives a triaxial shape for 1220 Crocus of a>b>c 24km:22km:12km that is 2.00:1.83:1.00.

The ratio $I_s/I = 2(a^2 + b^2) / (2c^2 + b^2 + a^2)$

so $I_s/I = 1.57$ and $\Omega/\omega = 1/93.3$ or 93.3

corresponding to $\cos\alpha = 0.0188$ or ~180

since $\cos\alpha$ cannot be less than 1 $\alpha = 88.9°$

$\tan\theta = I/I_s * \tan\alpha$ hence $\theta = 88.3°$

A synthetic light curve for a freely precessing pseudo-Crocus is given as Figure 8.3. This light curve is of a similar form to that given by Binzel as an illustration of free precession, namely a maximum light curve amplitude for the axial rotation. Also shown is a light curve which requires an external source of torque i.e. a forced precession where the maximum light curve amplitude represents the longer (precession) period. In this case the symmetry axis and the direction of the angular velocity vector have been taken as aligned. The light curves have been generated using an angular momentum vector 75° from the symmetry axis (since the light curve amplitude would not be easily seen if the derived value of 88.3° had been used to generate the light curve) The form agrees with that observed by Binzel.

There is a second shape, of approximately 2.0:1.14:1, which yields two rotational lightcurves of the required amplitude. Calculation shows that the values for the angles α and θ are similar to those derived above and that the light curve for the free precession case is not similar to the light curve observed by Binzel.

As the shape of my free precession curve differs from the light curve measured by Binzel, this analysis supports the conclusion that an external source of torque is required to explain the observed lightcurve of 1220 Crocus. The most likely explanation would be a second body in the system at a high inclination to the equator of the primary body. Assuming a density for Crocus of 2.500 kg m^{-3} and a mean radius of the primary of 10km this second body would be very close to the primary (50km-100km distant) to achieve the required short period. If the true nature of the 1220 Crocus system is that of a binary asteroid then the shapes derived above would not apply as they have been calculated for a single rotating body.

8.6 Newly Measured Light Curves Analysed using the Simple Photometric Model

A major part of this project has been the observation of 10 asteroids using my equipment design described in chapter 7. 12 light curves have been produced. Due to variable weather conditions four have been derived from continuous observation during a single night, three from observations during a week or two and the remainder assembled from observations taken over several months. Estimates of the errors in the light curve data points are given in the table. The internal consistency of each data set is good (usually better than 0.015 magnitudes) however external factors (such as transparency) may vary during the course of a night so that the adoption of this value would imply higher precision than justifiable. The errors in the light curve data points have been estimated from the phase plot at $\frac{2}{3}$ the maximum spread from the mean value which gives a higher error in most cases.

Various methods have been employed in the past to determine rotation periods when observations have been taken over several nights. The traditional method is to use the eye to align definite features and use these to successively refine the estimate of the period. Though simple in application the method suffers the shortcoming that there is a subjective element and unconsciously the observer may try to impose his preconceptions of the true period on the data.

A more objective method has been prepared by Harris and Lupishko (1989), using a Fourier Analysis of Light Curves (FALC) program. As explained in 8.2, Fourier analysis gives few clues as to the underlying mechanisms and has the drawback that if there are gaps in the data a synthetic light curve may deviate markedly from that expected from the rotation of a real body. In addition it is quite possible that successive cycles of the synthetic light curves have differing shapes.

To overcome the repeatability problem the analysis has been carried out using a reduced χ^2 fit to the synthetic model described in 8.3 (Bevington and Robinson 1992).

$$\chi_\nu^2 = \sum_{j=1}^{n} \frac{[\text{calculated-observed}]^2}{\sigma^2 * \nu} \quad \text{.....(8.2)}$$

where χ_ν^2 = the reduced χ^2

ν = the number of degrees of freedom - in this model (n - p)

n is the number of observations

p is the number of fixed parameters - four in this model semi-major axis
semi-minor axis
spot radius
spot longitude

σ = standard deviation of the observations

calculated-observed = the difference between the calculated and measured values for each data point.

The value of the reduced χ^2 is computed for a range of trial periods and the minimum value is derived. A graph of brightness vs phase should show a simple smooth curve. If this is the case then the period is taken as a true representation of the data. The adequacy of the model was tested using synthetic light curve data. 100 complete cycles of sin curve of amplitude 0.3 magnitudes and period of 9 hours were calculated using a random data temporal spacing and a random error of ±0.02 magnitudes. Most of the data was then deleted leaving 5 sets of data 4 to 6 hours long mimicking real observation data. When several different sets were run through the model the correct period was derived each time. This was also found to be the case when an albedo feature was introduced into the synthetic data set.

The crudity of the model does not allow modelling of fine structure in the lightcurve since the synthetic lightcurve is not a precise match. It is however periodic and makes use of all the data. It is quite adequate for determining periods, the estimate of which depends mainly on matching phase over extended periods, rather than on detailed light curve shapes. Corrections for varying Solar and Geocentric distance are used to correct brightness to a standard distance. Light travel time corrections are small and have, in general, not been applied. For example even a change in geocentric distance of 0.5 AU over 30 days for an asteroid with a rotation period of 12 hours would produce a mean error of only 4 seconds in an individual rotation cycle (0.001 hours) and changes near opposition are less than this. An estimate of the ratio of a:b (long axis to short axis) is given: this is a *lower bound* solution as a and b only represent the length of principal axes when the asteroid presents an equatorial aspect to Earth. The derived values of a:b have large errors as they depend both on the accuracy of the measurements and the goodness of fit of the model (the errors are greater for low amplitude light curves than for those with a greater variation).

The composite light curves are shown for 1.2 cycles. The repeated points are shown to illustrate the continuity of the light curve though, naturally, they are not used in the analysis. A typical measurement error bar is also shown on the graphs.

The accuracy of any period fit, especially if there is asymmetry in the light curve, must be tested by plotting the composite light curve. If the measured points lie close to a smooth curve then it may be assumed that the fit is satisfactory. Real fine structure on the light curve can easily result in an

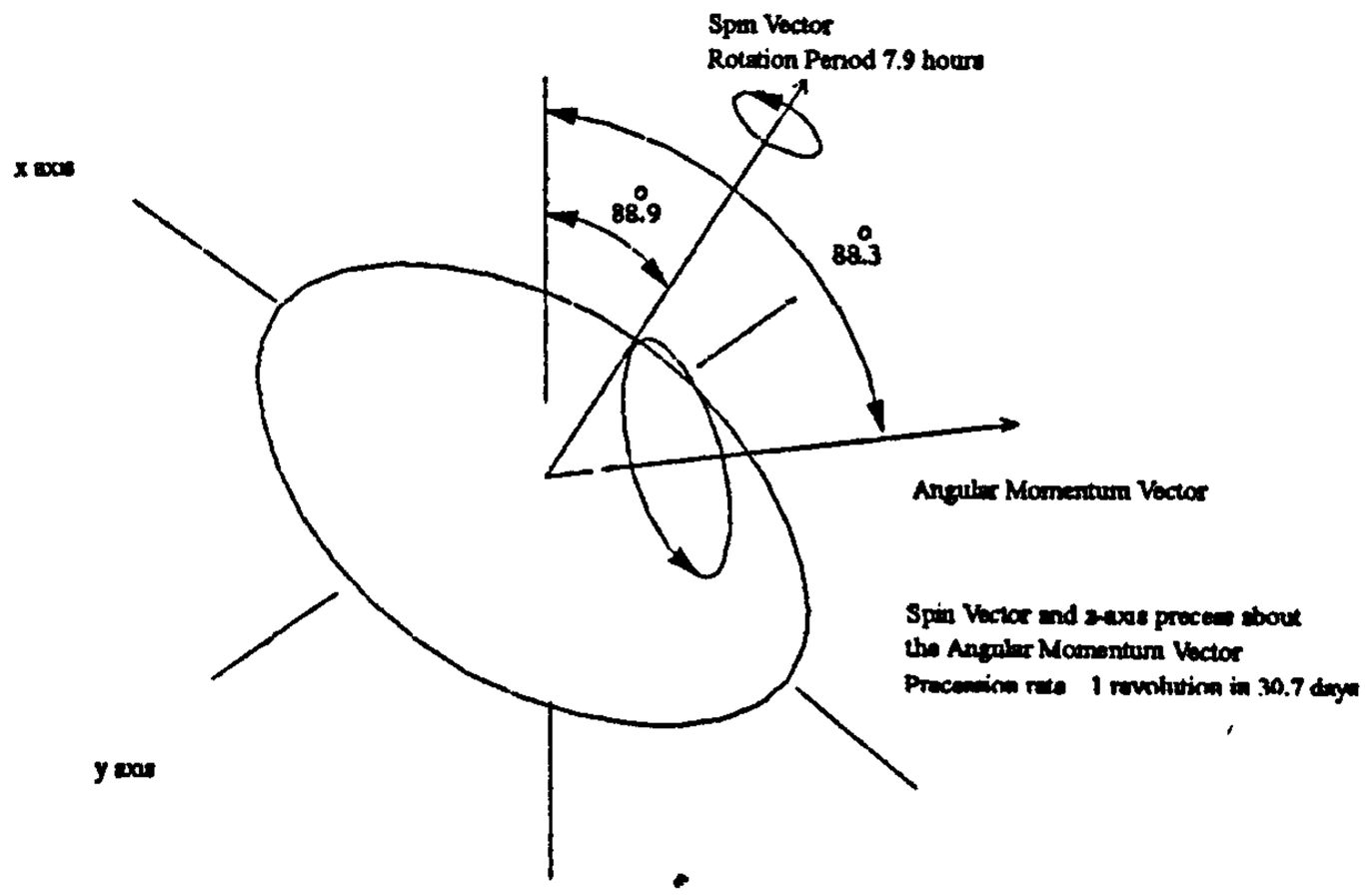

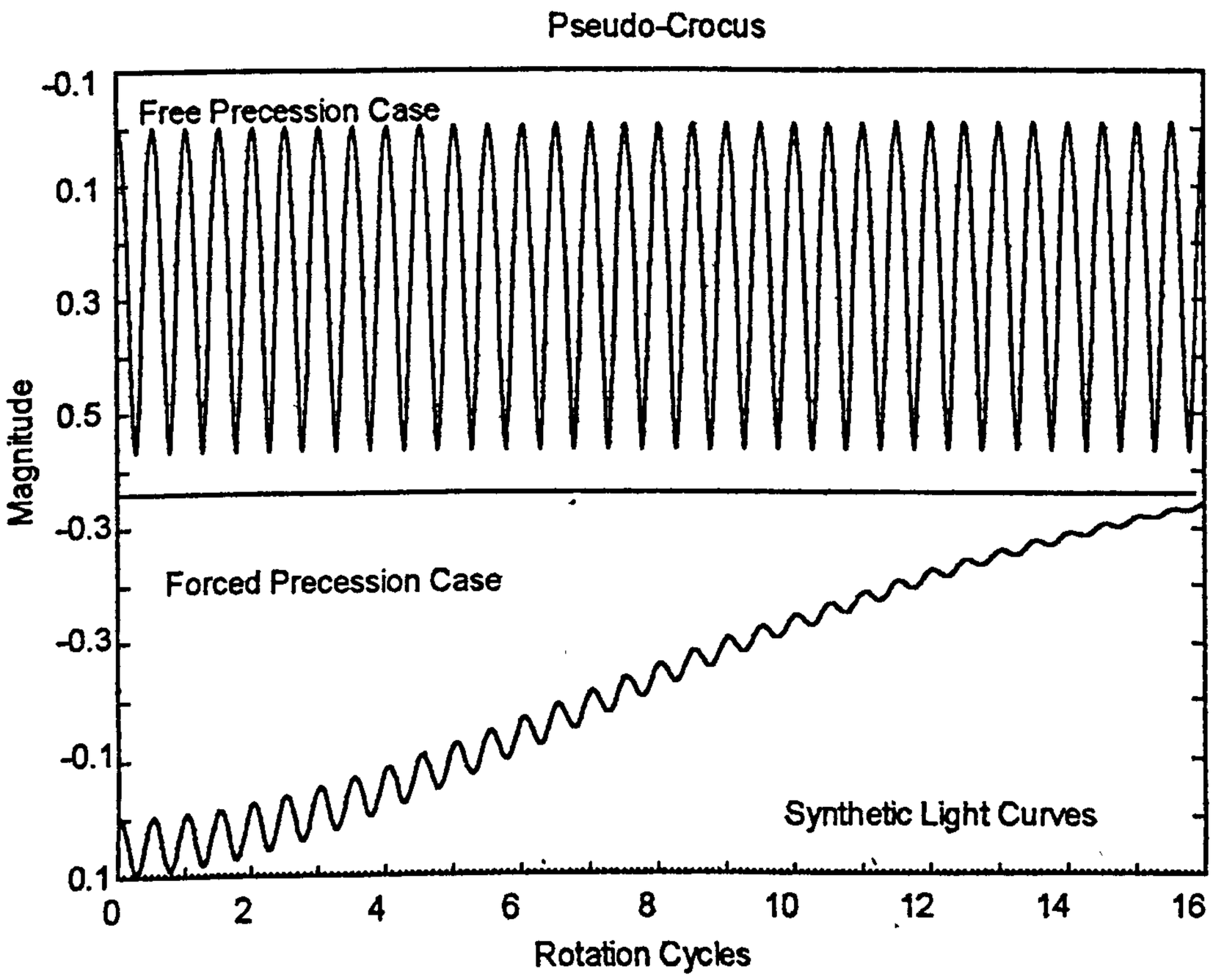

Figure 8.3 - The rotation geometry of 1220 Crocus and synthetic light curves for Free and Forced Precession cases derived in this work

erroneous period being highlighted which can be discounted by a visual inspection of the composite curve. This is illustrated in the case of 115 Thyra when a period apparently compatible with observations made in 1978 and new observations in 1983 for this work is discounted as it does not provide a good fit to the 1983 measurements.

The results are summarised in Table 8.1 and discussed in Sections 8.7 to 8.16. A discussion of the method of assembling composite light curves and how to derive accurate periods when weather conditions impose constraints on the availability of observing time is given in 8.17.

Table 8.1

Asteroid	Derived Period (Hrs)	Error in each point (mag)	Class	New Class	Observers	a:b	
1 Ceres	9.075 ±0.015	0.005	G	Ceres-like	A.J.Hollis	1.071:1	1986 Mar 1 & 2
2 Pallas	7.797 ±0.002	0.02	B	Pallas-like	A.J.Hollis	1.09:1	1991 Apr 22,25 1991 May 2, 5
4 Vesta	5.320 ±0.040	0.01	V	Vesta-like	R.Miles/A.J.Hollis	1.030:1	1985 Apr 23
7 Iris	7.140±0.030	0.015	S	Juno-like	J.Ells	1.17:1	1989 Feb 15
7 Iris	7.137±0.005	0.02			A.J.Hollis	1.138:1	1991 Aug31,Sep 1,7 Oct 3 Nov 1
8 Flora	26.03±0.03	0.015	S	Flora-like	A.J.Hollis/R.Miles M.Dumont,C.Bembrick	1.026:1	1984 Jul 24, Oct 1,3 1984 Oct 22, 23
15 Eunomia	6.080 ±0.002	0.015	S	Flora-like	A.J.Hollis/F.Mellilo	1.471:1	1985 Oct 7, 13, 14, 17
44 Nysa	6.432 ±0.004	0.01	E	Psyche-like (high p_v)	R.Miles/A.J.Hollis	1.347:1	1983 Oct 28
44 Nysa	6.493 ±0.020	0.005			R.Miles/A.J.Hollis	1.322:1	1988 Jan 7
44 Nysa	6.434 ±0.030	0.01			A.J.Hollis	1.347:1	1992 Jan 9
115 Thyra	7.797 ±0.005	0.025	S	Juno-like	R.Miles/A.J.Hollis	1.158:1	1983 Feb 3, 8, 11, 16
416 Vaticana	5.372 ±0.001	0.01	S	Juno-like	R.Miles/A.J.Hollis	1.384:1	1989 Mar 7, 8, 28 1989 Apr 4,15 1989 May 6,7,10
751 Faina	23.680±0.03	0.005	C	Pallas-like	R.Miles/A.J.Hollis	1.367:1	1988 Oct 31, Nov 2, 3, Nov 14,20, Dec6,16,30 1989 Jan 4,10,12

Comparison is made to data from other observers in the light curve database. This is a machine readable file of data digitised from published light curves held at Uppsala Observatory and is referred to simply as "the database". Initially this was published in printed form as a catalogue. Composite light curves (where several night's data are shown on a single light curve) have been separated (where

possible) so that individual night's measurements are listed. No estimate of the errors in the data sets have been made though likely errors can be gauged from the scatter in the lightcurves. Several of the light curves measured for this project have already been incorporated in this database and the remainder will in due course.

Reference to the reduced χ^2 plots on Figures 8.4 to 8.17 show that the curves are smooth and show minimum values indicating well defined periods. Alias periods indicated by minima near to the prime minimum are to be expected due to the large gaps in the data due to daylight and poor weather.

8.7 The rotation of 1 Ceres (Figure 8.4)

Ceres was observed by Hollis at Ormada observatory on 1986 March 1 & 2. Approximately 70% of a complete light curve was obtained when the two night's measurements are combined. Ceres is the largest of the asteroids (a diameter of 913km from IRAS data) and the rotational light curve is of low amplitude (0.06 mag during this data run). Though bright, its light curve has not been well studied and this is probably due to the low amplitude as errors in observation can significantly affect the shape of the measured light curve.

Using the least squares fit to a rotating 'spotty' ellipsoid, a period of 9.075 ±0.015 hours provides the best fit to the measured data. The adopted period in the master database is also 9.075 hours and an amplitude of 0.04 magnitudes (Batrakov et al (1994)). An indicated shape of 1.08:1 for the observed a:b was derived at this opposition - no estimated figure is given by Magnusson (1989). No error ranges for periods are given in the database.

The results in this work are in complete agreement with the values given in the database though it is possible that the amplitude of the light curve has been underestimated slightly in the database at 0.04 magnitudes as a value of 0.06 was measured in 1986.

8.8 The rotation of 2 Pallas (Figure 8.5)

2 Pallas was observed on six nights in 1991 over a period of just over two weeks by Hollis at Marton Green. Approximately 80% of a complete light curve was obtained. The rotating ellipsoid fit gave a solution of 7.797 ±0.002 hours for the observed synodic rotation period. This compares with a derived period of 7.811 hrs in Batrakov et al. The derived value of a:b is 1.09:1 which is within the range of 1.06:1 to 1.14:1 given by Magnusson.

The error reflects both the incompleteness of the light curve and, more significantly, the poor observing conditions during the course of the observing runs. None of these was longer than 2 hours.

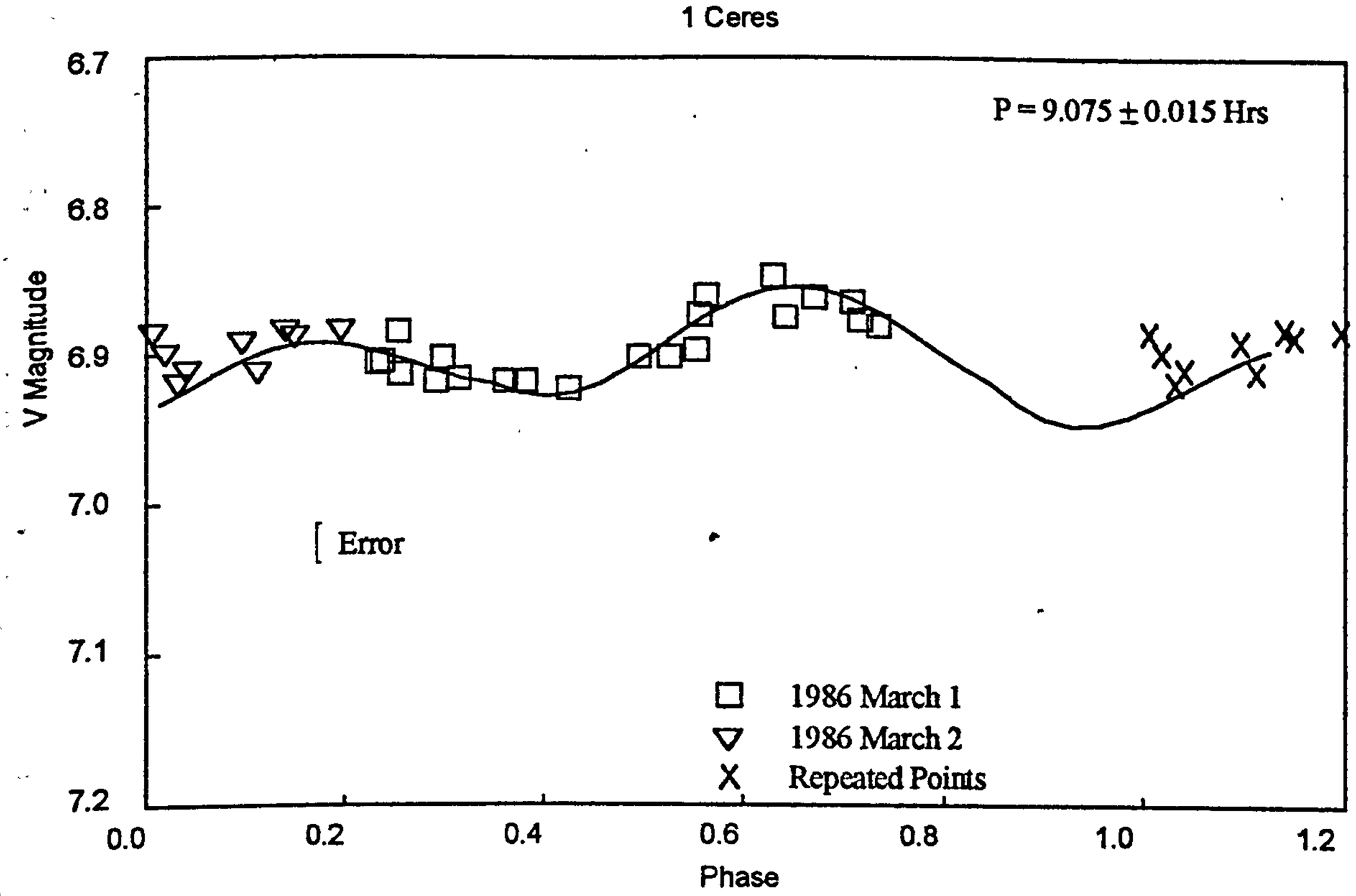

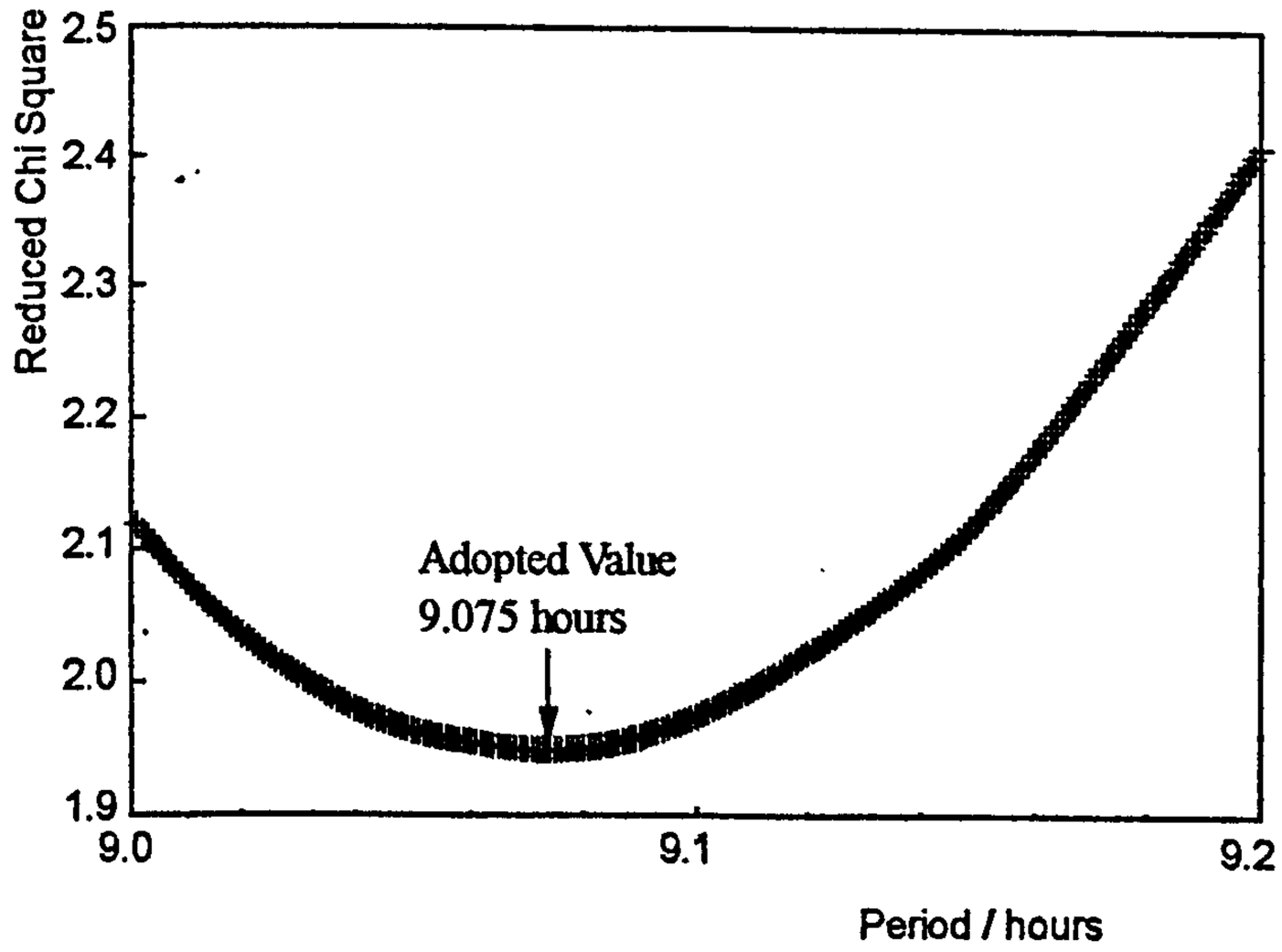

Figure 8.4 - Measured light curve and modelled fit for 1 Ceres

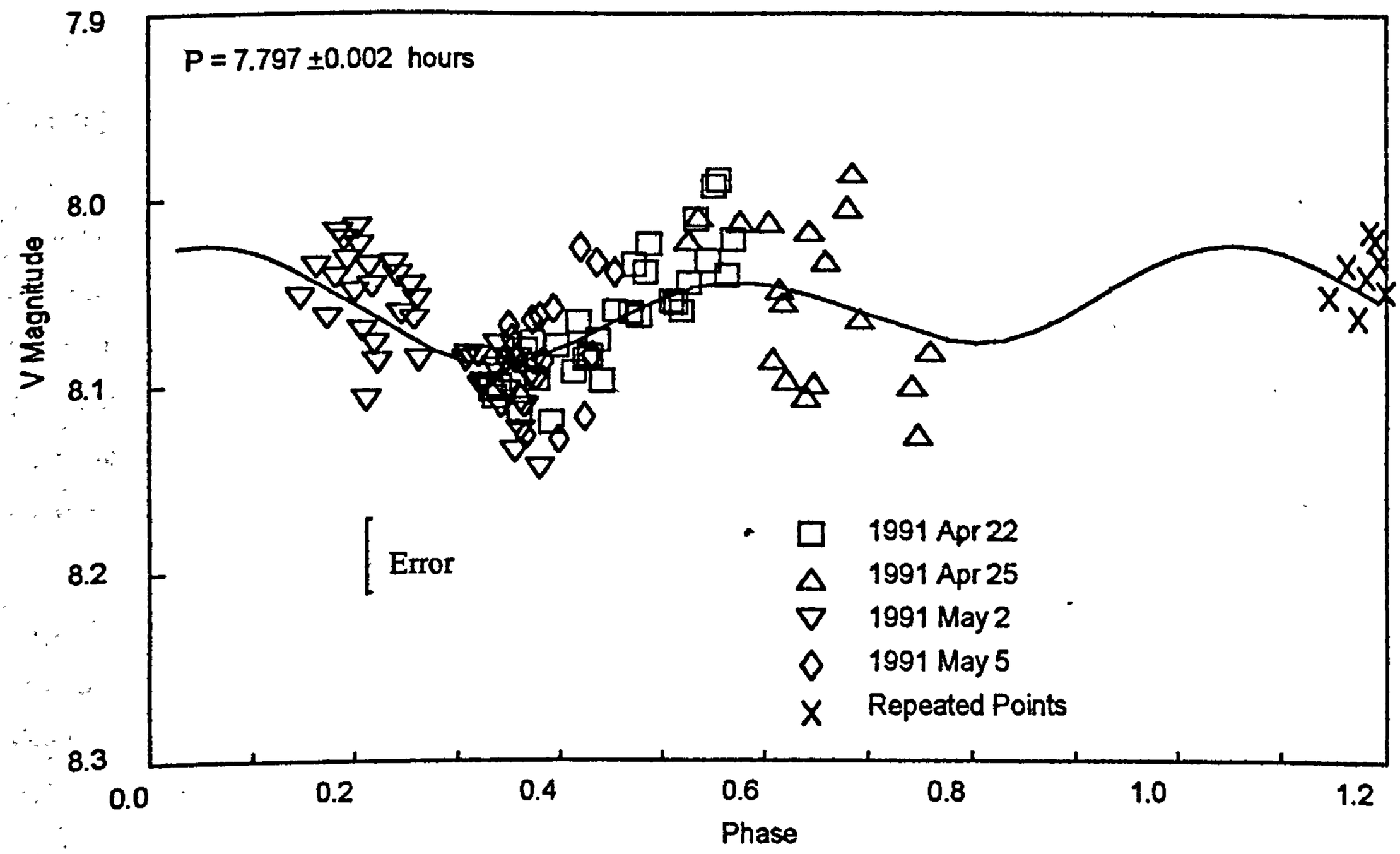

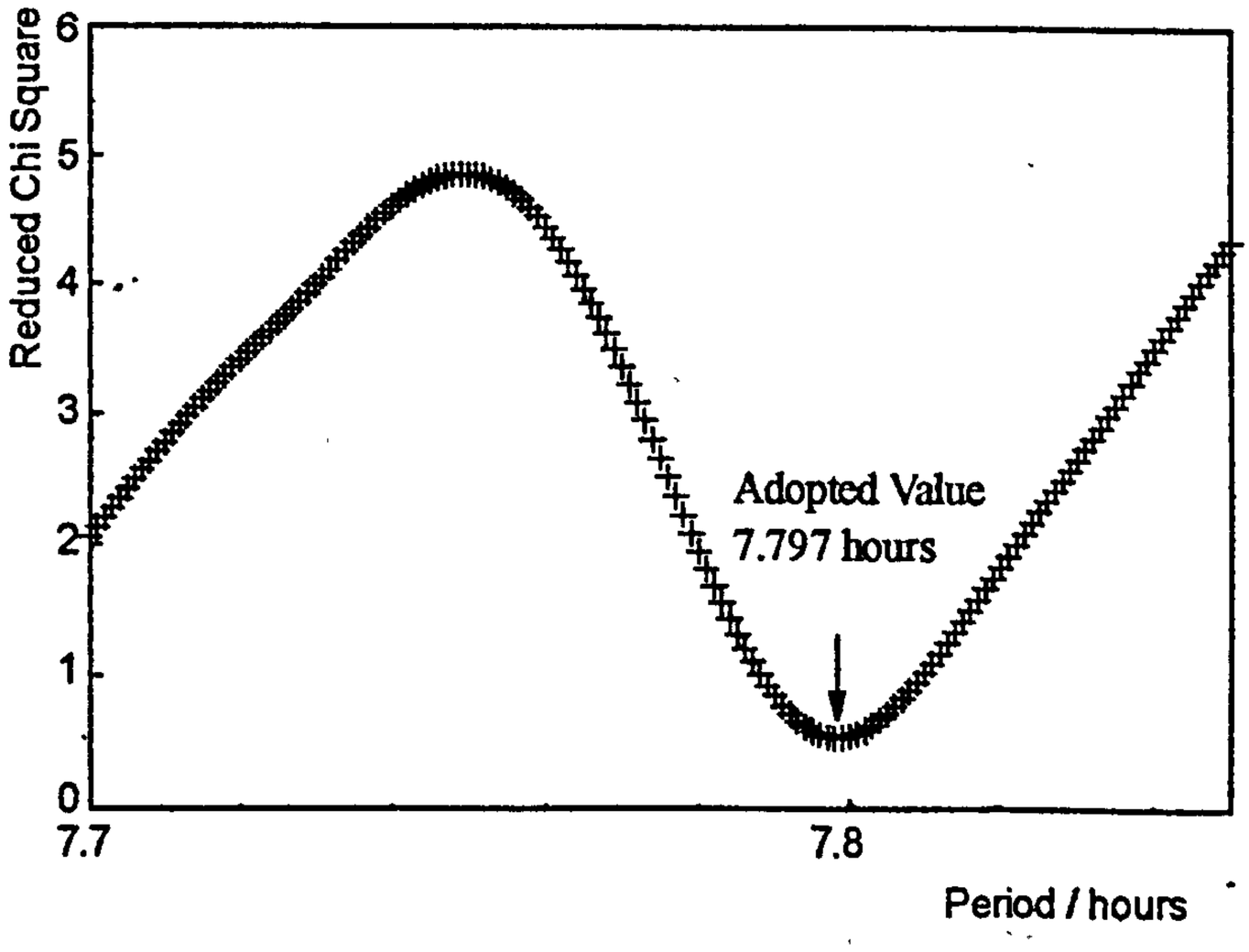

Figure 8.5 - Measured light curve and modelled fit for 2 Pallas

8.9 The rotation of 4 Vesta (Figure 8.6)

4 Vesta is the third largest of the asteroids and probably the most studied. This is not hard to understand since it is easily the brightest asteroid and frequently appears brighter than the nominal limit for naked eye visibility (mag 6). It was observed by Miles and Hollis at Manley on 1985 April 23 when a complete light curve for one rotation was obtained. The rotation is well documented from photoelectric lightcurves and only one maximum and one minimum per rotation is seen rather than the more usual two (this result being inferred from the change in colour during the course of a rotation). The light curve was interpreted as the rotation of a nearly spherical asteroid with a single dark albedo feature. The albedo feature was originally inferred from studies of light polarisation throughout several rotation cycles and it is from this data that the single periodicity has been deduced. The recent publication of a set of images from the Space Telescope showing most of one rotation of Vesta has confirmed these interpretations (Sky and Telescope 1995). It is pleasing to note that the shape and variegation calculation was performed before the publication of the Space Telescope images which serve to validate the conclusions presented in this work.

A model has been published by Cellino et al (1987) which makes use of all the then published light curves. They assume that Vesta is an ellipsoid with a:b equal to 1:1 (ie a spheroid). They model the light curve by assuming the presence of a single bright spot but their synthetic light curve is unsatisfactory as it is smooth and does not have the characteristic hump on the ascending branch of the light curve which is present on nearly all the measured light curves.

The light curve of Vesta, obtained by Hollis and Miles during the course of this project, is typical of all those recorded. The form is of a sharp minimum with a slow rise to maximum with a short standstill during the rise. From the broad maximum there is a sharp fall to minimum.

Using the light curve synthesis program it is possible to break down the curve into its component parts and then reassemble a synthetic light curve. Using this fit a synodic period of 5.320 ±0.040 hours has been derived and a:b shape parameters of 1.018:1 from a model assuming a single dark spot. The χ^2 curve shows a well defined minimum. The curve with a second spot is also given and the shape factor a:b from this fit is 1.030:1. This result is indicative that the main variation is derived from albedo variations rather than shape. This contrasts with the conclusion reached by Cellino et al (1987), however it should be noted that their synthetic light curve does not well model the characteristic hump on the light curve just before maximum. This feature is just noticeable in figure 8.6, but has also been recorded on most of the published light curves and therefore appears to be real. The currently adopted synodic rotation period for 4 Vesta is 5.342 hours (Batrakov et al 1994) and the shape factors range from 1.01:1 to 1.17:1 (Magnusson 1989). The results from this work support the lower

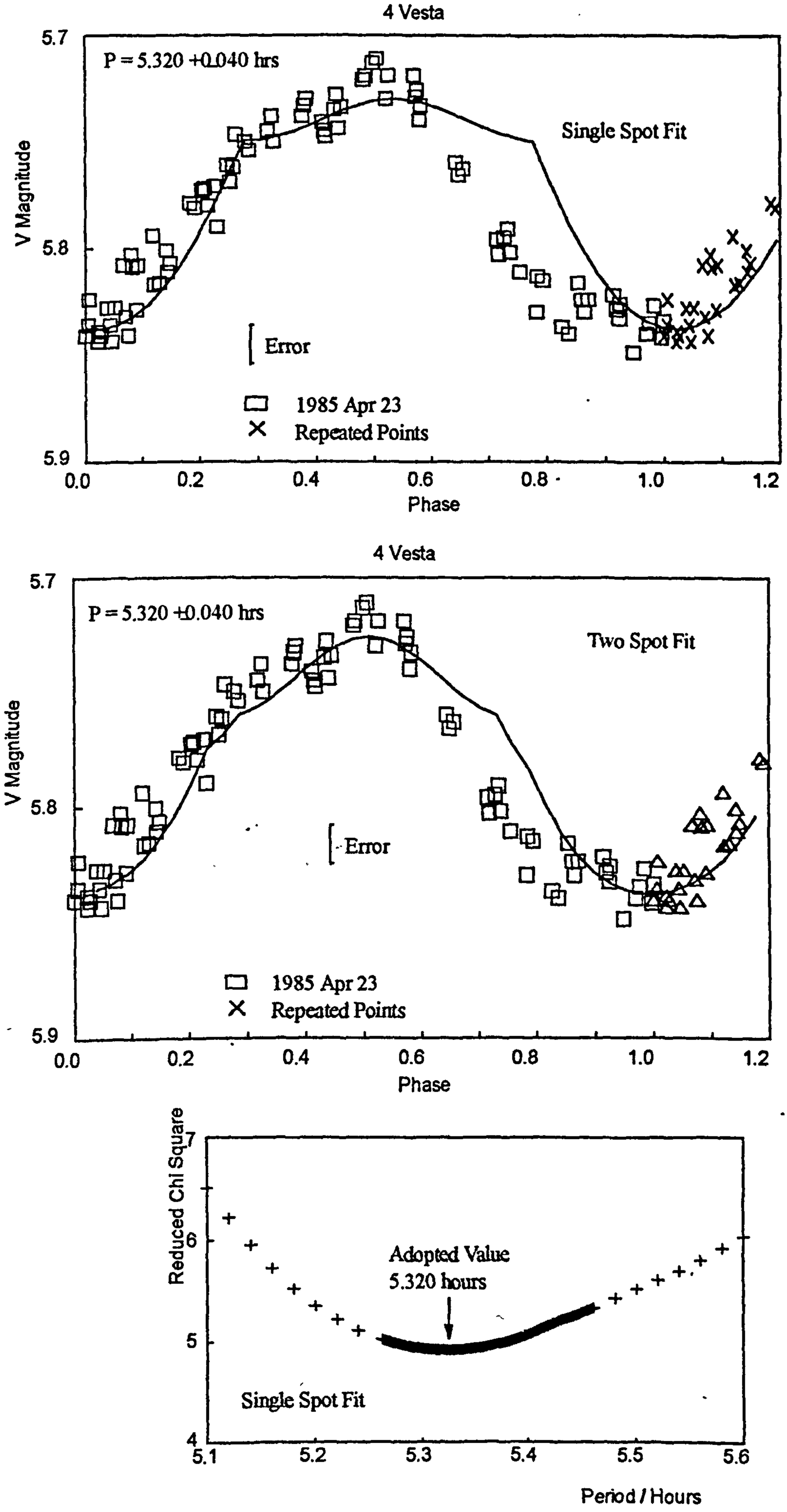

Figure 8.6 - Measured light curve and modelled fit for 4 Vesta
Upper curve modelled with a single spot
Lower curve modelled with two spots

estimate. The synthetic curve deviates from the measured curve during the fade from maximum. This suggests that a second dark 'spot' would be necessary to model the shape - this deduction is confirmed by referring to the published images where two dark regions can be seen.

The large error in the period (0.04 hours) reflects the fact that insufficient overlap of the light curve for the next cycle was obtained. Alternatively (and probably to be more accurate) a second night's observation should have been attempted had weather conditions allowed.

The two synthetic curves give a poor match to the descending branch of the light curve. The two circular spot solution is a much better approximation and it seems likely that a single elliptical spot would improve this. Reference to the Hubble Space Telescope images suggest that the dark patches are far from circular and it is thus unlikely that an exact match can be achieved without introducing a more complicated shape to the fit.

8.10 The rotation of 7 Iris (Figures 8.7 and 8.8)

7 Iris was observed at two oppositions. Firstly, on 1989 February 15 by the late J Ells from Dartford in Kent. This observation was requested by the writer as a suitable test for the Ells Semi-Automatic Telescope's suitability to follow and measure a moving target over a period of 7 hours. In addition it was also observed, by Hollis, over five nights during a two month period in 1991 when approximately 90% of the light curve was measured.

The rotating ellipsoid fit gives synodic periods of 7.140 ±0.030 hours and 7.137 ±0.005 hours respectively for the two oppositions. The earlier result is poorly constrained as a complete rotation cycle was not measured and results from a second night's observation are not available. The results for the second opposition show considerable scatter, but the measurements are spread over a long timescale so the period is well constrained. The shape factors derived for a:b are 1.17:1 and 1.138:1 respectively. The period given by Batrakov et al is 7.139 hours and the shape factor given by Magnusson are 1.19:1. *The results are in excellent agreement with these values.*

8.11 The rotation of 8 Flora (Figures 8.9 and 8.10)

8 Flora is one of the most enigmatic of the asteroids. Despite its early discovery and frequent bright oppositions it has not been well studied. This is because at most oppositions the light variation exhibits a very low amplitude (~0.04 magnitudes). Few complete light curves have been obtained and they are typically relatively featureless. Frequently the scatter in the measurements is nearly as great as the amplitude, making interpretation very difficult.

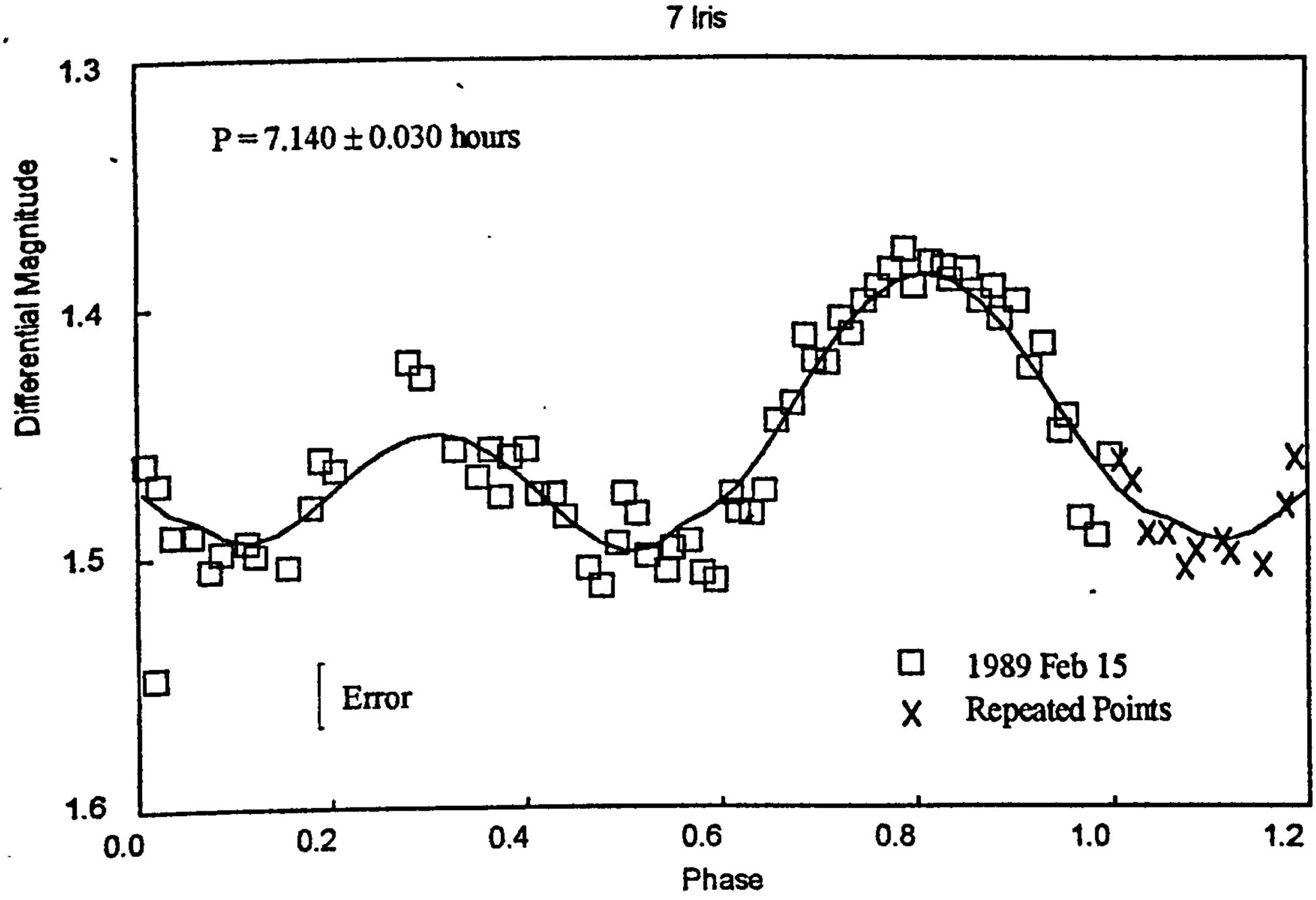

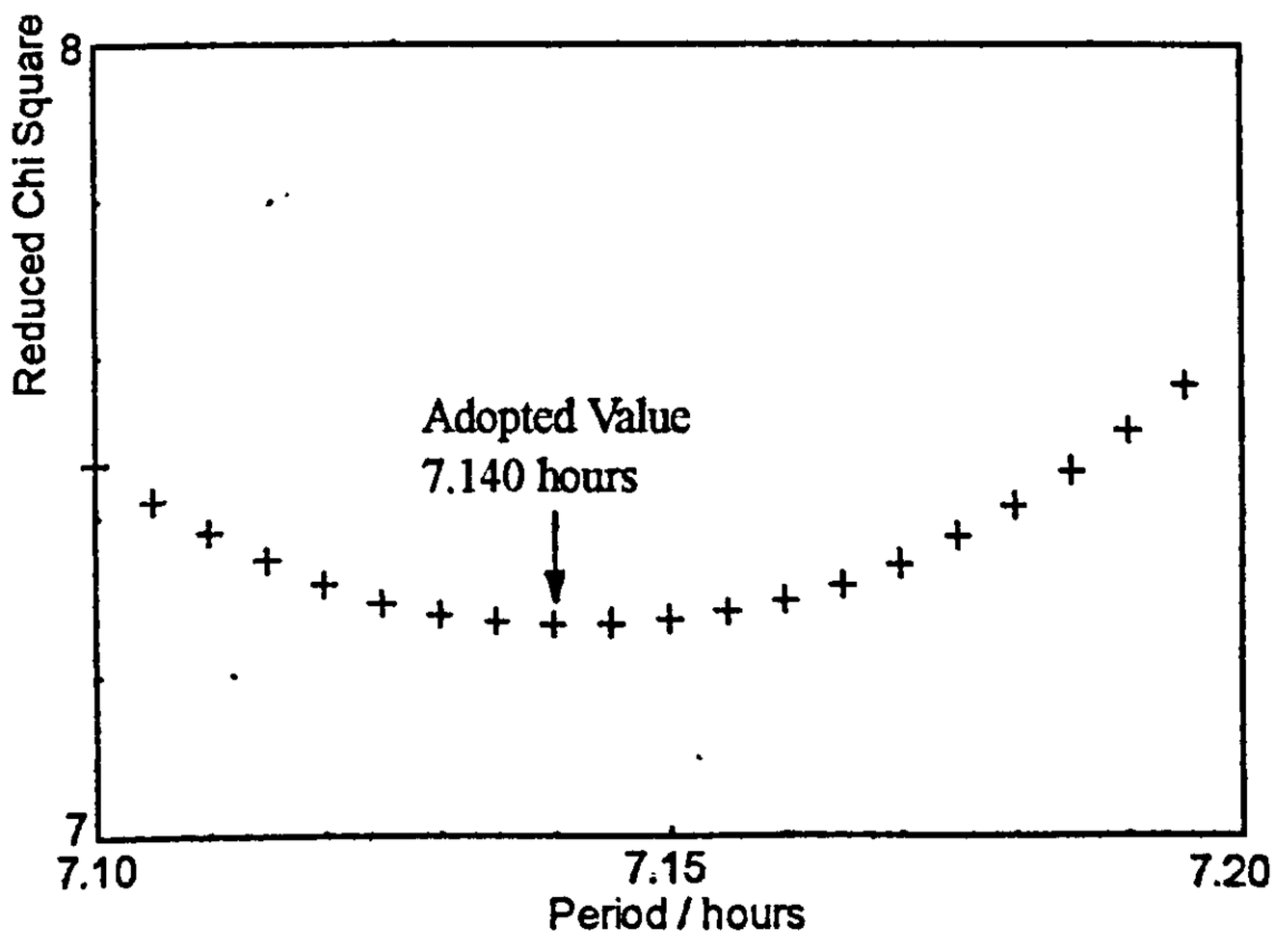

Differential Magnitude with respect to Comparison Star

Figure 8.7 - Measured light curve and modelled fit for 7 Iris

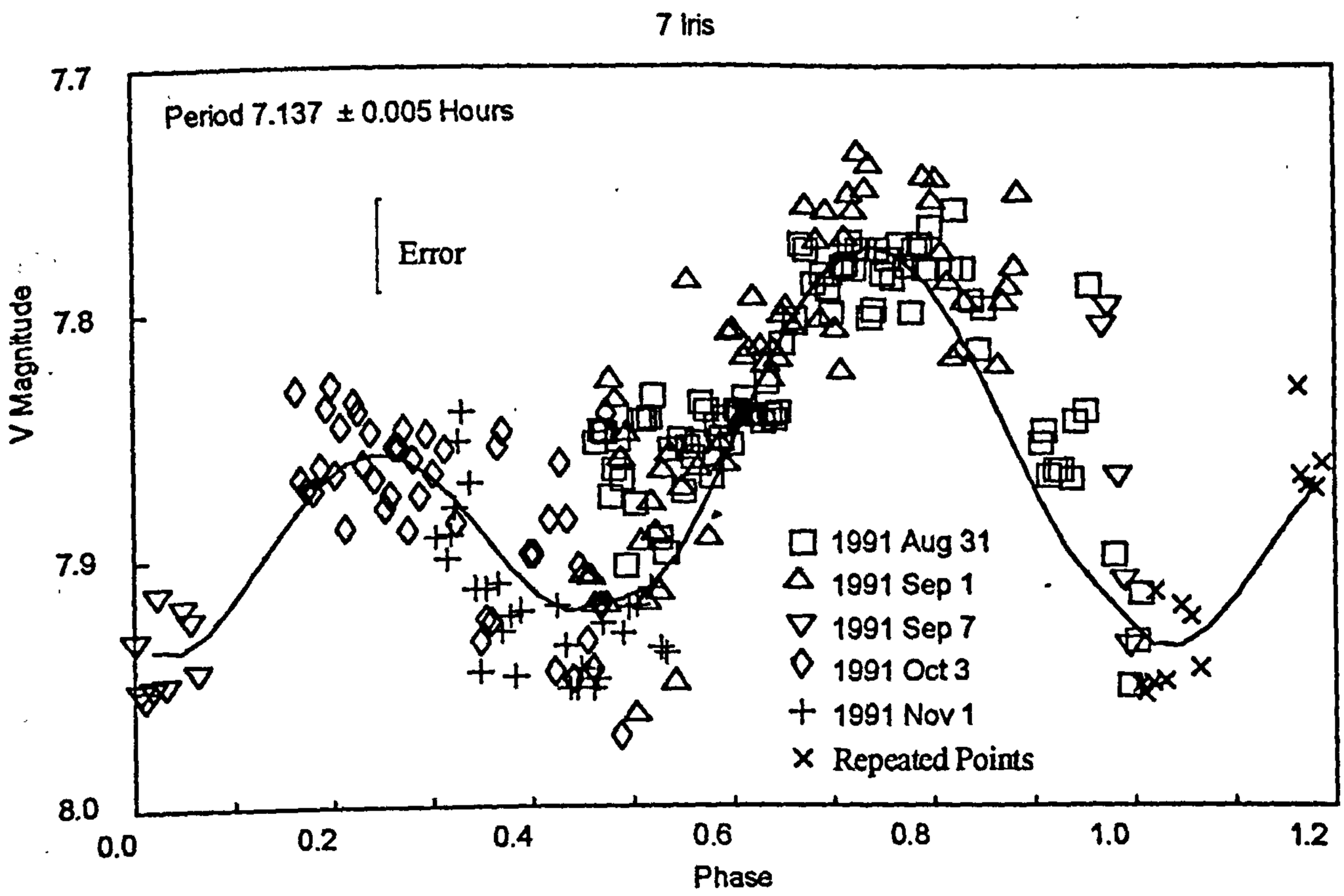

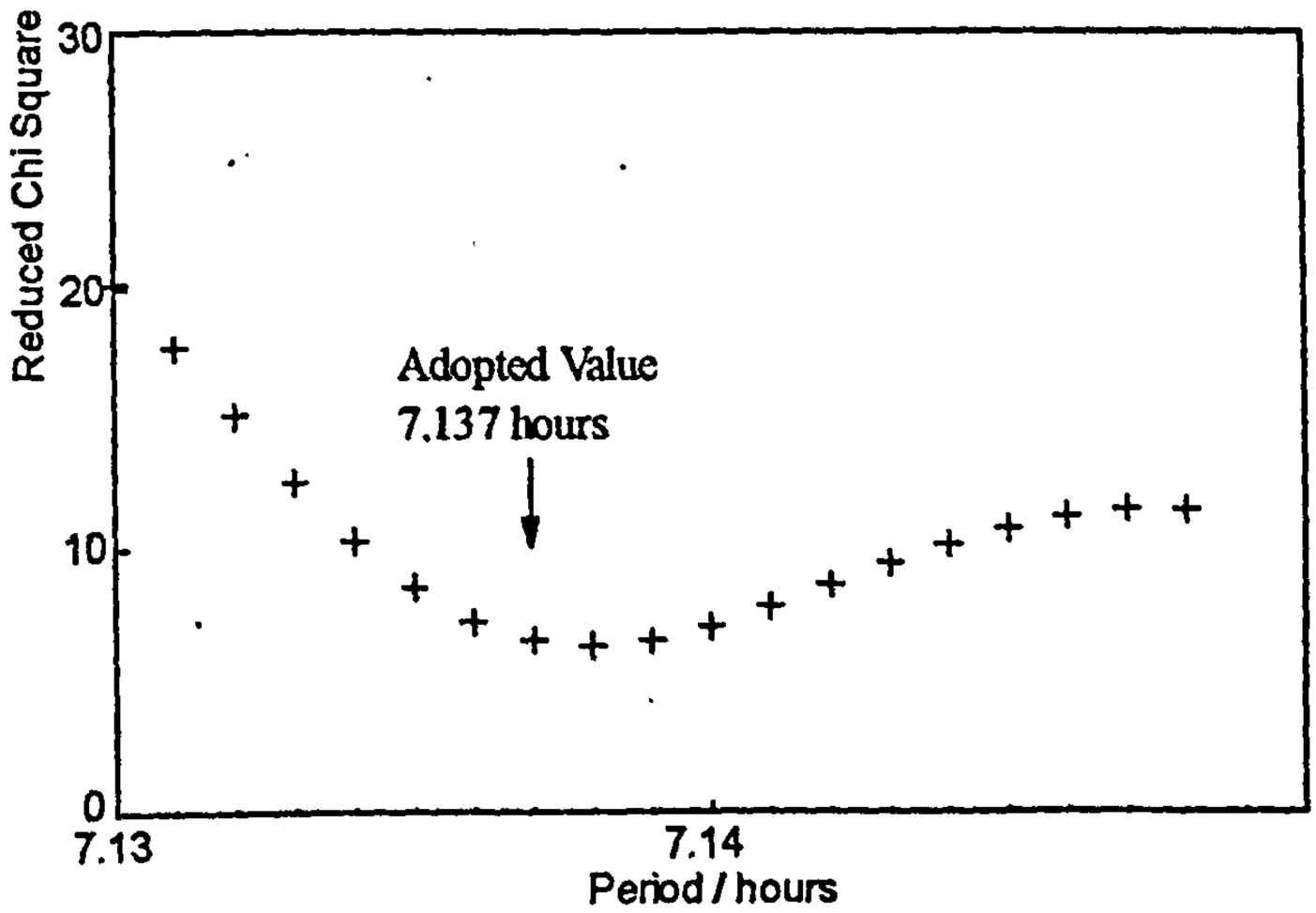

Figure 8.8 - Measured light curve and modelled fit for 7 Iris

Prior to this work the adopted period was listed as 13.6 hours. This was derived from a low amplitude light curve and was no better than a rough approximation. In 1984 the writer organised an international campaign to observe 8 Flora. Five nights of data were secured over a three month period by Hollis at Ormada, Miles at Manley, Dumont in France and Bembrick in Australia. Despite the problems in period searching a best fit period of 12.790 ±0.050 hours was derived and published (Hollis et al 1987). This value was adopted until the publication of other observations made in 1984 (Di Martino et al 1989). These comprised observations made just before and just after those from my project. Each set of the Di Martino data was assembled into a separate light curve with a period of 12.87 hours reworking my international campaign results using the rotating ellipsoid model indicates that the best fit also occurs at a period of 12.870 ±0.050 hours.

The periods appear to be so close to half a day that there are problems both in data acquisition and reduction. Rotation periods close to a sub-multiple of a day are awkward to determine as the same portion of the light curve is all that is available for several days. It can take several months to measure a complete light curve sufficiently well for an unambiguous determination of the rotation period (see the results for 751 Faina later).

The complete data set has been re-analysed in this work. The data sets cannot be combined and assembled satisfactorily using either of the previously derived periods. The conclusion must be that both periods are incorrect. The data sets have therefore been combined and a period search carried out in the range of 25 to 26.5 hours (being approximately double the two periods). The results were positive and several likely periods were found (see the RCS plot on Figure 8.10). The most satisfactory (and that with the minimum error) is 26.03 ±0.03 hours and corresponds to an ellipsoid with a:b of 1.026:1. This implies that Flora is closer to spherical than previously thought and that the main contributions to the variation in the light curve are either albedo variations or possibly shadows from topographic features. Many observers have noted a very low amplitude light curve though the light curves in the database show many occasions when a variation of amplitude of between 0.05-0.08 magnitude appears.

The rotation period for Flora may well be approximately twice as long as previously quoted. The wide error quoted reflects the low amplitude as several trial periods within the search range provide a similar value for χ^2. Further observation is necessary to try and resolve the period unambiguously but the knowledge that the period could be substantially longer than previously thought should assist in the formulation of the correct approach to secure the necessary data.

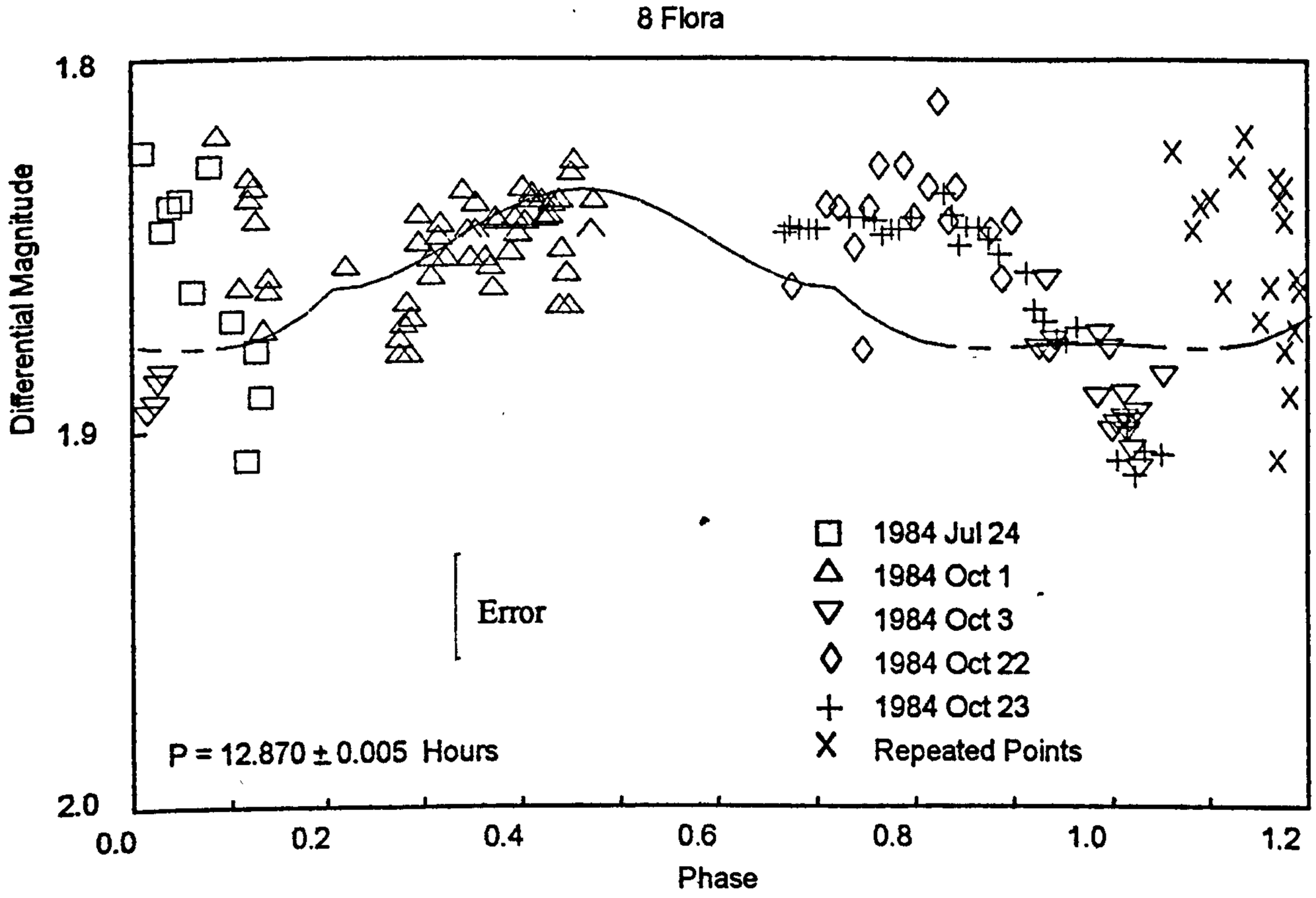

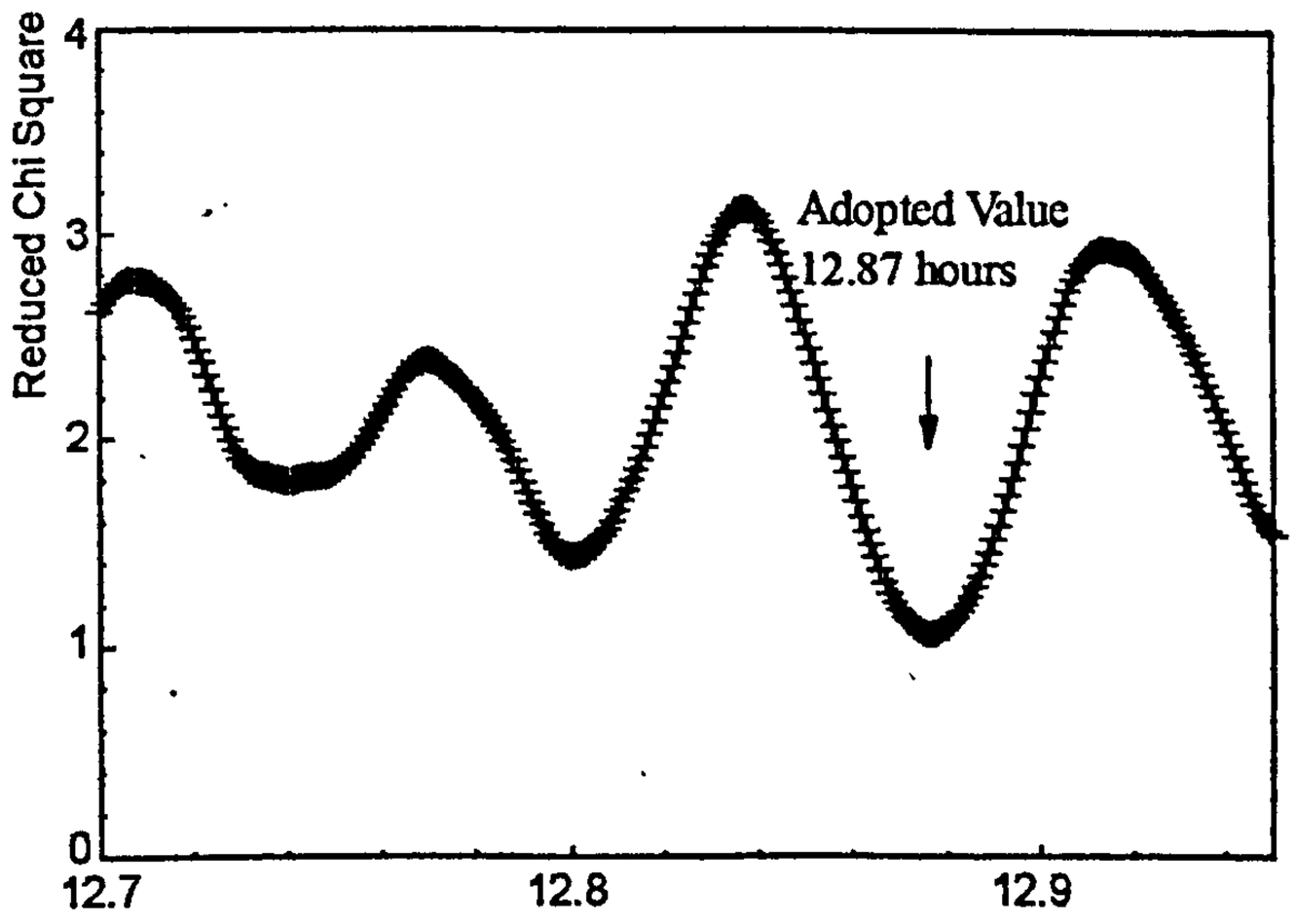

Differential Magnitude with respect to Comparison Star

Figure 8.9 - Measured light curve and modelled fit for 8 Flora
This was the original value derived in this work

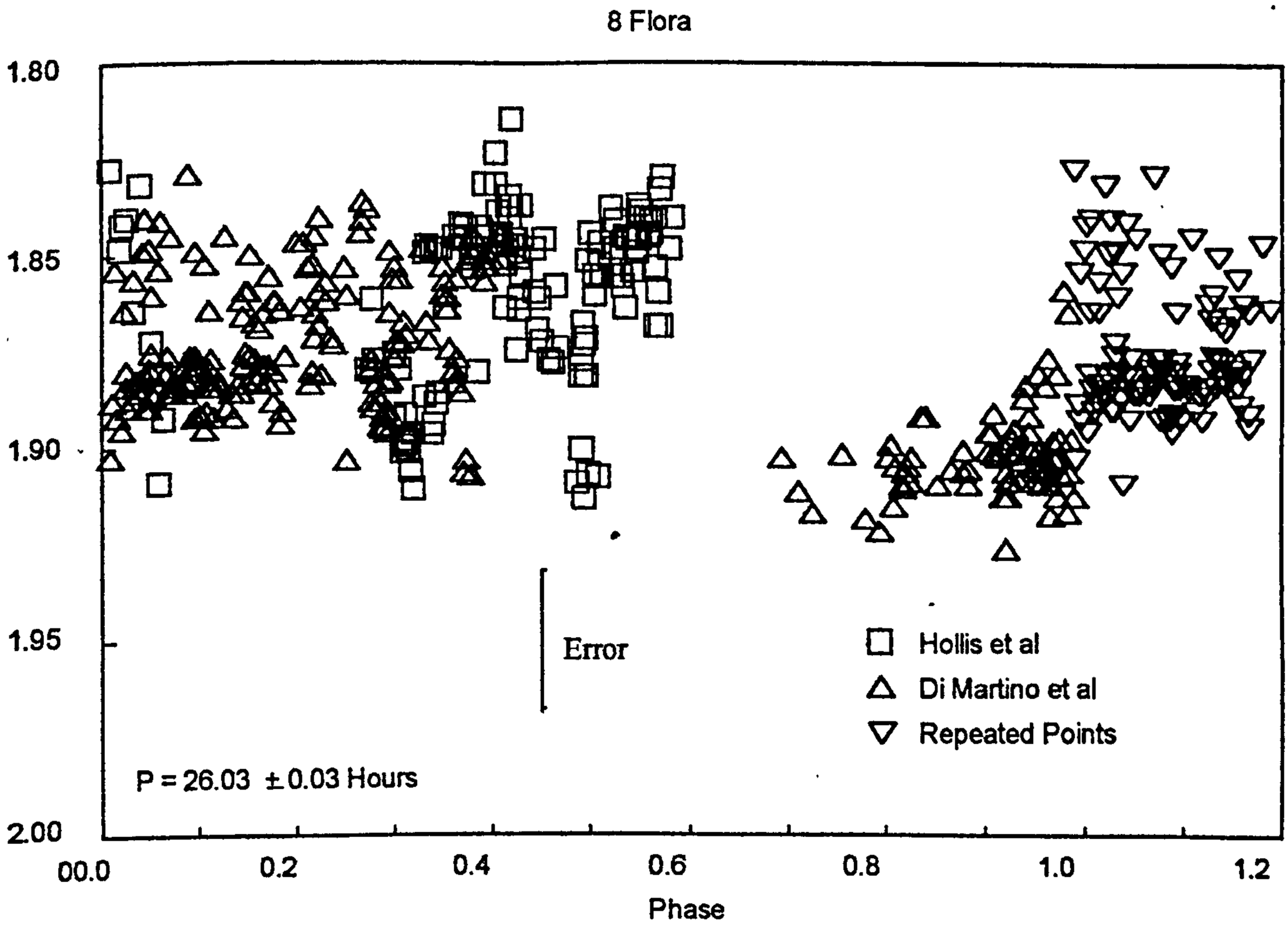

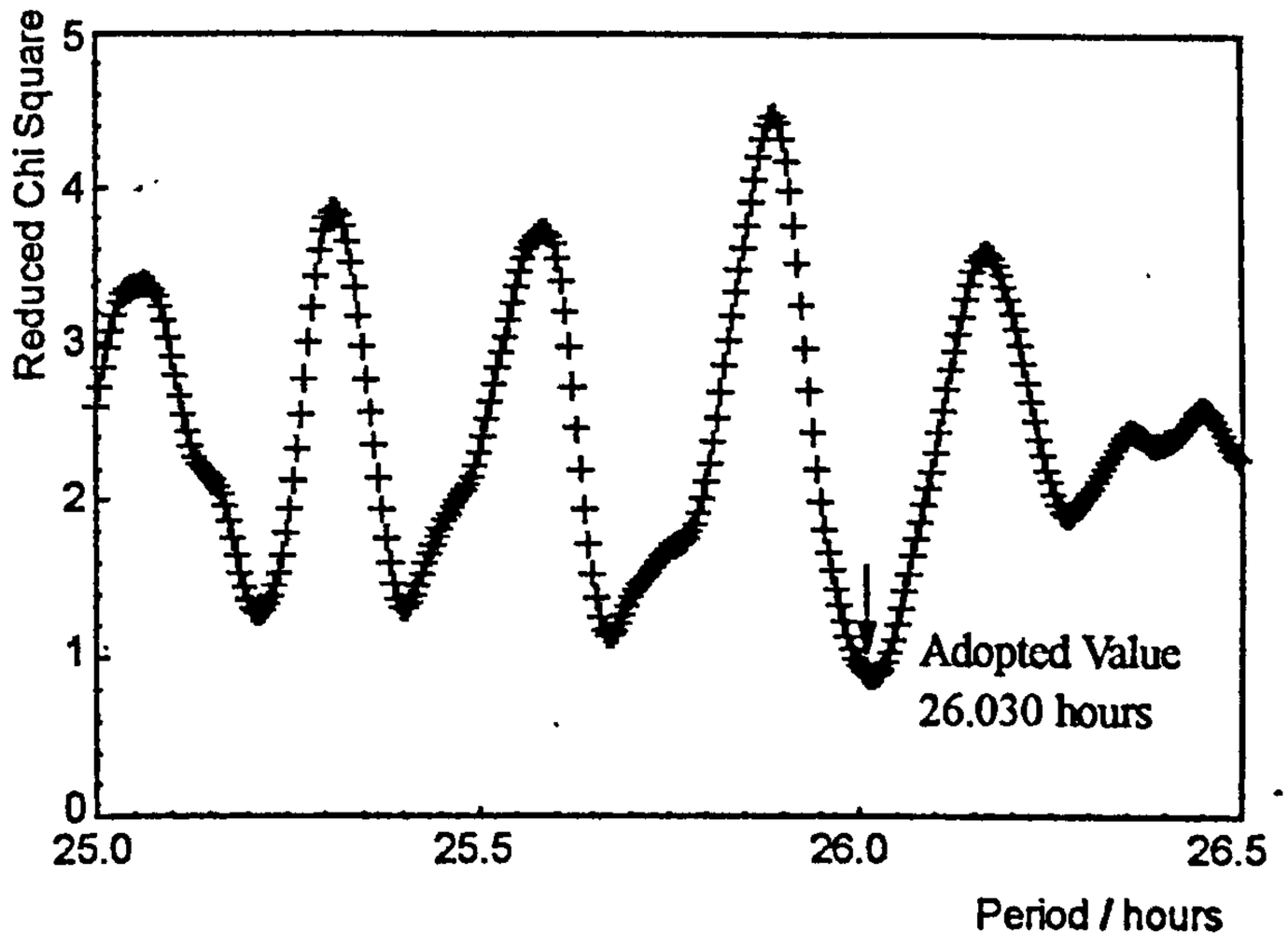

Differential Magnitude with respect to Comparison Star

Figure 8.10 - Composite light curve of 8 Flora from all published observations in 1984. The derived rotation period of 25.873 hours produces a realistic light curve with two maxima and two minima. Shorter periods do not produce smooth curves when all data sets are combined.

8.12 The rotation of 15 Eunomia (Figure 8.11)

15 Eunomia is one of the few large asteroids which have a large amplitude lightcurve. Its orbit has a relatively high inclination. A composite light curve was derived during March 1985 by Mellilo (Observing from New York State) and Hollis (observing from Cheshire). Eunomia has been extensively observed for one half of its orbit and is not well observed in the other - this is because its apparent declination varies between +45° and -45°. There are few observatories in the Southern Hemisphere and the number undertaking observation of asteroids is severely limited.

The light curve has two maxima and two minima per rotation. Some observations show these as at the same brightness but most show a secondary maximum which is approximately 0.03 magnitudes fainter than the primary.

A rotation period of 6.080 ±0.002 hours was derived, in excellent agreement with the period of 6.083 hours given in the database. The maximum amplitude corresponds to rotation where the aspect angle is 90°. This present work gives an estimate of the ratio a:b of 1.68:1 which does not correspond with the range of 1.40 to 1.50 given in the database (Magnusson 1989) and probably indicates that the value of a:b has been underestimated in the database. There is no strong evidence for very high values of a:b especially amongst the larger asteroids, with only a few possible exceptions (624 Hektor, 216 Kleopatra for example which have observed lightcurve amplitudes in excess of 1 magnitude implying a:b is greater than 2.5:1).

There is a small difference in the magnitude of adjacent maxima amounting to approximately 0.03 magnitudes. This can be accounted for by a single low albedo area on the central meridian (using the definition for this given in Section 8.3).

Albedo markings can only reasonably be inferred where the contrast with adjoining areas is relatively high (differing by the order of 50% from the mean level). Areas which differ in albedo by only a few percent will not be detectable as they will have a small effect on the lightcurve. They may however be detectable by other means - such as polarisation measurements.

8.13 The rotation of 44 Nysa (Figures 8.12, 8.13 and 8.14)

44 Nysa was observed at three oppositions in 1983 October 28 by Miles at Manley, 1988 January 8 by Miles and Hollis at Manley and 1992 January 9 by Hollis at Marton Green. The first and last oppositions produced complete rotational light curves whilst in 1988 only about 30% of a complete rotation was observed due to poor weather conditions.

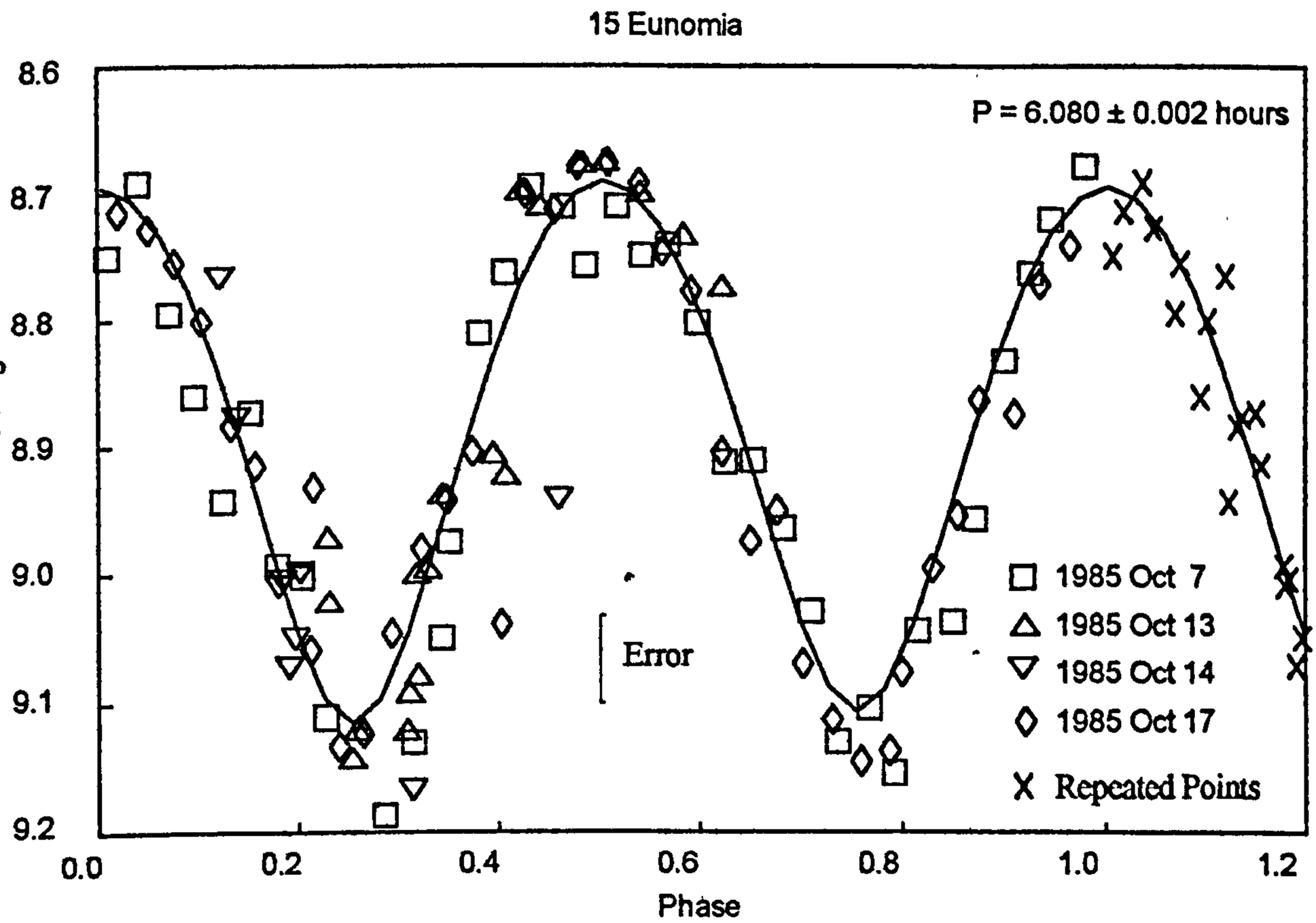

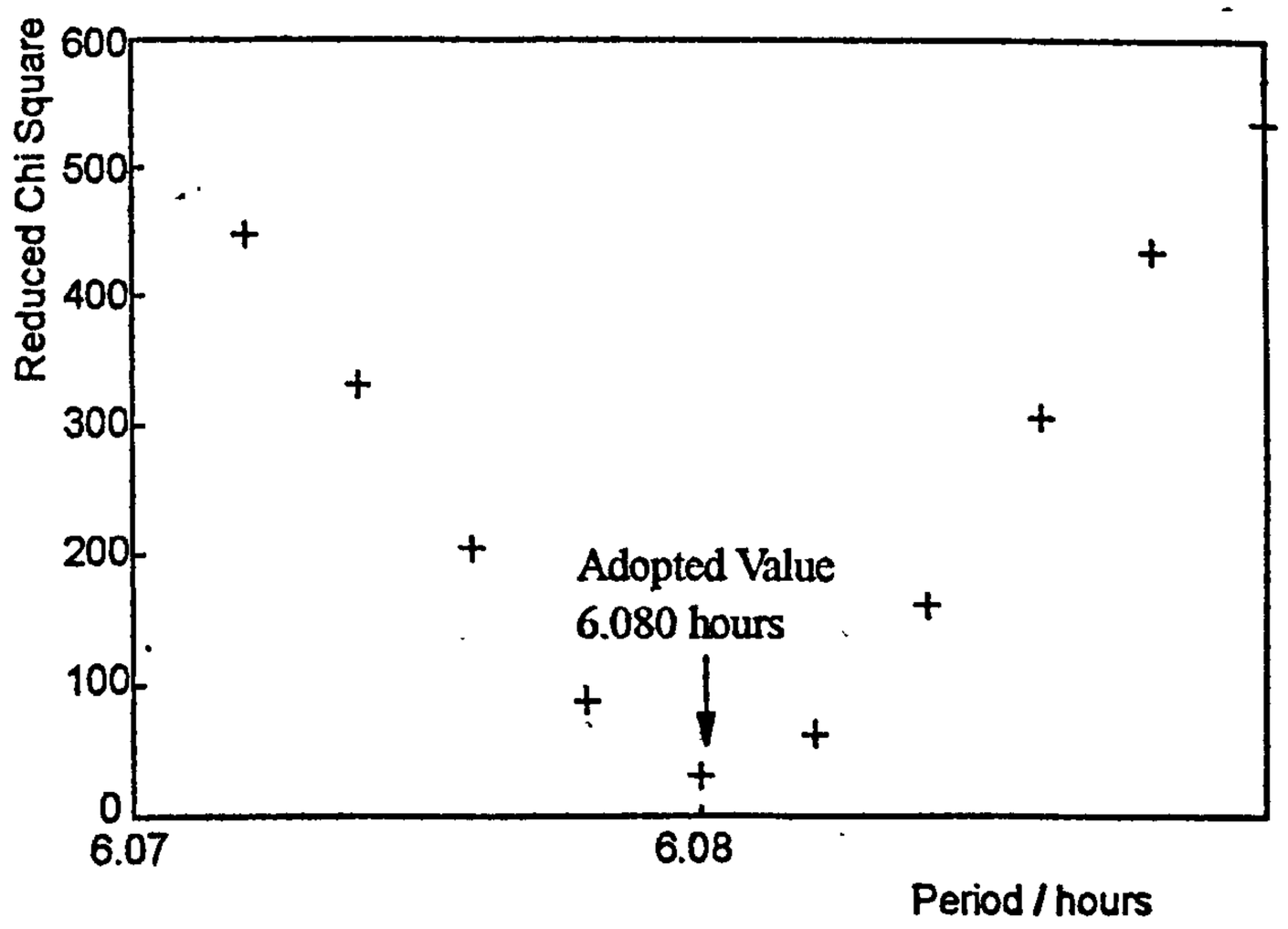

Differential Magnitude with respect to Comparison Star

Figure 8.11 - Measured light curve and modelled fit for 15 Eunomia

All three have been analysed using the ellipsoid model and periods of 6.432 ±0.004 hours, 6.493 ± 0.020 hours and 6.434 ±0.030 hours have been derived for 1983, 1988 and 1992 respectively. The values do not compare precisely with the database period of 6.422 hours. In 1988 only a small part of the light curve was measured on a single night and the derived period illustrates the errors to be expected from limited data. The period and errors obtained at the other two oppositions are within 30 seconds of the adopted period but illustrate the typical magnitude of errors when data from a single night alone is used for period derivation. Unfortunately measurements from different oppositions cannot be assembled to form a composite light curve as factors such as estimating the number of intervening rotation cycles, and the differing light curve shapes at different oppositions provide insuperable difficulties.

The shape factors derived for a:b are 1.347:1, 1.322:1 and 1.347:1 respectively. This suggests that the true value of a:b is at the lower end of the range of 1.37:1 to 1.58:1 given by Magnusson (1989).

Of particular note is the different depths of primary and secondary minima (0.4 and 0.2 magnitudes rspectively) seen in 1992. This opposition was near the polar longitude and hence at a near polar aspect. Gehrels observed two equal minima of amplitude 0.2 magnitudes during the 1960s when a polar aspect was presented. Most other aspects show an amplitude of 0.4 magnitudes as is seen in the other light curves. *The model indicates that there is a very bright patch visible at high latitude but off centre from the rotation pole.*

8.14 The rotation of 115 Thyra (Figure 8.15)

115 Thyra was observed at Manley in 1983 over 4 nights in March by Miles. Hollis was assisting during two of these.

A rotation period of 7.797 ±0.005 hours was derived. The current period given in the database is 7.241 hours which was derived in 1978 by Scaltriti and a composite light curve is presented in the Asteroid Photometric Catalogue. The machine readable database observations from 1978 however cannot be reassembled to give the correct composite. Either there is either an error in the machine readable catalogue or else the data has been altered since the composite was published. The 1983 observations cannot be assembled to give a smooth light curve at the database period of 7.241 hours. Each data set covers almost a complete rotation of the asteroid though the shape of the light curve is different at each opposition due to a different aspect angle to the Earth.

The data sets for 1978 and 1983 were separately searched to try and find a period common to both. A value of 8.000 ±0.005 hours appears to be the most compatible to the two data sets. It is therefore likely that the period is close to one third of a day. As an integral sub-multiple of a day it means that

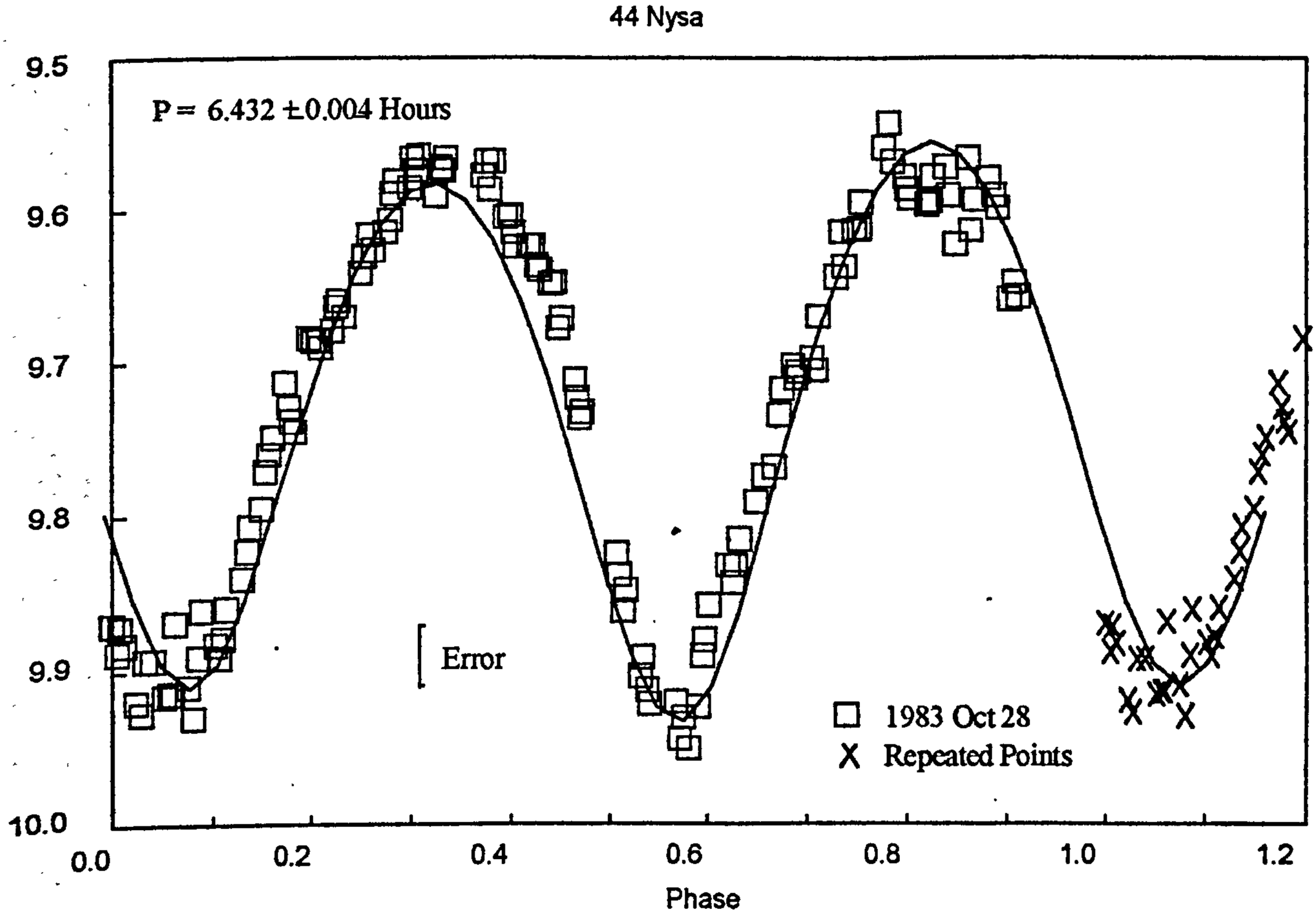

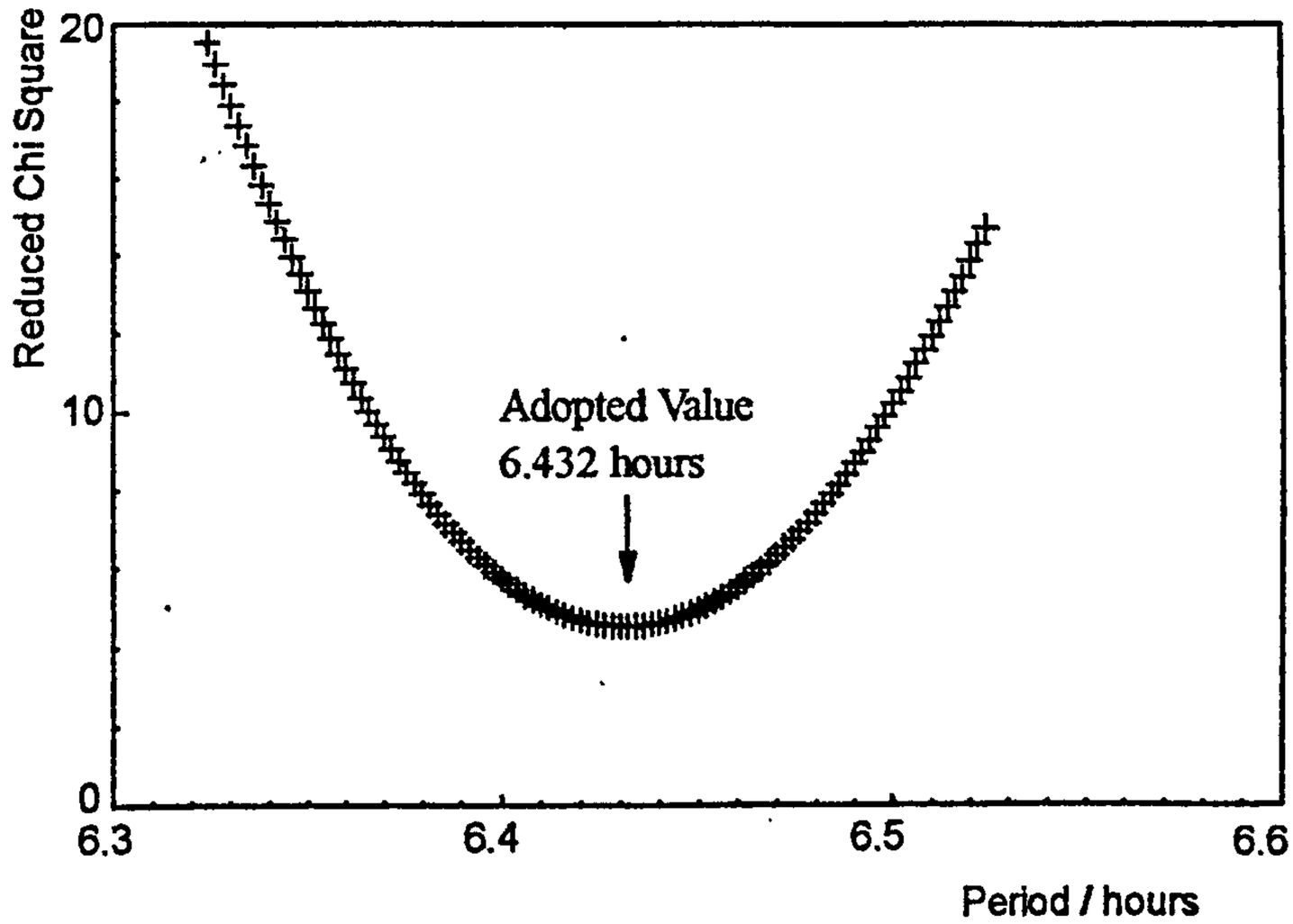

Figure 8.12 - Measured light curve and modelled fit for 44 Nysa in 1983

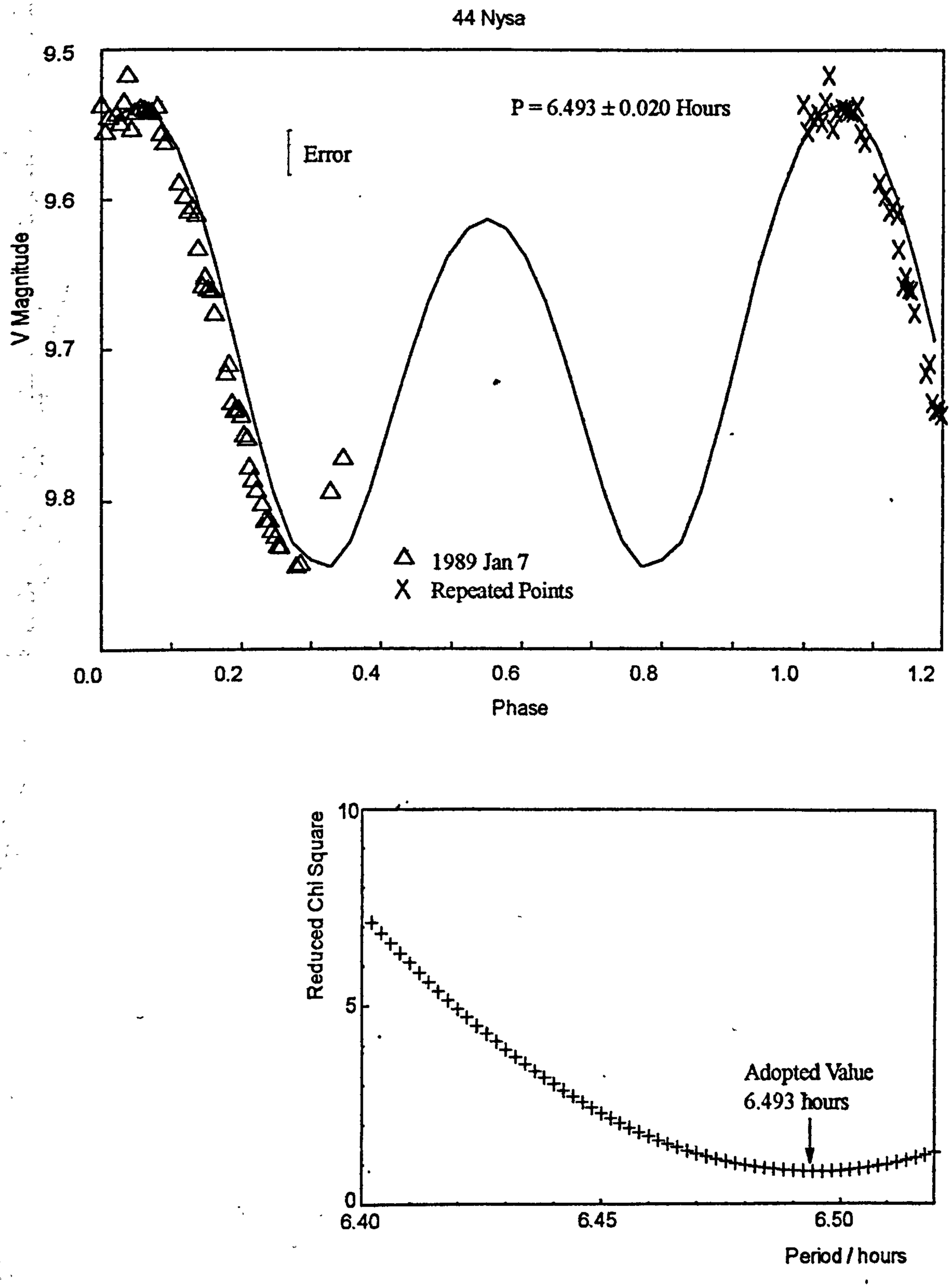

Figure 8.13 - Measured light curve and modelled fit for 44 Nysa in 1989

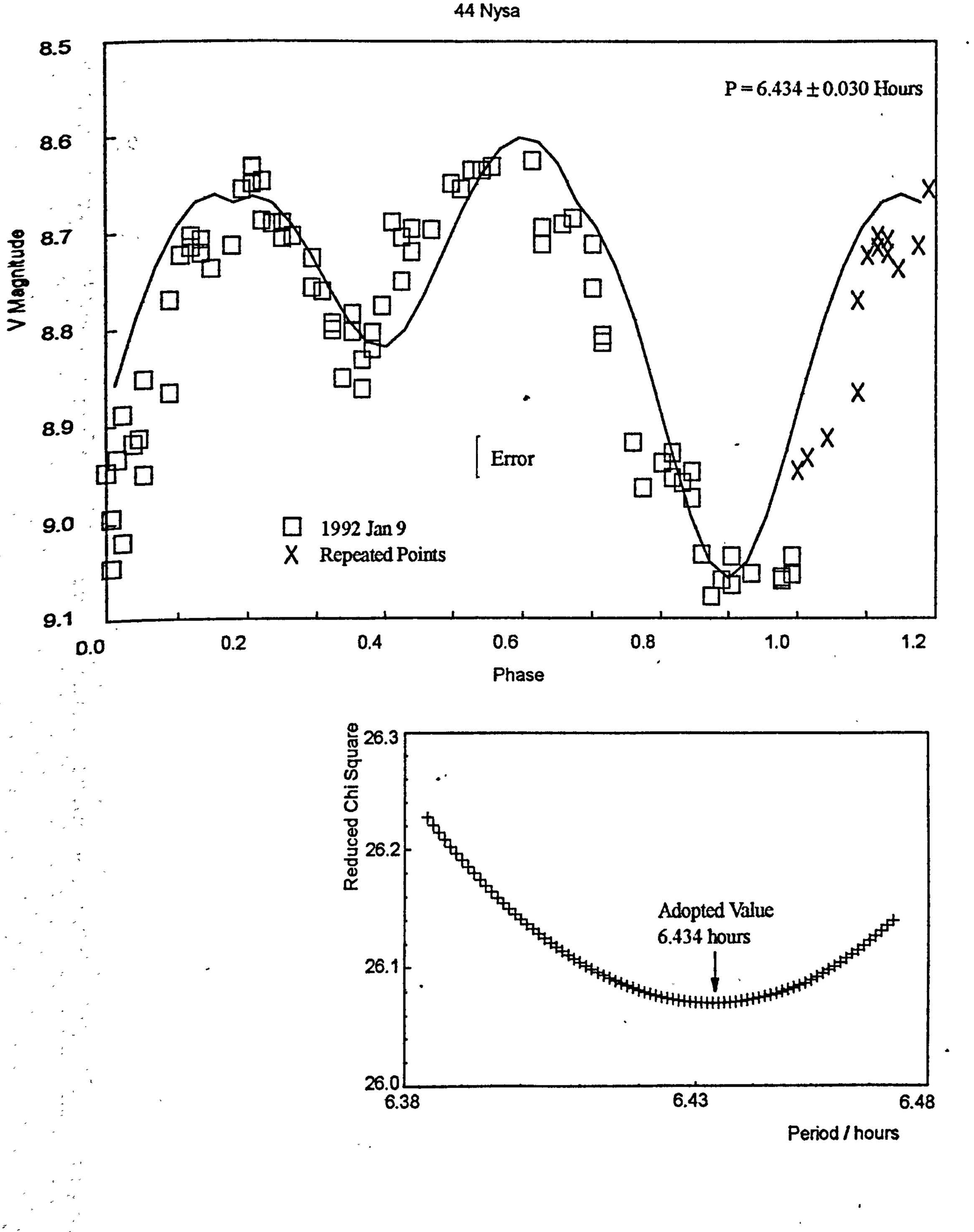

Figure 8.14 - Measured light curve and modelled fit for 44 Nysa in 1992

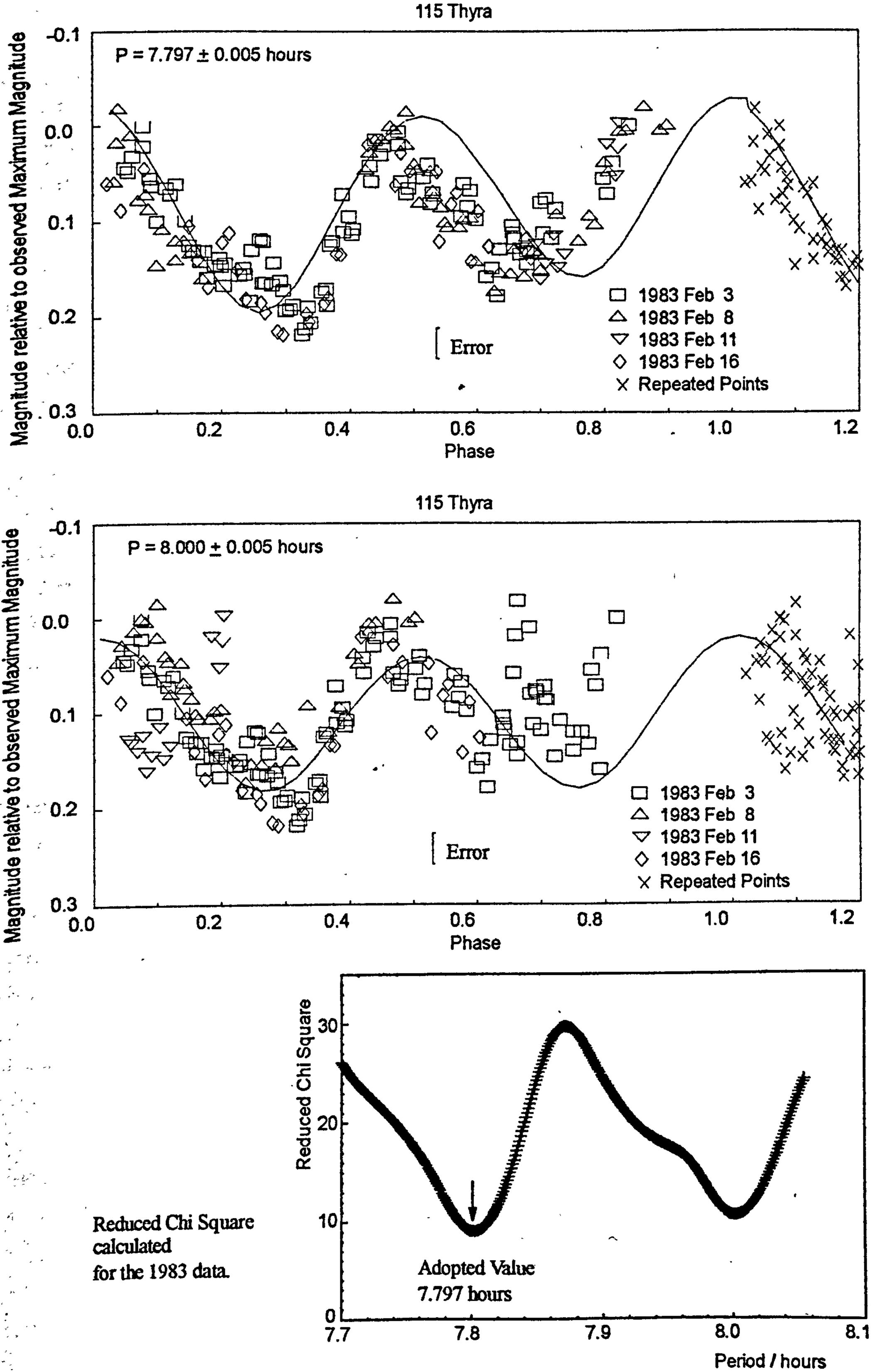

Reduced Chi Square calculated for the 1983 data.

Figure 8.15 - Measured light curve and modelled fits for 115 Thyra
Upper curve based on a best fit period of 7.797 hours
Lower curve based on a period of 8.000 hours more compatible with previous measurements made in 1978 - the fit is relatively poor.

a similar portion of the light curve is always seen at the same time on successive days. However the composite light curve in 1983 assembled with this period is not satisfactory and, in view of the apparent error in the 1978 data it seems preferable at least for the time being to assume the value of 7.797 hrs is correct. The 1983 measurements are plotted to both the derived periods in Figure 8.15.

8.15 The rotation of 416 Vaticana (Figure 8.16)

Light curves for Vaticana were obtained in March, April and May 1989 by Miles at Manley. Hollis was assisting during two observing runs. It had not previously been observed photoelectrically and so no rotation period had been derived.

Using the two complete light curves (March 28 and May 6) periods of 5.372 hours and 5.741 hours fitted the data. It was encouraging to find that incorporating the additional partial light curves resolved this ambiguity (the value of the reduced chi square for the shorter period was 5.999 and for the period of 5.742 hours came to 133.385 with all the observations included confirming that this period is not valid). A period of 5.372 ±0.001 hours was derived and this has been adopted in the database. A shape of a:b 1.384:1 has been deduced from the data.

8.16 The rotation of 751 Faina (Figure 8.17)

751 Faina was observed on 11 nights over a three month period from 1988 October 31 to 1989 January 12. From this a period of 23.680 ±0.030 hours was derived and this period has been adopted. A lower bound shape factor of a:b = 1.367:1 was found. No previous observations by others exist in the database. The minimum value shown on the RCS fit suggests a rotation period of 24.03 hours however, when plotted, the light curve shows irregularities which were not present on the individual observing runs implying that this value is not valid.

The rotation period is relatively long and well illustrates the difficulty in assembling the light curve when the period is close to one day. There is very little overlap between successive night's measurements so that similar portions of the light curve were only measured by successive sets of dta and not later in the observing series.. Changes in the form of the light curve could occur and not be detected as the typical observing run of from 4 to 6 hours only covers a small portion of a complete rotation. A fine structure feature can be detected on the curve (and can be seen at the mid point of the descending branch after each maximum) which is visible on both the primary and secondary minima. This feature may represent a topographic feature which can be detected when it is on the limb and thus be visible twice during each complete rotation cycle (when it reaches first the preceding limb and then the following limb). It is also possible that this is an albedo feature and that the rotational light

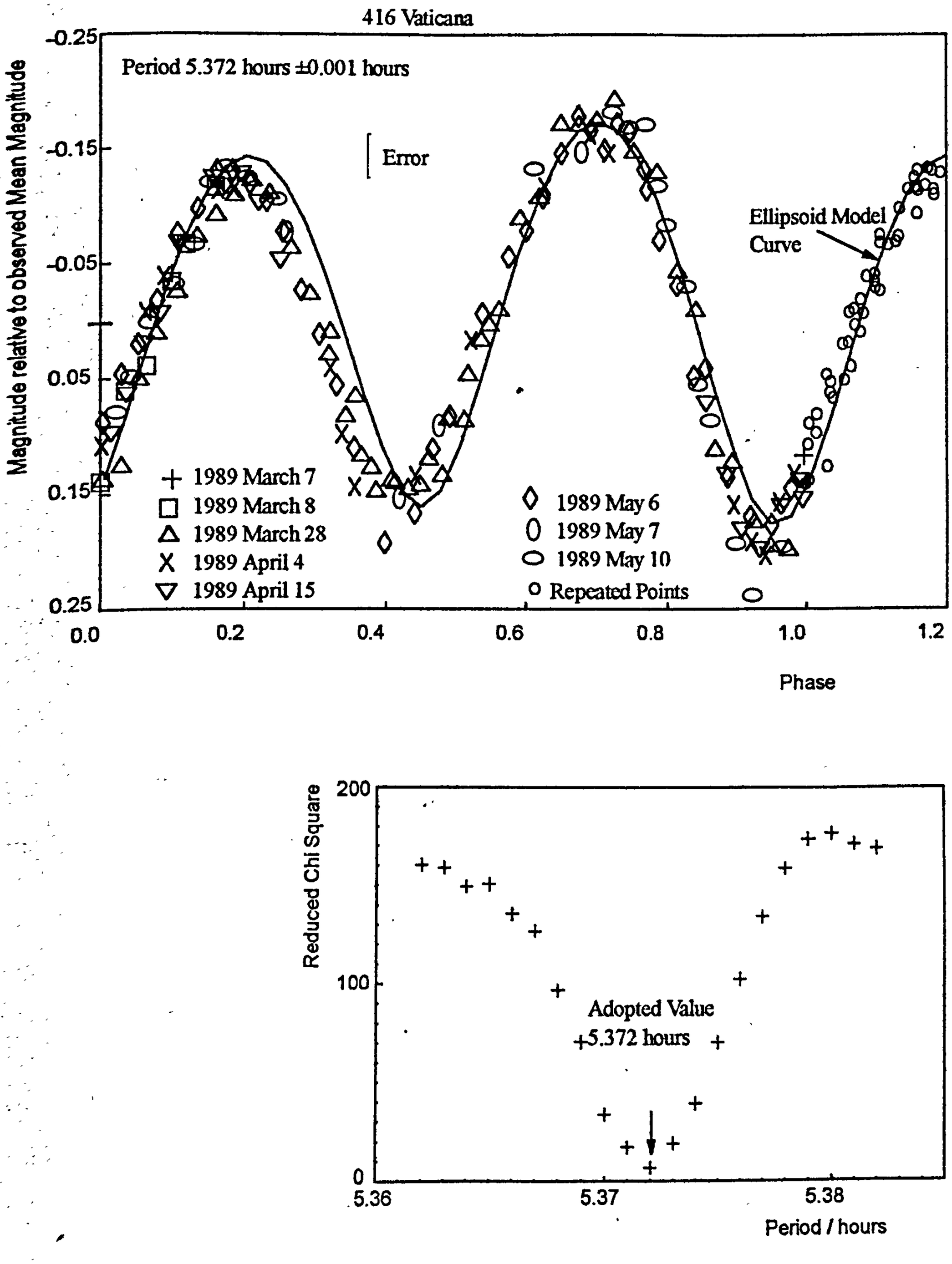

Figure 8.16 - Measured light curve and modelled fit for 416 Vaticana

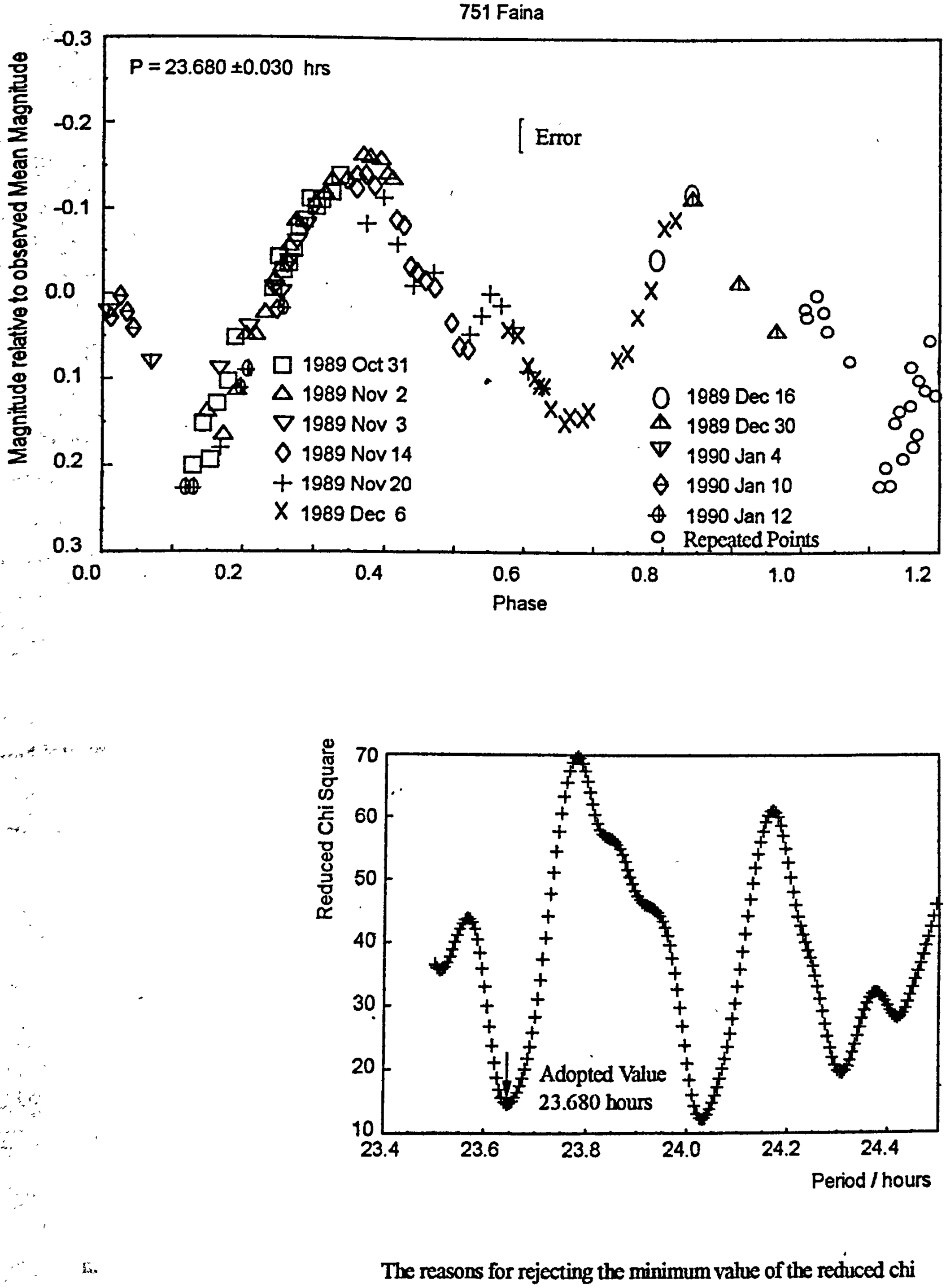

The reasons for rejecting the minimum value of the reduced chi square for the adopted period are discussed in the text.

Figure 8.17 - Measured light curve for 751 Faina

curve is singly periodic. Polarisation or multi colour photometry may help decide which of these options is most appropriate.

The rotating spheroid model did not provide a good match directly and the period was derived using a combination of this method and FALC (see Section 8.6). Final confirmation was made by a visual examination of 30 phase plots centred on the derived period. The quoted error is the limit beyond which the composited light curve ceased to be smooth.

8.17 Comments on data acquisition and errors.

During this project, various formats for taking measurements have been adopted - with the constraints frequently imposed by the UK weather.

Light curves have been taken over a single night, several nights close together, or scattered during the course of several months. A few general guidelines have emerged from experience.

1. The UK weather is so unpredictable that it is preferable to secure as much coverage of the light curve during the first night as is practicable (a second opportunity may not arise). At least thirty minutes phase overlap of the initial coverage is desirable. Accurate period determination is difficult from a single night's measurements alone.

2. Short fragments (say less than 1 hour) will only be significant if either there is definite variation during the period of observation, or where an asteroid exhibits a large amplitude light curve so that isolated photometric measurements can be used to reject unrealistic periods if they fall well away from the composite light curve.

3. Long partial coverage will allow period searching as long as three maxima or minima are obtained (so that ambiguities can be resolved). The derived period will be accurate if the form of the light curve does not change much during the course of an apparition.

4. If the rotation period is long, or close to a sub-multiple of 24 hours, there is no short cut. Substantial coverage of short periods, such as 6 hours and 8 hours, can be derived by long observing during a single night. 12 hours and 24 hours (and to some extent 18 hours) can only be adequately covered by collaborative efforts from several observatories at a range of longitudes or by observation from a single observatory over several months (or from space over the course of a single rotation!).

The error of the individual data points is typically ±0.02 magnitudes and this has been demonstrated over many night's observation. However there are several factors which can introduce systematic errors. The most significant of these is variable sky extinction. During the course of a night there is frequently a steady drift in atmospheric transparency. This will not show in the individual pairs of measurements forming each data point, but may mean that data points taken over the course of a night may include an error due to this variation. Observations made over a series of nights could also include an error due to variations in atmospheric absorption due to airborne dust aerosols as well as water vapour. Scatter (random variations) on any given night is likely to arise due to unsteadiness in the atmosphere. The more turbulence is present, the greater the stellar scintillation and image walk. The internal consistency of each night's measurements is usually good provided that the effects of variable transparency are taken into account. When measurements are made over several nights the internal consistency is poor. This effect is well illustrated by the two light curves of 7 Iris. The effect of these errors is much greater where the amplitude of the light curve is low and may well account for the poor constraints on the rotation period of 8 Flora.

The data presented in this Chapter is unsmoothed and represents two ten second integrations for each data point. Smoothing of the data is not reasonable where fine detail may be present as it will be removed. However a lower mean error can be achieved if each data point is produced from four ten second integrations. This reduces the number of data points by one half, the mean error is reduced by a factor of $1/\sqrt{2}$. Though this exercise has not been carried out in this work smoother light curves could be produced in this manner. In general this technique suggests that the smoothness of the light curve can be increased when the number of photoelectrons detected for each data point is increased - a conclusion reached in the theoretical analysis of the photometer performance in the previous Chapter.

8.18 Conclusion

The calculations presented at the start of the Chapter show that Comet P/Halley appears to be in a state of free-precession with axial rotation and precession occurring about the principal axis. 1220 Crocus is confirmed to be in a state of forced precession (the geometry being incompatible with a state of free precession). This seems to indicate a binary nature for the 1220 Crocus system.

The new light curves presented here show no evidence of complex rotation since all the observed features on the light curves can be explained in terms of albedo markings. The rotating ellipsoid model gives a valid method for estimating the rotation period and lower bound of the shape, however its use has limitations if there is significant fine structure in the light curve (as for example in the case of 751 Faina) as it is not feasible to fit these to a multiple spot model..

Individually the data presented in this work suggest several modifications and additions to the current database.

8 Flora has not been well modelled in the past due to the low amplitude of its light curve which is also relatively featureless. Its rotation period may well be approximately twice as long as previously thought and part of the light variation due to other factors than shape.

The calculations carried out here showed a derived shape for 4 Vesta with a:b of 1.018:1. The light variation was modelled as probably due to two dark albedo features. This conclusion is in agreement with the photographic record of a rotation of 4 Vesta secured from the Space Telescope and published after these calculations were made (but before the work was submitted).

The adopted period of 115 Thyra is incorrect. The best fit for the light curve in this work is 7.797 hours. Though both data sets can be reconciled to a period of 8.000 hours the composite light curve does not appear smooth and so this suggested period is probably incorrect.

There appears to be no direct evidence in this data (or the light curve database) of freely precessing asteroids. There is thus no direct evidence for recent collisions amongst those asteroids whose light curve has been measured. This is perhaps not surprising as the damping times for the larger asteroids are relatively short (as considered in chapter 1).

9 Extensions of the Current Work

This current work has highlighted several fundamental questions which are worthy of more detailed study.

9.1 Asteroid Classification

Barucci et al (1988) have used the same data set as used in Chapter 3 of this work (the 8-colour photometry of Tedesco et al. 1986). Their intention was to extend and refine the currently accepted classification scheme. In this work the conclusions are that the current scheme has shortcomings. Some quite dissimilar bodies are grouped together whilst similar bodies are separated into different classes. It is apparent that classification schemes can be constructed from published data which differ from, and perhaps improve on, that currently accepted. The introduction of Artificial Neural Networks (Howell et al 1994) to help in classification has given the potential to establish a system that will self modify as additional data becomes available.

It would now seem appropriate to investigate the strengths and shortcomings of asteroid classifications making use of all the published data by numerical methods. Whilst this would undoubtedly confirm that the classification of the majority of the asteroids is correct however it would certainly also adjust the scheme. In particular this work confirms the work of Gaffey et al (1993) that even without additional data, the S group asteroids can be subdivided, and that these subdivisions are more pronounced than those already in use for the lower albedo C, G, F classes.

9.2 Photoelectric Photometry

In this work it has been found that dehumidifying photomultipliers produces striking reductions in the dark current. The reduction is a factor of the order of 80 to 100 times. A valuable project would be an investigation into the relative and combined benefits of drying and dry ice cooling on the dark noise of a photomultiplier. This research should be applied to both pulse-counting and analogue (dc) systems. The indications of this work is that drying with silica gel produces major improvements in the performance of Sb-Cs side-window tubes in analogue mode.

In order to gain a complete understanding, the effect of increasing the relative humidity of the air around the tube should also be studied.

The use of robotic telescopes tracking using CCDs and the Guide Star Catalogue could potentially allow the acquisition of light curve data for many asteroids during the course of a single night and potentially several thousand light curves during the course of a single season. This could provide data on a more systematic basis than the relatively unstructured approach currently being undertaken

9.3 Synthesis and Inversion of Light Curves

To date the majority of efforts have involved modelling asteroids as regular ellipsoids. Several authors have indicated that they are modelling asteroids in terms of albedo variations across the surface or else large scale topographic features. However there are no landmark papers in the literature to date. The difficulty of this was identified by Russell in 1903.

With the large amount of imagery of irregular bodies that now exists it would be valuable to use known shape to synthesise lightcurves and compare these with the results of observation. The modelling should not only include the topography but also phase effects introduced by various surface roughness. One area for further investigation would be the effect that errors in the observations would introduce into the models.

9.4 Evolution of Asteroids and the Asteroid Belt

Using the basic ideas outlined in this work and the distribution of planetesimals inferred from models of the Solar Nebula it would be possible to model the accretion phase of the evolution of asteroids. The dynamics and composition could be modelled and the internal processes included in the evolutionary study. It should prove feasible to incorporate fragmentation processes to identify the possible structures of the current asteroid belt and its sensitivity to various conditions - eg initial composition, gravitational interactions between asteroids, gravitational stirring from proto-Jupiter.

9.5 Observation

Earlier in this chapter the potential for obtaining data using robotic telescopes was mentioned. This would significantly enhance the amount of data available for analysis. In particular a continuing programme of observation of small asteroids, to determine spin frequency and spin axis orientation will be necessary for some years to come as a means of refining the statistics. One area of study that has not been fully investigated for more than a small number of asteroids requires intensive observation during several oppositions. This will allow phase effects to be studied for various solar aspects and will lead to determination of the photometric homogeneity of the surface besides accurate determination of the synodic rotation period and spin axis orientation. To date, the most precisely determined spin parameter for any asteroid is less accurately known than was the case for Mars in 1900 - a time when data was taken from drawings and photographs: precision photometry was still some decades from systematic use in astronomy.

By extension, a study of the methods of deriving the physical characteristics from observation should also be examined to confirm whether they are the most effective methods and whether the results are satisfactory.

The relatively small number of research projects being carried out world-wide, by a comparatively small number of observers and theoreticians, means it is especially important to plan and, if possible, co-ordinate the work. The IAU does not have any such plan at present though Dr Alan Harris at JPL and his colleagues maintain a database of observations for the IAU and provide advice on favourable observing projects. Organisations, such as the Asteroids and Remote Planets Section of the British Astronomical Association, mount specific projects - such as that for 8 Flora described in Chapter 8 - which can provide valuable data.

The digitised set of lightcurve data for all published lightcurves derived photoelectrically is now available in PC compatible form. Detailed analysis of this data set both for individual asteroids and also for classes of asteroids should allow refinement of both analytical methods and physical characteristics. The data from 44 Nysa obtained in the early 1980s have been composited and utilised to derive its basic parameters, however this is only feasible if the light curve is regular. The problems with attempting this for other asteroids with ill defined light curves is shown in the case of 8 Flora where three separate light curves for observations in 1984 do not composite well.

The Hubble Space Telescope has been used to image a complete rotation cycle of 4 Vesta. It would be a great assistance to asteroid research if this could be extended to other asteroids. One specific topic would be to image 8 Flora as this could serve to resolve its rotation period and variegation.

Further photometry of 115 Thyra is necessary to confirm the rotation period derived in this work.

Acknowledgements

I would like to thank my wife and family for their great forbearance during the course of this project, and for their acceptance of the importance of minor solar system bodies when more mundane problems arose.

My thanks go to the late Professor Zdenek Kopal for supervising the early part of this work and setting its direction and to Dr David Hughes for his willingness to supervise the final stages and chop my ideas into a sensible shape. Special thanks a due to Dr Alan. Cooper who has shown great patience in ensuring that not only is each topic fully explored but also written up! All my supervisors have given their encouragement in my pursuit of different lines of research and advised how they could be expanded and investigated more fully.

I owe much to my friend Dr Richard Miles who has long provided a collaboration in asteroid research and a ready ear which has listened to many of the ideas presented in this research. Without his comments the conclusions here would have been less well explored and presented.

I would like to thank the British Astronomical Association for establishing an Asteroids Section in 1984 and inviting me to propose an observing programme and become its inaugural Director.

I would like to thank the IAU for honouring me by naming asteroid 4084 Hollis. I hope that I can live up to this by furthering the course of asteroid study in the future.

Finally I must acknowledge a debt to the astronomical community in general - amateur as well as professional. It has given me a lifetimes' interest and an opportunity to discuss various theories - both sound and outrageous - prior to forming a rational view and making what I hope is a practical contribution to the subject.

REFERENCES

Alfven H., 1964, On the origin of the Asteroids, *Icarus*, 3, pp52-56

Allen, C. W., 1973, *Astrophysical Quantities*, 3rd Ed Athlone, London

Anon., 1802, Some Particulars relating to the new Planet Ceres Ferdinandia, *Phil. Mag.*, 12, pp80-83

BAA, 1995, *Handbook of the British Astronomical Association*, London

Ball, R. S., 1901, *The Story of the Heavens*, London

Barucci, M. A., and Fulchignoni, M., 1983, On the inversion of asteroidal Lightcurve Functions in *Comets, Asteroids and Meteors* eds Lagerkvist, C. I., and Rickman, H., pp.101-105 Uppsala University

Barsuhn J., 1983, The Light Curves of a Freely Precessing Spheroidal Minor Planet, *Astron. Astrophys.* 122, pp237-240

Barucci, M.A., Capria, M.T., Coradinini, A., and Fulchignoni, M., 1987 Classification of Asteroids using G-Mode analysis, *Icarus*, 72, pp304-324

Barucci, M. A., Casacchia, R., Fulchignoni, M., Burchi, R., Dipaoloantonio, A., Giuliani, C., Milano, L., Scaltriti, F., and Zappala, V., 1982, Laboratory Simulation of Photometric Light Curves of Asteroids, *Moon and Planets* 27, pp387-395

Batrukov, Y.V, et al, 1993, *Ephemerides of the Minor Planets 1994*, Institute for Theoretical Astronomy, St Petersburg

Bell, J.F., Davis, D.R., Hartmann, W.K.,and Gaffey, M.K., 1989, Asteroids : The Big Picture, in *Asteroids II* eds Binzel R.P., Gehrels T., and Matthews M.S., pp921-845, Arizona

Belton, M.J.S., 1990, Rationalization of Comet Halley's Periods, *Icarus*, 86, pp30-51

Bevington, P.R.,and Case, D.K., 1992, Data Reduction abd Error Analysis for the Physical Sciences, McGraw-Hill, New York

Bien, R., and Schubart, J., 1983, Methods of Determination of Periods in the Motion of Asteroids in *Comets, Asteroids, and Meteors* eds Lagerkvist, C. I., and Rickman, H., pp.161-166 Uppsala University

Binzel, R. P., 1985, Is 1220 Crocus a Precessing Binary Asteroid?, *Icarus*, 63, pp99-108

Binzel R.P., 1986, *Collision Evolution of the Asteroid Belt: An observational and numerical study*, Ph.D Thesis, Univ of Texas

Binzel, R.P., Farinella, P., Zappala, V., and Cellino, A., 1989, Asteroid Rotation Rates: Distributions and Statistics, in *Asteroids II* eds Binzel R.P., Gehrels T., and Matthews M.S., pp416-441, Arizona

Bode, J. E., 1772, *Anleitung zur Kenntniss des gestirnten Himmels*, Hamburg

Bottke, W.F., Nolan, M.C., Greenberg, R., and Kolvoord, R.A., 1994, Velocity Distributions among Colliding Asteroids, *Icarus*, 107, pp255-268

Bowell, E., and Lumme, K., 1979, Colorimetry and Magnitudes of Asteroids, in *Asteroids* ed Gehrels, T., pp132-169, Arizona

Bowell, E., Chapman, C.R., Morrison, D and Zellner B., 1978, Taxonomy of Asteroids,

Icarus, 35, pp313-335

Bowell, E., Gehrels, T., and Zellner, B., 1979, Magnitudes Colours, Types and Adopted Diameters of the Asteroids in *Asteroids* ed Gehrels, T., pp.1108-1129, Arizona

Bowell, E., Hapke, B., Domingue, D., Lumme, K., Petroniemi, J., and Harris, A.W., 1989, Application of Photometric Models to Asteroids, in *Asteroids II* eds Binzel R.P., Gehrels T., and Matthews M.S., pp524-556, Arizona

Boyd, L. J., Genet, R. M., and Hall, D. S., 1984, Automatic Photoelectric Telescopes at the Fairborn Observatory in *Microcomputers in Astronomy II* eds Genet, R. M., and Genet, K. A.,pp3.1-3.12 Fairborn, Ohio

Burns, J.A., and Tedesco, E.F.,1979, Asteroid lightcurves: Results for rotations and Shapes in Asteroids in *Asteroids* eds Gehrels T., and Matthews M.S., pp494-527, Arizona

Cameron, A. G. W., 1975, The Origin and Evolution of the Solar System, in *The Solar System*, pp.15-23, Scientific American

Cameron, A. G. W., 1978, Physics of the Primitive Solar Accretion Disc, *Moon and Planets*, 18, pp5-40

Carusi, A., and Valsecchi, G. B., 1979, Numerical Simulations of Close Encounters between Jupiter and Minor Bodies, in *Asteroids* ed Gehrels, T., pp391-416, Arizona

Cellino, A., Zappala, V., Di Martino, M., Farinella, P., and Paolicchi, P., 1987 Flattening, Pole, and Albedo Features of 4 Vesta from Photometric Data, *Icarus*, 70 ,pp546-565

Chandrasekar, S, 1969 *Ellipsoidal Figures of Equilibrium*, Yale University Press, New Haven

Chapman, C. R., 1979, The Asteroids : Nature, Interrelations, Origins and Evolution in *Asteroids* ed. Gehrels, T., pp.25-60 Arizona

Chapman, C. R., 1981, Asteroids, in *The New Solar System* eds. Beatty, J. K., O'Leary, B., and Chaikin, A., Cambridge University Press

Chapman, C. R., Morrison, D., and Zellner, B., 1975, Surface Propertities of Asteroids: A Synthesis of Polarimetry, Radiometry and Spectrophotometry *Icarus*, 25, pp.104-130

Cole, G.H.A., 1978, *The Structure of Planets*, Wykeham London

Cole, G.H.A., 1984, *Physics of Planetary Interiors*, Adam Hilger - Bristol

Curdt W., and Keller H.U., 1988, Collisions with Cometary Dust recorded by the Giotto HMC Camera, *ESA Journal* 12, pp189-208

Davis D.R., Weidenscilling S.J., Farinella P., Paolicchi P., and Binzel R.P., 1989, Asteroid Collision History: Effects on Sizes and Spins,in *Asteroids II*"eds Binzel R.P., Gehrels T., and Matthews M.S., pp805-826, Arizona

Degewij, J., and van Houten, C. J., 1979, Distant Asteroids and the Outer Jovian Satellites in *Asteroids*, ed. Gehrels, T., pp.417-435, Arizona

Dermott, S. F., Harris, A. W., and Murray, C. D., 1984 Asteroid Rotation Rates, *Icarus*, 57, pp14-34

Dobrovoskis, A. R., and Burns, J. A., 1984, Angular Momentum Drain: A Mechanism for Despinning Asteroids, *Icarus*, 57, pp464-476

DuPuy, D. L., 1983, An ultra low-dirft DC amplifier for use with Photomultipliers *Publ. Astron. Soc. Pacific*, **95**, pp86-91

DuPuy, D. L., and Hoffman, G. A., A Jurkevich Period Search Programme, *IAPPP Communications*, **20**, .pp1-18

Ealing-Beck, 1994, *Ealing Optics Catalogue*,Watford

Farinella, P., Davis, D.R., Paolicchi, P., Cellino, A., and Zappala, V., 1992, Asteroid Collisional Evolution: An integrated model for the evolution of asteroid rotation rates, *Astron. Astrophys*, **253**, pp604-614

Farinella, P., Paolicchi, P., and Zappala, V., 1981 On the shape of rapidly rotating Asteroids *Adv. Space Res.*, **1**, pp187-189

Farinella P., Paolicchi P., Tedesco E., and Zappalla V., 1981, Triaxial equilibrium ellisoids among the asteroids, *Icarus*, **64**, pp113-123

Fertig J., Marc X., and Schoenmaekers J., 1988, Analysis of Giotto encounter dynamics and post encounter status based on AOCS Data, *ESA Journal*, **12**, pp171-188

Fitzgerald, M. P., and Shelton, I., 1982, A Simple and Accurate On-line Data Acquistion Program, *J. R. Astron Soc. Canada*, **76**, pp337-367

van Flandern, T. E., Tedesco, E. F., and Binzel, R. P., 1979, Satellites of Asteroids in *Asteroids*, ed. Gehrels, T., pp.443-465 Arizona

Fowles G.R., 1981, *Analytical Mechanics*, Holt Rinehart and Winston, New York

French A.P., *Newtonian Mechanics*, 1971, WW Norton - London

Fried, R. E., and Mannery, E. J., 1983, GORT-1 Automatic Photometer, in *Microcomputers in Astronomy*, eds. Genet, R. M., and Genet, A. M., pp 96-115 Fairborn, Ohio

Fujiwara, A., Cerroni, P., Davis, D., Ryan, E., Di Martino, M., Holsapple, K., and Housen, K., 1989, Experiments and Scaling Laws for Catastrophic Collisions, in *Asteroids II* eds Binzel R.P., Gehrels T., and Matthews M.S., pp240-265, Arizona

Fujiwara, A., Kamimoto, G., and Tsukamoto, A., 1977, Destruction of basaltic bodies by high velocity impact, *Icarus*, **31**, pp277-288

Gaffey, M. J., and McCord, T. B., 1979, Mineralogical and Petrological Characteristics of Asteroid Surface Materials in *Asteroids*, ed. Gehrels, T., pp.688-723, Arizona

Gaffey, M. J., Bell, J. F., Hamilton Brown, R., Brubine, T. H., Piatek, J. L., Reed, K. L., and Chaky, D. A., 1993, Mineralogical Variations within the S-Type Asteroid Class, *Icarus*, **106**, pp573-602

Gehrels, T., 1979, The Asteroids : History, Surveys, Techniques and Future Work in *Asteroids* eds. Gehrels, T., pp.3-24 Arizona

Gehrels, T., 1984, A Study of Asteroid Topography, *National Geograph. Soc. Res. Reps.*, **21**, pp.187-191

Genet, R. M., 1980 (i), A Photoelectric Data Reduction Program in BASIC for Microcomputers *IAPPP Communications*, **2**, .pp23-28

Genet, R. M., 1980 (ii), A Microcomputer based System for Photoelectric Photometry *IAPPP Communications*, **3**, pp12-18

Goldreich, P., and Ward, W. R., 1973, The Formation of Planetesimals, *Astrophys. J.*, **183**, pp1061-1061

Gradie, J. C., Chapman, C. R., and Williams, J. G., 1979, Families of Minor Planets in *Asteroids*, ed. Gehrels, T., pp. 359-390 Arizona

Gradie, J. C., and Tedesco, E. F., 1982, Compositional Structure of the Asteroid Belt, *Science*, **216**, p.1405-1407

Greenberg, R., and Scholl, H., 1979, Resonances in the Asteroid Belt in *Asteroids*, ed. Gehrels, T., pp.310-333 Arizona

Greenberg, R., and Nolan, M.C., 1989, Delivery of asteroids and Meteorites to the Inner Solar System in *Asteroids II* eds Binzel R.P., Gehrels T., and Matthews M.S., pp778-804, Arizona

Greenberg, R., Wacker, J. F., Hartmann, W. K., and Chapman, C. R., 1978, Planetesimals to Planetoids : Numerical Simulation of Collision Evolution, *Icarus*, **35**, 1-26

Hall, D. S., and Genet, R. M., 1982, *Photoelectric Photometry of Variable Stars*, Fairborn, Ohio

Halling, R., 1984, Can gravitational compaction explain the Spin-Diameter relation for the Asteroids *Astrophys. and Space Sci.*, **103**, pp379-383

Hamamatsu, 1982, *Catalogue of Photomultiplier Tubes*, Catalogue SC-5

Harris, A. W., 1979, Asteroid Rotation Rates II : A Theory for the Collisional Evolution of Rotation Rates *Icarus*, **49**, pp145-153

Harris, A.W., 1994, Tumbling Asteroids, *Icarus*, **107**, pp209-211

Harris A. W., and Burns, J. A., 1979, Asteroid Rotation Rates I: Tabulations and Analysis of Rates, Pole Positions and Shapes, *Icarus*, **49**, pp115-144

Harris, A.W., Lupishko, D.F., 1989, Photometric Lightcurve Observations, in *Asteroids II* eds Binzel R.P., Gehrels T., and Matthews M.S., pp39-53, Arizona

Harris A. W., and Young, J. W., 1984, *Asteroid Rotation List Update 1* November 1984, Jet Propulsion Laboratory, Pasadena

Hartmann, W. K., 1978, Planet Formation: Mechanism of Early Growth, *Icarus*, **33**, pp50-61

Hartmann, W. K., 1979, Diverse Puzzling Asteroids and a Possible Unified Explanation in *Asteroids* ed. Gehrels, T., pp.466-479 Arizona

Hartmann, W. K., 1981, Small Bodies and their Origin, in *The New Solar System*, eds. Beatty, J. K., O'Leary, B., and Chaikin, A., pp197-204, Cambridge University Press

Henden, A. A., and Kaitchuck, R. H., 1982, *Astronomical Photometry*, Van Nostrand Reinhold, New York

Heppenheimer, T. A., 1978, On the Origin of the Kirkwood Gaps and of Satellite-Satellite Resonances *Astron. and Astrophys.*, **70**, pp457-465

Herschel, W., 1781, Account of a comet, *Phil. Trans. R. Soc.*, **92**, pp213-232

Herschel, W., 1802, Observations of the two lately discovered celestial bodies *Phil. Trans R. Soc.*, 92, pp213-232

Hirayama, K., 1918, Groups of asteroids probably of a common origin, *Proc. Imp, Acad, Japan* 9, pp482-485

Hollis, A.J., Bemrick, C.S., Dumont, M., Miles, R., 1987, Photometric Studies of the Minor Planets - Observations of 8 Flora, J. Brit., Astron Assoc., 97, pp220-223

Hopkins, J. L., 1981, PMT High Voltage Power Supply,*IAPPP Communications*, 4, pp23-25

Horowitz, P., and Hill, W., 1980, *The Art of Electronics* Cambridge University Press

Howell, E.S, Merenyi, E, and Lebofsky, L. A., 1994, Classification of asteroid spectra using a neural network, *J. Geophys. Research*, 99, pp10847-10865

Hoyle, F.,1978, *The Cosmogony of the Solar system*, University College Cardiff Press

Hughes, D. W., 1981, The Influx of Comets and Asteroids to the Earth, *Phil. Trans. R. Soc.*, 303, pp353-368

Hughes, *D. W., 1982, Asteroidal size* distribution, *Mon. Not. R. astr. Soc.* 199, pp1149-1157

Hughes, D.W., 1991, The largest asteroids ever, *Q. J. Roy. astr. Soc.*, 32, pp133-145

Hughes, D.W., 1994, Comets and Asteroids, *Contemporary Physics* 35, pp75-93

Intersil, 1980, *ICL7650 Chopper Stabilised Operational Amplifier Data Sheet*

Ip, W.H., 1977, On the Orbital dependence of the asteroid collision process, *Icarus*, 32, pp378-380

Issacman, R., and Sagan, C. 1977, Computer Simulations of Planetary Accretion Dynamics: Sensitivity to Initial Conditions, *Icarus*, 31, pp510-533

Johnson, H. L., and Harris, D. L., 1954, Three-Colour Observations of 108 stars intended for use as Photometric Standards, *Astrophys. J.*, 120, pp196-199

Johnson, H. L., and Morgan, W. W., 1953, Fundamental Stellar Photometry for Standards of Spectral Type on The revised System of the Yerkes Spectral Atlas *Astrophys. J.*, 117, pp313-352

Julian, W.H., 1987, Free Precession of the Comet Halley Nucleus, *Nature*, 326, pp57-58

KenKnight, C. E., 1985, Light Scattered from Polished Optical Surfaces : Wings of the Point Spread Function, in *Proc. Workshop on Improvements in Photometry* NASA CP2350

Kepler, J., 1595, *Mysterium Cosmographicum*, Tubingen

Kopal, Z., 1970, The axial rotation of asteroids, *Astrophys. Space Sci.*, 6, pp33-35

Kresak, L., 1979, Dynamical Interrelations among Comets and Asteroids in *Asteroids* ed. Gehrels, T., pp289-309 Arizona

Lamy P.L., and Burns, J.A., 1972, Geometrical Approach to Torque Free Motion of a Rigid Body having Internal Energy Dissipation, *Amer. J. Phys.*, 40, pp441-444

Ley, W., 1963, *Watchers of the Sky*,London

Lumme, K., and Bowell, E., 1981 (i), Radiative Transfer in the Surface of Atmosphereless Bodies - I Theory *Astron. J.*, 86, pp1690-1704

Lumme, K., and Bowell, E., 1981 (ii), Radiative Transfer in the Surface of Atmosphereless Bodies - II Interpretation of Phase Curves, *Astron. J.*, **86**, pp1705-1712

Lupishko, D. F., Akimov, L. A., and Belskaya, I. N., 1983, On Photometric Heterogeneity of Asteroid Surfaces in *Comets, Asteroids and Meteors* eds. Lagerkvist, C. I., and Rickman, H., pp63-70, Uppsala University

McAdoo, D. C., and Burns, J. A., 1974, Approximate Alignment Times for Spinning Bodies *Icarus*, **21**, pp86-93

McCheyne, R. S., 1985, *Optical and Infra-Red Studies of Asteroids*, Ph.D. Thesis, Leicester University

Magnusson, P., 1989, Pole Determinations of Asteroids, in *Asteroids II* eds Binzel R.P., Gehrels T., and Matthews M.S., pp1180-1190, Arizona

Magnusson, P, Barucci, M.A., Drummond, J.D., Lumme, K., Ostro, S., Surdej, J., Taylor, R.C., and Zappala, V., 1989, Determination of Pole Orientations and Shapes of Asteroids, in *Asteroids II* eds Binzel R.P., Gehrels T., and Matthews M.S., pp68-97, Arizona

Maley, P., 1984, Measuring the shape of an Asteroid *Astronomy*, **12**, pp51-54

Marsden, B. G., 1986, *Minor Planet Circular 11199 - Oct 17*, Smithsonian Astrophys. Obs., Harvard

Marsden, B.G., 1985, Notes from the IAU General Assembly , *MPC 10193*

Meadows, A. J., 1978, *Stellar Evolution*, Pergamon, Oxford

Meech and Belton, 1989, *IAU Circular 4770*

Miles, R., 1986, Ohmic Leakage Currents and the Dark Performance of the 1P21 side-window Photomultiplier, *IAPPP Communications*, **24**, pp6-21

Millis, R. L., and Elliot, J. L., 1979, Direct Determination of Asteroid Diameters from Occultation Observations in *Asteroids* ed. Gehrels, T., pp98-118Arizona

Millis, R. L., and Schleicher, D. G., 1986, Rotation period of Comet Halley, *Nature*, **324**, pp646-649

Napier, W. McD., and Dodd, R. J., 1973, The Missing Planet, *Nature*, **242**, pp250-251

Nieto, M. M., 1972, *The Titius-Bode Law of Planetary Distances Its History and Theory*,Pergamon, London

O'Keefe, J.D., and Ahrens, T.J., 1977, Meteorite impact ejecta : Dependence of mass and energy lost on planetary escape velocity, *Science*, **198**, pp1249-1251

von Oppolzer, E., 1901, Notiz betr. planet (433) Eros, *Astron. Nach.*, **154**, p297

Piazzi, G., 1802, Results of Observations of the new star discovered on the 1st January 1801 at the Royal Observatory of Palermo, *Phil. Mag.*, **12**, pp54-62

Pospieszalska-Surdej, A., and Surdej, J, 1985, Determination of the pole orientation of an asteroid : The amplitude-aspect relation revisited, *Astron. Astrophys.*, **149**, pp186-194

RS Components, 1982, *Universal Counter 7226A*, Data Sheet R/4412

Rosen, W. A., and Chromey, F. R., 1985, Gain instabilities in Photomultipliers - How accurate are photon counting measurements in *Proc. Workshop Improvements in Photometry*, NASA CP2350

Russell, H. N., 1906, On the light variations of Asteroids and Satellites, *Astrophys. J.*, **24**, pp1-18

Ruzmaikina, T.V., Safronov, V.S., and Weidenschilling, S.J., 1989, Radial Mixing of Material in the Asteroidal Zone in *Asteroids II* eds Binzel R.P., Gehrels T., and Matthews M.S., pp681-700 Arizona

Sagdeev, R. Z., Blamont, J., Galeev, A. A., Moroz, V. I., Shapiro, V.D., Shevchenko, V.I., Szego, K., 1986, Vega Spacecraft encounters with Comet Halley, *Nature*, **321**, pp259-262

Samarasinha, N.N, and A'Hearn, M. F. A., 1991, Observational and Dynamical Constraints on the Rotation of Comet P/Halley, *Icarus*, **93**, pp194-225

Schott, 1985, *Colour Filter Glass*, Catalogue 3531/4e

Schultz, P., and Gault, D.E., 1986, Momentum Transfer from oblique impacts, *Proc.Lunar Planet Sci. Conf. XVII*, pp781-784

Schwehm, G, and Hechler, M., 1994, "Rosetta" - ESA's Planetary Cornerstone Mission, *ESA Bulletin* 77, pp7-18

Sekaninia, Z., 1987, Nucleus of comet Halley as a torque-free rigid rotator, *Science*, **325**, pp326-328

Sher, D., 1971, On the Variation in light of Tumbling Bodies, *Astrophys and Space Sci.*, **11**, pp222-231

Shoemaker, E. M., 1981, The Collison of Solid Bodies, in *The New Solar System*, eds. Beatty, J. K., O'Leary, B.,and Chaikin, A., pp33-44, Cambridge University Press

Shoemaker, E. M., Williams, J. G., Helin, E. F., and Wolfe, F. F., 1979, Earth-Crossing Asteroids Orbital Class, Collision Rates with Earth and Origin in *Asteroids* ed. Gehrels, T., pp253-282 Arizona

Singh, J., 1970, *Modern Cosmology*,Pelican, London

Sky and Telescope, *News and Notes*, April 1995, p14

Sokal, R. R., and Sneath, P. H. A., 1963, *Principles of Numerical Taxonomy*,Freeman, London

Stern, S.A., 1995, The Chiron Perihelion Campaign, *Sky and Telescope*, **89**, pp32-34

Stokes, A., A Compact Rotating Disk Photometer Head *IAPPP Communications*, **11**, pp43-45

Stubberfield, R. A., 1985, Getting the most from your Photomultiplier, *Photonics Spectra*, pp94-97 Feb. 1985

Sykes, M.V., Greenberg, R., Dermott, S.F., Nicholson, P.D., Burns, J.A., Gautier, T.N., 1989, Dust Bands in the Asteroid Belt, , in *Asteroids II* eds Binzel R.P., Gehrels T., and Matthews M.S., pp336-367, Arizona

Szecesnyi-Nagy, G., 1983, 127 Johanna : Is it really the most quickly spinning Asteroid known at the moment? in *Comets, Asteroids and Meteors* eds. Lagerkvist, C. I., and Rickman, H., pp49-53 Uppsala University

Taff, L. G., 1984, Optimal Searches for Asteroids *Icarus*, **57**, pp259-266

Taylor, R. C., 1979, Pole Orientations, in *Asteroids*, ed. Gehrels, T., pp480-493 Arizona

Tedesco, E.F., 1989, Asteroid Magnitudes, UBV Colors, and IRAS Albedos and Diameters in *Asteroids II* eds Binzel R.P., Gehrels T., and Matthews M.S., pp1151-1161, Arizona

Tedesco, E.F., Williams, J.G., Matson, D.L., Veeder, G.J., Gradie, J.C., and Lebofsky, L.A., 1989, A Three Parameter Asteroid Taxonomy, *Astron. J.*, 97, pp580-606

Tedesco, E. F., and Zappala V., 1980, Rotational Properties of Asteroids : Correlations and Selection Effects *Icarus*, 43, pp33-50

Teledyne Inc., 1980, *9400 9401 9402 Voltage-to-Frequency Converter*, Data Sheet

Tholen, D.J., and Barucci, M.A., 1989, Asteroid Taxonomy, in *Asteroids II* eds Binzel R.P., Gehrels T., and Matthews M.S., pp298-315, Arizona

Thompson, G. A., 1905, Variability and the Asteroids, *Pop. Astron.*, 13, [[378-384

Titius von Wittenberg, J. D., 1766, translation into German of *Betractung uber die Natur, vom Karl Bonnet*, Leipzig

Trueblood, M., and Genet, R. M., 1985, *Microcontrol of Telescopes*, William-Bell, Dundee, Mich.

Vaïberg, O.L., et al., 1986, Comet Halley dust environment from SP-2 detector measurements, *Nature*, 321, pp262-266

Walker, E. N., 1986, The Joint European Amateur Photometer, *IAPPP Communications*, 21, pp21-23

Watson, J. R., 1983, *Mastering Electronics*, Macmillan, London

Weidenschilling, S.J., 1980, Hektor : Nature and Origin of a Binary Asteroid, *Icarus*,44, pp807-809

Weidenschilling, S. J., 1981, How Fast Can an Asteroid Spin, *Icarus*, 46, pp124-126

Weissman, P.R., A'Hearn, M.F., McFadden, L.A., and Rickman, H, 1989, Evolution of Comets into Asteroids, in *Asteroids II* , eds Binzel R.P.,Gehrels T., and Matthews M.S., pp880-920, Arizona

Wetherill, G. W., 1981, The Formation of the Earth from Planetesimals, *Sci. American*, June 1981, pp131-140

Wetherill, G.W.,1989, Origin of the Asteroid Belt, in *Asteroids II* , eds Binzel R.P.,Gehrels T., and Matthews M.S., pp661-680, Arizona

Whipple, A. L., and White, K.L.K., 1985, Stability of Binary Asteroids,*Celestial Mech.*, 35, pp95-104

Whipple F., 1981, The spin of the Comets, in *Readings from Scientific American : Comets* ed. Brandt, J. C., pp56-63W. H. Freeman, San Francisco

Whipple, F., 1986, *The Mystery of Comets*, Cambridge University Press

Wood, J. A., 1979, *The Solar System*,New Jersey

Yanagisawa, M., Eluszkiewicz, J., Ahrens, T.J., 1991, Angular Momentum Transfer in Low Velocity Oblique Impacts: Implications for Asteroids, *Icarus*, 94, pp272-282

Young, A. T., 1985, Filter and Passband Problems in *Proc. Workshop Improvements in Photometry*, NASA CP2350

Young, A. T., Talbert, F., and Angione, R., 1984, On the Optical Design of Photoelectric Stellar Photometers,*Mon. Not. R. Astron. Soc.*, 25, pp56-62

von Zach, F. X., 1802, (i), letter to Sir Joseph Banks March 30 1802, RGO Archive 4/119(ix)

von Zach, F. X., 1802 (ii), letter to Maskelyne

May 4 1802, RGO Archive 4/119 (x)

von Zach, F. X., 1802, (iii), Forgesetzte Nachrichten uber den langst vermutheten neuen Haupt-Planeten unseres SonnenSystem, *Monat. Correspon.*, 4, pp89-95

von Zach, F. X., 1802 (iv), Forgesetzte Nachrichten uben den zwischen Mars und Jupiter richtig vermutheten nun wirklich entdeckten neuen Haupt-Planeten unseres Sonnen Systems Ceres Ferdinandia. *Monat. Correspon.*, 4, pp170-183

Zappala, V., 1981, A Semi-analytic Method for Pole Determination of Asteroids, *Moon and Planets*, 24, pp170-183

Zeilik, M., and Elston, R., 1982, Intelligent Photometry at Capilla Peak Observatory *IAPPP Communications*, 10, pp22-25

Zellner, B., 1979 (i), Asteroid Taxonomy and the distribution of the Compositional Types in *Asteroids* ed. Gehrels, T., pp788-806 Arizona

Zellner, B., 1979 (ii), The Tucson Revised Index of Asteroid Data in *Asteroids* ed. Gehrels, T., pp1011-1013 Arizona

Zellner, B., Thirunagari, A., and Bender, D., 1985, The Large Scale Structure of the Asteroid Belt *Icarus*, 62, pp505-511

Zellner, B., Tholen, D. J., Tedesco, E. F., 1985, The Eight-Colour Asteroid Survey : Results for 589 Minor Planets, *Icarus*, 61, pp355-416

Ziolkowski, K., 1983, Do Nongravitational Forces exist in the motion of Asteroids? in *Comets, Asteroids and Meteors* eds. Lagerkvist, C. I., and Rickman, H., pp171-174 Uppsala University